

NRC Publications Archive Archives des publications du CNRC

High performance roofing and walls technologies: task 5, parametric study of curtain wall systems for selection of components and optimization of thermal performance

Saber, Hamed H.; Lacasse, Michael A.

For the publisher's version, please access the DOI link below./ Pour consulter la version de l'éditeur, utilisez le lien DOI ci-dessous.

Publisher's version / Version de l'éditeur:

<https://doi.org/10.4224/23002872>

Client Report (National Research Council of Canada. Construction), 2016-02-18

NRC Publications Archive Record / Notice des Archives des publications du CNRC :

<https://nrc-publications.canada.ca/eng/view/object/?id=338ae785-f1e5-4165-a253-1e05baf3ab56>

<https://publications-cnrc.canada.ca/fra/voir/objet/?id=338ae785-f1e5-4165-a253-1e05baf3ab56>

Access and use of this website and the material on it are subject to the Terms and Conditions set forth at

<https://nrc-publications.canada.ca/eng/copyright>

READ THESE TERMS AND CONDITIONS CAREFULLY BEFORE USING THIS WEBSITE.

L'accès à ce site Web et l'utilisation de son contenu sont assujettis aux conditions présentées dans le site

<https://publications-cnrc.canada.ca/fra/droits>

LISEZ CES CONDITIONS ATTENTIVEMENT AVANT D'UTILISER CE SITE WEB.

Questions? Contact the NRC Publications Archive team at

PublicationsArchive-ArchivesPublications@nrc-cnrc.gc.ca. If you wish to email the authors directly, please see the first page of the publication for their contact information.

Vous avez des questions? Nous pouvons vous aider. Pour communiquer directement avec un auteur, consultez la première page de la revue dans laquelle son article a été publié afin de trouver ses coordonnées. Si vous n'arrivez pas à les repérer, communiquez avec nous à PublicationsArchive-ArchivesPublications@nrc-cnrc.gc.ca.

High Performance Roofing and Walls Technologies

Task 5: Parametric study of Curtain Wall Systems for Selection of Components and Optimization of Thermal Performance

Client Report: A1-002844-06

Hamed H. Saber and Michael A. Lacasse

18 February, 2016



Table of Contents

Table of Contents	i
List of Figures.....	iii
List of Tables.....	ix
Summary.....	xi
Acknowledgements	xiii
1. Introduction.....	1
2. Description of Curtain Wall Components	2
2.1 Spandrel Panels	3
2.2 Frame	3
2.3 Vision Panels.....	3
2.3.1 Vision Glass.....	3
2.3.2 Insulating Glass Unit (IGU)	4
3. Overview of Thermal Performance of Enclosed Spaces in IGUs	5
3.1 Basic physics of heat transfer across enclosed spaces of IGUs.....	5
4. Approach to Simulation & Description of Curtain Wall Configurations.....	10
4.1 Approach for Simulation of NFRC Compliant CW Configurations.....	10
4.2 Description of curtain wall panel modelling configurations.....	11
4.2.1 Detailed curtain wall manufactured product configuration	11
4.2.2 Description of curtain wall panel modelling configuration	11
4.2.3 Description of NFRC curtain wall panel model configuration	14
5. Results derived from simulation.....	16
5.1 Simulation Results for manufactured product configurations	16
5.1.1 – Results for Double glazed CW product configurations.....	16
5.1.2 – Results for Triple glazed CW manufactured product configuration	19
5.2 Simulation Results for NFRC-Compliant CW configurations	21
5.2.1 Results for Double-glazed NFRC-Compliant CW Configurations	21
5.2.2 Results for Triple-glazed NFRC-Compliant CW Configurations.....	43
6. Summary.....	65
7. References.....	66
Appendix 1	73
Appendix 2 Results of Simulation of Double-glazed Curtain Wall Manufactured Products	75
A2.1 Predicted total heat loss through curtain wall panel derived from simulation	75
A2.2 Predicted R-value in relation to emissivity of glazing as derived from simulation.....	75

Appendix 3 Results of Simulation of Triple-glazed Curtain Wall Manufacturers Product.....	81
Effect of Glazing to Wall Area Ratio / Case-I: 90% Ar and 10% Air, Low-e Coating ($e_{coat} = 0.054$)	81
Effect of Glazing to Wall Area Ratio / Case-II: 90% Kr and 10% Air, Low-e Coating ($e_{coat} = 0.054$)	83
Effect of Glazing to Wall Area Ratio / Case-III: 90% Xe and 10% Air, Low-e Coating ($e_{coat} = 0.054$)	85
Effect of Glazing to Wall Area Ratio / Air, Low-e Coating ($e_{coat} = 0.054$)	87
Effect of Glazing to Wall Area Ratio/Case-IV: Air filled IGU; Low-e Coating vs. no Coating ($e_{coat}=0.054 / e$)	89
Effect of Glazing to Wall Area Ratio/Case-IV: 90 % Ar, 10 % Air-filled IGU; Low-e Coating vs. no Coating ($e_{coat}=0.054 / e$	91
Effect of Glazing to Wall Area Ratio/Case-IV: 90 % Kr, 10 % Air-filled IGU; Low-e Coating vs. no Coating ($e_{coat}=0.054 / e$	93
Effect of Glazing to Wall Area Ratio/Case-IV: 90 % Xe, 10 % Air-filled IGU; Low-e Coating vs. no Coating ($e_{coat}=0.054 / e$	95
Effect of Coating ($e_{coat} = 0 - 0.84$), 90 % Ar, 10 % Air-filled IGU; Solid Symbols: Epsilon CW having triple-glazed vision and spandrel panel	97
Effect of Coating ($e_{coat} = 0 - 0.84$), 90 % Kr, 10 % Air-filled IGU; Solid Symbols: Epsilon CW having triple-glazed vision and spandrel panel	99
Effect of Coating ($e_{coat} = 0 - 0.84$), 90 % Xe, 10 % Air-filled IGU; Solid Symbols: Epsilon CW having triple-glazed vision and spandrel panel.....	101
Effect of Coating ($e_{coat} = 0 - 0.84$), Air-filled IGU; Solid Symbols: Epsilon CW having triple-glazed vision and spandrel panel.....	103
Appendix 4 Effect of Inclination Angle and Direction of Heat Flow.....	111
Appendix 5 - Summary of Previous Model Benchmarking	123

List of Figures

Figure 1. Basic components of a typical curtain wall system [6].....	2
Figure 2. Components of a standard double-glazed insulating glass unit	4
Figure 3 - Dependence of R-value ($\text{ft}^2 \cdot \text{hr} \cdot ^\circ\text{F}/\text{BTU}$) on effective emissivity, ϵ_{eff} given values of $T_{\text{avg}}/\Delta T$ ($10^\circ\text{C}/\Delta T = 16.7^\circ\text{C}$; $-45.6^\circ\text{C}/\Delta T = 11.1^\circ\text{C}$), and different values of H for an airspace of depth 13 mm;	9
Figure 4. Schematics of enclosed space with and without thin sheet of low emissivity on both sides, placed in the middle of the space of Insulating Glass Units (IGUs).	Error! Bookmark not defined.
Figure 5 – Sectional drawings of triple-glazed curtain wall mullion at vision panel; Sectional drawing of triple-glazed curtain wall mullion at opaque panel	1
Figure 6 – Sectional drawing of double-glazed curtain wall mullion; Photo showing end portion of horizontal section; Sectional drawing of double-glazed curtain wall mullion at opaque panel.....	1
Figure 7 – Elevation view of “exterior” of double- and triple-glazed curtain wall assembly.....	2
Figure 8 – Elevation view of “interior” of double- and triple-glazed curtain wall assembly.....	2
Figure 9 - Reference Curtain Wall assembly conforming to NFRC (2m x 2m vision; 2 m x 1.2 m spandrel)	14
Figure 10 - Double Glazing (2G) Curtain Wall sectional views; Surface 2 with low-e of emissivity = 0.054; Other surfaces (1, 3, 4) emissivity = 0.84; Filling gas: 90% gas and 10% air.....	15
Figure 11 - Triple Glazing (3G) Curtain Wall sectional views and detail of IGU and characteristic surfaces	15
Figure 12 – Risk of Condensation on Interior Surface of CW components for NFRC test conditions; Two Options: Option B: ASHRAE 160 (40% RH); Option D: Modified ASHRAE 160 (32% RH)	17
Figure 13 – Simulated exterior temperature (i) and values of temperature index T_{Index} (ii) of double-glazed thermally broken CW product having IGU with 90% Ar & 10% Air; Surface 2, $E_{\text{coat}} = 0.054$	18
Figure 14 – Simulated results of relative humidity on interior surface of double-glazed IGU thermally broken CW product; (i) Option D: Modified ASHRAE 160 (32% RH); (ii) Option B: ASHRAE 160 (40% RH)	18
Figure 15 – Simulated results of temperature difference (ΔT °C) on exterior surface of double-glazed CW product: (i) Option D: Modified ASHRAE 160 (32% RH); (ii) Option B: ASHRAE 160 (40% RH)	18
Figure 16 – Simulated temperature differences between surface (T_{int}) and dew point (T_{Dewpoint}) of double-glazed thermally broken CW product having IGU with 90% Ar & 10% Air; Surface 2, $E_{\text{coat}} = 0.054$	19
Figure 17 – Simulated exterior temperature (i) and values of temperature index T_{Index} (ii) of triple-glazed thermally broken CW product having IGU with 90% Ar & 10% Air; Surface 2, $E_{\text{coat}} = 0.054$	20
Figure 18 – Simulated results of relative humidity on interior surface of triple -glazed IGU thermally broken CW product; (i) Option D: Modified ASHRAE 160 (32% RH); (ii) Option B: ASHRAE 160 (40% RH)	20
Figure 19 – Simulated results of temperature difference (ΔT °C) on exterior surface of triple-glazed CW product: (i) Option D: Modified ASHRAE 160 (32% RH); (ii) Option B: ASHRAE 160 (40% RH)	20
Figure 20 – Simulated temperature differences between surface (T_{int}) and dew point (T_{Dewpoint}) of triple-glazed thermally broken CW product having IGU with 90% Ar & 10% Air; Surface 2, $E_{\text{coat}} = 0.054$	21
Figure 21 – Simulated exterior (i) & interior (ii) temperature; values of temperature index T_{Index} (iii) of double-glazed thermally broken NFRC-compliant CW having IGU with 90% Ar & 10% Air.....	23
Figure 22 – Simulated results of RH on interior surface of double-glazed IGU thermally broken NFRC-compliant CW; (i) Option D: Modified ASHRAE 160 (32% RH); (ii) Option B: ASHRAE 160 (40% RH)	23
Figure 23 – Simulated results of temperature difference on exterior surface of double-glazed NFRC-compliant CW: (i) Option D: Modified ASHRAE 160 (32% RH); (ii) Option B: ASHRAE 160 (40% RH)	23
Figure 24 – Simulated temperature differences between surface and dew point (T_{Dewpoint}) of double-glazed thermally broken NFRC compliant CW having IGU with 90% Ar & 10% Air; Surface 2, $E_{\text{coat}} = 0.054$	24
Figure 25 - Predicted (by simulation) R-value (i) and U-value (ii) (air-to-air; surface-to-surface) of double-glazed low-e coated ($e = 0.054$) thermally broken curtain wall section in relation to glazing to Wall Area Ratio	26
Figure 26 - Predicted (by simulation) R-value (i) & U-value (ii) (air-to-air; surface-to-surface) of double-glazed low-e coated ($e = 0.054$) thermally broken curtain wall section in relation to glazing to Wall Area Ratio.....	26
Figure 27- Predicted (by simulation) R-value (i) and U-value (ii) (air-to-air; surface-to-surface) of double-glazed low-e coated ($e = 0.054$) thermally broken curtain wall section in relation to glazing to Wall Area Ratio	27
Figure 28 - Predicted (by simulation) R-value (i) and U-value (ii) (air-to-air; surface-to-surface) of double-glazed low-e coated ($e = 0.054$) thermally broken curtain wall section in relation to glazing to Wall Area Ratio	27
Figure 29 - Predicted (by simulation) R-value (i) and U-value (ii) (air-to-air; surface-to-surface) of double-glazed low-e coated or not coated thermally broken CW in relat ⁿ to Glaz ^{ng} to Wall Area Ratio	28
Figure 30 - Predicted (by simulation) R-value (i) and U-value (ii) (air-to-air; surface-to-surface) of double-glazed low-e coated or not coated thermally broken CW in relat ⁿ to Glaz ^{ng} to Wall Area Ratio	28
Figure 31 - Predicted (by simulation) R-value (i) ; U-value (ii) (air-to-air; surface-to-surface) of double-glazed, low-e thermally broken curtain wall in relation to Glazing to Wall Area Ratio.....	29

Figure 32 - Predicted (by simulation) R-value (i) ; U-value (ii) (air-to-air; surface-to-surface) of double-glazed, low-e thermally broken curtain wall in relation to Glazing to Wall Area Ratio.....	29
Figure 33 – Predicted (by simulation) R-value (surface-to-surface) of double-glazed low-e coated (e = 0.054) thermally broken curtain wall in relation to Glazing to Wall Area Ratio for IGU filled with 100 % Air; 90 % Ar, 10 % Air; 90 % Kr, 10 % Air; 90 % Xe, 10 % Air.....	30
Figure 34 - Predicted (by simulation) R-value (surface-to-surface) of double-glazed low-e coated (e = 0.054) thermally broken curtain wall in relation to glazing to Wall Area Ratio for IGU filled with 100 % Air; 90 % Ar, 10 % Air; 90 % Kr, 10 % Air; 90 % Xe, 10 % Air.....	30
Figure 35 – Predicted (by simulation) R-value (i) ; U-value (ii) of double-glazed, thermally broken curtain wall as a function of coating emissivity for IGU filled with 90% Ar & 10 % Air.....	32
Figure 36 - Predicted (by simulation) R-value (i) ; U-value (ii) of double-glazed, thermally broken curtain wall as a function of coating emissivity for IGU filled with 90% Kr and 10 % Air	32
Figure 37 - Predicted (by simulation) R-value (i); U-value (ii) (air-to-air; surface-to-surface) of double-glazed, thermally broken curtain wall as a function of coating emissivity.....	33
Figure 38 - Predicted (by simulation) R-value (i) ; U-value (ii) (air-to-air; surface-to-surface) of double-glazed, thermally broken curtain wall as a function of coating emissivity.....	33
Figure 39 – Predicted (by simulation) (i) R-value (surface-to-surface) as a function of coating emissivity (surface S2) and; (ii) rate of change in R-value in relation to emissivity for a NFRC-compliant, thermally-broken Curtain Wall, with a double-glazed, Air-, Ar-, Xe-, or Kr-filled IGU.....	34
Figure 40 – Predicted (by simulation) (i) U-value (surface-to-surface) as a function of coating emissivity (surface S2) and; (ii) rate of change in U-value in relation to emissivity for a NFRC-compliant, thermally-broken Curtain Wall, with a double-glazed, Air-, Ar-, Xe-, or Kr-filled IGU.....	34
Figure 41 – Predicted (by simulation) (i) R-value and (ii) U-value (air-to-air; surface-to-surface) as a function of Spandrel panel insulation for a NFRC-compliant, thermally-broken double-glazed Ar-filled IGU curtain wall assembly with and without low-e coating on surface 2.....	36
Figure 42 – Predicted (by simulation) (i) R-value and (ii) U-value (air-to-air; surface-to-surface) as a function of Spandrel panel insulation for a NFRC-compliant, thermally-broken double-glazed Kr-filled IGU curtain wall assembly with and without low-e coating on surface 2.....	36
Figure 43 – Predicted (by simulation) (i) R-value and (ii) U-value (air-to-air; surface-to-surface) as a function of Spandrel panel insulation for a NFRC-compliant, thermally-broken double-glazed Xe-filled IGU curtain wall assembly with and without low-e coating on surface 2.....	37
Figure 44 – Predicted (by simulation) (i) R-value and (ii) U-value (air-to-air; surface-to-surface) as a function of Spandrel panel insulation for a NFRC-compliant, thermally-broken double-glazed Air filled IGU curtain wall assembly with and without low-e coating on surface 2.....	37
Figure 45 – Predicted (by simulation) (i) R-value and (ii) U-value as a function of Spandrel panel insulation for a NFRC-compliant, thermally-broken double-glazed curtain wall assembly incorporating an IGU with low-ε coating (surface 2) and filled with either Ar, Kr, Xe, or Air.....	38
Figure 46 – Predicted (by simulation) (i) R-value and (ii) U-value as a function of Spandrel panel insulation for a NFRC-compliant, thermally-broken double-glazed curtain wall assembly incorporating an IGU without low-ε coating (surface 2) and filled with either Ar, Kr, Xe, or Air.....	38
Figure 47 - Typical doubled & triple-glazed IGUs and their respective components	39
Figure 48 – Predicted (by simulation) (i) R-value and (ii) U-value (air-to-air; surface-to-surface) as a function of thermal conductivity of spacer for a NFRC-compliant, thermally-broken double-glazed Ar-filled IGU curtain wall assembly with and without low-e coating on surface 2.....	40
Figure 49 – Predicted (by simulation) (i) R-value and (ii) U-value (air-to-air; surface-to-surface) as a function of thermal conductivity of spacer for a NFRC-compliant, thermally-broken double-glazed Kr-filled IGU curtain wall assembly with and without low-e coating on surface 2.....	40
Figure 50 – Predicted (by simulation) (i) R-value and (ii) U-value (air-to-air; surface-to-surface) as a function of thermal conductivity of spacer for a NFRC-compliant, thermally-broken double-glazed Xe-filled IGU curtain wall assembly with and without low-e coating on surface 2.....	41
Figure 51 – Predicted (by simulation) (i) R-value and (ii) U-value (air-to-air; surface-to-surface) as a function of thermal conductivity of spacer for a NFRC-compliant, thermally-broken double-glazed Air filled IGU curtain wall assembly with and without low-e coating on surface 2.....	41
Figure 52 – Predicted (by simulation) R-value (surface-to-surface) as a function of thermal conductivity of Spacer for a NFRC-compliant, thermally-broken double-glazed curtain wall assembly incorporating an IGU with low-ε coating (ε = 0.054; surface 2) and filled with either Ar, Kr, Xe, or Air.....	42
Figure 53 – Predicted (by simulation) (i) R-value (surface-to-surface) as a function of thermal conductivity of Spacer for a NFRC-compliant, thermally-broken double-glazed curtain wall assembly incorporating an IGU without low-ε coating and filled with either Ar, Kr, Xe, or Air.....	42
Figure 54 – Simulated exterior (i) & interior (ii) temperature; values of temperature index T_{Index} (iii) of triple-glazed thermally broken NFRC-compliant CW having IGU with 90% Ar & 10% Air.....	44

Figure 55 – Simulated results of RH on interior surface of triple-glazed IGU thermally broken NFRC-compliant CW; (i) Option D: Modified ASHRAE 160 (32% RH); (ii) Option B: ASHRAE 160 (40% RH)44

Figure 56 – Simulated results of temperature difference (ΔT °C) on exterior surface of triple-glazed NFRC-compliant CW: (i) Option D: Modified ASHRAE 160 (32% RH); (ii) Option B: ASHRAE 160 (40% RH) 44

Figure 57 – Simulated temperature differences between surface (T_{int}) and dew point ($T_{Dewpoint}$) of triple-glazed thermally broken NFRC compliant CW having IGU with 90% Ar & 10% Air;.....45

Figure 58 – Predicted (by simulation) (i) R-value and (ii) U-value (air-to-air; surface-to-surface) of triple-glazed low-e ($e = 0.054$) coated thermally broken Curtain Wall in relation to Glazing to Wall Area Ratio for IGU filled with 90 % Ar, 10% Air 48

Figure 59 – Predicted (by simulation) (i) R-value and (ii) U-value (air-to-air; surface-to-surface) of triple-glazed low-e ($e = 0.054$) coated thermally broken Curtain Wall in relation to Glazing to Wall Area Ratio for IGU filled with 90 % Kr, 10% Air 48

Figure 60 – Predicted (by simulation) (i) R-value and (ii) U-value (air-to-air; surface-to-surface) of triple-glazed low-e ($e = 0.054$) coated thermally broken Curtain Wall in relation to Glazing to Wall Area Ratio for IGU filled with 90 % Xe, 10% Air 49

Figure 61 – Predicted (by simulation) (i) R-value and (ii) U-value (air-to-air; surface-to-surface) of triple-glazed low-e ($e = 0.054$) coated thermally broken Curtain Wall in relation to Glazing to Wall Area Ratio for IGU filled with 100 % Air 49

Figure 62 – Predicted (by simulation) (i) R-value and (ii) U-value (air-to-air; surface-to-surface) of triple-glazed low-e ($e = 0.054$) or no low-e ($e = 0.84$) coated thermally broken Curtain Wall in relation to Glazing to Wall Area Ratio for IGU filled with 90 % Ar, 10% Air50

Figure 63 – Predicted (by simulation) (i) R-value and (ii) U-value (air-to-air; surface-to-surface) of triple-glazed low-e ($e = 0.054$) or no low-e ($e = 0.84$) coated thermally broken Curtain Wall in relation to Glazing to Wall Area Ratio for IGU filled with 90 % Kr, 10% Air50

Figure 64 – Predicted (by simulation) (i) R-value and (ii) U-value (air-to-air; surface-to-surface) of triple-glazed low-e ($e = 0.054$) or no low-e ($e = 0.84$) coated thermally broken Curtain Wall in relation to Glazing to Wall Area Ratio for IGU filled with 90 % Xe, 10% Air51

Figure 65 – Predicted (by simulation) (i) R-value and (ii) U-value (air-to-air; surface-to-surface) of triple-glazed low-e ($e = 0.054$) or no low-e ($e = 0.84$) coated thermally broken Curtain Wall in relation to Glazing to Wall Area Ratio for IGU filled with 100 % Air51

Figure 66 – Predicted (by simulation) (i) R-value and rate of change in R-value in relation to emissivity and; (ii) U-value (surface-to-surface) as a function of Glazing to Wall Area Ratio, for a NFRC-compliant, thermally-broken Curtain Wall, having a triple-glazed, low-e coated Air-, Ar-, Xe-, or Kr-filled IGU .52

Figure 67 – Predicted (by simulation) (i) R-value and rate of change in R-value in relation to emissivity and; (ii) U-value (surface-to-surface) as a function of Glazing to Wall Area Ratio, for a NFRC-compliant, thermally-broken Curtain Wall, having a triple-glazed, Air-, Ar-, Xe-, or Kr-filled IGU (no low-e coating; $e = 0.84$) 52

Figure 68 – Predicted (by simulation) R-value (i) ; U-value (ii) of triple-glazed, thermally broken curtain wall as a function of coating emissivity for IGU filled with 90% Ar and 10 % Air54

Figure 69 – Predicted (by simulation) R-value (i) ; U-value (ii) of triple -glazed, thermally broken curtain wall as a function of coating emissivity for IGU filled with 90% Kr and 10 % Air54

Figure 70 – Predicted (by simulation) R-value (i) ; U-value (ii) of triple-glazed, thermally broken curtain wall as a function of coating emissivity for IGU filled with 90% Xe and 10 % Air55

Figure 71 – Predicted (by simulation) R-value (i) ; U-value (ii) of triple -glazed, thermally broken curtain wall as a function of coating emissivity for IGU filled with 100 % Air55

Figure 72 – Predicted (by simulation) (i) R-value (surface-to-surface) as a function of coating emissivity (surface S2) and; (ii) rate of change in R-value in relation to emissivity for a NFRC-compliant, thermally-broken Curtain Wall, with a triple-glazed, Air-, Ar-, Xe-, or Kr-filled IGU56

Figure 73 – Predicted (by simulation) (i) U-value (surface-to-surface) as a function of coating emissivity (surface S2) and; (ii) rate of change in U-value in relation to emissivity for a NFRC-compliant, thermally-broken Curtain Wall, with a triple-glazed, Air-, Ar-, Xe-, or Kr-filled IGU56

Figure 74 – Predicted (by simulation) (i) R-value and (ii) U-value (air-to-air; surface-to-surface) as a function of Spandrel panel insulation for a NFRC-compliant, thermally-broken triple-glazed Ar-filled IGU curtain wall assembly with and without low-e coating on surface 258

Figure 75 – Predicted (by simulation) (i) R-value and (ii) U-value (air-to-air; surface-to-surface) as a function of Spandrel panel insulation for a NFRC-compliant, thermally-broken triple-glazed Kr-filled IGU curtain wall assembly with and without low-e coating on surface 258

Figure 76 – Predicted (by simulation) (i) R-value and (ii) U-value (air-to-air; surface-to-surface) as a function of Spandrel panel insulation for a NFRC-compliant, thermally-broken triple-glazed Xe-filled IGU curtain wall assembly with and without low-e coating on surface 259

Figure 77 – Predicted (by simulation) (i) R-value and (ii) U-value (air-to-air; surface-to-surface) as a function of Spandrel panel insulation for a NFRC-compliant, thermally-broken triple-glazed Air filled IGU curtain wall assembly with and without low-e coating on surface 2.....59

Figure 78 – Predicted (by simulation) (i) R-value and (ii) U-value (air-to-air; surface-to-surface) as a function of Spandrel panel insulation for a NFRC-compliant, thermally-broken triple-glazed curtain wall assembly incorporating an IGU with low-ε coating and filled with either Ar, Kr, Xe, or Air.....60

Figure 79 – Predicted (by simulation) (i) R-value and (ii) U-value (air-to-air; surface-to-surface) as a function of Spandrel panel insulation for a NFRC-compliant, thermally-broken triple-glazed curtain wall assembly incorporating an IGU without low-ε coating and filled with either Ar, Kr, Xe, or Air.....60

Figure 80 – Predicted (by simulation) (i) R-value and (ii) U-value (air-to-air; surface-to-surface) as a function of thermal conductivity of spacer for a NFRC-compliant, thermally-broken triple-glazed Ar-filled IGU curtain wall assembly with and without low-e coating on surface 2.....62

Figure 81 – Predicted (by simulation) (i) R-value and (ii) U-value (air-to-air; surface-to-surface) as a function of thermal conductivity of spacer for a NFRC-compliant, thermally-broken triple-glazed Kr-filled IGU curtain wall assembly with and without low-e coating on surface 2.....62

Figure 82 – Predicted (by simulation) (i) R-value and (ii) U-value (air-to-air; surface-to-surface) as a function of thermal conductivity of spacer for a NFRC-compliant, thermally-broken triple-glazed Xe-filled IGU curtain wall assembly with and without low-e coating on surface 2.....63

Figure 83 – Predicted (by simulation) (i) R-value and (ii) U-value (air-to-air; surface-to-surface) as a function of thermal conductivity of spacer for a NFRC-compliant, thermally-broken triple-glazed Air filled IGU curtain wall assembly with and without low-e coating on surface 2.....63

Figure 84 – Predicted (by simulation) R-value (surface-to-surface) as a function of thermal conductivity of Spacer for a NFRC-compliant, thermally-broken triple-glazed curtain wall assembly incorporating an IGU with low-ε coating (ε = 0.054; surface 2) and filled with either Ar, Kr, Xe, or Air64

Figure 85 – Predicted (by simulation) (i) R-value (surface-to-surface) as a function of thermal conductivity of Spacer for a NFRC-compliant, thermally-broken triple-glazed curtain wall assembly incorporating an IGU without low-ε coating and filled with either Ar, Kr, Xe, or Air.....64

Figure 86 – Summary of Thermal performance of NFRC compliant double- and triple-glazed CW assemblies65

Figure A87 – Predicted (by simulation) R-value (surface-to-surface) of double-glazed thermally broken curtain wall panel in relation to fraction (by volume) of air present in the low-e (0.054) IGUs.....76

Figure A88 – Predicted (by simulation) R-value (air-to-air) of double-glazed thermally broken curtain wall panel in relation to fraction (by volume) of air present in the low-e (0.054) IGUs.....76

Figure A89 - Predicated (by simulation) U-value (surface -to-surface) of double-glazed thermally broken curtain wall panel in relation to fraction (by volume) of air present in the low-e (0.054) IGUs.....77

Figure A90 – Predicated (by simulation) U-value (air-to-air) of double-glazed thermally broken curtain wall panel in relation to fraction (by volume) of air present in the low-e (0.054) IGUs.....77

Figure A91 - Predicated (by simulation) total heat loss through double-glazed thermally broken curtain wall panel in relation to fraction (by volume) of air present in the low-e IGUs; red marker shows test value78

Figure A92 - Predicted (by simulation) R-value (surface-to-surface) of double-glazed thermally broken curtain wall panel in relation to glazing emissivity on surface 2 of IGUs; 90% Ar filled IGU78

Figure A93 - Predicted (by simulation) U-value (surface-to-surface) of double-glazed thermally broken curtain wall panel in relation to glazing emissivity on surface 2 of IGUs; 90% Ar filled IGU79

Figure A94 - Predicted (by simulation) R-value (air-to-air) of double-glazed thermally broken curtain wall panel in relation to glazing emissivity on surface 2 of IGUs; 90% Ar filled IGU.....79

Figure A95 - Predicted (by simulation) U-value (air-to-air) of double-glazed thermally broken curtain wall panel in relation to glazing emissivity on surface 2 of IGUs; 90% Ar filled IGU.....80

Figure A96 - Predicted (by simulation) R-value of triple-glazed low-e coated (e = 0.054) thermally broken curtain wall panel in relation to glazing to Wall Area Ratio; 90% Ar filled IGU81

Figure A97 - Predicted (by simulation) R-value of triple-glazed low-e coated (e = 0.054) thermally broken curtain wall panel in relation to glazing to Wall Area Ratio; 90% Ar filled IGU81

Figure 98 - Predicted (by simulation) U-value of triple-glazed low-e coated (e = 0.054) thermally broken curtain wall panel in relation to glazing to Wall Area Ratio; 90% Ar filled IGU82

Figure 99 - Predicted (by simulation) U-value of triple-glazed low-e coated (e = 0.054) thermally broken curtain wall panel in relation to glazing to Wall Area Ratio; 90% Ar filled IGU82

Figure A100 – Predicted (by simulation) R-value of triple-glazed low-e coated (e = 0.054) thermally broken curtain wall panel in relation to glazing to Wall Area Ratio; 90% Kr filled IGU83

Figure A101 - Predicted (by simulation) R-value of triple-glazed low-e coated (e = 0.054) thermally broken curtain wall panel in relation to glazing to Wall Area Ratio; 90% Kr filled IGU83

Figure A102 - Predicted (by simulation) U-value of triple-glazed low-e coated (e = 0.054) thermally broken curtain wall panel in relation to glazing to Wall Area Ratio; 90% Kr filled IGU84

Figure A103 - Predicted (by simulation) U-value of triple-glazed low-e coated (e = 0.054) thermally broken curtain wall panel in relation to glazing to Wall Area Ratio; 90% Kr filled IGU84

Figure A132 - Predicted (by simulation) R-value (air-to-air; surface-to-surface) of triple-glazed vision & spandrel panel low-e coated (e = 0.054; surfaces S2 and S4) thermally broken curtain wall in relation to coating emissivity; 90 % Kr, 10 % Air-filled IGU	99
Figure A133 - Predicted (by simulation) R-value (air-to-air; surface-to-surface) of triple-glazed vision & spandrel panel low-e coated (e = 0.054; surfaces S2 and S4) thermally broken curtain wall in relation to coating emissivity; 90 % Kr, 10 % Air-filled IGU	99
Figure A134 – Predicted (by simulation) U-value (air-to-air; surface-to-surface) of triple-glazed vision & spandrel panel low-e coated (e = 0.054; surfaces S2 and S4) thermally broken curtain wall in relation to coating emissivity; 90 % Kr, 10 % Air-filled IGU	100
Figure A135 - Predicted (by simulation) U-value (air-to-air; surface-to-surface) of triple-glazed vision & spandrel panel low-e coated (e = 0.054; surfaces S2 and S4) thermally broken curtain wall in relation to coating emissivity; 90 % Kr, 10 % Air-filled IGU	100
Figure A136 - Predicted (by simulation) R-value (air-to-air; surface-to-surface) of triple-glazed vision & spandrel panel low-e coated (e = 0.054; surfaces S2 and S4) thermally broken curtain wall in relation to coating emissivity; 90 % Xe, 10 % Air-filled IGU	101
Figure A137 - Predicted (by simulation) R-value (air-to-air; surface-to-surface) of triple-glazed vision & spandrel panel low-e coated (e = 0.054; surfaces S2 and S4) thermally broken curtain wall in relation to coating emissivity; 90 % Xe, 10 % Air-filled IGU	101
Figure A138 - Predicted (by simulation) U-value (air-to-air; surface-to-surface) of triple-glazed vision & spandrel panel low-e coated (e = 0.054; surfaces S2 and S4) thermally broken curtain wall in relation to coating emissivity; 90 % Xe, 10 % Air-filled IGU	102
Figure A139 - Predicted (by simulation) U-value (air-to-air; surface-to-surface) of triple-glazed vision & spandrel panel low-e coated (e = 0.054; surfaces S2 and S4) thermally broken curtain wall in relation to coating emissivity; 90 % Xe, 10 % Air-filled IGU	102
Figure A140 - Predicted (by simulation) R-value (air-to-air; surface-to-surface) of triple-glazed vision & spandrel panel low-e coated (e = 0.054; surfaces S2 and S4) thermally broken curtain wall in relation to coating emissivity; Air-filled IGU	103
Figure A141 - Predicted (by simulation) R-value (air-to-air; surface-to-surface) of triple-glazed vision & spandrel panel low-e coated (e = 0.054; surfaces S2 and S4) thermally broken curtain wall in relation to coating emissivity; Air-filled IGU	103
Figure A142 - Predicted (by simulation) U-value (air-to-air; surface-to-surface) of triple-glazed vision & spandrel panel low-e coated (e = 0.054; surfaces S2 and S4) thermally broken curtain wall in relation to coating emissivity; Air-filled IGU	104
Figure A143 - Predicted (by simulation) U-value (air-to-air; surface-to-surface) of triple-glazed vision & spandrel panel low-e coated (e = 0.054; surfaces S2 and S4) thermally broken curtain wall in relation to coating emissivity; Air-filled IGU	104
Figure A144. Sample stacks tested at NRC [28]	111
Figure A145. Vertical velocity contours and flow field in the air cavity of sample stacks with different inclinations ..	114
Figure A146. Horizontal velocity contours and flow field in the air cavity of sample stacks with different inclinations	115
Figure A147. Effect of inclination angle of sample stack and direction of heat flow on the effective R-value in the case of foil emissivity of 0.05	116
Figure A148. Effect of inclination angle of sample stack shown in Figure 129, foil/coating emissivity and direction of heat flow on the effective R-value	117
Figure A149. Effect filling gas in sample stack shown in Figure 129 and foil/coating emissivity on the effective R-value for the case of $\theta = 90^\circ$ (vertical)	118
Figure A150. Effect filling gas in sample stack heated from bottom and shown in Figure 129 and foil/coating emissivity on the effective R-value for the case of $\theta = 0^\circ$ (horizontal)	119
Figure A151. Effect filling gas in sample stack heated from top and shown in Figure 129 and foil/coating emissivity on the effective R-value for the case of $\theta = 0^\circ$ (horizontal)	120
Figure A152. Effect filling gas in sample stack heated from bottom and shown in Figure 129 and foil/coating emissivity on the effective R-value for the case of $\theta = 30^\circ$ (sloped)	121
Figure A153. Effect filling gas in sample stack heated from top and shown in Figure 129 and foil/coating emissivity on the effective R-value for the case of $\theta = 30^\circ$ (sloped)	122

List of Tables

<i>Table 1. Properties of gases used to fill Insulating Glass Units (IGUs)</i>	<i>4</i>
<i>Table 2 - R-value and U-values (air-to-air) of double-glazed curtain wall assembly incorporating IGUs having different gases at selected glazing to wall-area ratios</i>	<i>24</i>
<i>Table 3 - R-value and U-values (air-to-air) of double-glazed curtain wall assembly at selected glazing to wall-area ratios and incorporating IGUs having different gases and higher emissivity (e = 0.84)</i>	<i>25</i>
<i>Table 4 - R-value and U-values (air-to-air) of triple-glazed curtain wall assembly incorporating IGUs having different gases at selected glazing to wall-area ratios</i>	<i>46</i>
<i>Table 5 - R-value and U-values (air-to-air) of double-glazed curtain wall assembly at selected glazing to wall-area ratios and incorporating IGUs having different gases and higher emissivity (e = 0.84)</i>	<i>47</i>
<i>Table 6 – Simulation Results of Thermal Performance of NFRC Compliant DOUBLE-Glazed CW Configuration</i>	<i>67</i>
<i>Table 7 - Simulation Results of Thermal Performance of NFRC Compliant TRIPLE-Glazed CW Configuration</i>	<i>68</i>
<i>Table A8 – Material Properties</i>	<i>73</i>
<i>Table A9 – Test Results & Calculated U-value for curtain wall assembly for Ar (90%) filled IGU; model dimensions (M) used as basis for calculations</i>	<i>105</i>
<i>Table A10 – Test Results & Calculated U-value for curtain wall assembly with overfilling of Argon in IGU; model dimensions (M) used as basis for calculations</i>	<i>106</i>
<i>Table A11 – Test Results and Calculated U-value for Curtain Wall Assembly Specimen size of 12 ft. x 12 ft., as reported in test for Ar (90%) filled IGU</i>	<i>107</i>
<i>Table A12 – Test Results and Calculated U-value for Curtain Wall Assembly of 12 ft. x 12 ft. Specimen size, as reported in test with overfilling of Argon in IGU</i>	<i>108</i>

Summary

In 2012 the NRC-Construction initiated a project on the “High Performance Walls and Roofing Technologies Next Generation Technologies R&D – Building Envelopes”. Partnership and funding for the project was obtained from NRCan (Housing and Buildings /Sustainable Building and Communities CANMET / Group) under the Program of Energy Research and Development (PERD).

In commercial buildings, curtain wall systems often cover a significant part of the building envelope, and therefore their impact on the overall thermal performance of the building is important. In order to evaluate, compare and improve curtain wall designs, one requires insights to the different calculation and evaluation methods, and as well, knowledge of the state-of-the-art in thermal optimization of curtain walls.

The overall objective of this project was to improve the thermal efficiency of commercial building envelopes. This was achieved by using different approaches to improve the overall effective R-values of the curtain wall systems.

The project consisted of a number of Tasks in which curtain walls were evaluated, compared and suggestions made for improvement to the thermal performance of such systems, and include:

- Task 1: Literature review on Curtain Walls
- Task 2: Curtain Walls and National Energy Code for Buildings 2011
- Task 3: Thermal Optimization in Curtain Walls: Part I - Modelling
- Task 4: Thermal Performance Testing of a Curtain Wall Panel
- Task 5: Benchmarking the Thermal Performance of a Curtain Wall Panel through Simulation
- Task 5: Parametric study of Curtain Wall Systems for Selection of Components and Optimization of Thermal Performance

The results from simulation of double and triple-glazed CW modelling configurations of both manufactured products as well as NFRC compliant CW assemblies using the simulation model hygIRC-C were compared and results of simulations derived from varying the thermal properties of the CW components to permit determining the relative effect of different components on the overall thermal performance of the CW assembly.

In respect to results from simulation of manufacturer’s products, results were provided for the risk to condensation of double and triple-glazed CW assemblies. The results showed that both double and triple-glazed CW indeed have components that are potentially vulnerable to the formation of condensation; these are located along the frame at the periphery of the glazing unit.

As regards the NFRC compliant CW assemblies, the results from simulation provided information on the R-value and respective U-values of the assemblies for different gas filling the IGU. Triple-glazed CW assemblies, as might were demonstrated to perform better than the double-glazed assemblies, and the thermal performance was also affected by the type of gas that fills the IGU. Using the R-value of double-glazed Air-filled IGU as reference (i.e. $0.555 \text{ m}^2 \cdot \text{K}/\text{W}$), the degree of improvement in R-value was: 9.4%, 21%, and 26% respectively, for Ar, Kr, and Xe filled double-glazed IGUs, whereas these values were 8.4%, 18.6%, 23.2% respectively, for Ar, Kr, and Xe filled triple-glazed IGUs, when using the triple-glazed Air-filled IGU as

reference (i.e. $0.736 \text{ m}^2\cdot\text{K}/\text{W}$). Improvements in R-value of the CW assembly for double- to triple-gazed IGUs provide enhancements of 33%, 31.4%, 29.9% and 29.3% when filled respectively, with air, Ar, Kr, and Xe gas.

The results from simulation of both the double and triple-glazed NFRC compliant CW assemblies were also provided in terms of:

- (i.) Risk to the formation of condensation;
- (ii.) Effect of glazing to wall-area ratio;
- (iii.) Effect of changes to coating emissivity;
- (iv.) Effect of thermal resistance of the spandrel panel insulation, and;
- (v.) Effect of IGU spacer thermal conductivity

As regards the results for the Risk to the formation of condensation, the results showed that both double and triple-glazed CW indeed have components that are potentially vulnerable to the formation of condensation as was the case for the manufactured products; locations of vulnerability are along the frame at the periphery of the glazing unit.

Results were also provided in terms of changes to R-value and U-values (both air-to-air and surface to surface) as a function of changes to the specific parameter of interest (i.e. glazing to wall-area ratio, coating emissivity; thermal resistance of the spandrel panel insulation, or IGU spacer thermal conductivity).

At the end of each section of results, summary results were provide together with information on how each of the respective parameters affected changes to the thermal resistance of the CW assembly. Relationships between expected changes in thermal resistance of the CW assembly to corresponding changes in the given simulation parameter permitted gauging the significance of each these effects.

Taken as a whole, this substantive and in-depth set of information of CW thermal performance provides the basis for developing guidelines to the selection of components of double and triple-gazed metal-glass CW assemblies.

Acknowledgements

NRC wishes to acknowledge the partnership and funding for the project as provided by NRCan (Housing and Buildings /Sustainable Building and Communities CANMET / Group) under the Program of Energy Research and Development (PERD).

High Performance Roofing and Walls Technologies

**Parametric study of Curtain Wall Systems for Selection of
Components and Optimization of Thermal Performance**

Forming part of Task 5

Authored by:

Hamed H. Saber, Ph.D. and Michael A. Lacasse, Ph.D., P.Eng.

A Report for the

**Natural Resources Canada (NRCan)
Housing and Buildings
Sustainable Building and Communities CANMET / Group**

ATT: Mr. Anil Parekh

National Research Council Canada
Ottawa ON K1A 0R6 Canada

18 February, 2016

This report may not be reproduced in whole or in part without the written consent of both the client and the National Research Council of Canada

High Performance Roofing and Walls Technologies

Parametric study of Curtain Wall Systems for Selection of Components and Optimization of Thermal Performance

Report forming part of Task 5

Hamed H. Saber and Michael A. Lacasse

1. Introduction

In regions having cooler climatic conditions as Canada, a substantial share of energy is used for heating the buildings [10] and in those portions of the country where a continental climate prevails, the humid warm summers have, over the years, motivated energy use for cooling, and thus cooling is also a factor in the overall energy usage of a building. The overall energy consumption of the building sector is high and although the situation differs from country to country, buildings are responsible for about 30-40% of the total energy demand [11]. In Europe, however, buildings are responsible for 40-50% of energy use and the largest share of energy in buildings is used for heating [12]. The design of building enclosures with the intent of achieving energy savings can necessarily help reduce building operating loads and thus the demand for energy over time [13, 14]. A practical and logical first step towards achieving energy efficiency in buildings located across Canada can evidently be achieved by increasing the effective thermal resistance (R-value) of the building envelope components (walls, roofs, windows, curtain walls, and skylights). This report is focused on providing insight into the factors that contribute to energy transfer across curtain wall (CW) assemblies and the contribution of several different CW components to the overall thermal performance of the assembly. This was accomplished by presenting results derived from simulation, using NRC's simulation model, hygIRC-C¹, for which a parametric study was completed of specific curtain wall assemblies and variations of these assemblies based on the thermal performance attributes of selected CW components. The thermal performance assessment of the curtain wall assemblies was completed in accordance with established industry standards. The intent was to provide information useful for developing guidelines to the selection of components for CW assemblies in compliance with industry guidelines.

In this report, a general description of curtain wall systems is provided and thereafter, an overview is given of the basic physics of heat transfer of primary importance to understanding the thermal performance of enclosed spaces within insulated glass units (IGU), a primary component of CW assemblies. In the subsequent section, the modelling approach is described as are the curtain wall configurations modelled for the parametric study. Results of simulation are then provided of a select set of manufactured CW products and CW assemblies compliant with the National Fenestration Rating Council (NFRC). The parametric study is summarized at the end of the report. The report also includes several useful appendices in which can be found basic information on the thermal properties of components and materials, information on benchmarking the simulation model, as well as results derived from simulation but not included in the main report.

¹ hygIRC-C – Comsol Multiphysics package

2. Description of Curtain Wall Components

Common curtain wall assemblies consist of a metal frame (mullions) and a combination of transparent and opaque infill panels (Figure 1). The primary materials used are aluminum, steel and glass, together with secondary materials such as sealant products, rubber or polymer-based gaskets and insulation products. The metal frame is structurally secured to the building at each floor slab and can have a tubular- or open-shaped profile. Spandrel panels are made of coated glass or metal, stone, plastic, ceramic, or other rigid material, and are used for both opacity and to provide added thermal insulation to the CW assembly. Clear transparent glass panels are used as infills to provide the interior with vision to the exterior. A brief description of each of the different components of a CW system follows [2].

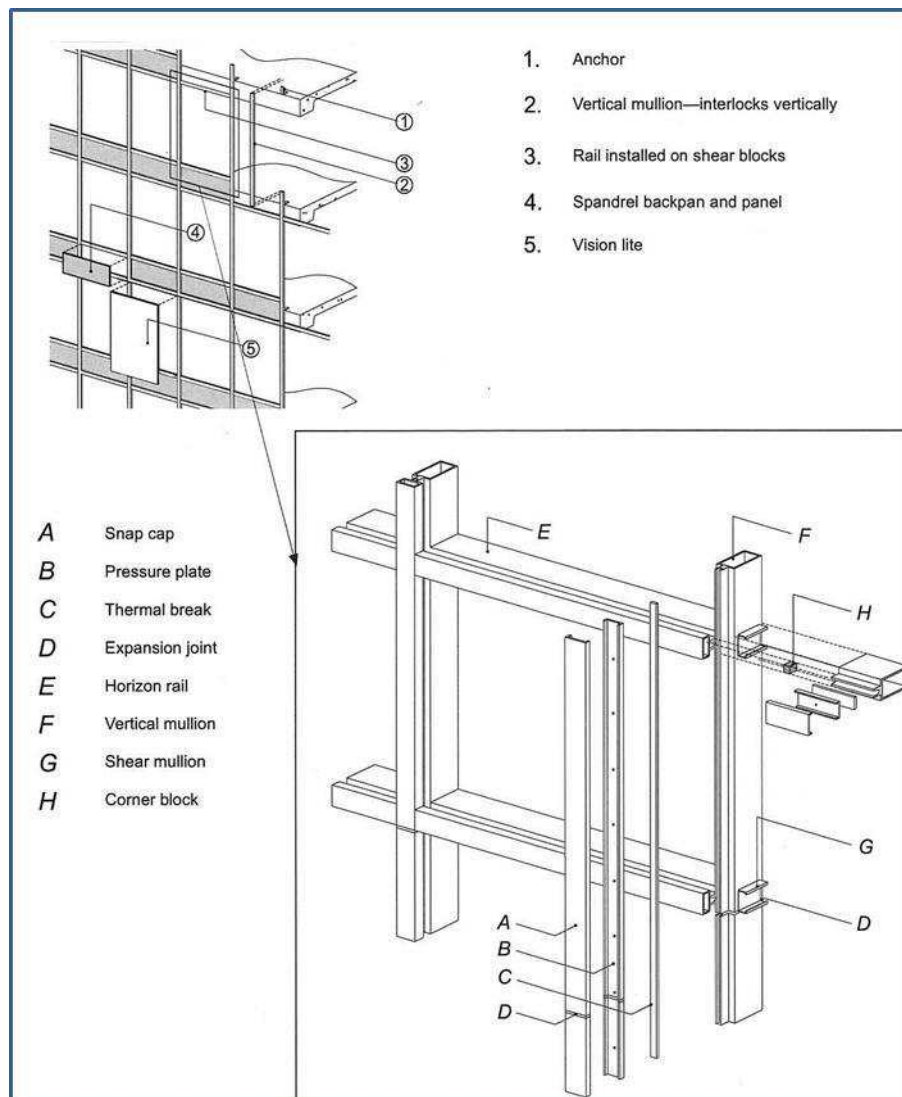


Figure 1. Basic components of a typical curtain wall system [15]

² H. H. Saber, G. Ganapathy and M. A. Lacasse (2016), High Performance Roofing and Walls Technologies; Task 5: Benchmarking the Thermal Performance of a Curtain Wall Panel through Simulation; Client Report: A1-002844.05; NRC-Construction, National Research Council of Canada, Ottawa, Canada, January; 42 p.

2.1 Spandrel Panels

Spandrel panels are commonly used to cover construction elements and materials on the outside of a building. Heat-strengthened (tinted or opaque) *spandrel glass* is the most commonly used panel type to resist thermal, wind and other climatic loads. Reflective film coatings and insulation can considerably enhance the thermal performance of the spandrel glass panel. Metal or stone panels are also commonly used as spandrel infills. Metal panels are usually made of aluminum, or sheets of steel/aluminum and a core (e.g., composite panels). The most common stone used in curtain wall applications is granite.

2.2 Frame

The most common framing material for metal-glass CW systems in North America is the aluminum extrusion (e.g., alloy AA6063) although fiberglass framing has also been used in some applications. Steel anchors are used to structurally secure the CW frame to the building slabs at every floor, or every other level. Rubber gaskets or tapes made of neoprene, ethylene-propylene-diene-monomer (EPDM) or silicone are used to seal the glass panel perimeter to prevent water penetration to or air leakage from the interior. Gaskets rely on their elasticity and interface pressure to create and maintain a seal, however, over time, these polymer-based materials they can shrink and crack, creating small openings through which air, water or moisture can enter and damage the integrity of the curtain wall assembly. Corners are the most susceptible areas for water and air leakage. Obtaining adequate performance from the joints at the interface between the curtain wall and the building is of utmost importance.

2.3 Vision Panels

2.3.1 Vision Glass

Due to the brittle nature of glass, it is significantly affected by the presence of cracks and defects on its surface that arise due to bending and point pressures as induced by wind and thermal loads. As such, the vision glass panels used in CW assemblies require special designs and considerations to ensure that performance requirements for the safety, stability, impact-resistance, and durability of the panels at met and at the most competitive cost. There are different types of glasses that are currently being used in curtain walls.

- *Float, sheet or plate glass* not typically used in CW assemblies as it tends to breaks into large and sharp pieces or fragments, which constitutes a safety hazard;
- *Annealed float glass* withstands wind loads and some thermal loads relatively well, however, when used with coatings in Insulating Glass Units (IGUs), the thermal stresses rise considerably;
- *Tempered glass* - Factory-treated heat-tempering process strengthens *annealed float glass* to increase resistance to thermal breakage;
- *Chemically strengthened glass* involves chemical tempering instead of heat tempering and is similar to tempered glass in its qualities and use;
- *Laminated glass* is made of two or more layers of glass with an invisible plastic interlayer, usually polyvinyl butyral (PVB), which keeps the glass from shattering. Combining laminated and tempered glass in a single pane produces a strong and secure glazing product;
- *Tinted (green, bronze, grey, blue) glass* and *reflective glass* are used to control the solar and light transmittance, as well as for aesthetic reasons.

2.3.2 Insulating Glass Unit (IGU)

The IGUs are the standard vision units used in curtain wall assemblies and have three basic components: *glass lite, spacer and sealant* (

). IGUs are made of two or more lites of glass with a hermetically sealed dry-air or gas-filled space(s) between the lites, the space imparting some degree of thermal insulation.

IGU cavity spacer gases — There are a number of heavy gases that are currently being used to fill the spaces between the glass lites. Argon (Ar) is the most commonly used gas to fill the spacer cavity due to its low cost and UV-stability, and as well, given its colorless, non-corrosive and non-toxic nature. Krypton (Kr), or much less frequently, Xenon (Xe) gases are used as fill gases, mostly in narrow IGUs.

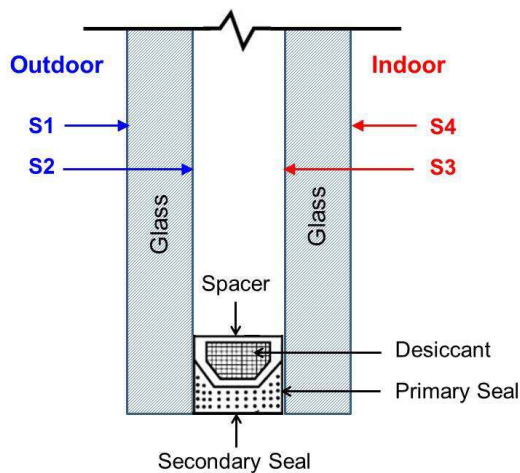


Figure 2. Components of a standard double-glazed insulating glass unit

At atmospheric pressure and a temperature of 300 K, the molecular weight, density and thermal conductivity of Air, Ar, Kr and Xe are provided in Table 3.

Within the enclosed cavity of the IGU, the heat transfer modes are by conduction, convection and radiation. The more dense gases provide lower convective heat transfer rates across the two glass lites of the IGU due to the buoyancy effect. As well, the lower the value of the thermal conductivity of the gas, the lower the heat transfer rate by conduction. As shown in Table 3, Xe has the lowest thermal conductivity and highest density amongst the gasses that are used to fill IGUs. Thus, the thermal resistance (R-value) of IGUs if filled with either Xe and Kr gas, would be lower than that of an IGU filled with either Ar or Air. Nevertheless, Xe is an order of magnitude greater in cost than Kr, and Kr gas

is 2 orders of magnitude more in cost as compared to Ar.³

Table 1. Properties of gases used to fill Insulating Glass Units (IGUs)

Gas	Molecular Weight (g/mole)	*Density (kg/m ³)	*Thermal Conductivity (mW/(m·K))
Air	29	1.179	26.2
Argon (Ar)	40	1.626	17.9
Krypton (Kr)	84	3.415	9.5
Xenon (Xe)	131	5.325	5.5

* Properties at atmospheric pressure and 300 K

³ Häussinger, Peter; Glatthaar, Reinhard; Rhode, Wilhelm; Kick, Helmut; Benkmann, Christian; Weber, Josef; Wunschel, Hans-Jörg; Stenke, Viktor; Leicht, Edith; Stenger, Hermann (2001). "Noble Gases". Ullmann's Encyclopedia of Industrial Chemistry (6th ed.). Wiley. doi:10.1002/14356007.a17_485. ISBN 3-527-20165-3.

Coatings for glass lites — Reflective and low-emissivity (low-e) coatings made of thin pure metal or metal oxide layers can also be applied for solar (ultraviolet and infrared radiation) control, as either hard (e.g., cobalt, iron, chrome, tin) or soft coatings (e.g., silver, copper, chrome, titanium, stainless steel) products. Soft coatings are vulnerable to scratching and corrosion and are sealed within the space in the IGU (surface S2 or S4, see Figure 2). Reflective coatings act like a mirror reflecting the heat back to the exterior, whereas low-e coatings reflect the heat back to the warmer side, reducing either the solar gains in the summer or retaining the interior heat in the winter and thus increasing the overall IGU thermal performance. When combined with the thickness of the glass lite, the overall thickness of an IGU ranges generally between 22 – 25 mm for the case of 3 mm glass lite, and 28 – 31 mm for the case of 6 mm glass lite.

Typically, standard double-glazed IGUs consisting of two clear uncoated glass lites with air in the spacer cavity have U-factors of 2.85 W/m²K (R-values of 0.35 m²K/W). Standard double-glazed IGUs filled with inert gas have lower U-factors ranging between 0.2-0.5 W/m²K (R-values 2-5 m²K/W), whereas triple-glazed IGUs have U-factors ranging between 0.16-0.25 W/m²K (R-values 4-6 m²K/W). However, their depth and weight makes them uncommon in standard curtain wall applications. Suspended coated films between the inner and outer panes have also been used to replace the third and fourth lites of glass and thereby reduce the IGUs overall weight.

Spacers for IGUs — Conventionally, *spacers* have been made of aluminum or galvanized steel. However, these metal spacers have high thermal conductivity and act as a heat conductor (i.e. thermal bridges), undermining the ability of the IGU to reduce the heat flow, resulting in condensation at the bottom of the sealed unit. To reduce the heat transfer rate through the spacer and hence increase the overall IGU's thermal performance, spacers can be made of less-conductive materials (e.g., stainless steel, pre-desiccated structural foam, thermoplastic).

Sealants for IGUs — For curtain wall applications, IGUs are produced with *double-seal designs*, which use a primary sealant (e.g., polyisobutylene) as a barrier to vapour flow, and a secondary sealant (e.g., hot melt butyl, polysulphide, polyurethane and silicone) that ensures the structural integrity of IGU. In addition, IGUs used for structural glazing systems (where the glass is adhesively bonded to the framing) differ from non-structural silicone glazing. More information about spacers and edge seals can be found in [16].

3. Overview of Thermal Performance of Enclosed Spaces in IGUs

3.1 Basic physics of heat transfer across enclosed spaces of IGUs

Low-emissivity (low-e) coatings, typically used in IGUs, were introduced as a promising technology for enhancing the thermal performance of Insulating Glass Units (IGUs) in windows, curtain walls and skylight devices [19, 20, 21]. To be used effectively however, low-e coatings must have at least one coated surface facing a space filled with air and other gasses (e.g., Argon, Krypton, Xenon). It is important to accurately determine the effective R-values of the enclosed spaces of different dimensions, effective emittances, inclination angles, directions of heat flow, mean airspace temperatures, and temperature differences across the airspaces. Many studies were conducted to determine the R-values of low-e coatings in IGUs [11-12, 18-46].

A review about the use of reflective materials to reduce heat transfer by radiation across enclosed airspaces was conducted by Gross and Miller [22]. Fricker and Yarbrough [23] conducted literature review on four

computational methods for evaluating the R-values of enclosed reflective airspaces. Those four methods involved an assumption of one-dimensional heat transfer between large parallel surfaces (infinite parallel planes). In IGUs, however, there are surfaces connecting the parallel planes (e.g., framing, and spacers in IGUs). These surfaces absorb, emit and reflect thermal radiation. Glicksman [24] has shown that the heat transfer process that included radiation interaction between the parallel surfaces and the framing resulted in a decrease in the overall thermal performance (i.e. lower R-values) across the parallel surfaces.

The parameters that affect the R-value of an enclosed space are: (a) the physical properties of the gas filling the space, (b) temperature of all surfaces of the space, (c) emissivity of all surfaces of the space, (d) temperature differences across the space, (e) dimensions of the space, (f) direction of heat flow through the space, and (g) orientation of the space. The R-values of enclosed airspaces were calculated by many investigators; e.g., see Robinson et al. [48-50] for various orientations of airspaces and reflective boundaries by using heat transfer coefficient data.

The heat transfer coefficient data were obtained from measurements of panels of different thicknesses using the test method described in the ASTM C236-53 [51]. In those studies, the steady-state heat transmission rates were corrected for heat transfer occurring along parallel paths between hot and cold boundaries. Thereafter, the convective heat transfer coefficients were obtained from the data by subtracting a calculated radiative heat transfer rate from the total corrected heat transfer rate; and the radiative heat transfer was calculated using an emissivity of 0.028 for the aluminum surfaces.

Generally, the value for the effective heat conductance, U-value (the reciprocal of the R-value) of an enclosed space accounts for the contribution of heat transfer in the enclosed space due to heat transfer by conduction, convection and radiation. In the absence of heat transfer by radiation, the contribution of heat transfer by convection and conduction in an enclosed space is normally given in terms of the Nusselt number, Nu ($Nu = h \delta / \lambda$), where h is convective heat transfer coefficient, δ is the thickness (depth) of the space, and λ is the thermal conductivity of the gas filling the space such as air, Argon (Ar), Krypton (Kr) or Xenon (Xe). According to many authors [19-21, 52], the convective heat transfer coefficient for an enclosed space can be given as:

$$Nu = h \delta / \lambda = a (Gr \cdot Pr)^b A_R^c = a (Ra)^b A_R^c, \text{ and } Gr = g \beta \rho^2 \delta^3 \Delta T / \mu^2. \quad (1)$$

In Eq. (1), the coefficients a , b and c are dimensionless constants, derived from experiments, A_R is the aspect ratio of the enclosed space ($A_R = \text{height (H)}/\text{thickness } (\delta)$), Gr is the Grashoff number, Ra is the Raleigh number ($Ra = Gr \cdot Pr$), Pr is the Prandtl number, g is the gravitational acceleration, β is the thermal expansion coefficient, ρ is the density, and μ is the dynamic viscosity.]

To derive the coefficients a , b and c (Eq. (1)) from which the heat transfer coefficient, h , due to the convective and conductive components of heat transfer can be determined, the emissivity of all surfaces that bound the enclosed space must be zero (i.e. purely reflective surfaces). However, it is not possible in practice to use materials having zero emissivity when conducting such experiments. Hence, to derive the values of these coefficients from experiments, the rate of radiative heat transfer across the enclosed space should be subtracted from the total rate of heat transfer across the space, as was done by Robinson et al. [48-50].

A number of correlations for the value of Nu in the form of the relationship given in Eq. (1) and for different ranges of values of Ra , A_R and Pr are provided in several studies as described in the IEA Annex XII report

[52]. Some of these correlations showed the dependence of the Nu on the aspect ratio of the enclosed space (A_R). As such, it is anticipated that the effective thermal conductance or the effective thermal resistance of the enclosed space would be affected by the aspect ratio of the enclosed space; this will be discussed later.

Based on the heat transfer data reported by Robinson et al. [48-50], the 2009 ASHRAE Handbook of Fundamentals, Chapter 26 [53] provides a table that contains the R-values for enclosed spaces filled by air of three inclination angles (θ) of 0°, 45° and 90°. These R-values are being extensively used by modellers, architects and building designers to determine the R-values of building enclosures and IGUs filled by air. The R-values provided in the ASHRAE Handbook were obtained by combining the convective and radiative components of heat transfer from which the effective R-value for an enclosed airspace was provided for airspaces of different parameters, namely:

- (a) Thickness ($\delta = 13$ mm (0.5 in), 20 mm (0.75 in), 40 mm (1.5 in), and 90 mm (3.5 in)),
- (b) Mean temperature ($T_{avg} = 32.2^\circ\text{C}$ (90°F), 10.0°C (50°F), -17.8°C (0°F) and -45.6°C (-50°F)),
- (c) Temperature difference across the airspace ($\Delta T = 5.6^\circ\text{C}$ (10°F), 11.1°C (20°F) and 16.7°C (30°F)),
- (d) Effective emittance ($\epsilon_{eff} = 0.03, 0.05, 0.2, 0.5$ and 0.82), and
- (e) Direction of heat flow through the airspace.

Note that the effective emittance (ϵ_{eff}) of an enclosed airspace is given as [53]:

$$1/\epsilon_{eff} = 1/\epsilon_1 + 1/\epsilon_2 - 1 \quad (2)$$

In Eq. (2), the parameters ϵ_1 and ϵ_2 are the emissivity of the hot and cold surfaces (see **Error! Reference source not found.a**).

More recently, and following the work published in Chapter 26 of the ASHRAE Handbook of Fundamentals [53], Saber likewise undertook studies [42-46] to predict the R-values of vertical, horizontal, high-sloped (45°) and low-sloped (30°) enclosed airspaces that included the same parameters as were published in the ASHRAE Handbook, but in addition, the following parameters were investigated:

- (i) Length / height ($H = 203$ mm (8 in) – 2438 mm (96 in));
- (ii) Range of values for effective emittance ($\epsilon_{eff} = 0 - 0.82$), and;
- (iii) Direction of heat flow.

NRC's hygrothermal model, hygIRC-C, was used to complete the work. It is worth mentioning that the R-values of low-sloped enclosed airspaces were not previously available in the ASHRAE table [53], nor was the effect of the aspect ratio (length/thickness) of the enclosed airspace on the R-values as provided in the ASHRAE table.

Practical Correlation for the R-values of Enclosed Airspaces — For the case of an enclosed space filled with air, a practical correlation was developed by Saber [42-46] to determine the R-values as a function of all parameters that affect the thermal performance of the enclosed airspaces, namely: Average temperature (T_{avg}); temperature differential (ΔT); aspect ratio (A_R), and; effective emittance (ϵ_{eff}).

The ranges of these parameters cover most building applications. This correlation is given as:

$$R\text{-value} = R_c(T_{avg}) + a_0 A_R^{\alpha_1} T_{avg}^{\alpha_2} (\Delta T)^{\alpha_3} + a \epsilon_{eff}^{\beta} T_{avg}^{\alpha_2} (\Delta T)^{\alpha_3} \sum_{i=1}^4 g_i A_R^i + A_R^{\alpha_2} T_{avg}^{\alpha_3} (\Delta T)^{\alpha_3} \sum_{i=1}^4 b_i \epsilon_{eff}^i \quad (3)$$

Note that the R-value correlation given by Eq. (3) is applicable *only* for the case of the enclosed space filled with air. In this correlation, $R_c(T_{avg})$ is the R-value in (ft²hr°F/BTU) of the enclosed airspace due to heat transfer by conduction only, which is given as:

$$R_c(T_{avg}) = \delta / \lambda(T_{avg}). \quad (4)$$

Where $\lambda(T_{avg})$ is the thermal conductivity of the air filling the enclosed space, which is given as:

$$\lambda(T_{avg}) = \sum_{i=0}^4 f_i T_{avg}^i, f_0 = -0.0022758562, f_1 = 1.15480022 \times 10^{-4}, \quad (5)$$

$$f_2 = -7.9025286 \times 10^{-8}, f_3 = 4.11702505 \times 10^{-11}, f_4 = -7.4386433 \times 10^{-15}$$

Note that $\lambda(T_{avg})$ in Eq. (5) is the average thermal conductivity of air in (W/(m•K)), which is evaluated at the average temperature of the airspace, T_{avg} in (K). It is important to point out that the calculated value of $R_c(T_{avg})$ from Eq. (4) and (5) must be converted to (ft²hr°F/BTU) in order to be used in Eq. (3).

In Eq. (3), the units of T_{avg} and ΔT must be in (K). The other coefficients in this equation

($a_0, a, b_1, b_2, b_3, b_4, \alpha_1, \alpha_2, \beta, a_1, a_2, a_3, c_1, c_2, c_3, g_1, g_2, g_3,$ and g_4) are provided in the references [42-46] for enclosed airspace of different inclination angles and directions of heat flow. The results showed that the calculated R-values using Eq. (3) for different inclination angles and directions of heat flow were in good agreements with those obtained using the benchmarked model (within ±3% to ±5%; more details are available in [42-46]).

In these recent studies [42-46], the dependence of the R-value on the aspect ratio, A_R ($A_R = \text{length (H)}/\text{thickness } (\delta)$) of vertical enclosed spaces ($\theta = 90^\circ$) were also investigated. The ranges of values for the aspect ratio (H/δ) in those studies were:

- $A_R = 16$ to 188 for $\delta = 13$ mm (0.5 in),
- $A_R = 10$ to 122 for $\delta = 20$ mm (0.75 in),
- $A_R = 5$ to 61 for $\delta = 40$ mm (1.5 in), and
- $A_R = 2$ to 27 for $\delta = 90$ mm (3.5 in).

Depending on the thickness (depth) of the space and the operating conditions, the results of those studies showed that the aspect ratio can have a significant effect on the R-value (see [4] for more details).

Thus based on the correlation provide in Eq. 3, and as shown in , the dependence of R-value on the effective emissivity, ϵ_{eff} , of an enclosed space is provided for selected values of T_{avg} , ΔT , ϵ_{eff} and values of H (provided in), given an airspace depth of 13 mm. The values published in ASHRAE are clearly evident as is the range of R-values attributable to variations in values of effective emissivity, ϵ_{eff} . As such, the correlation provides a means to readily predict spacer cavity R-values for IGUs having different values of glass lite coating emissivity provided the aspect ratio and height of the IGU, as well as the temperature difference across and mean temperature within the IGU are known.

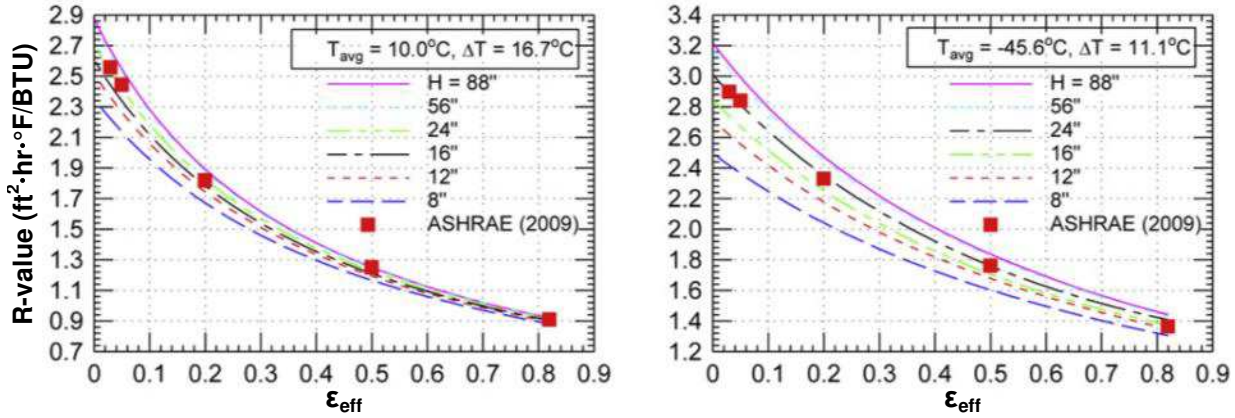
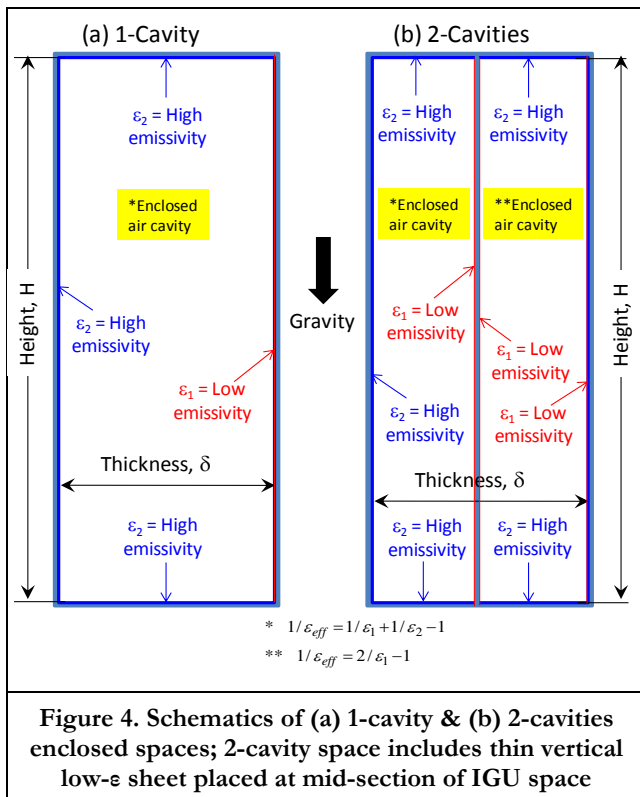


Figure 3 - Dependence of R-value (ft²·hr·°F/BTU) on effective emissivity, ϵ_{eff} given values of $T_{avg}/\Delta T$ (10 °C/ ΔT = 16.7 °C; -45.6 °C/ ΔT = 11.1 °C), and different values of H for an airspace of depth 13 mm

Effect of Installing Thin Sheet in the Middle of Enclosed Space — Saber also investigated [42-46] the



potential increase in the R-value of the enclosed airspace when a thin sheet having different values of emissivity on either side was placed in the middle of the airspace as shown in Figure 4b. Dividing an enclosed space into 2 or more cavities by thin sheet(s) would increase the R-value of the enclosed space. In fact, the results [42] showed that the R-value could be doubled due to installing a thin sheet in the middle of a vertical enclosed airspace ($\theta = 90^\circ$).

Figure 4a shows a case of 1-Cavity (i.e. without thin sheet) and Figure 4b shows a case of 2-Cavities (i.e. with thin sheet). For the applications of planar skylights, windows and curtain walls, the thin sheet should be transparent low-e materials. The benefits of installing a thin sheet are: (i) reducing heat transfer by convection, and (ii) reducing heat transfer by radiation due to low effective emittance. These benefits resulted in higher R-value for the “2-Cavities” case compared to the “1-Cavity” case.

To broaden the range of application for Insulating Glass Units (IGUs) used in windows, curtain walls and skylight devices, similar correlations were developed for the cases of enclosed space filled with other gases such as Argon, Krypton, and Xenon (see Table 1)

4. Approach to Simulation & Description of Curtain Wall Configurations

4.1 Approach for Simulation of NFRC Compliant CW Configurations

The following conditions were used for the determination of U-value:

$$\begin{aligned}
 T_{in} &= \text{interior ambient temperature of } 21.0 \text{ }^\circ\text{C (69.8 }^\circ\text{F)} \\
 T_{out} &= \text{exterior ambient temperature of } -18.0 \text{ }^\circ\text{C (-0.4 }^\circ\text{F)} \\
 V &= \text{wind speed of } 5.5 \text{ m/s (12.3 mph)} \\
 T_{m,out} &= T_{out} \\
 T_{m,in} &= T_{in} \\
 I_s &= 0 \text{ W/m}^2 \text{ (0 Btu/h}\cdot\text{ft}^2\text{)}
 \end{aligned}$$

The convective film coefficients on the interior and exterior of the window product were determined as follows:

- The indoor side convective heat transfer coefficient was based on the center of glass temperature and the entire window height; this film coefficient was used on all glass and edge of glass indoor surfaces.
- Frame section indoor convective film coefficients were constants that depended on the type of frame material; these values are listed in Table 2.
- The outdoor side convective heat transfer coefficient was calculated based on wind speed and was applied to all of outdoor surfaces, both glass and frame. Standard values for outdoor convective surface heat transfer coefficients are listed in Table 2.
- On the indoor side of a fenestration product, a detailed gray body radiation model was applied to both glass and frame surfaces for all products.
- The use of detailed radiation model on indoor fenestration surfaces makes the use of “slightly or partially ventilated cavities” on the indoor frame surfaces redundant
- The standard frame convective film coefficients (h_c) provided in Table 2 and the detailed radiation model referenced above was applied to all interior frame surfaces.
- On the outdoor side of a fenestration product, a black body radiation model, as defined [ref] was used; this model was applied to both glass and frame surfaces.

Table 2. Boundary Conditions

Boundary Condition	Radiation Model	Convective film coefficient boundary conditions	
		Tilt = 90° W/m ² K (Btu/h·ft ² °F)	Tilt = 20° W/m ² K (Btu/h·ft ² °F)
NFRC 100-2001 Exterior	Blackbody	26.00 (4.578)	26.00 (4.578)
Interior Aluminum Frame (convection only)	Gray Body Diffuse	3.29 (0.579)	4.94 (0.869)
Interior Thermally Broken Frame (convection only)	Gray Body Diffuse	3.00 (0.528)	4.38 (0.771)
Interior Thermally Improved Frame (convection only)	Gray Body Diffuse	3.12 (0.549)	4.60 (0.810)
Interior Wood/Vinyl Frame (convection only)	Gray Body Diffuse	2.44 (0.429)	3.38 (0.595)
Interior Glazing System boundary condition	Gray Body Diffuse	Calculated by WINDOW	

4.2 Description of curtain wall panel modelling configurations

4.2.1 Detailed curtain wall manufactured product configuration

Horizontal sectional drawings are provided in Figure 5 and in Figure 6⁴ showing the vision panel and the same for the opaque panel of the double- and triple-glazed curtain wall assemblies of the manufactured products; corresponding photos of the anodized aluminum curtain wall mullion are also provided. From these drawings the different curtain wall components can be identified and in which it is apparent that the opaque panels are insulated with mineral wool to the depth of the mullion and a polyimide compound was used as thermal break.

The elevation drawings for both the double- and triple-glazed curtain wall assemblies are given in Figure 7 (exterior side of CW) and Figure 8 (interior side of CW). As can also be seen in these figures, the curtain wall assembly consisted of three equal size opaque panels, each conventionally insulated and superimposed over three vision panels of the same width. The overall test specimen area, A_s , was 13.37 m². The glazed area, A_g , was ca. 8.29 m², the opaque panel area, A_o , ca. 3.88 m², and the frame area, A_f , ca. 1.37 m². As such, the proportion of vision glass to the overall wall area (A_g/A_s) was ca. 62 %; the frame to wall area, (A_f/A_s) ca. 10%, and; the vision to opaque panel ratio (A_g/A_o) was estimated to be ca. 2.14. The perimeter length of glazing was 20.97 m and that of the opaque panels, ca. 13.64 m.

The vision panel was comprised of a double- or triple-glazed insulated glass unit (IGU), a metal spacer, the IGU cavity being filled with air or a mixture of air and argon, krypton or Xenon gas. Surface 2 of the double-glazed IGU had a low-e coating (emissivity, $\epsilon = 0.054$).

4.2.2 Description of curtain wall panel modelling configuration

Model representations of the configuration of the curtain wall assembly for the manufactured products are provided in Figure 7 and Figure 8; these are each of the figures adjacent to the elevations drawings of the exterior and interior surfaces of the test specimen; the model for the exterior surface of the panel is shown in Figure 7, and the interior surface in Figure 8. For both of these representations, only half of the overall specimen size was modelled as the specimen was symmetric about its vertical centerline.

The assumed values for thermal conductivity of the different curtain wall components is provided in Table A9, located in the Appendix.

⁴ All drawings were provided by the curtain wall manufacturer.

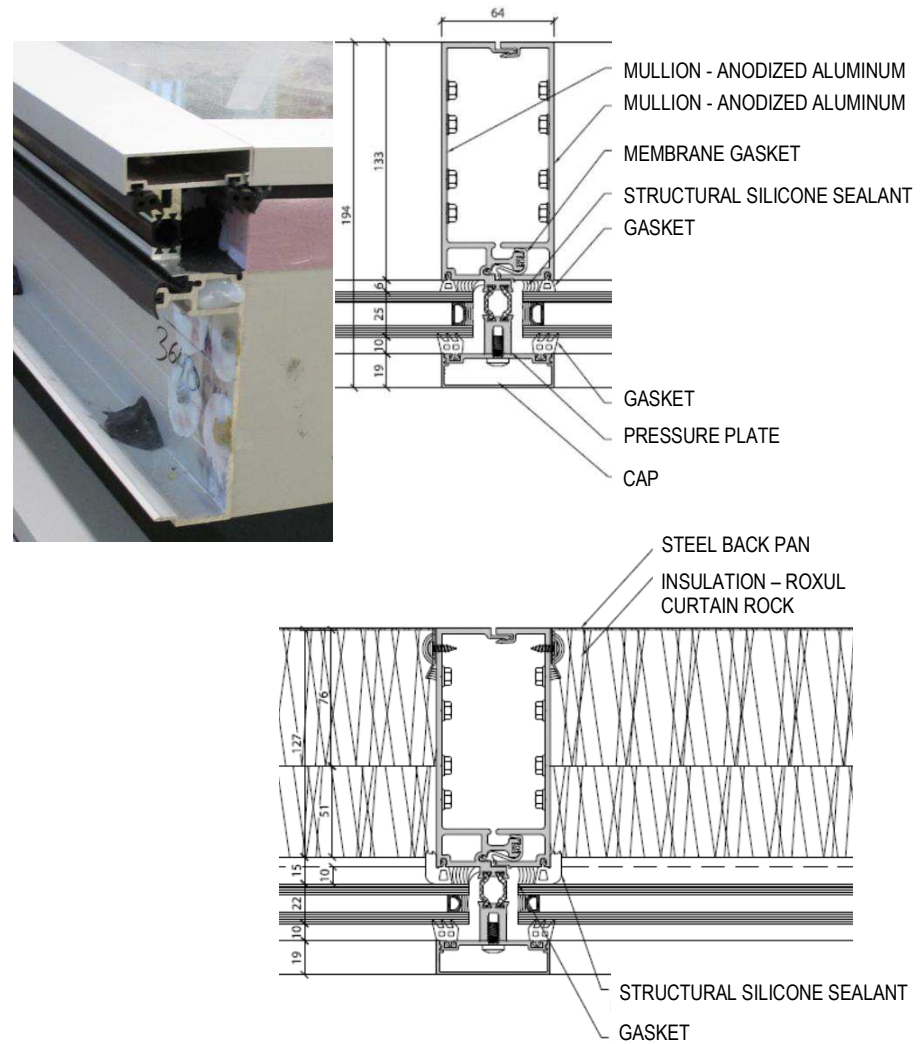
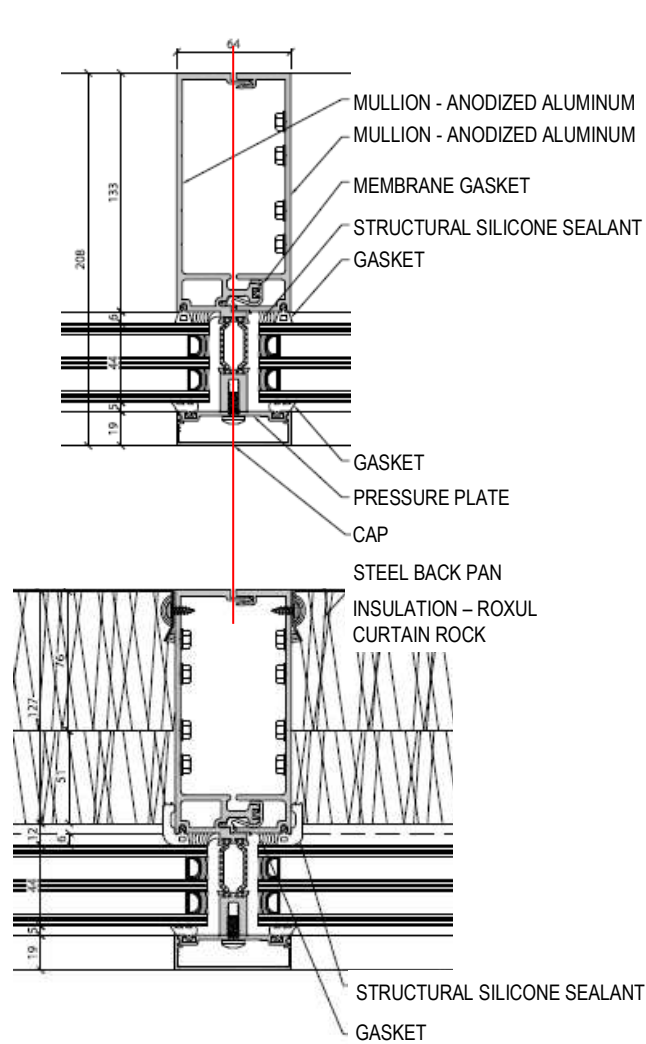
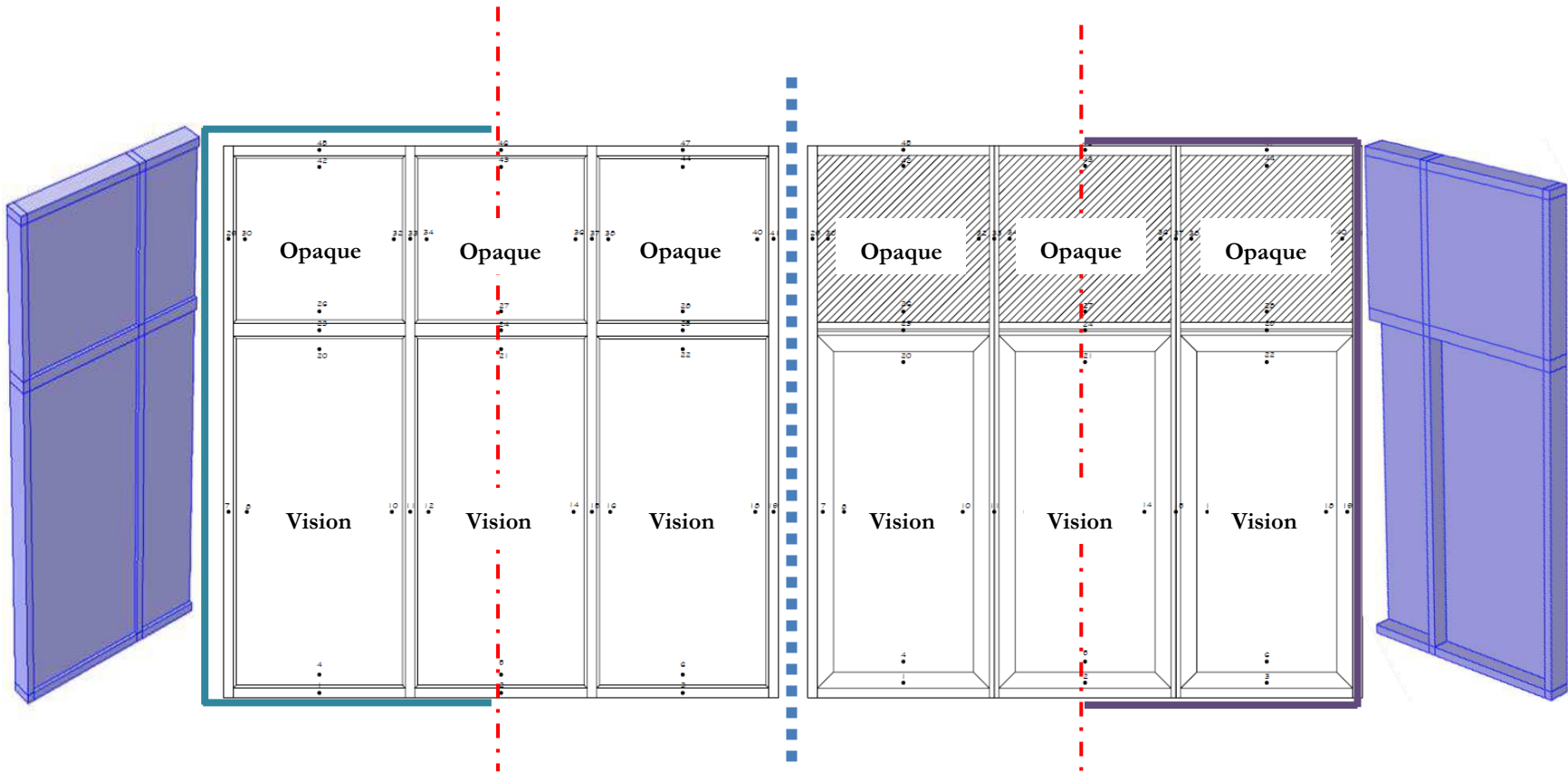


Figure 5 – Sectional drawings of triple-glazed curtain wall mullion at vision panel; Sectional drawing of triple-glazed curtain wall mullion at opaque panel

Figure 6 – Sectional drawing of double-glazed curtain wall mullion; Photo showing end portion of horizontal section; Sectional drawing of double-glazed curtain wall mullion at opaque panel



<p>Figure 7 – Elevation view of “exterior” of double- and triple-glazed curtain wall assembly</p>	<p>Figure 8 – Elevation view of “interior” of double- and triple-glazed curtain wall assembly</p>
---	---

4.2.3 Description of NFRC curtain wall panel model configuration

Curtain wall assembly size & configuration — The Reference curtain wall assembly conforming to NFRC is shown in Figure 9. It consists of two adjacent 2-m x 1-m vision panels and two adjacent 1-m x 1.2-m opaque spandrel panels. Given the symmetry about the centreline of the assembly only half of each assembly was configured for modelling, as is shown in the figure to the right of the elevation drawing of Figure 9. The overall size of the assembly configured for modelling was thus 1-m wide by 3.2-m high.

Vertical sectional views of the double-glazed CW assembly are given in Figure 10 and comparable views for the triple-glazed CW assembly in Figure 11. The location of the IGU in the respective aluminium mullions is evident in both figures; the same thermally broken aluminium sections were used for the model configuration of the NFRC compliant CW assembly as were used for the CW assembly of the manufactured products. The opaque panels were insulated with mineral wool of the same type and properties as used for the manufactured products.

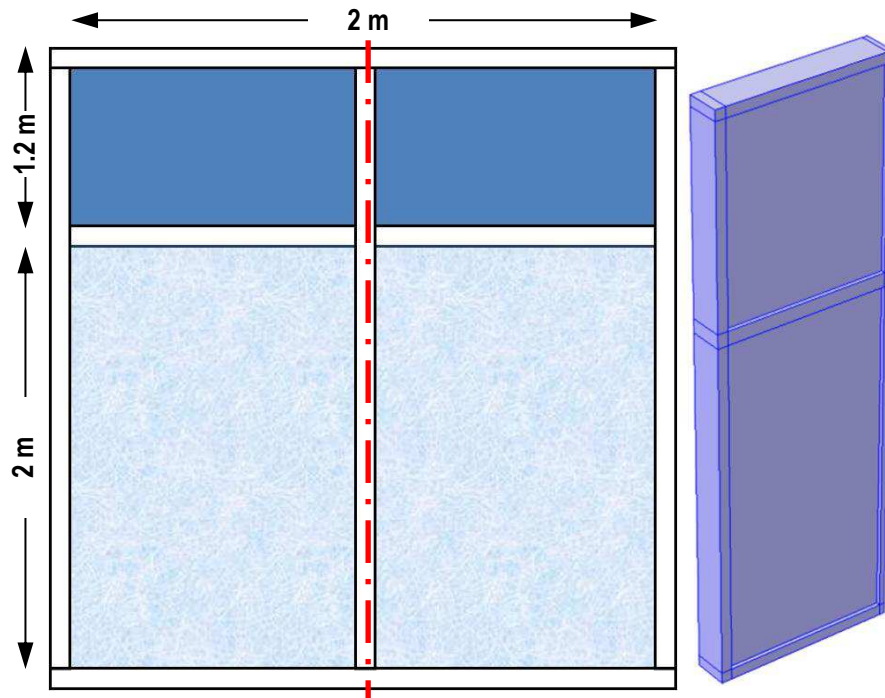


Figure 9 - Reference Curtain Wall assembly conforming to NFRC (2m x 2m vision; 2 m x 1.2 m spandrel)

Configuration of IGUs — The configuration of the IGU for the double-glazed IGU is shown in Figure 10 and for the triple-glazed unit in Figure 11. For the double-glazed IGU incorporating a low- ϵ coating, surface 2 was the low- ϵ surface of emissivity = 0.054; for all other surfaces (1, 3, 4), the emissivity was = 0.84. The IGU was filled with Air (reference) or mixtures of 10% Air and 90% of either, Argon, Krypton, or Xenon gas.

The triple-glazed IGU incorporated a low- ϵ coating on surfaces 2 and 4 as shown Figure 11; the low- ϵ surface emissivity = 0.054; for all other surfaces (1, 3, 5, 6), the emissivity was = 0.84. gas filling was the same as that for the double-glazed IGU.

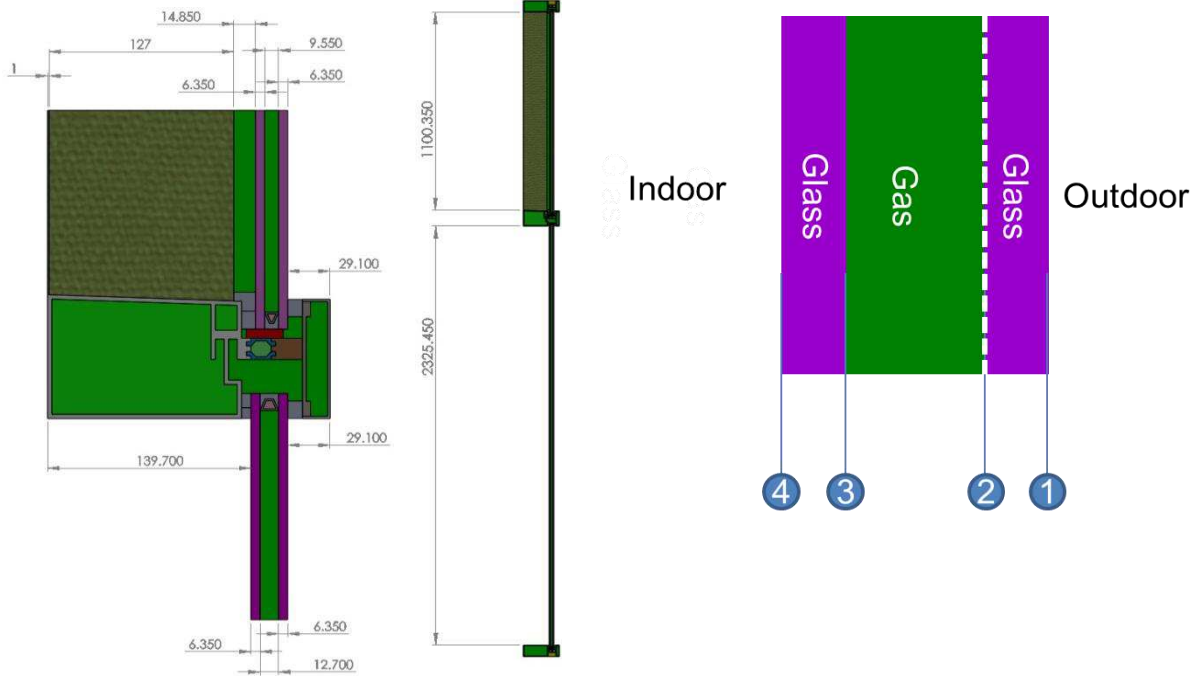


Figure 10 - Double Glazing (2G) Curtain Wall sectional views; Surface 2 with low-e of emissivity = 0.054; Other surfaces (1, 3, 4) emissivity = 0.84; Filling gas: 90% gas and 10% air

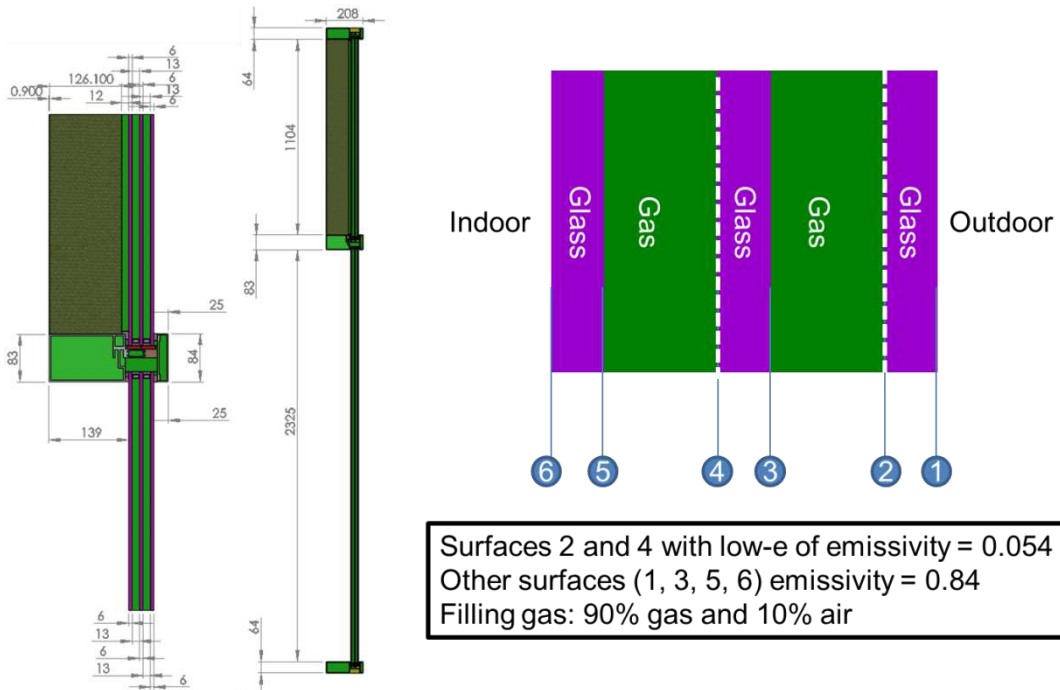


Figure 11 - Triple Glazing (3G) Curtain Wall sectional views and detail of IGU and characteristic surfaces

5. Results derived from simulation

The results derived from simulation are provided for two sets of curtain wall (CW) configurations that include the:

- CW manufactured product configurations, and;
- NFRC compliant CW configurations

The results of simulation are provided for each of these configurations in turn. In respect to results of simulation for the CW manufactured product configurations, only simulation results required to assess the risk to condensation of the manufactured products are provided in the main body of the report. Whereas, the broader range of simulation results that form the basis of the parametric study focus on results derived for the NFRC compliant CW configurations; these results are those given in the main body of the report and are discussed in some detail. Where additional results were generated for the CW manufactured products but not presented in the main body of this report, these have been provided in the Appendix as noted in the respective sections of the report.

5.1 Simulation Results for manufactured product configurations

Simulation results for manufactured product configurations are first provided for the double-glazed and thereafter the triple-glazed CW product configuration.

5.1.1 – Results for Double glazed CW product configurations

The risk to the formation of condensation relates to whether there is likelihood for the formation of condensation on the interior side of the frame or glazed portion of the vision panel. The risk is related to the surface temperature on the exterior and interior of the curtain wall components, and the relative humidity on the interior side.

Three known (but different) condensation rating systems are available: (i) the AAMA Condensation Resistance Factor (CRF) [5]; (ii) the National Fenestration Rating Council (NFRC) Condensation Rating (CR) [6], and; (iii) the Canadian Standards Association (CSA) Temperature Index (I) [7]. -

The Temperature Index (I), is the ratio of the temperature difference between the inside surface temperature and the outside air temperature, divided by temperature difference between the inside and outside air, and is given as:

$$\text{Temperature Index (I): } T_{Index} = \frac{T_s - T_o}{T_i - T_o} \quad (1)$$

Where T_i is indoor air temperature; T_o is outdoor air temperature; T_s is the temperature of the interior surface of the assembly.

⁵ AAMA 1503-09 (2009), Voluntary Test Method for Thermal Transmittance and Condensation Resistance of Windows, Doors and Glazed Wall Sections, American Architectural Manufacturers Association Schaumburg, IL, USA;

⁶ NFRC-500-2010 (2010), Procedure for Determining Fenestration Product Condensation Resistance Values, National Fenestration Rating Council, Greenbelt, MD, USA, 32 p.

⁷ CSA A440. Canadian Standards Association (CSA) Temperature Index

This ratio remains fairly stable regardless of the size of the temperature difference, so that if one has data on the temperature index, one can predict the interior surface condition given an outdoor temperature. The values of the Condensation Resistance Factor (CRF) used in US window standards is a Temperature Index, as is the I value used in Canadian standards, the difference being in how the interior surface temperature is defined for their respective methods of calculation.

When evaluating the risk to the formation of condensation on the interior surface of the CW components, two different interior conditions were considered, as shown in :

- Option B: representative of ASHRAE 160 conditions of 40% RH;
- Option D: representative of Modified ASHRAE 160 conditions of 32% RH

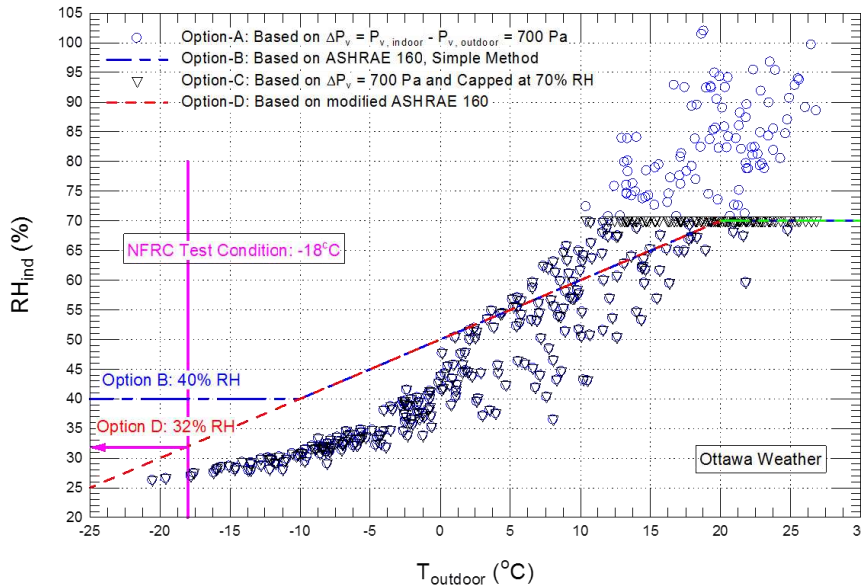


Figure 12 – Risk of Condensation on Interior Surface of CW components for NFRC test conditions; Two Options: Option B: ASHRAE 160 (40% RH); Option D: Modified ASHRAE 160 (32% RH)

Accordingly, results derived from simulation of a double-glazed thermally broken curtain wall assembly of a manufactured product for the exterior (i) and (ii) temperature index, as given in Equation 1, are provided in Figure 13. The double-glazed Ar filled IGU (i.e. 90% Ar and 10% Air) has a low-e coating on surface 2 ($\epsilon_{coat} = 0.054$). The range in values for the respective set of results can be found in the scale adjacent to each of the three figures of the assembly, for which can be found that the exterior surface temperature of the assembly ranges between ca. -4 °C and -18 °C, and the value of the temperature index (I) between 0.43 and 0.97.

Simulated results of relative humidity (% RH) on exterior surface of double-glazed CW are given in Figure 14 and for temperature difference (ΔT °C) in Figure 15; in the two plots provided of either figure, Option D represents a modified ASHRAE 160 interior RH conditions of 32 %, whereas Option B has the ASHRAE 160 interior RH conditions of 40 %; values of surface temperature difference less than 0 ($\Delta T < 0$ °C) represent locations for risk of condensation. The range in RH values for the respective set of results can be found in the scale adjacent to each of the plots; results for Option D (i) range from ca. 34% to 100 % RH and for Option B (ii) from ca. 42.5 to 100% RH.

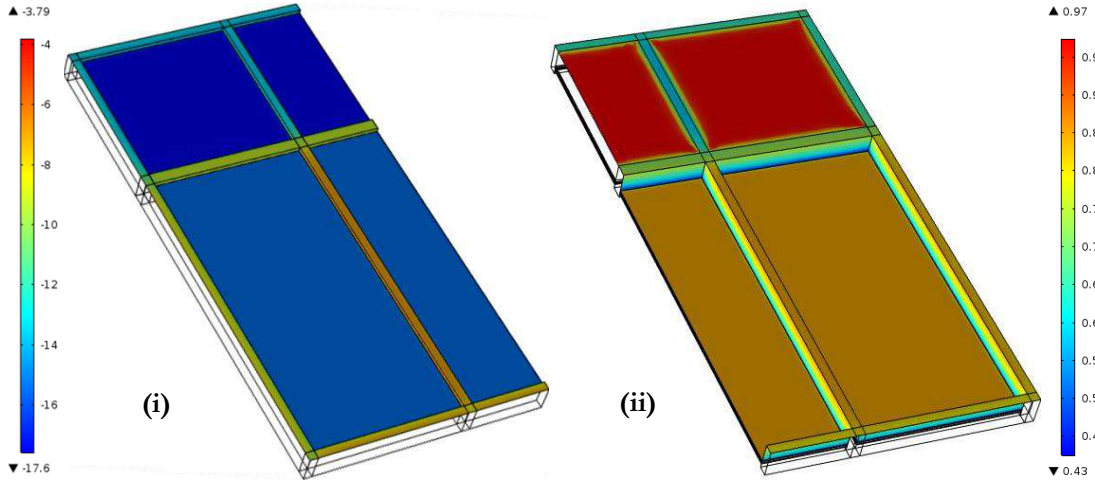


Figure 13 – Simulated exterior temperature (i) and values of temperature index T_{Index} (ii) of double-glazed thermally broken CW product having IGU with 90% Ar & 10% Air; Surface 2, $E_{coat} = 0.054$.

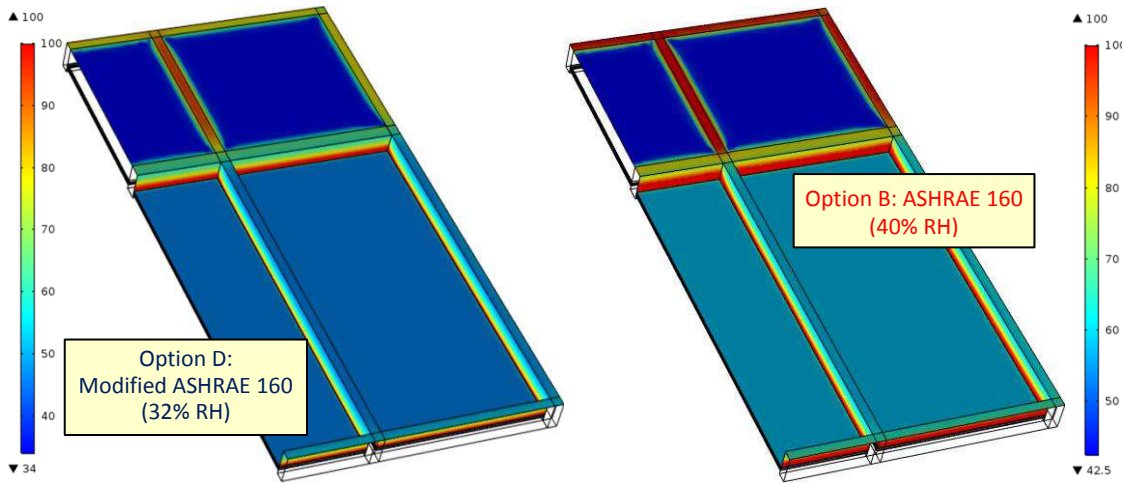


Figure 14 – Simulated results of relative humidity on interior surface of double-glazed IGU thermally broken CW product; (i) Option D: Modified ASHRAE 160 (32% RH); (ii) Option B: ASHRAE 160 (40% RH)

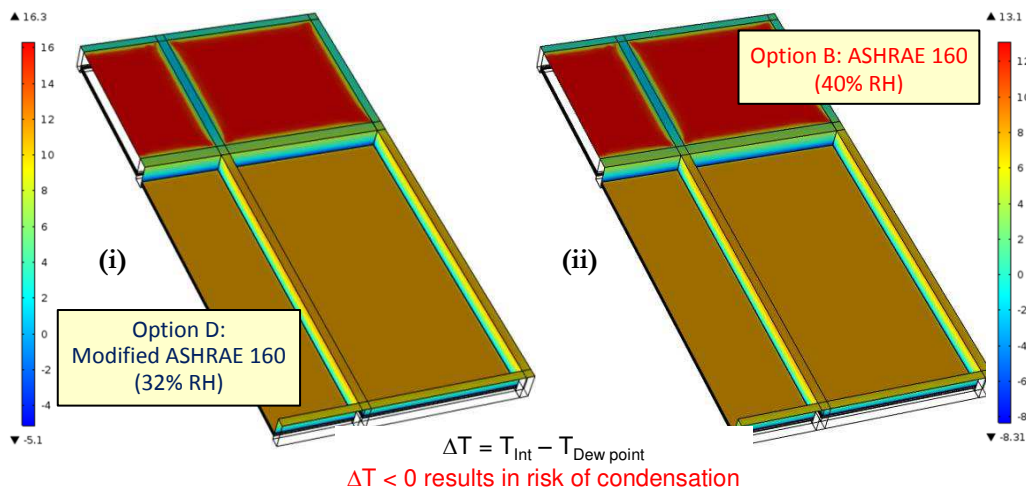
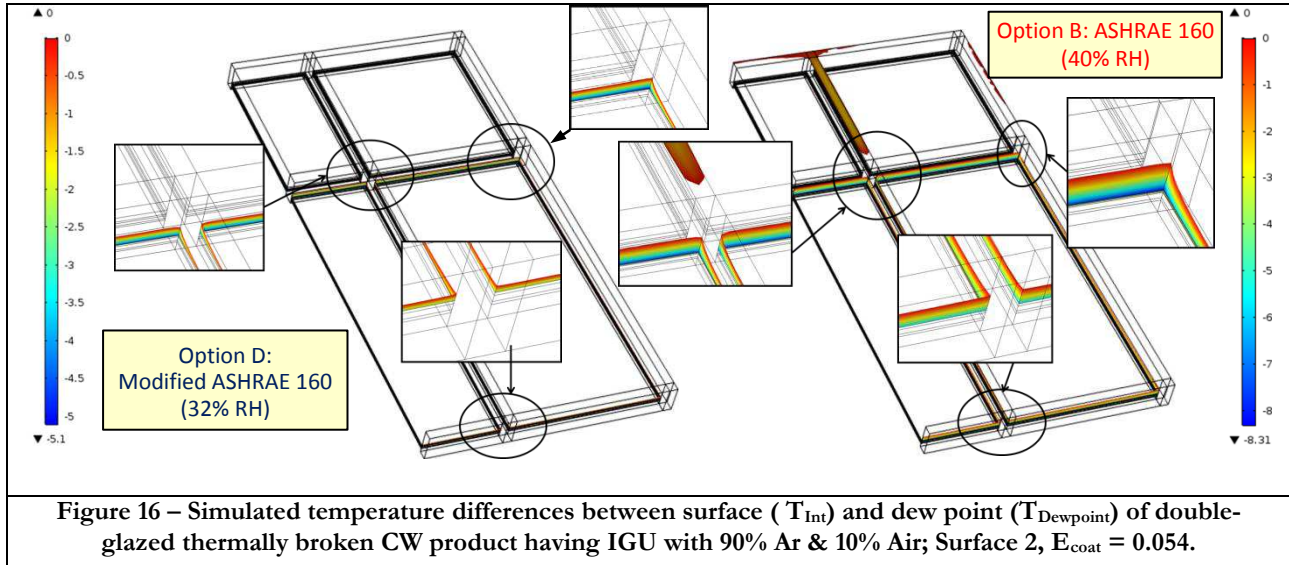


Figure 15 – Simulated results of temperature difference (ΔT °C) on exterior surface of double-glazed CW product; (i) Option D: Modified ASHRAE 160 (32% RH); (ii) Option B: ASHRAE 160 (40% RH)



Finally, the results derived from simulation of the same double-glazed curtain wall assembly and in respect to the temperature differences between the interior surface temperature (T_{Int}) of the assembly and the dew point temperature ($T_{Dewpoint}$) are given in Figure 16. In Figure 16, the locations for risk to condensation, specifically, where the temperature difference is < 0 have been highlighted in two plots: the one on the right-hand side showing locations at risk to condensation where the interior RH is 40 % (Option B); and the other on the left hand side (Option D) representative of interior RH conditions of 32 %. Values of temperature difference (i.e. $\Delta T = T_{Int} - T_{Dewpoint}$) for Option D range between ca. $-8.3\text{ }^{\circ}\text{C}$ and 0°C whereas for Option B between ca. $-5.1\text{ }^{\circ}\text{C}$ and 0°C . Values below zero represent locations at risk of formation of condensation. Whichever interior RH conditions used, both show similar locations for the formation on condensation on the assembly, specifically, along frame edges.

5.1.2 – Results for Triple glazed CW manufactured product configuration

Condensation risk: — Results derived from simulation of a triple-glazed thermally broken curtain wall assembly of a manufactured product for the exterior (i) and (ii) temperature index, as given in Equation 1, are provided in Figure 17. The triple-glazed Ar filled IGU (i.e. 90% Ar and 10% Air) has a low-e coating on surface 2 ($\epsilon_{coat} = 0.054$). The range in values for the respective set of results can be found in the scale adjacent to each of the three figures of the assembly, for which can be found that the exterior surface temperature of the assembly ranges between ca. $-3.8\text{ }^{\circ}\text{C}$ and $-117.6\text{ }^{\circ}\text{C}$, and the value of the temperature index (I) between 0.43 and 0.97.

Simulated results of relative humidity (% RH) on exterior surface of double-glazed CW are given in Figure 18 and for temperature difference ($\Delta T\text{ }^{\circ}\text{C}$) in Figure 19; in the two plots provided of either figure, Option D represents a modified ASHRAE 160 interior RH conditions of 32 %, whereas Option B has the ASHRAE 160 interior RH conditions of 40 %; values of surface temperature difference less than 0 ($\Delta T < 0\text{ }^{\circ}\text{C}$) represent locations for risk of condensation. The range in RH values for the respective set of results can be found in the scale adjacent to each of the plots; results for Option D (i) range from ca. 34% to 100 % RH and for Option B (ii) from ca. 42.5 to 100% RH.

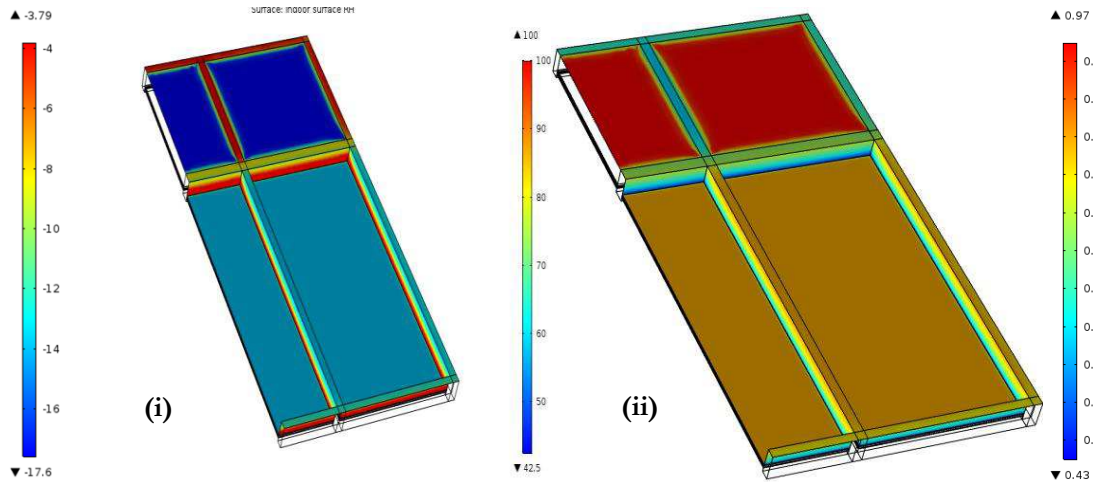


Figure 17 – Simulated exterior temperature (i) and values of temperature index T_{Index} (ii) of triple-glazed thermally broken CW product having IGU with 90% Ar & 10% Air; Surface 2, $E_{coat} = 0.054$.

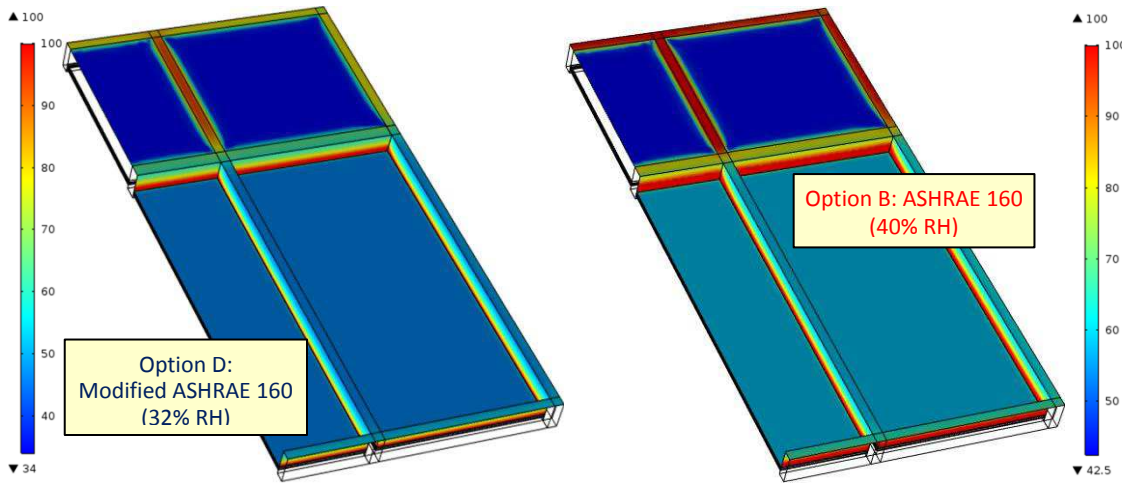


Figure 18 – Simulated results of relative humidity on interior surface of triple-glazed IGU thermally broken CW product; (i) Option D: Modified ASHRAE 160 (32% RH); (ii) Option B: ASHRAE 160 (40% RH)

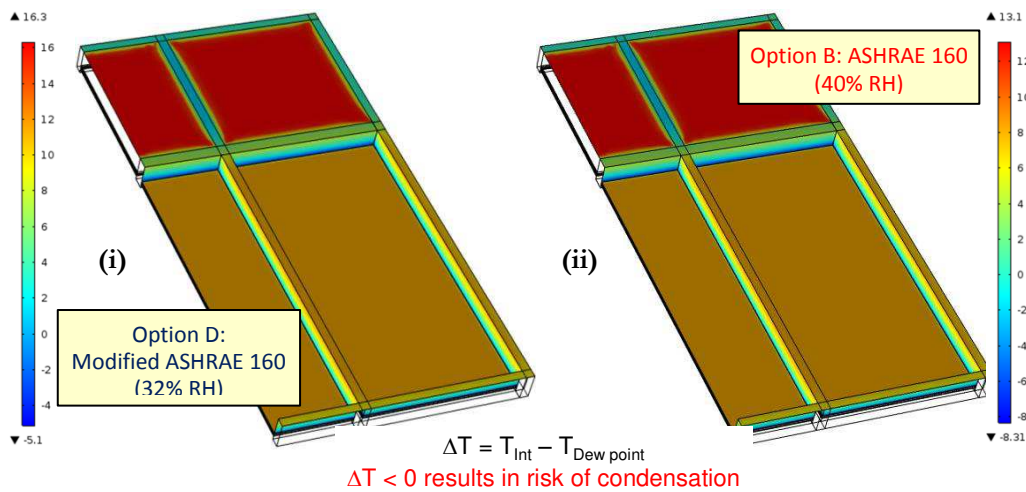


Figure 19 – Simulated results of temperature difference (ΔT °C) on exterior surface of triple-glazed CW product; (i) Option D: Modified ASHRAE 160 (32% RH); (ii) Option B: ASHRAE 160 (40% RH)

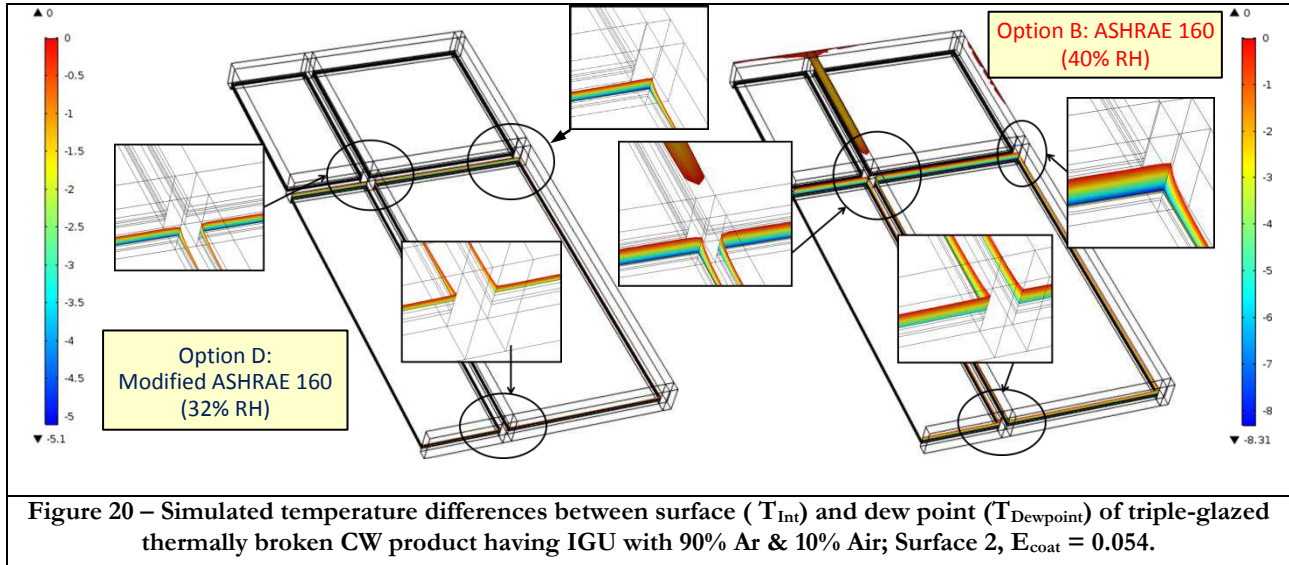


Figure 20 – Simulated temperature differences between surface (T_{Int}) and dew point ($T_{Dewpoint}$) of triple-glazed thermally broken CW product having IGU with 90% Ar & 10% Air; Surface 2, $E_{coat} = 0.054$.

Finally, the results derived from simulation of the same double-glazed curtain wall assembly and in respect to the temperature differences between the interior surface temperature (T_{Int}) of the assembly and the dew point temperature ($T_{Dewpoint}$) are given in Figure 20. In Figure 20, the locations for risk to condensation, specifically, where the temperature difference is < 0 have been highlighted in two plots: the one on the right-hand side showing locations at risk to condensation where the interior RH is 40 % (Option B); and the other on the left hand side (Option D) representative of interior RH conditions of 32 %. Values of temperature difference (i.e. $\Delta T = T_{Int} - T_{Dewpoint}$) for Option D range between ca. -5.1 °C and 0 °C whereas for Option B between ca. -8.3 °C and 0 °C. Values below zero represent locations at risk of formation of condensation. Whichever interior RH conditions used, both show similar locations for the formation on condensation on the assembly, specifically, along frame edges.

5.2 Simulation Results for NFRC-Compliant CW configurations

5.2.1 Results for Double-glazed NFRC-Compliant CW Configurations

Results derived from simulation for the double-glazed NFRC-compliant curtain wall configurations are provided in terms of the:

- (i.) Risk to the formation of condensation;
- (ii.) Effect of glazing to wall-area ratio;
- (iii.) Effect of changes to coating emissivity, and;
- (iv.) Effect of thermal resistance of the spandrel panel insulation
- (v.) Effect of spacer thermal properties

Results for each of these topics are provided in turn.

5.2.1.1 — Condensation risk:

Results derived from simulation of a double-glazed thermally broken NFRC-compliant curtain wall assembly for the exterior (i) and interior (ii) surface temperatures and (iii) temperature index, as given in Equation 1, are provided in Figure 21. The double-glazed Ar filled IGU (i.e. 90% Ar and 10% Air) has a low-e coating on surface 2 ($e_{coat} = 0.054$). The range in values for the respective set of results can be found in the scale adjacent

to each of the three figures of the assembly, for which can be found that the exterior surface temperature of the assembly ranges between ca. -7 °C and -18 °C, the interior temperature between -3.7 °C and 19.9 °C and the value of the temperature index (I) between 0.37 and 0.97.

The results derived from simulation for the relative humidity on interior surface of the double-glazed NFRC-compliant curtain wall assembly are provided in Figure 22. In Figure 22, two plots are provided: the one on the right-hand side (ii) for which the interior RH is 40 % (Option B) and which follows the interior RH conditions as recommended in ASHRAE 160 [8]; and the other (i) on the left hand side (Option D) and that represents a modified ASHRAE 160 interior RH conditions of 32 %. The range in RH values for the respective set of results can be found in the scale adjacent to each of the plots; results for Option D (i) range from ca. 34 to 100 % RH and for Option B (ii) from ca. 42 to 100% RH.

Simulated results of temperature difference (ΔT °C) on exterior surface of double-glazed NFRC-compliant CW are given in Figure 23; in the two plots provided, Option D represents a modified ASHRAE 160 interior RH conditions of 32 %, whereas Option B has the ASHRAE 160 interior RH conditions of 40 %; values of surface temperature difference less than 0 ($\Delta T < 0$ °C) represent locations for risk of condensation.

Finally, the results derived from simulation of the same double-glazed NFRC-compliant curtain wall assembly and in respect to the temperature differences between the interior surface temperature (T_{Int}) of the assembly and the dew point temperature ($T_{Dewpoint}$) are given in Figure 24. In Figure 24, the locations for risk to condensation, specifically, where the temperature difference is < 0 have been highlighted in two plots: the one on the right-hand side showing locations at risk to condensation where the interior RH is 40 % (Option B); and the other on the left hand side (Option D) representative of interior RH conditions of 32 %. Values of temperature difference (i.e. $\Delta T = T_{Int} - T_{Dewpoint}$) for Option D range between ca. -7.3 °C and 0°C whereas for Option B between ca. -10.5 °C and 0 °C. Values below zero represent locations at risk of formation of condensation. Whichever interior RH conditions used, both show similar locations for the formation on condensation on the assembly, specifically, along frame edges.

5.2.1.2 — Effect of Glazing to Wall Area Ratio:

The effect of glazing to wall-area ratio (window-to-wall ratio / A_R) on the R-value and corresponding U-value of double-glazed thermally broken NFRC-compliant curtain wall assemblies is elaborated in this section. As well, the influence on the thermal performance of the assembly in relation to the A_R for assemblies incorporating IGUs of different gas type and whether, or not, the IGU includes a low-e coating is also explored.

The results derived from simulation for the air-to-air and surface-to-surface R-value and U-value of a double-glazed thermally broken curtain wall assembly in relation to the glazing to wall area ratio (A_R) is provided in Figure 25 to Figure 34; results are first presented for curtain wall assemblies having low-e coated IGUs and thereafter, for IGUs of higher emissivity.

Thermal performance results for double-glazed curtain wall assembly with low-e coated IGU—

Simulation results for the R-value (uppermost plot) and U-value (lower-most plot) in relation to the A_R of a double-glazed curtain wall assembly that included a low-e coated IGU ($e = 0.054$; surface 2), and for which the

⁸ ANSI/ASHRAE Standard 160 (2009), *Criteria for Moisture-Control Design Analysis in Buildings*, ASHRAE, Atlanta, GA, USA.

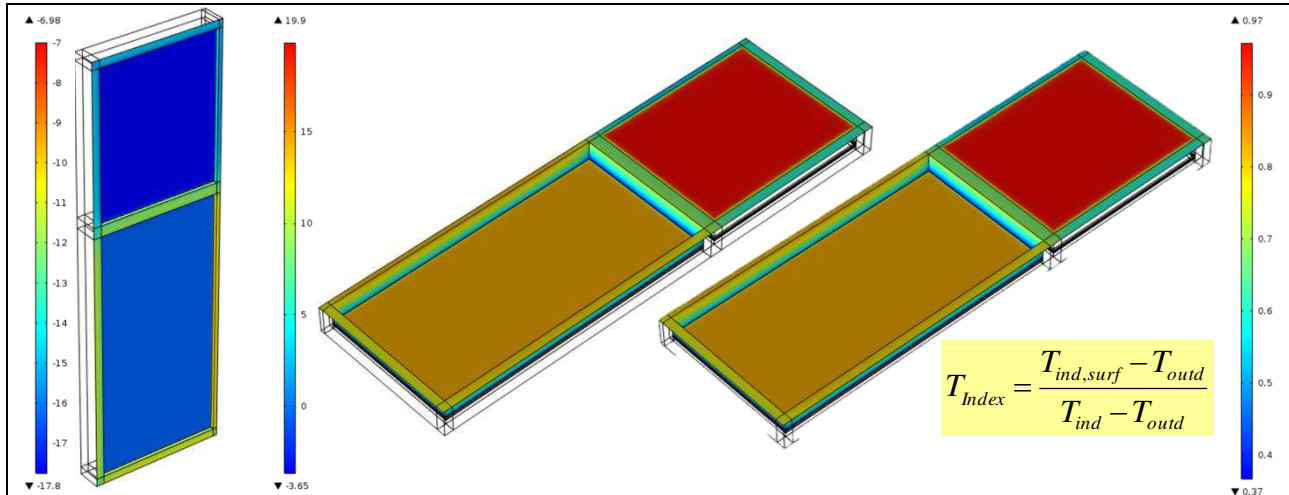


Figure 21 – Simulated exterior (i) & interior (ii) temperature; values of temperature index T_{Index} (iii) of double-glazed thermally broken NFRC-compliant CW having IGU with 90% Ar & 10% Air; Surface 2, $E_{coat} = 0.054$.

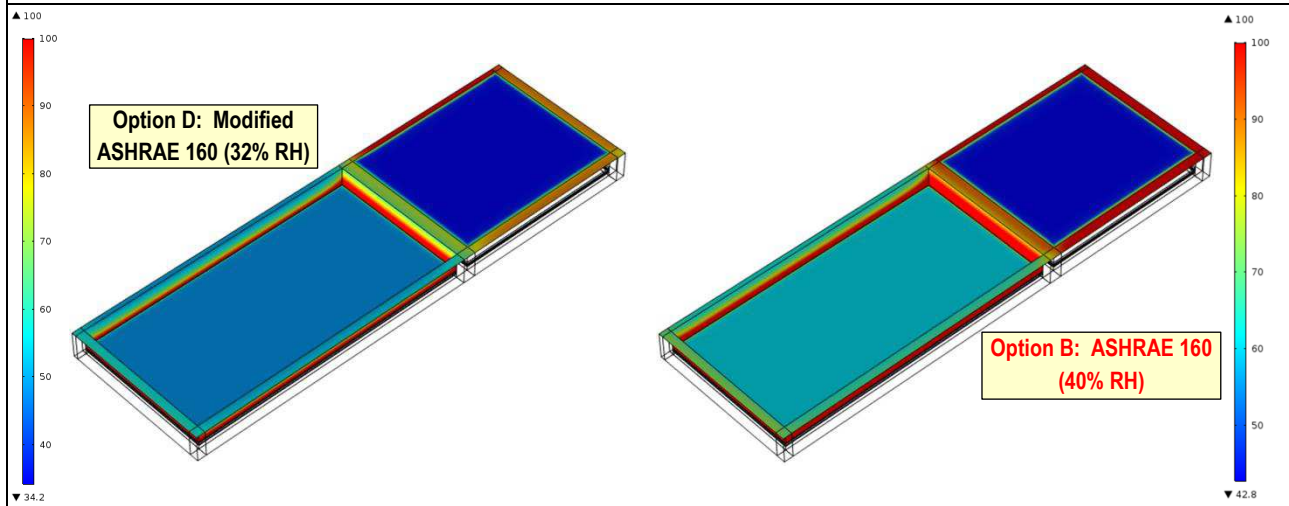


Figure 22 – Simulated results of relative humidity on interior surface of double-glazed IGU thermally broken NFRC-compliant CW; (i) Option D: Modified ASHRAE 160 (32% RH); (ii) Option B: ASHRAE 160 (40% RH)

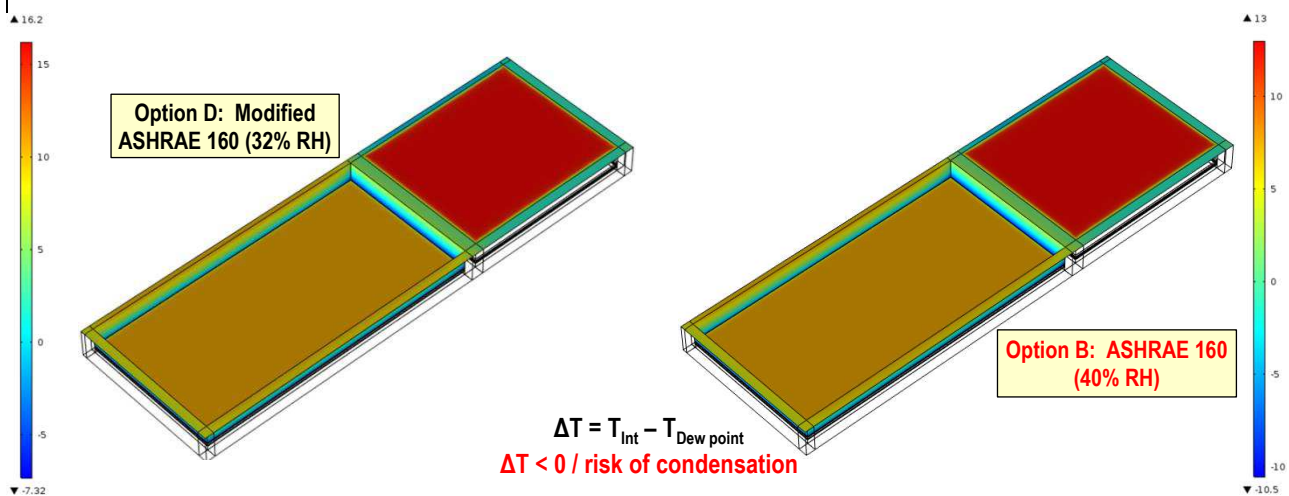
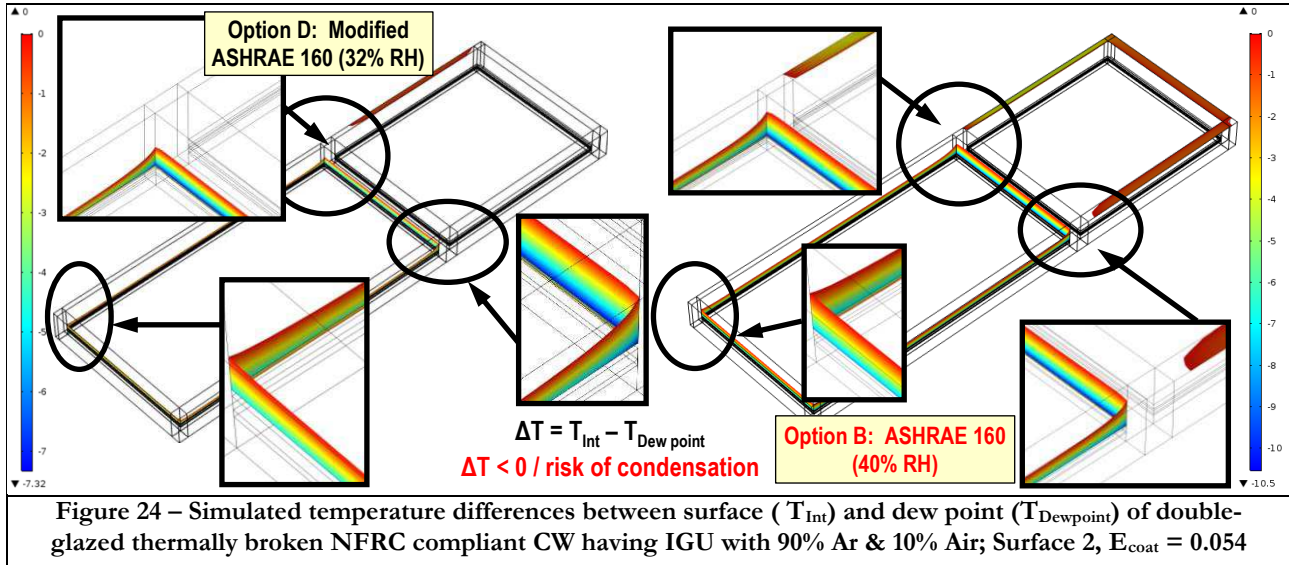


Figure 23 – Simulated results of temperature difference (ΔT °C) on exterior surface of double-glazed NFRC-compliant CW: (i) Option D: Modified ASHRAE 160 (32% RH); (ii) Option B: ASHRAE 160 (40% RH)



gas within the IGU was varied, is provided in the initial set of results given in Figure 25 to Figure 28; in the respective 4 figures, starting with Figure 25, the simulation results are given for the IGU incorporating a gas having:

- 90 % Ar and 10 % Air
- 90 % Kr and 10 % Air
- 90 % Xe and 10 % Air
- 100 % Air (Reference value)

From this set of results it is apparent that the R-value (air-to-air, or surface-to-surface) decreases with an corresponding increase in the A_R for all of the IGU simulated, irrespective of the type of gas incorporated in the IGU. The loss in thermal performance with increasing in A_R is entirely as might be expected given the reduced thermal performance of the vision as compared to the insulated spandrel panel (R22); R-values respectively range between ca. 0.45 to 1.1. The more significant decreases are evidently found for the least performing IGU which is filled with 100% air. The respective thermal performance range of the 4 different sets of results in terms of the air-to-air R-value ($m^2 \cdot K/W$) and U-value ($W/m^2 \cdot K$) at 10 % and 90 % A_R are provide in Table 3:

Table 3 - R-value and U-values (air-to-air) of double-glazed curtain wall assembly incorporating IGUs having different gases at selected glazing to wall-area ratios

IGU gas fill	R-value ($m^2 \cdot K/W$)		U-value ($W/m^2 \cdot K$)	
	10 % A_R	90 % A_R	10 % A_R	90 % A_R
100 % Air (Reference value)	0.93	0.45	1.30	2.20
90 % Ar and 10 % Air	0.96	0.50	1.15	2.00
90 % Kr and 10 % Air	0.98	0.57	1.05	1.80
90 % Xe and 10 % Air	1.12	0.60	0.99	1.66

Thermal performance results for double-glazed curtain wall assembly with & without low-e IGU— Simulation results for the R-value (uppermost plot) and U-value (lower-most plot) in relation to the A_R of a double-glazed curtain wall assembly that included an IGU either with or without a low-e surface (i.e. $e = 0.054$; surface 2) and for which the gas within the IGU was varied, is provided in this subsequent set of results given

in Figure 29 to Figure 32; in the respective 4 figures, starting with Figure 29, the simulation results are given, as for the previous set, for an IGU incorporating a gas having:

- 90 % Ar and 10 % Air
- 90 % Kr and 10 % Air
- 90 % Xe and 10 % Air
- 100 % Air (Reference value)

From this set of results it is evident that the R-value (air-to-air, or surface-to-surface) decreases with an corresponding increase in the A_R for all of the IGUs simulated, irrespective of the type of gas incorporated in the IGU and regardless of whether the low-e coating is applied to the IGU. As well, the R-value (air-to-air, or surface-to-surface) of the low-e coated IGU is characteristically greater than that of the high emissivity IGU for any given value of A_R . The loss in thermal performance with increasing in A_R is, as before, entirely as might be expected, whether for an IGU having a low-e glass surface or glass of higher emissivity, given the reduced thermal performance of the vision as compared to the insulated spandrel panel (R22); however these losses are more important for IGUs have higher emissivity glass. The more significant decreases are evidently found for the least performing IGU which is filled with 100% air. The respective thermal performance range of the 4 different sets of results in terms of the air-to-air R-value ($m^2 \cdot K/W$) and U-value ($W/m^2 \cdot K$) at 10 % and 90 % A_R are provide in Table 4:

Table 4 - R-value and U-values (air-to-air) of double-glazed curtain wall assembly at selected glazing to wall-area ratios and incorporating IGUs having different gases and higher emissivity ($\epsilon = 0.84$)

IGU gas fill	R-value ($m^2 \cdot K/W$)		U-value ($W/m^2 \cdot K$)	
	10 % A_R	90 % A_R	10 % A_R	90 % A_R
100 % Air (Reference value)	0.85	0.34	1.2	2.9
90 % Ar and 10 % Air	0.87	0.35	1.2	2.9
90 % Kr and 10 % Air	0.88	0.37	1.2	2.8
90 % Xe and 10 % Air	0.89	0.38	1.2	2.8

Summary of thermal performance results for double-glazed curtain wall assembly — Results derived from simulation for the surface-to-surface R-value (uppermost plot) and surface-to-surface U-value (lower-most plot) in relation to the A_R of a double-glazed curtain wall assembly having a low-e coated IGU, and for which the gas within the IGU was varied, is provided in Figure 33; similar sets of plots of thermal performance for the curtain wall assembly having an IGU of higher emissivity ($\epsilon = 0.84$), is given in Figure 34.

The relative thermal performance of the curtain wall assembly in relation to A_R and amongst the different types of IGUs is clearly evident in Figure 33 for the assembly incorporating the low-e IGU; this is much less evident for the assembly with the higher emissivity IGU, as shown in Figure 34. The least performing assembly, irrespective of the emissivity of the glass, was the assembly, having the air filled IGU; the most performing having the Xe filled IGU.

The rate of change, in this instance decrease in R-value for a corresponding increase in A_R is also provided in the uppermost plot of Figure 33 and Figure 34. The effect is greatest for changes of A_R ranging between 5 and 35%; thereafter, the changes in R-value are less significant for corresponding changes in A_R . The vertical line at $A_R = 57\%$ represents the value of A_R of the NFRC compliant curtain wall assembly. It is evident from this information that there is little to be gained in terms of thermal performance for changes in the type of IGU gas for double-glazed curtain wall assembly having values of A_R exceeding say 40 %.

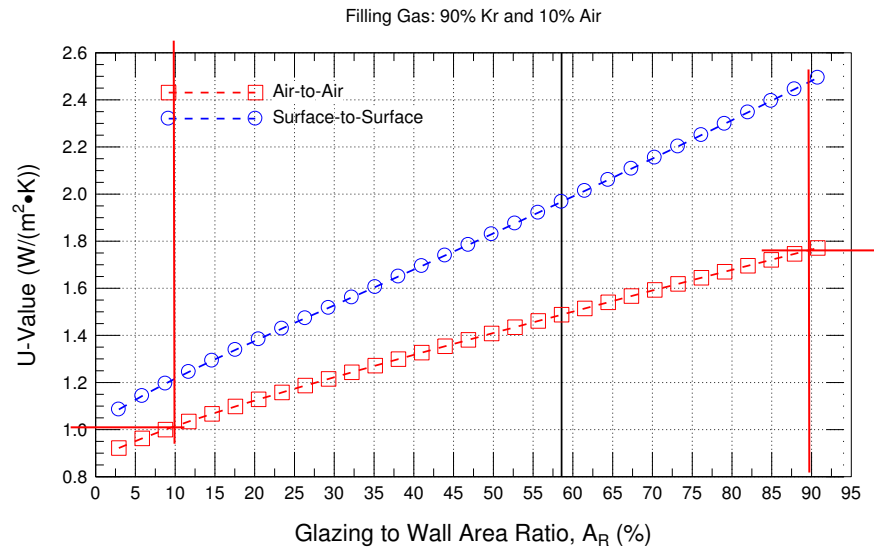
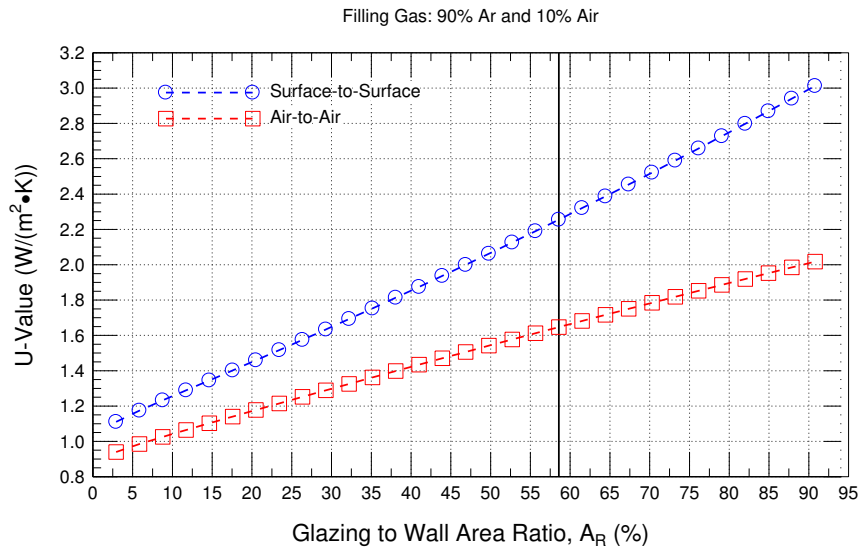
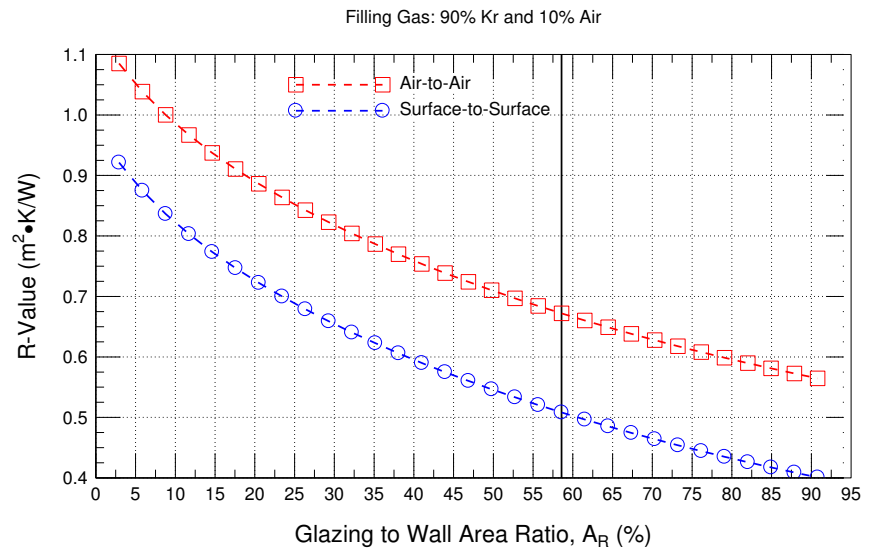
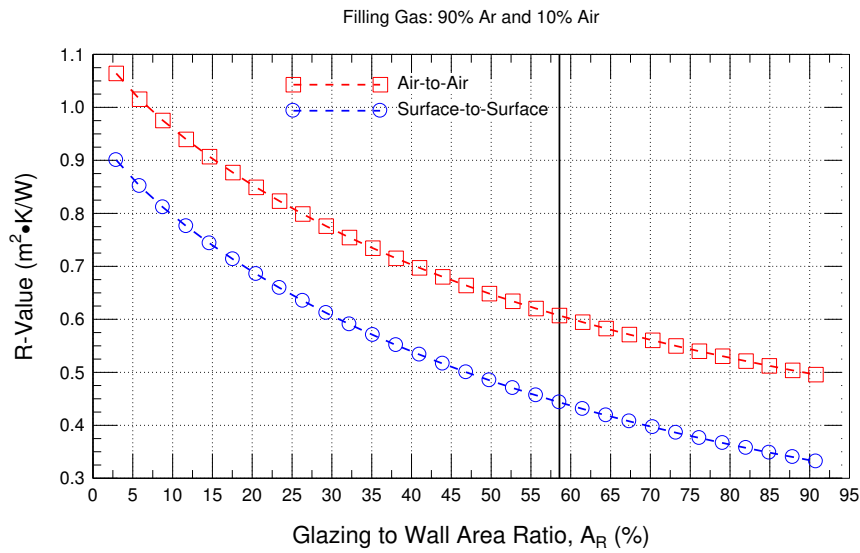


Figure 25 - Predicted (by simulation) R-value (i) and U-value (ii) (air-to-air; surface-to-surface) of double-glazed low-e coated ($e = 0.054$) thermally broken curtain wall section in relation to glazing to Wall Area Ratio

Figure 26 - Predicted (by simulation) R-value (i) & U-value (ii) (air-to-air; surface-to-surface) of double-glazed low-e coated ($e = 0.054$) thermally broken curtain wall section in relation to glazing to Wall Area Ratio

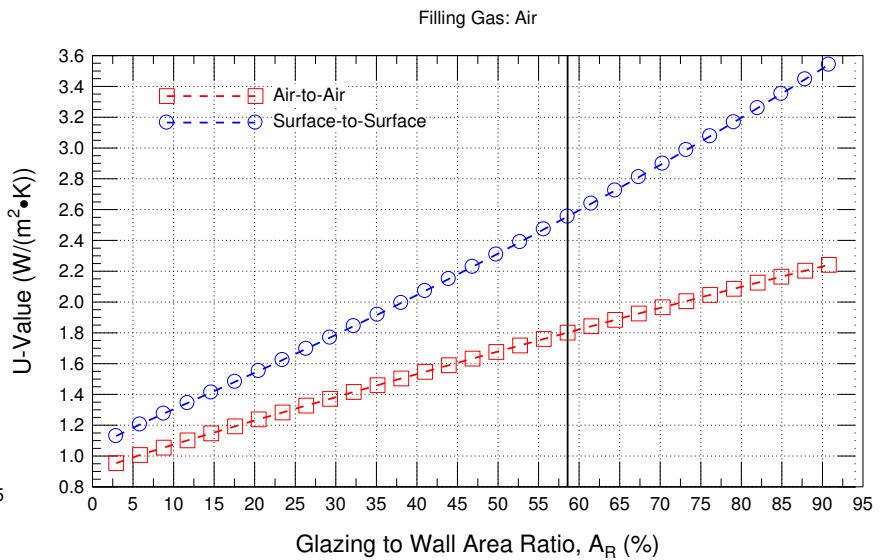
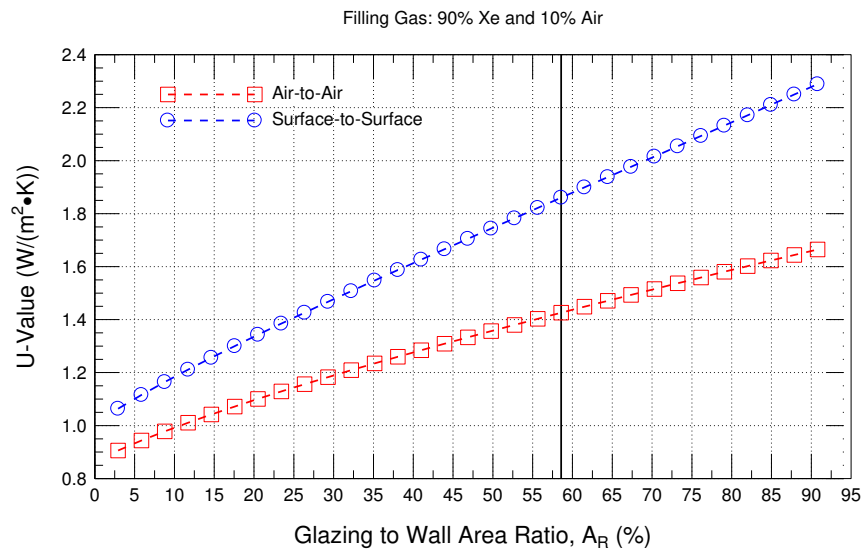
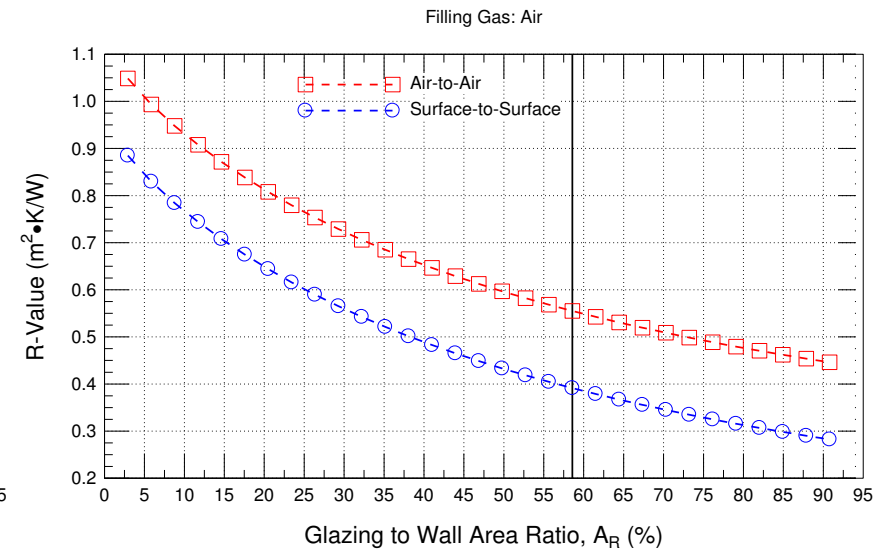
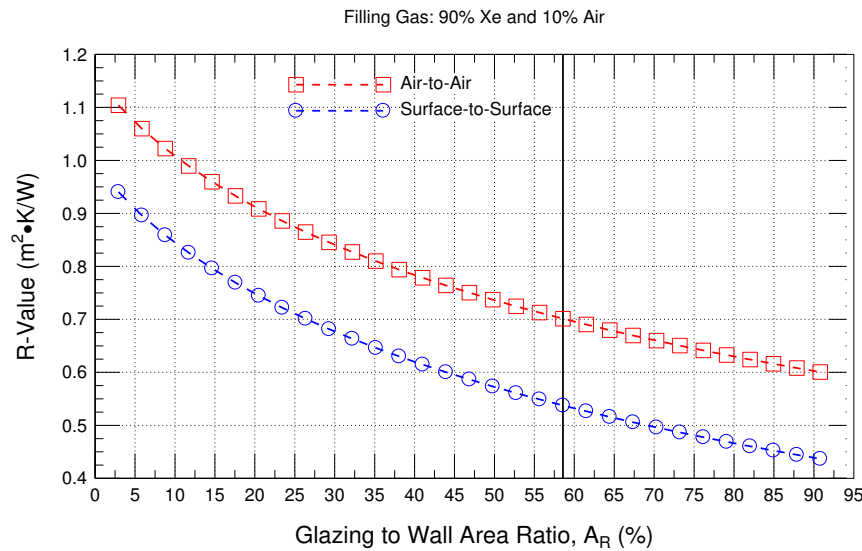


Figure 27- Predicted (by simulation) R-value (i) and U-value (ii) (air-to-air; surface-to-surface) of double-glazed low-e coated ($e = 0.054$) thermally broken curtain wall section in relation to glazing to Wall Area Ratio

Figure 28 - Predicted (by simulation) R-value (i) and U-value (ii) (air-to-air; surface-to-surface) of double-glazed low-e coated ($e = 0.054$) thermally broken curtain wall section in relation to glazing to Wall Area Ratio

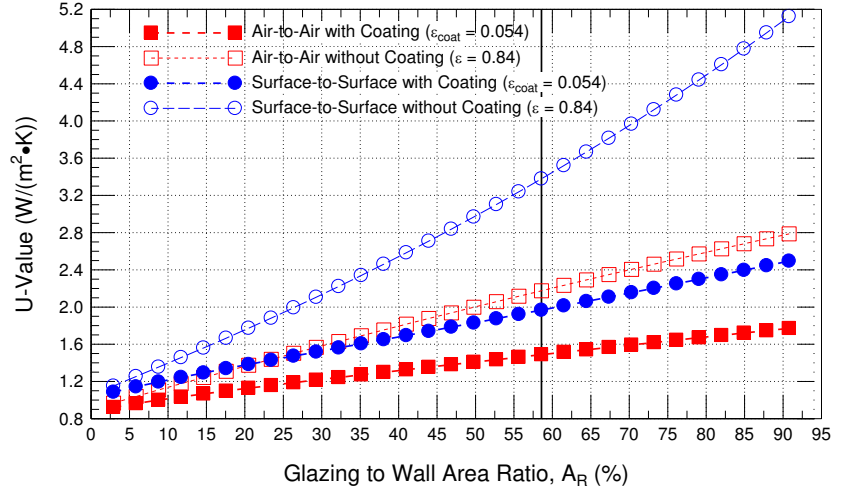
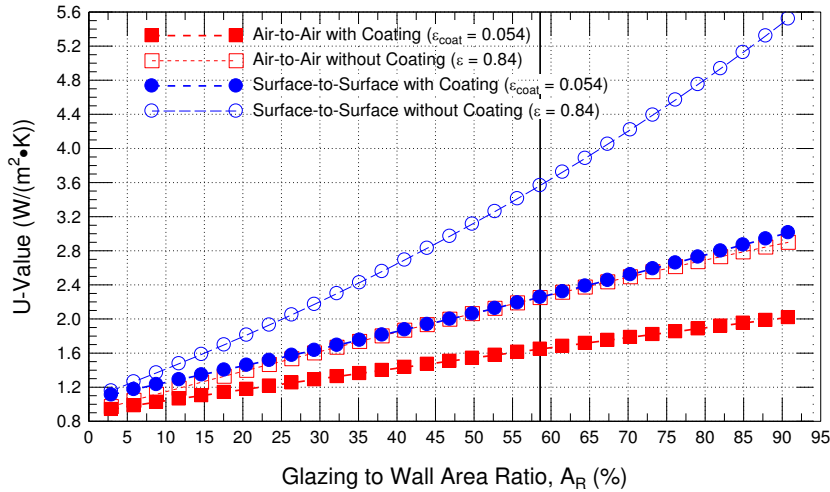
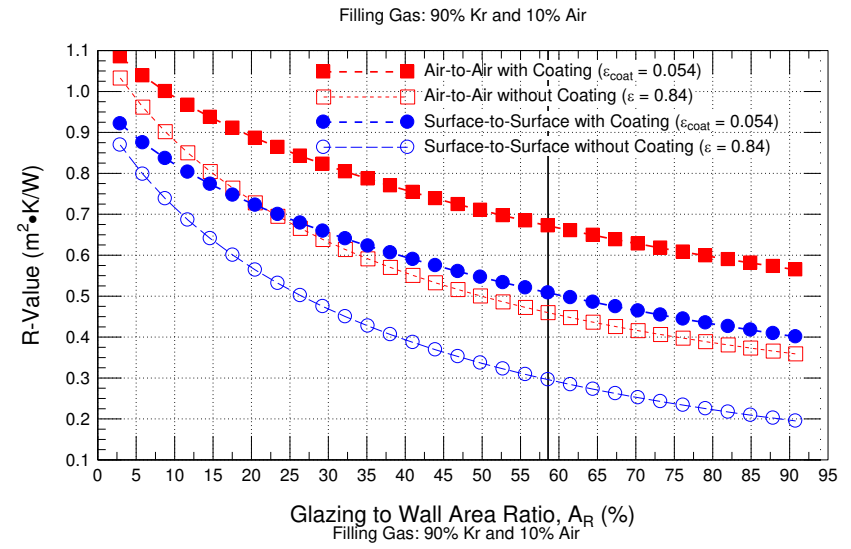
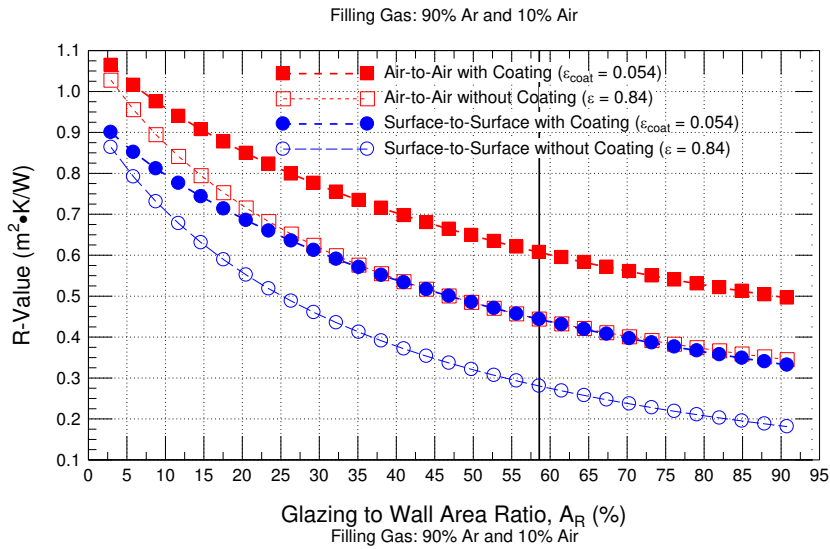


Figure 29 - Predicted (by simulation) R-value (i) and U-value (ii) (air-to-air; surface-to-surface) of double-glazed low-e coated ($\epsilon = 0.054$) or not coated ($\epsilon = 0.84$) thermally broken CW in relatⁿ to Glaz^{ng} to Wall Area Ratio

Figure 30 - Predicted (by simulation) R-value (i) and U-value (ii) (air-to-air; surface-to-surface) of double-glazed low-e coated ($\epsilon = 0.054$) or not coated ($\epsilon = 0.84$) thermally broken CW in relatⁿ to Glaz^{ng} to Wall Area Ratio

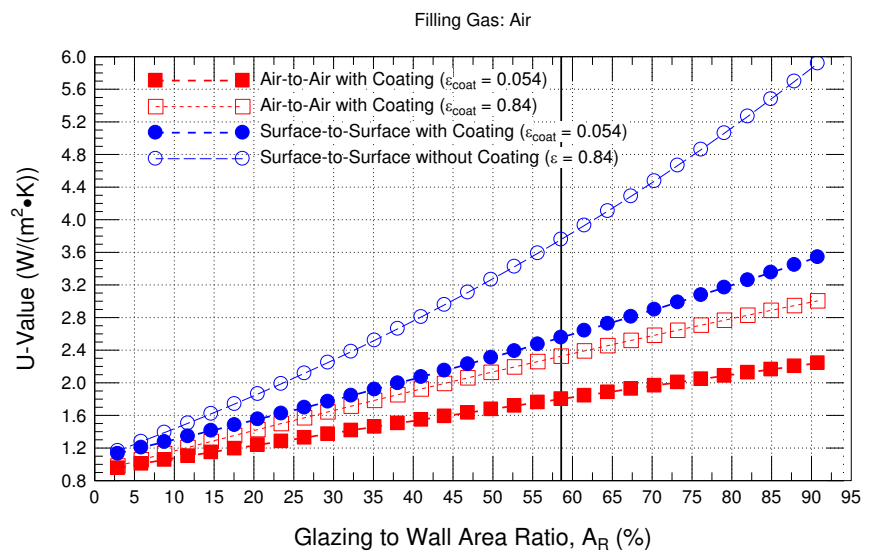
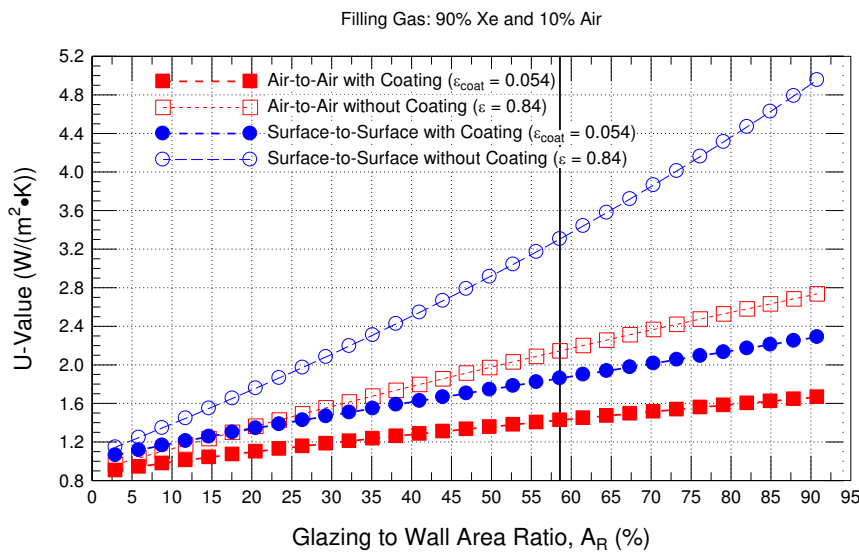
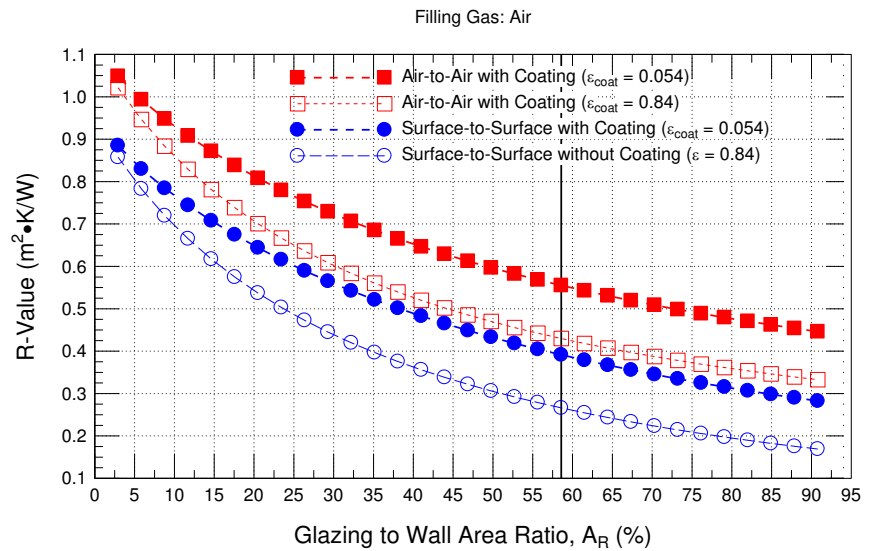
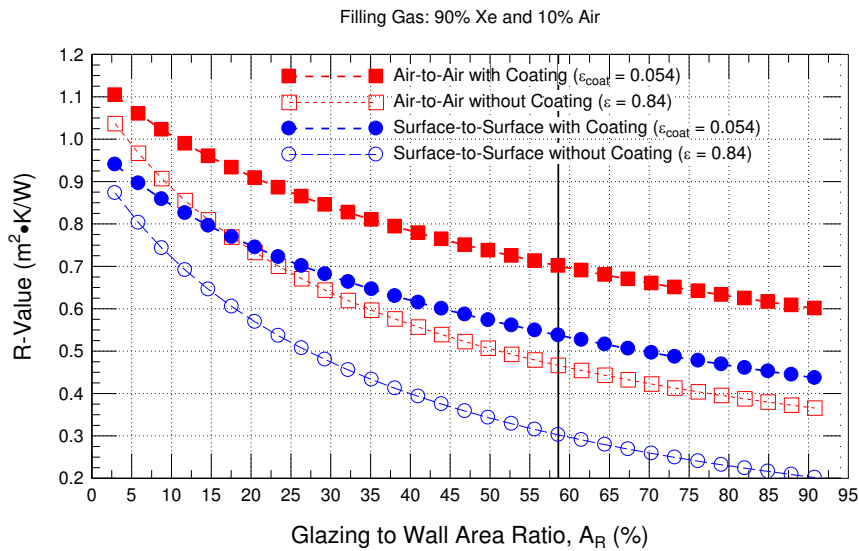


Figure 31 - Predicted (by simulation) R-value (i) ; U-value (ii) (air-to-air; surface-to-surface) of double-glazed, low-e ($e = 0.054$ / No coating $e = 0.84$) thermally broken curtain wall in relation to Glazing to Wall Area Ratio

Figure 32 - Predicted (by simulation) R-value (i) ; U-value (ii) (air-to-air; surface-to-surface) of double-glazed, low-e ($e = 0.054$ / No coating $e = 0.84$) thermally broken curtain wall in relation to Glazing to Wall Area Ratio

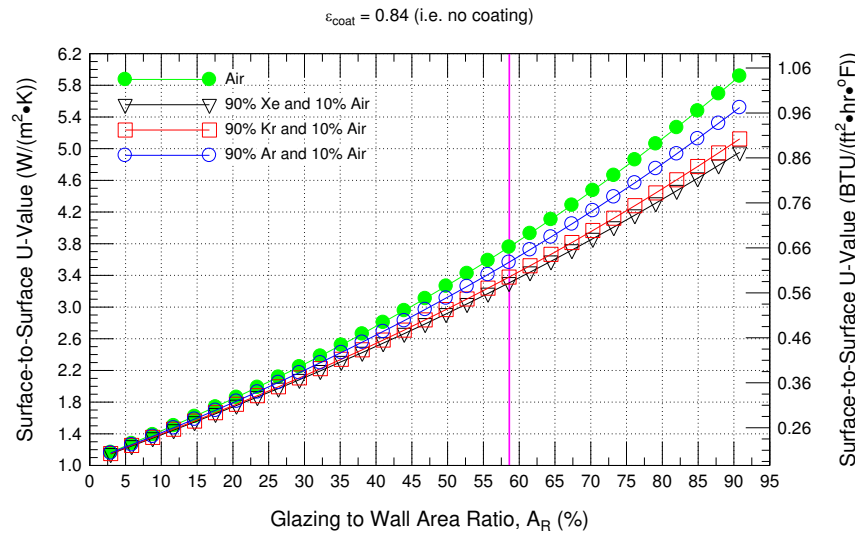
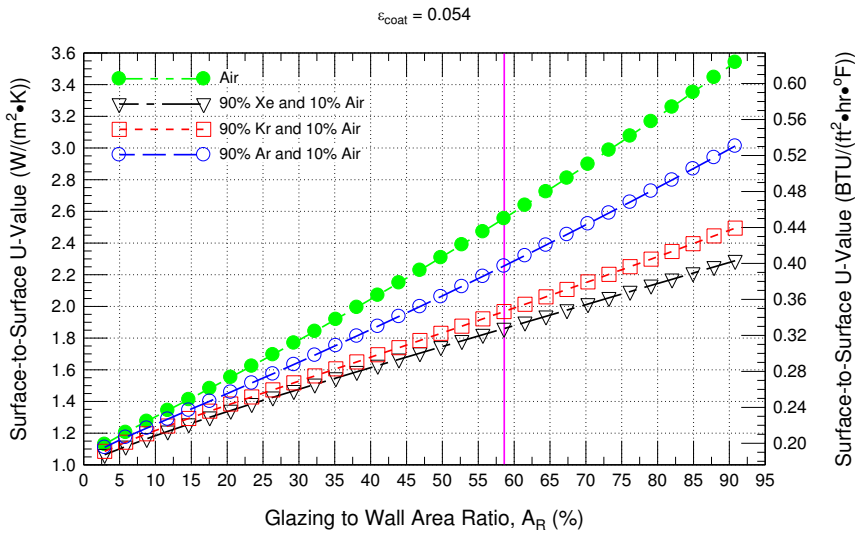
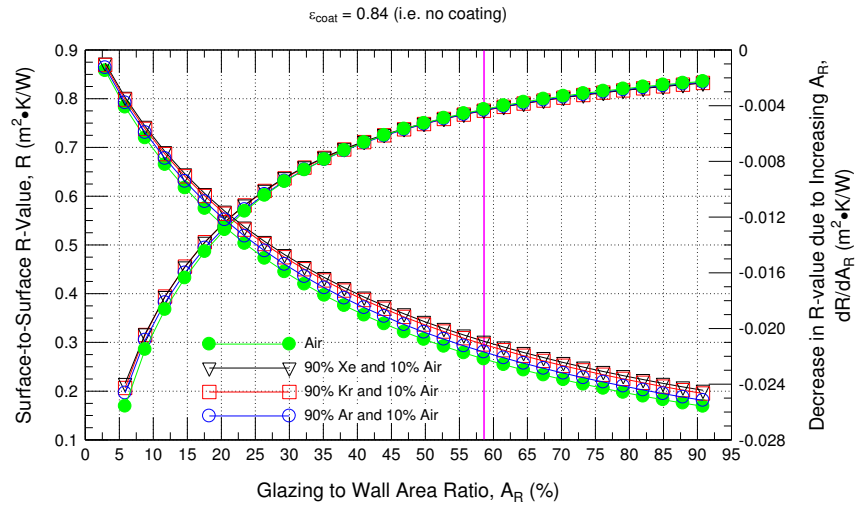
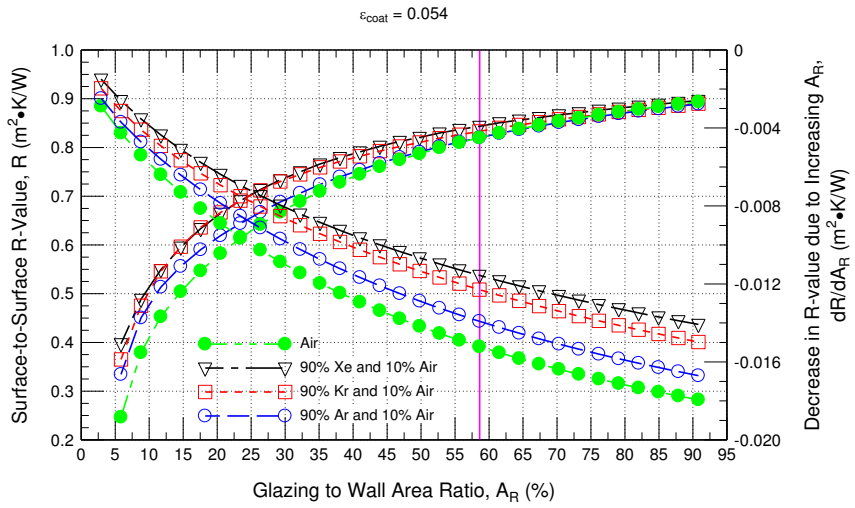


Figure 33 – Predicted (by simulation) R-value (surface-to-surface) of double-glazed low-e coated ($e = 0.054$) thermally broken curtain wall in relation to Glazing to Wall Area Ratio for IGU filled with 100 % Air; 90 % Ar, 10 % Air; 90 % Kr, 10 % Air; 90 % Xe, 10 % Air

Figure 34 - Predicted (by simulation) R-value (surface-to-surface) of double-glazed low-e coated ($e = 0.054$) thermally broken curtain wall in relation to glazing to Wall Area Ratio for IGU filled with 100 % Air, 90 % Ar, 10 % Air; 90 % Kr, 10 % Air; 90 % Xe, 10 % Air

5.2.1.3 — Effect of changes to Coating emissivity

The effect of changes to coating emissivity on the R-values and corresponding U-values of double-glazed thermally broken NFRC-compliant curtain wall assemblies is elaborated in this section. As well, the influence on the thermal performance of the assembly in relation to the coating emissivity for assemblies incorporating IGUs of different gas type is also examined.

The results derived from simulation for the air-to-air and surface-to-surface R-value and U-value of a double-glazed thermally broken curtain wall assembly in relation to the coating emissivity is provided in Figure 35 to Figure 39.

Simulation results for the R-value (uppermost plot) and U-value (lower-most plot) in relation to the coating emissivity (ϵ_{coat}) of surface 2 of the IGU for a double-glazed curtain wall assembly having an A_R of 0.57, and for which the gas within the IGU was varied, is provided in the initial set of results given in Figure 35 to Figure 38; in the respective 4 figures, starting with Figure 35, the simulation results are given for the IGU incorporating a gas having:

- 90 % Ar and 10 % Air
- 90 % Kr and 10 % Air
- 90 % Xe and 10 % Air
- 100 % Air (Reference value)

From this set of results it is apparent that the R-value (air-to-air, or surface-to-surface) decreases with an corresponding increase in the value of ϵ_{coat} for all of the IGUs simulated, irrespective of the type of gas incorporated in the IGU. The loss in thermal performance with a corresponding increase in value of ϵ_{coat} is completely expected given the increase in transmission of radiation for related increases in emissivity of the glass. The more significant decreases are evidently found for the least performing IGU which is filled with 100% air.

A summary of the effect of changes to coating emissivity on the thermal performance of the double-glazed curtain wall assembly is given in Figure 39. In Figure 39, the rate of change in R-value for a NFRC-compliant double-glazed thermally-broken curtain wall assembly in relation to the emissivity of surface 2 of the IGU is given for IGUs incorporating Air, or combinations of Air and Ar, Xe, or Kr. The vertical line in the plot shows the value of $\epsilon_{\text{coat}} = 0.054$, for which the low- ϵ coating is applied to surface 2. For an IGU having low- ϵ coating, significant changes to thermal performance can arise depending on the type of gas with which the IGU is filled; for $\epsilon_{\text{coat}} = 0.054$ on surface 2 of the IGU, the respective R-values for the curtain wall assembly for which the IGU is filled with air, or mixtures of air and Ar, Kr, or, Xe are: 0.391; 0.445; 0.509; and 0.538 $\text{m}^2 \cdot \text{K}/\text{W}$.

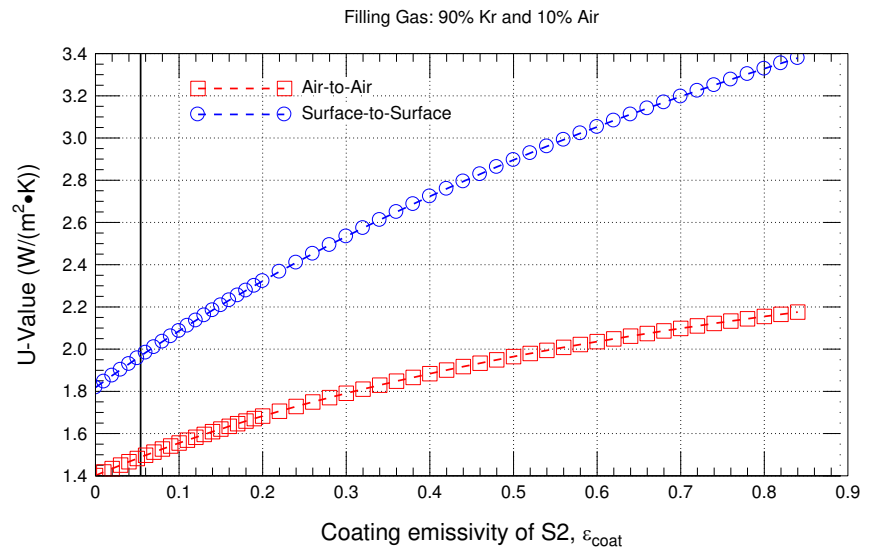
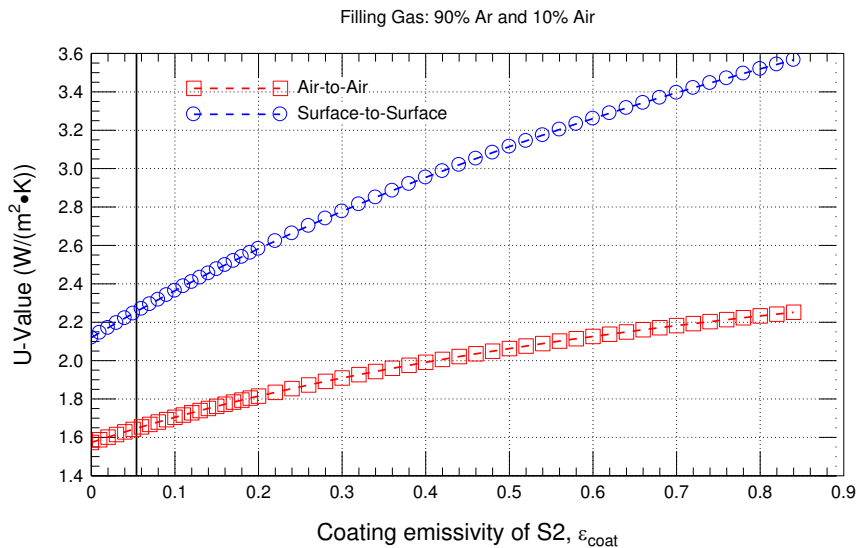
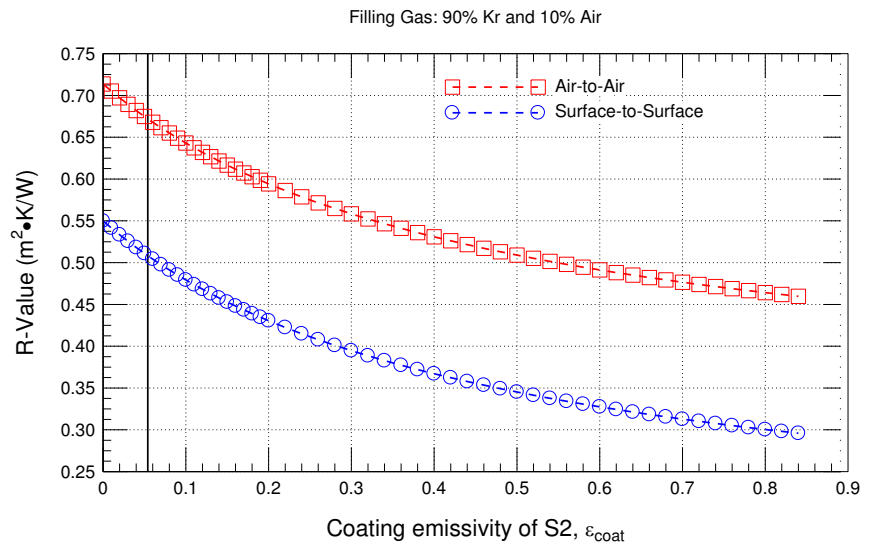
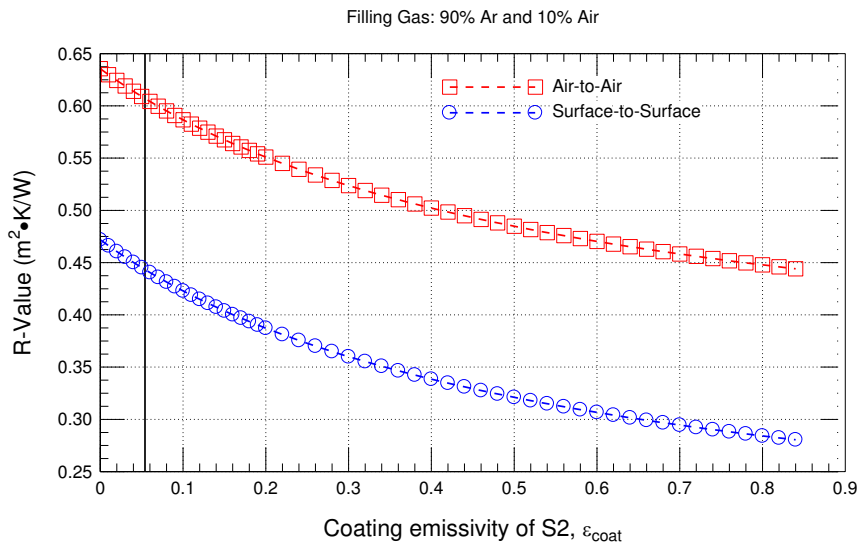


Figure 35 – Predicted (by simulation) R-value (i) ; U-value (ii) (air-to-air; surface-to-surface) of double-glazed, thermally broken curtain wall as a function of coating emissivity for IGU filled with 90% Ar and 10% Air

Figure 36 - Predicted (by simulation) R-value (i) ; U-value (ii) (air-to-air; surface-to-surface) of double-glazed, thermally broken curtain wall as a function of coating emissivity for IGU filled with 90% Kr and 10% Air

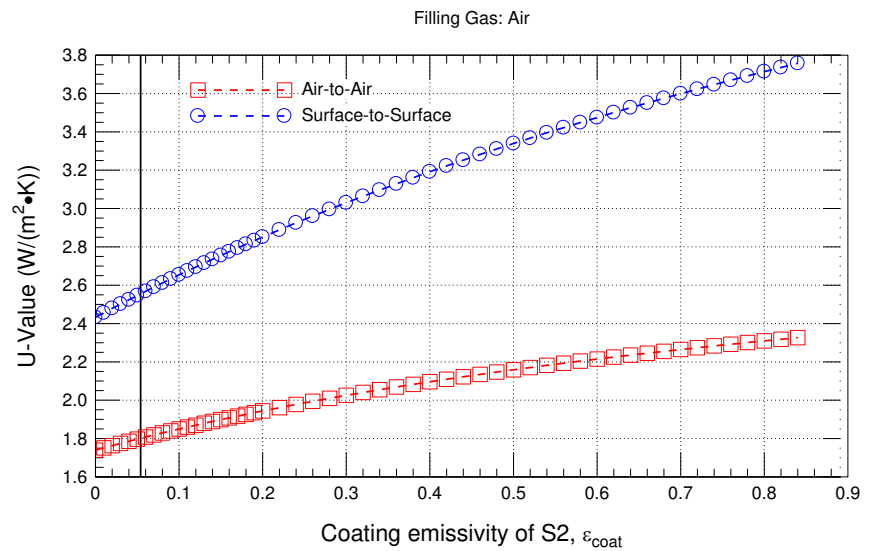
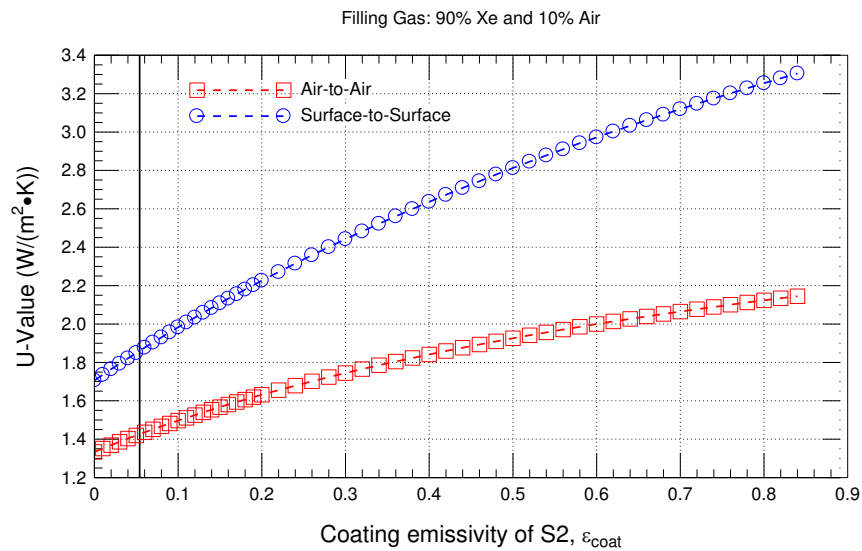
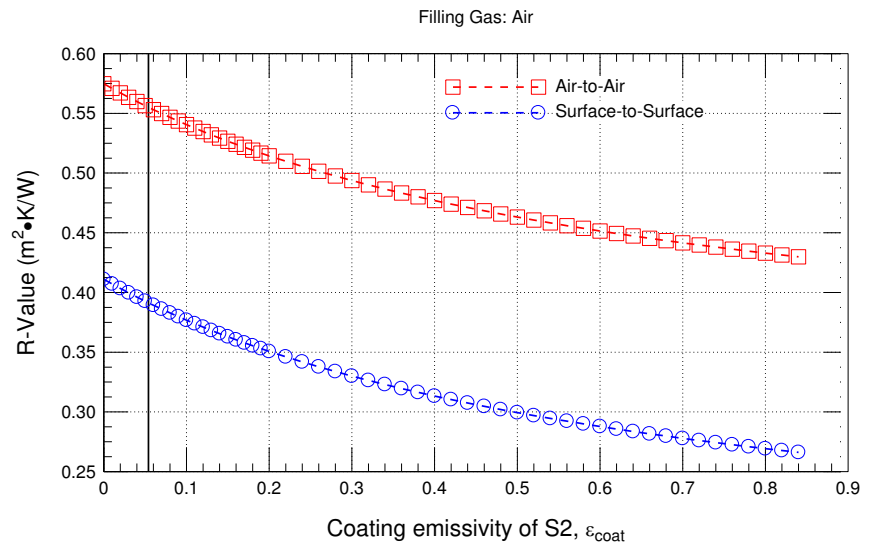
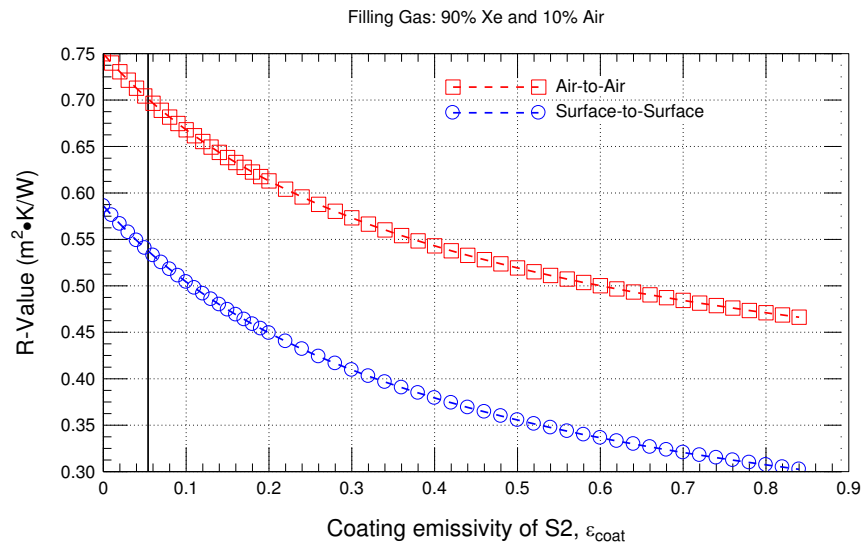


Figure 37 - Predicted (by simulation) R-value (i); U-value (ii) (air-to-air; surface-to-surface) of double-glazed, thermally broken curtain wall as a function of coating emissivity

Figure 38 - Predicted (by simulation) R-value (i) ; U-value (ii) (air-to-air; surface-to-surface) of double-glazed, thermally broken curtain wall as a function of coating emissivity

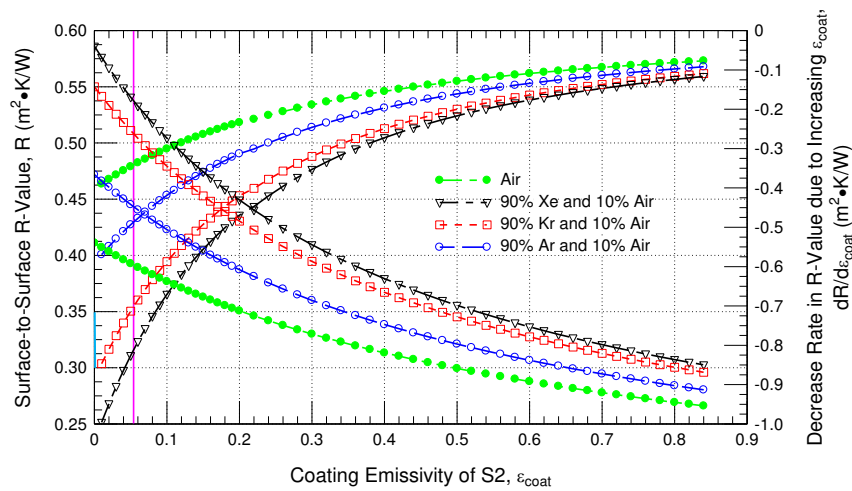


Figure 39 – Predicted (by simulation) (i) R-value (surface-to-surface) as a function of coating emissivity (surface S2) and; (ii) rate of change in R-value in relation to emissivity for a NFRC-compliant, thermally-broken Curtain Wall, with a double-glazed, Air-, Ar-, Xe-, or Kr-filled IGU

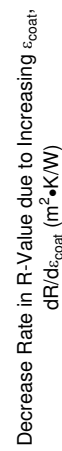


Figure 40 – Predicted (by simulation) (i) U-value (surface-to-surface) as a function of coating emissivity (surface S2) and; (ii) rate of change in U-value in relation to emissivity for a NFRC-compliant, thermally-broken Curtain Wall, with a double-glazed, Air-, Ar-, Xe-, or Kr-filled IGU

5.2.1.4 — *The effect of thermal resistance of the spandrel panel insulation*

The effect of thermal resistance of the spandrel panel insulation on the R-values and corresponding U-values of double-glazed thermally broken NFRC-compliant curtain wall assemblies is elaborated in this section. As well, the influence on the thermal performance of double-glazed curtain wall assemblies is also examined in relation to the different gases with which the IGUs are filled and that include Ar, Kr, Xe, and air; this portion also includes assessing the thermal performance of assemblies having IGUs that incorporate, or not, a low-e coating.

The results derived from simulation for the air-to-air and surface-to-surface R-value and U-value of a double-glazed thermally broken curtain wall assembly in relation to the spandrel panel insulation is provided in Figure 41 to Figure 46.

Simulation results for the R-value (uppermost plot) and U-value (lower-most plot) in relation to the spandrel panel thermal resistance ($\text{m}^2 \cdot \text{K}/\text{W}$) for a double-glazed curtain wall assembly having an A_R of 0.57, and for which the gas within the IGU was varied, is provided in the initial set of results given in Figure 41 to Figure 44; in the respective 4 figures, starting with Figure 41, the simulation results are given for the IGU incorporating a gas having:

- 90 % Ar and 10 % Air
- 90 % Kr and 10 % Air
- 90 % Xe and 10 % Air
- 100 % Air (Reference value)

The vertical line in each of the figures gives the R-value of the spandrel panel insulation for the curtain wall assembly as illustrated in Figure 6 and **Figure 10**.

From this set of results it is apparent that the R-value (air-to-air, or surface-to-surface) of the curtain wall assembly increases in relation to corresponding increases in thermal resistance of the spandrel panel although such increases are limited to ca. 10% of the initial and lowest R-value for the spandrel panel. The R-value of assemblies having a low- ϵ coated ($\epsilon = 0.054$) IGU are characteristically greater than the assemblies having a non-coated IGU ($\epsilon = 0.84$) although both assemblies have similar trends over the range of increase in thermal resistance of the spandrel panel. The differences in R-value of the curtain wall assembly increases as relate to the type of IGU (i.e. low- ϵ vs. no low- ϵ) differs depending on the gas which fills the IGU; increase in R-value of the curtain wall assembly were ca. 27%, 38% 49 % and 54%, respectively, for IGUs filled with Air, Ar, Kr, and Xe.

It is to be noted that the values for thermal resistance of the curtain wall, taken for an A_R of ca. 0.57, would not appreciably increase should additional insulation be added to the spandrel panel and thus do not provide a useful avenue for improved overall thermal performance. This is especially evident when reviewing summary results provided in Figure 58 and Figure 59. In Figure 58 is shown the R-value (surface-to-surface) of the same curtain wall assembly having a low-e coated IGU in relation to the thermal resistance of the spandrel panel and for all gases which filled the IGU; whereas Figure 59 provides the same information for an assembly having no low-e coated IGU. In addition, the rate of change in curtain wall R-value to that of the spandrel panel is also provided and for each type of IGU. The trades are now evident, in that only very small changes in assembly R-value can be expected for corresponding changes in spandrel R-value and these are in the order of 1%, or less, for enhancements to the thermal resistance of the spandrel panel beyond the vertical line that delineates the R-value for the spandrel panel of the manufactured product.

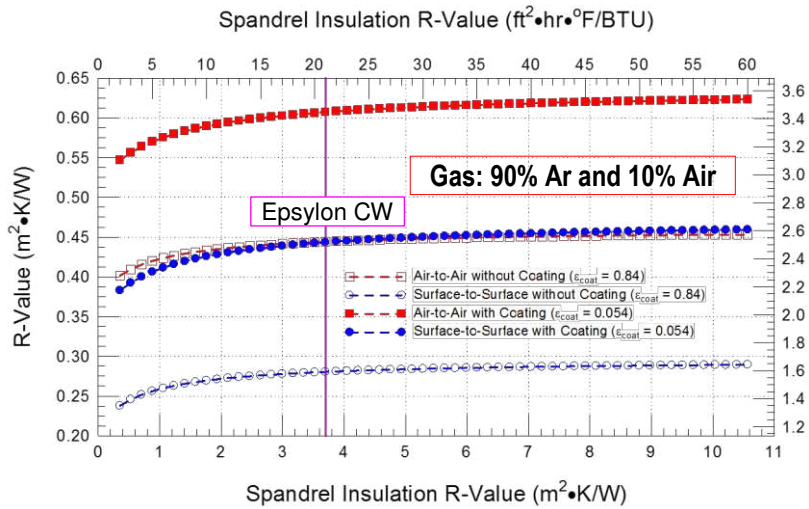


Figure 41 – Predicted (by simulation) (i) R-value and (ii) U-value (air-to-air; surface-to-surface) as a function of Spandrel panel insulation for a NFRC-compliant, thermally-broken double-glazed Ar-filled IGU curtain wall assembly with and without low-e coating on surface 2

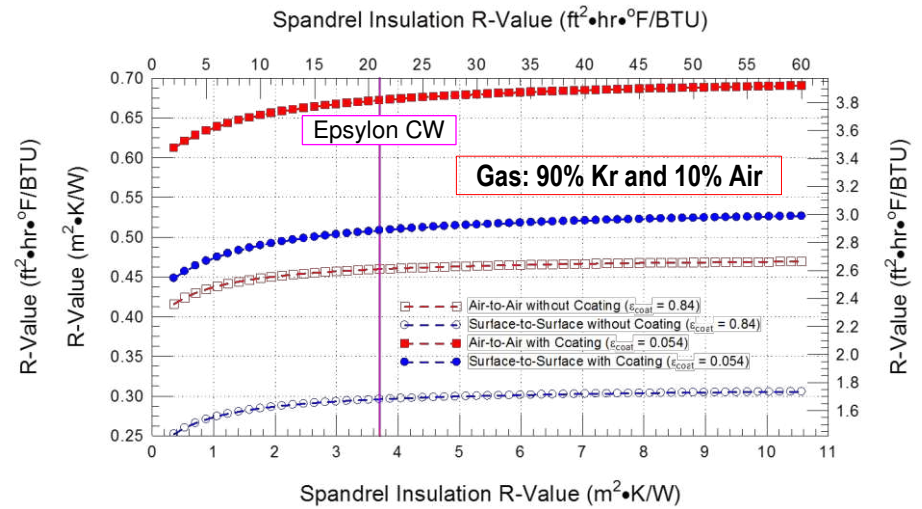


Figure 42 – Predicted (by simulation) (i) R-value and (ii) U-value (air-to-air; surface-to-surface) as a function of Spandrel panel insulation for a NFRC-compliant, thermally-broken double-glazed Kr-filled IGU curtain wall assembly with and without low-e coating on surface 2

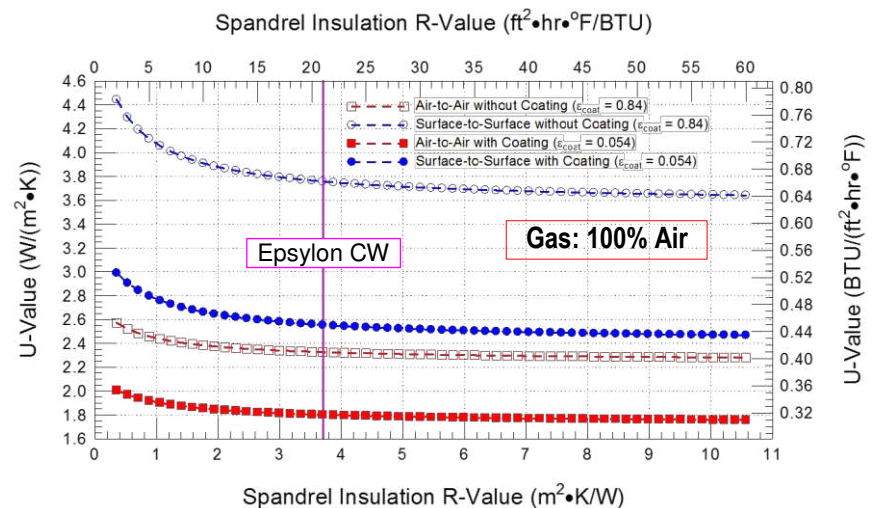
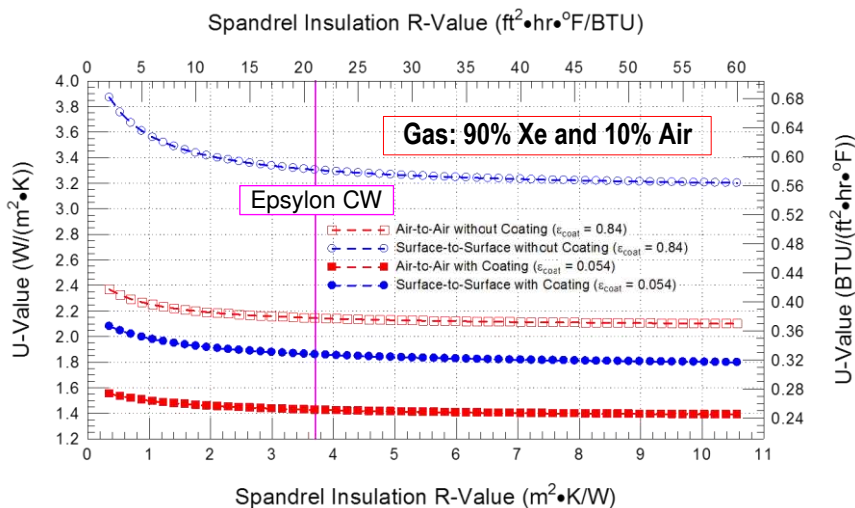
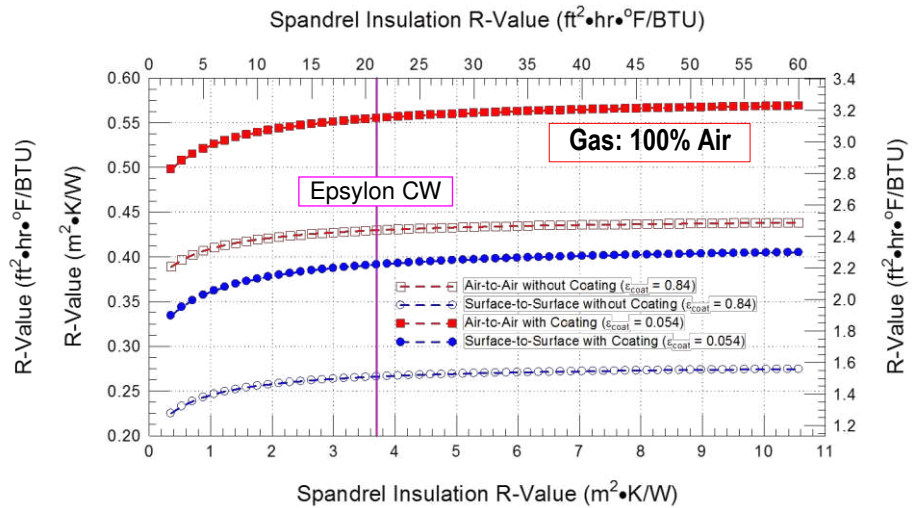
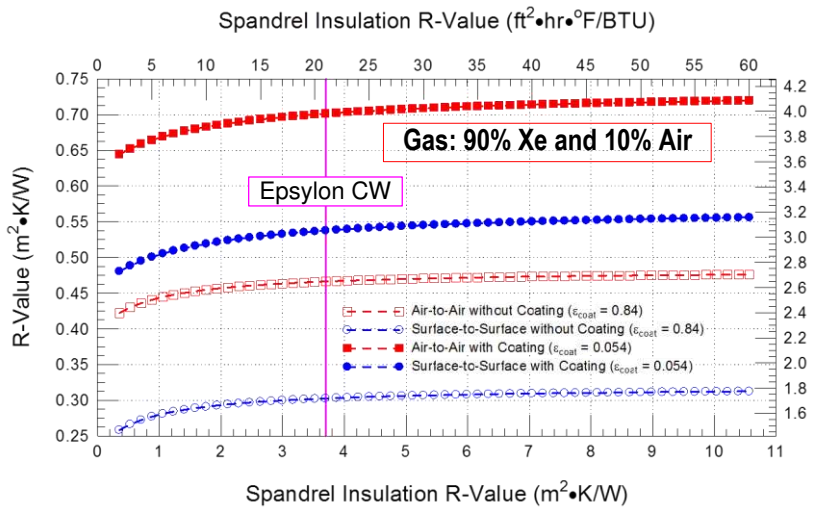


Figure 43 – Predicted (by simulation) (i) R-value and (ii) U-value (air-to-air; surface-to-surface) as a function of Spandrel panel insulation for a NFRC-compliant, thermally-broken double-glazed Xe-filled IGU curtain wall assembly with and without low-e coating on surface 2

Figure 44 – Predicted (by simulation) (i) R-value and (ii) U-value (air-to-air; surface-to-surface) as a function of Spandrel panel insulation for a NFRC-compliant, thermally-broken double-glazed Air filled IGU curtain wall assembly with and without low-e coating on surface 2

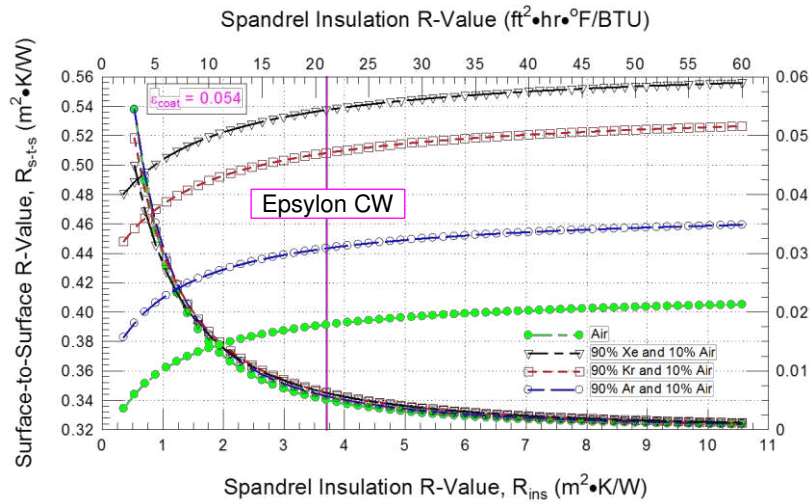


Figure 45 – Predicted (by simulation) (i) R-value and (ii) U-value (air-to-air; surface-to-surface) as a function of Spandrel panel insulation for a NFRC-compliant, thermally-broken double-glazed curtain wall assembly incorporating an IGU with low-ε coating (surface 2) and filled with either Ar, Kr, Xe, or Air

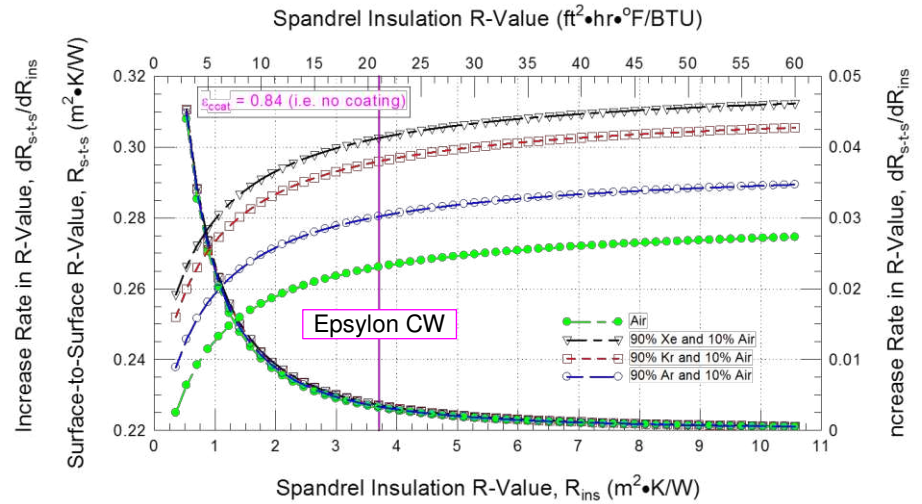
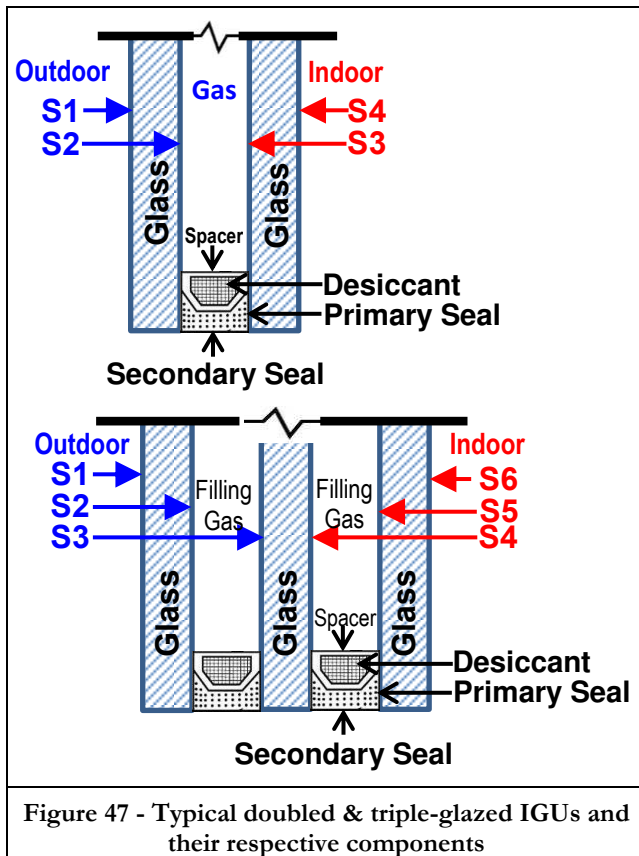


Figure 46 – Predicted (by simulation) (i) R-value and (ii) U-value (air-to-air; surface-to-surface) as a function of Spandrel panel insulation for a NFRC-compliant, thermally-broken double-glazed curtain wall assembly incorporating an IGU without low-ε coating (surface 2) and filled with either Ar, Kr, Xe, or Air

5.2.1.5 — The effect of IGU spacer thermal properties

The effect of the IGU spacer thermal properties on the R-values and corresponding U-values of double-glazed thermally broken NFRC-compliant curtain wall assemblies is elaborated in this section. As well, the influence on the thermal performance of double-glazed curtain wall assemblies is also examined in relation to the different gases with which the IGUs are filled and that include Ar, Kr, Xe, and air; this section also includes assessing the thermal performance of assemblies having IGUs that incorporate, or not, a low- ϵ coating.

Typical doubled and triple-glazed units and their respective IGU components are shown in Figure 47. The spacer configuration for both the double- and triple IGUs were modelled in such a fashion that the depth and height of the spacer and seals (primary and secondary) was consistent with actual product configurations but when completing the simulations, the thermal conductivity of this area varied from 0.1 to 2 W/m·K.. As such, spacer configurations resulting in different values of thermal conductivity were taken into consideration in the modelling. The information provided in Figure 47 in the uppermost schematic is pertinent to this section, whereas, information provided in the lower most schematic is pertinent to the simulation results given in § 5.2.2.5.



In this section, the results derived from simulation for the air-to-air and surface-to-surface R-value and U-value of a double-glazed thermally broken curtain wall assembly in relation to the thermal conductivity of the IGU spacer are provided in Figure 48 to Figure 53.

Simulation results for the R-value (uppermost plot) and U-value (lower-most plot) in relation to the thermal conductivity of the IGU spacer (W/m·K) for a double-glazed curtain wall assembly having an A_R of 0.57, and for which the gas within the IGU was varied, is provided in the initial set of results given in Figure 48 to Figure 51; in the respective 4 figures, starting with Figure 48, the simulation results are given for the IGU incorporating a gas having:

- 90 % Ar and 10 % Air
- 90 % Kr and 10 % Air
- 90 % Xe and 10 % Air
- 100 % Air (Reference value)

From this set of results it is apparent that the R-value (air-to-air, or surface-to-surface) of the curtain wall

assembly decreases in relation to corresponding increases in thermal conductivity of the IGU spacer although such decreases over the range of values for spacer thermal conductivity (i.e.) are limited to ca. 11-15% of the initial and lowest value for thermal conductivity of the IGU spacer. The R-value of assemblies having a low- ϵ ($\epsilon = 0.054$) IGU are characteristically greater than the assemblies having a non-coated IGU ($\epsilon = 0.84$) although both assemblies have similar trends over the range of reduction in thermal conductivity of the IGU

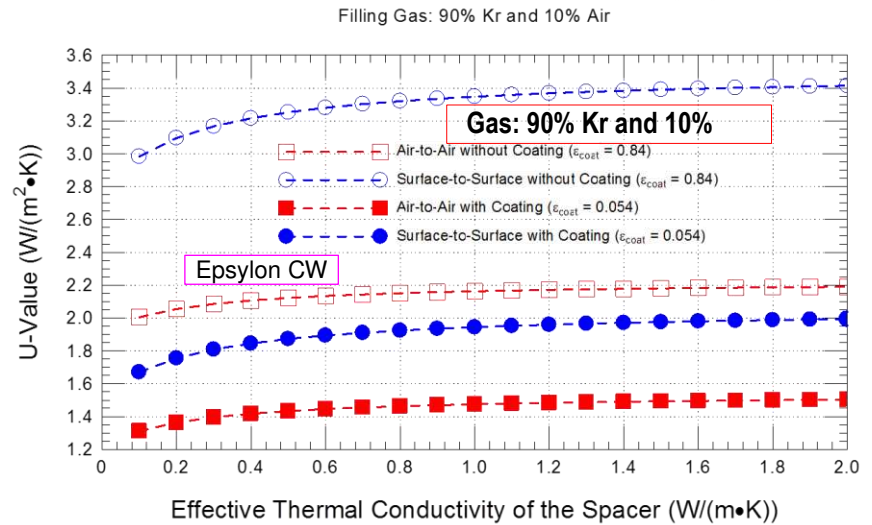
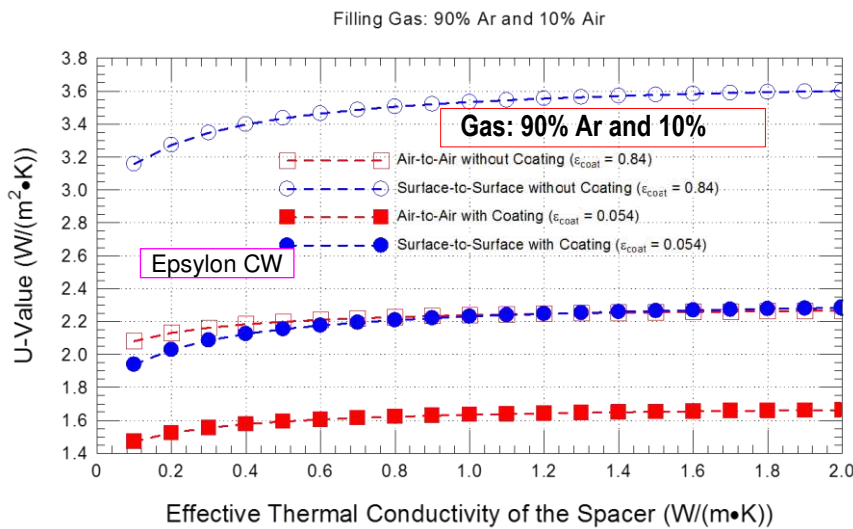
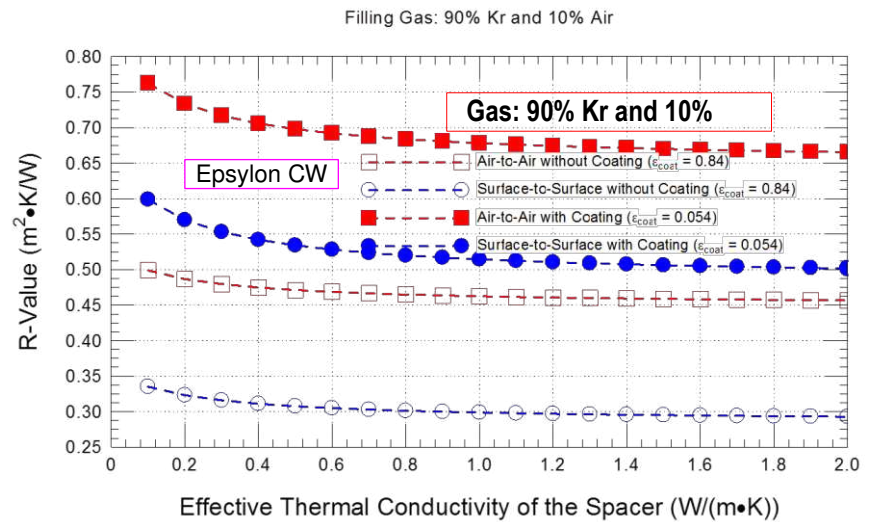
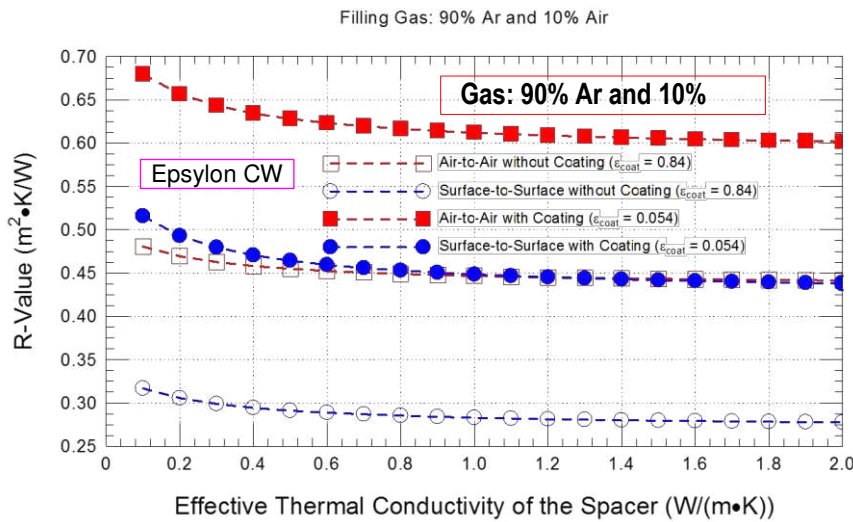


Figure 48 – Predicted (by simulation) (i) R-value and (ii) U-value (air-to-air; surface-to-surface) as a function of thermal conductivity of spacer for a NFRC-compliant, thermally-broken double-glazed Ar-filled IGU curtain wall assembly with and without low-e coating on surface 2

Figure 49 – Predicted (by simulation) (i) R-value and (ii) U-value (air-to-air; surface-to-surface) as a function of thermal conductivity of spacer for a NFRC-compliant, thermally-broken double-glazed Kr-filled IGU curtain wall assembly with and without low-e coating on surface 2

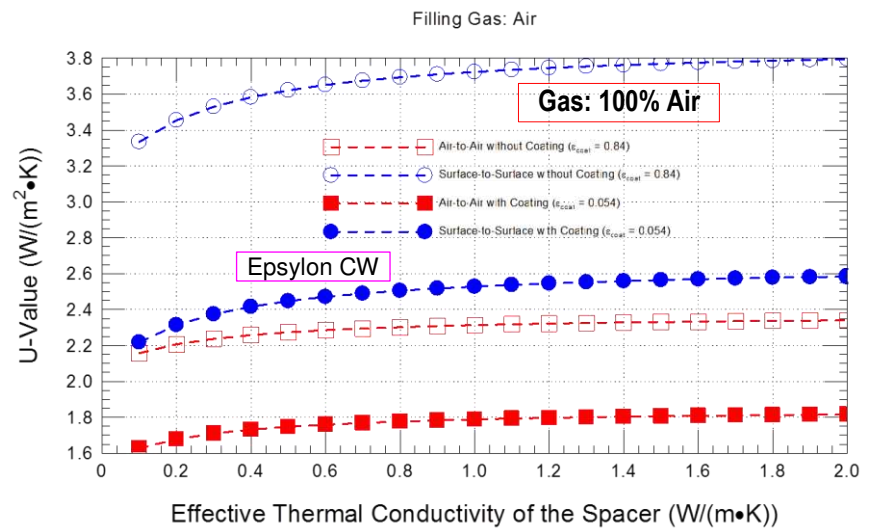
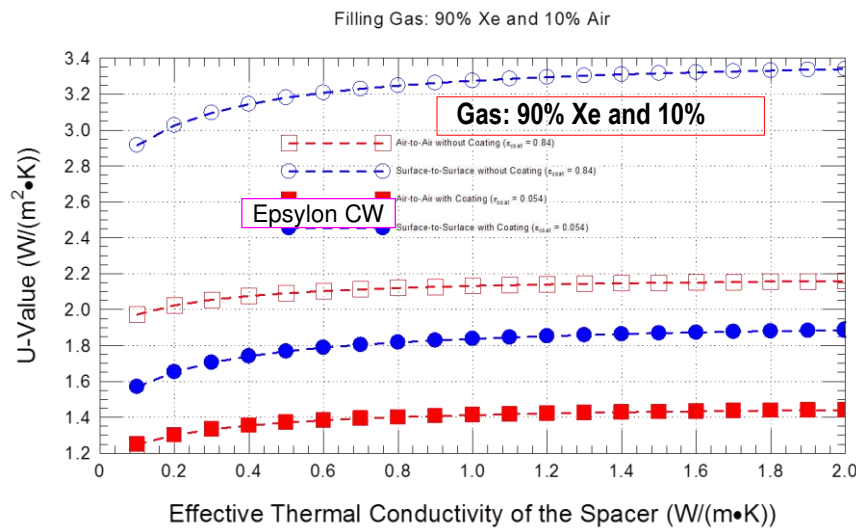
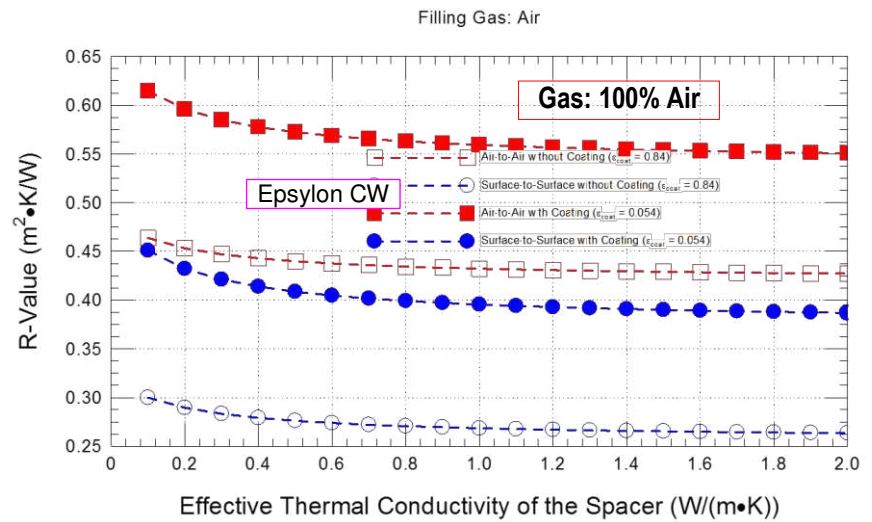
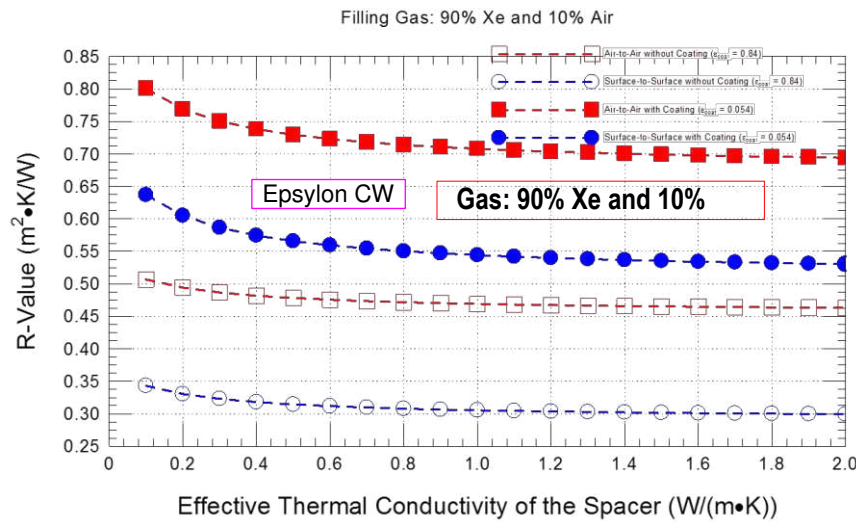


Figure 50 – Predicted (by simulation) (i) R-value and (ii) U-value (air-to-air; surface-to-surface) as a function of thermal conductivity of spacer for a NFRC-compliant, thermally-broken double-glazed Xe-filled IGU curtain wall assembly with and without low-e coating on surface 2

Figure 51 – Predicted (by simulation) (i) R-value and (ii) U-value (air-to-air; surface-to-surface) as a function of thermal conductivity of spacer for a NFRC-compliant, thermally-broken double-glazed Air filled IGU curtain wall assembly with and without low-e coating on surface 2

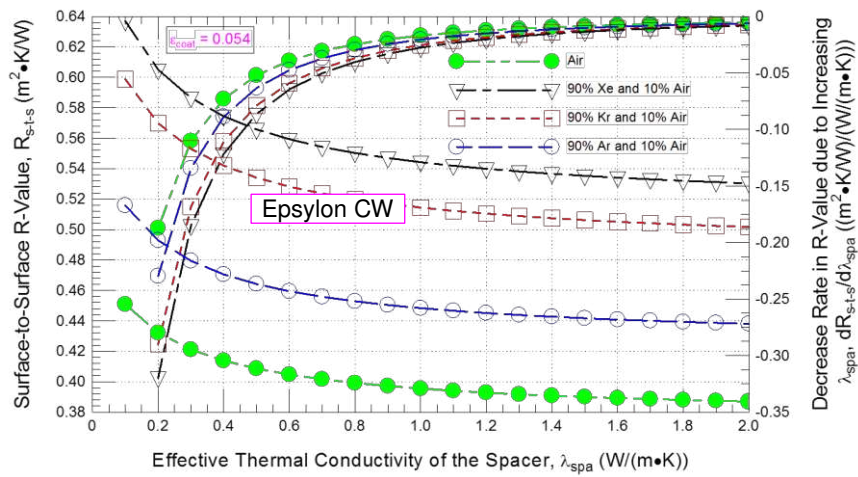


Figure 52 – Predicted (by simulation) R-value (surface-to-surface) as a function of thermal conductivity of Spacer for a NFRC-compliant, thermally-broken double-glazed curtain wall assembly incorporating an IGU with low- ϵ coating ($\epsilon = 0.054$; surface 2) and filled with either Ar, Kr, Xe, or Air

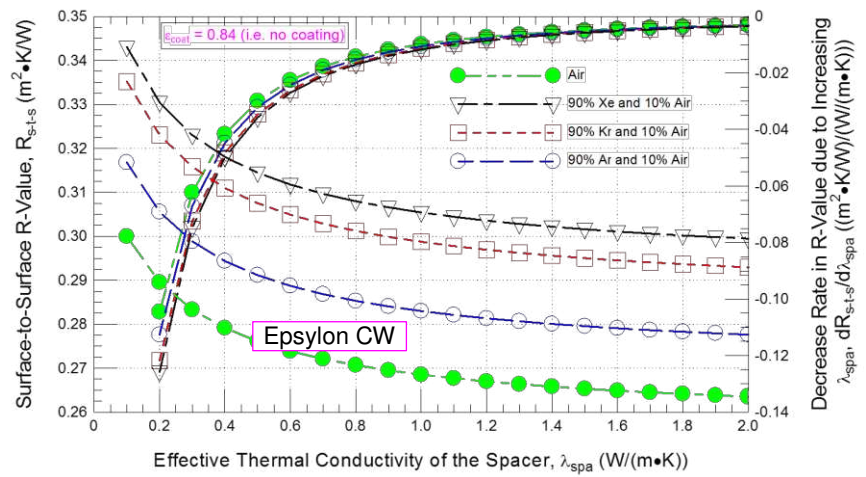


Figure 53 – Predicted (by simulation) (i) R-value (surface-to-surface) as a function of thermal conductivity of Spacer for a NFRC-compliant, thermally-broken double-glazed curtain wall assembly incorporating an IGU without low- ϵ coating and filled with either Ar, Kr, Xe, or Air

spacer. The differences in R-value of the curtain wall assembly as relates to the type of IGU (i.e. low- ϵ vs. no low- ϵ) differs depending on the gas which fills the IGU; decrease in R-value of the curtain wall assembly were ca. 27%, 38% 49 % and 54%, respectively, for IGUs filled with Air, Ar, Kr, and Xe.

It is to be noted that the values for thermal resistance of the curtain wall, taken for an A_R of ca. 0.57, would not appreciably increase should additional insulation be added to the spandrel panel and thus do not provide a useful avenue for improved overall thermal performance. This is especially evident when reviewing summary results provided in and Figure 58 and Figure 59. In Figure 58 is shown the R-value (surface-to-surface) of the same curtain wall assembly having a low-e coated IGU in relation to the thermal resistance of the spandrel panel and for all gases which filled the IGU; whereas Figure 59 provides the same information for an assembly having no low-e coated IGU. In addition, the rate of change in curtain wall R-value to that of the spandrel panel is also provided and for each type of IGU. The trades are now evident, in that only very small changes in assembly R-value can be expected for corresponding changes in spandrel R-value and these are in the order of 1%, or less, for enhancements to the thermal resistance of the spandrel panel beyond the vertical line that delineates the R-value for the spandrel panel of the manufactured product.

5.2.2 Results for Triple-glazed NFRC-Compliant CW Configurations

Results derived from simulation for the triple-glazed NFRC-compliant curtain wall configurations are provided in terms of the:

- (i.) Risk to the formation of condensation;
- (ii.) effect of glazing to wall-area ratio;
- (iii.) Effect of changes to coating emissivity, and;
- (iv.) Effect of thermal resistance of the spandrel panel insulation
- (v.) Effect of thermal conductivity of the IGU spacer

Results for each of these topics are provided in turn.

5.2.2.1 — Condensation risk:

Results derived from simulation of a triple-glazed thermally broken NFRC-compliant curtain wall assembly for the exterior (i) and interior (ii) surface temperatures and (iii) temperature index, as given in Equation 1, are provided in Figure 60. The triple-glazed Ar filled IGU (i.e. 90% Ar and 10% Air) has a low-e coating on surface 2 ($\epsilon_{\text{coat}} = 0.054$). The range in values for the respective set of results can be found in the scale adjacent to each of the three figures of the assembly, for which can be found that the exterior surface temperature of the assembly ranges between ca. -8 °C and -18 °C, the interior temperature between -1.7 °C and 20.1 °C and the value of the temperature index (I) between 0.42 and 0.98.

Simulated results of temperature difference (ΔT °C) on exterior surface of triple-glazed NFRC-compliant CW are given in Figure 55; in the two plots provided, Option D represents a modified ASHRAE 160 interior RH conditions of 32 %, whereas Option B has the ASHRAE 160 interior RH conditions of 40 %; values of surface temperature difference less than 0 ($\Delta T < 0$ °C) represent locations for risk of condensation.

Finally, the results derived from simulation of the same triple-glazed NFRC-compliant curtain wall assembly and in respect to the temperature differences between the interior surface temperature (T_{Int}) of the assembly and the dew point temperature (T_{Dewpoint}) are given in Figure 56. In Figure 56, the locations for risk to condensation, specifically, where the temperature difference is < 0 have been highlighted in two plots: the one

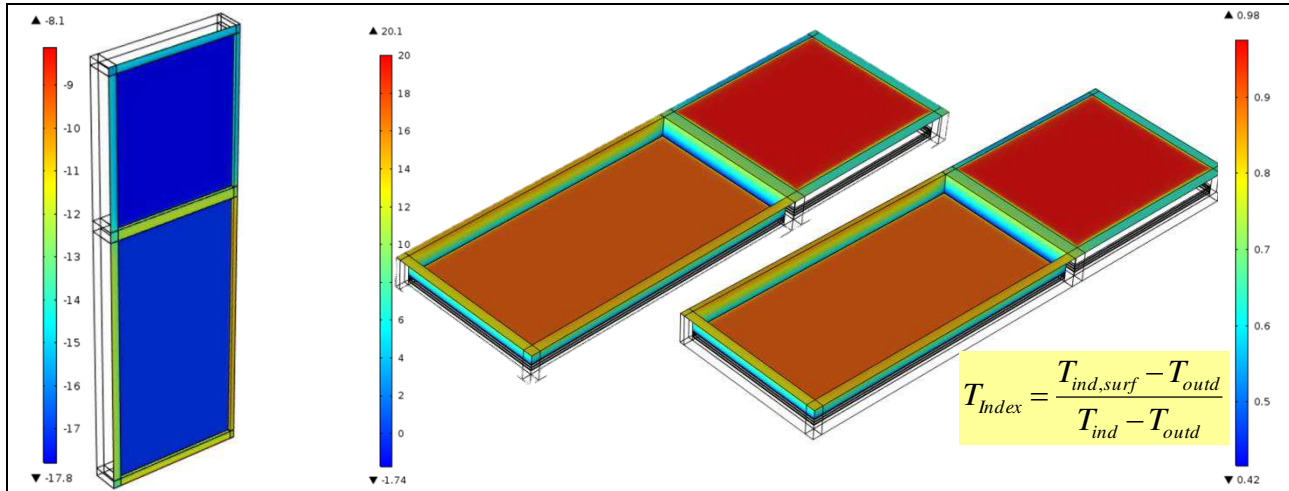


Figure 54 – Simulated exterior (i) & interior (ii) temperature; values of temperature index T_{Index} (iii) of triple-glazed thermally broken NFRC-compliant CW having IGU with 90% Ar & 10% Air; Surface 2, $E_{coat} = 0.054$.

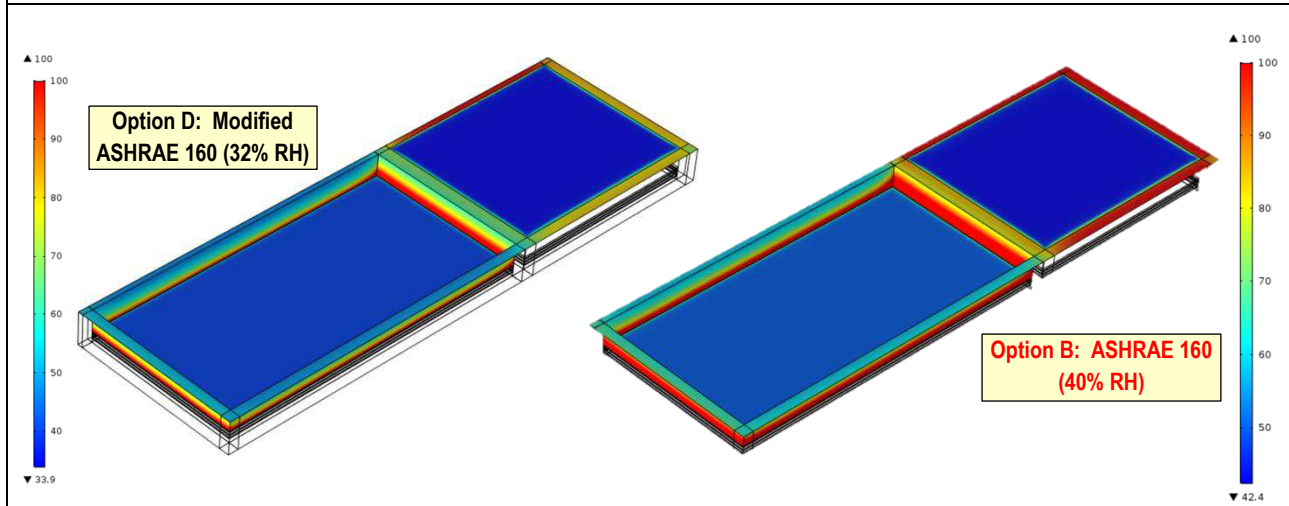


Figure 55 – Simulated results of relative humidity on interior surface of triple-glazed IGU thermally broken NFRC-compliant CW; (i) Option D: Modified ASHRAE 160 (32% RH); (ii) Option B: ASHRAE 160 (40% RH)

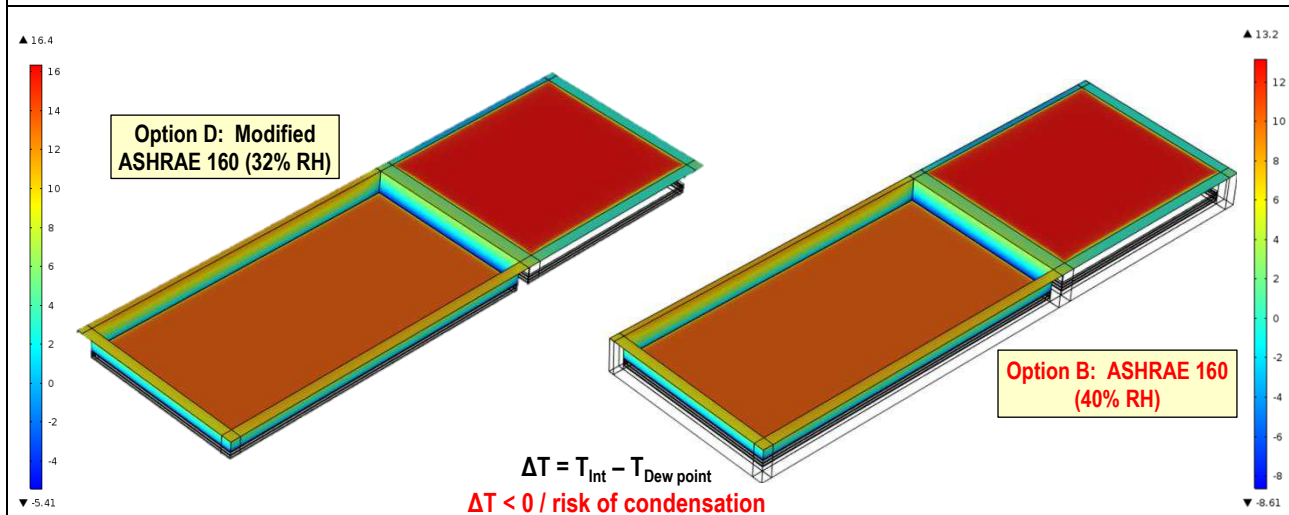


Figure 56 – Simulated results of temperature difference (ΔT °C) on exterior surface of triple-glazed NFRC-compliant CW: (i) Option D: Modified ASHRAE 160 (32% RH); (ii) Option B: ASHRAE 160 (40% RH)

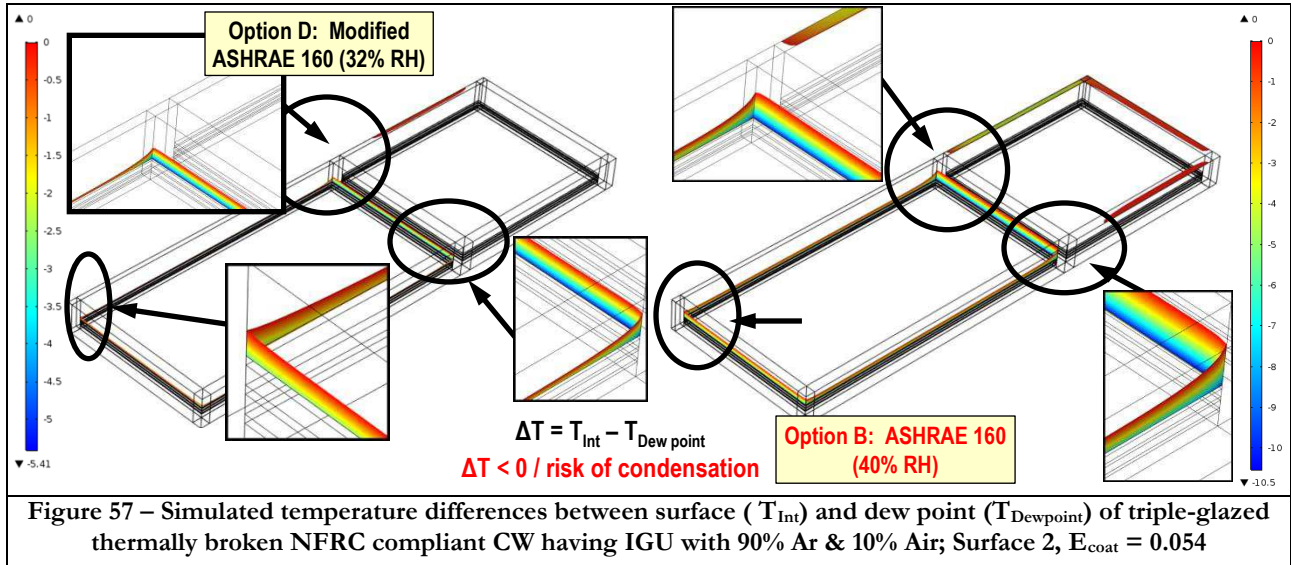


Figure 57 – Simulated temperature differences between surface (T_{Int}) and dew point ($T_{Dewpoint}$) of triple-glazed thermally broken NFRC compliant CW having IGU with 90% Ar & 10% Air; Surface 2, $E_{coat} = 0.054$

on the right-hand side showing locations at risk to condensation where the interior RH is 40 % (Option B); and the other on the left hand side (Option D) representative of interior RH conditions of 32 %. Values of temperature difference (i.e. $\Delta T = T_{Int} - T_{Dewpoint}$) for Option D range between ca. $-5.4\text{ }^{\circ}\text{C}$ and $16.4\text{ }^{\circ}\text{C}$ whereas for Option B between ca. $-8.6\text{ }^{\circ}\text{C}$ and $13.2\text{ }^{\circ}\text{C}$. Values below zero represent locations at risk of formation of condensation. Whichever interior RH conditions used, both show similar locations for the formation on condensation on the assembly, specifically, along frame edges.

Values below zero represent locations at risk of formation of condensation. Whichever interior RH conditions used, both show similar locations for the formation on condensation on the assembly, specifically, along frame edges.

5.2.2.2 — Effect of Glazing to Wall Area Ratio

The effect of glazing to wall-area ratio (window-to-wall ratio / A_R) on the R-value and corresponding U-value of triple-glazed thermally broken NFRC-compliant curtain wall assemblies is elaborated in this section. As well, the influence on the thermal performance of the assembly in relation to the A_R for assemblies incorporating IGUs filled with different gases IGU including, or not, a low-e coating, is also explored.

The results derived from simulation for the air-to-air and surface-to-surface R-value and U-value of a double-glazed thermally broken curtain wall assembly in relation to the glazing to wall area ratio (A_R) is provided in Figure 58 to Figure 67; results are first presented for curtain wall assemblies having low-e coated IGUs and thereafter, for IGUs of higher emissivity.

Thermal performance results for triple-glazed curtain wall assembly with low-e coated IGU—

Simulation results for the R-value (uppermost plot) and U-value (lower-most plot) in relation to the A_R of a double-glazed curtain wall assembly that included a low-e coated IGU ($e = 0.054$; surface 2), and for which the gas within the IGU was varied, is provided in the initial set of results given in Figure 58 to Figure 61; in the respective 4 figures, starting with Figure 58, the simulation results are given for the IGU incorporating a gas having:

- 90 % Ar and 10 % Air
- 90 % Kr and 10 % Air

- 90 % Xe and 10 % Air
- 100 % Air (Reference value)

From this set of results, and as was the case for the double-glazed CW assembly, it is apparent that the R-value (air-to-air, or surface-to-surface) decreases with an corresponding increase in the A_R for all of the IGU simulated, irrespective of the type of gas incorporated in the IGU. As before, the loss in thermal performance with increasing A_R is entirely as might be expected; R-values respectively range between ca. 0.45 to 1.1 $m^2 \cdot K/W$ for the set of assemblies having the low-e IGU and between ca. 0.25 to 1 $m^2 \cdot K/W$ for the CW assemblies having no low-e coated IGU. The more significant decreases are evidently found for the least performing IGU which is filled with 100% air. The respective thermal performance range of the 4 different sets of results in terms of the air-to-air R-value ($m^2 \cdot K/W$) and U-value ($W/m^2 \cdot K$) at 10 % and 90 % A_R are provide in Table 5:

Table 5 - R-value and U-values (air-to-air) of triple-glazed curtain wall assembly incorporating IGUs having different gases at selected glazing to wall-area ratios

IGU gas fill	R-value ($m^2 \cdot K/W$)		U-value ($W/m^2 \cdot K$)	
	10 % A_R	90 % A_R	10 % A_R	90 % A_R
100 % Air (Reference value)	1.075	0.625	0.925	1.625
90 % Ar and 10 % Air	1.125	0.688	0.900	1.475
90 % Kr and 10 % Air	1.150	0.780	0.875	1.325
90 % Xe and 10 % Air	1.175	0.800	0.850	1.250

Thermal performance results for triple-glazed curtain wall assembly with & without low-e IGU—

Simulation results for the R-value (uppermost plot) and U-value (lower-most plot) in relation to the A_R of a double-glazed curtain wall assembly that included an IGU either with or without a low-e surface (i.e. $e=0.054$; surface 2) and for which the gas within the IGU was varied, is provided in this subsequent set of results given in Figure 62 to Figure 65; in the respective 4 figures, starting with Figure 62, the simulation results are given, as for the previous set, for an IGU incorporating a gas having:

- 90 % Ar and 10 % Air
- 90 % Kr and 10 % Air
- 90 % Xe and 10 % Air
- 100 % Air (Reference value)

From this set of results it is evident that the R-value (air-to-air, or surface-to-surface) decreases with an corresponding increase in the A_R for all of the IGUs simulated, irrespective of the type of gas incorporated in the IGU and regardless of whether the low-e coating is applied to the IGU. As well, the R-value (air-to-air, or surface-to-surface) of the low-e coated IGU is characteristically greater than that of the non-coated IGU for any given value of A_R . The loss in thermal performance with increasing in A_R is, as before, entirely as might be expected, whether for an IGU having a low-e glass surface or glass of higher emissivity. However, these losses are more important for IGUs that are not coated and have the higher emissivity glass. The more significant decreases are evidently found for the least performing IGU which is filled with 100% air. The respective thermal performance range of the 4 different sets of results for CW assemblies having the non-coated higher emissivity glass in terms of the air-to-air R-value ($m^2 \cdot K/W$) and U-value ($W/m^2 \cdot K$) at 10 % and 90 % A_R are provided in Table 6:

Table 6 - R-value and U-values (air-to-air) of double-glazed curtain wall assembly at selected glazing to wall-area ratios and incorporating IGUs having different gases and higher emissivity (e = 0.84)

IGU gas fill	R-value (m ² •K/W)		U-value (W/m ² •K)	
	10 % A _R	90 % A _R	10 % A _R	90 % A _R
100 % Air (Reference value)	0.98	0.45	1.05	2.25
90 % Ar and 10 % Air	1.0	0.475	1.0	2.15
90 % Kr and 10 % Air	1.02	0.480	0.95	2.05
90 % Xe and 10 % Air	1.025	0.50	0.90	2.00

Summary of thermal performance results for triple-glazed curtain wall assembly — Results derived from simulation for the surface-to-surface R-value (uppermost plot) and surface-to-surface U-value (lower-most plot) in relation to the A_R of a triple-glazed curtain wall assembly having a low-e coated IGU, and for which the gas within the IGU was varied, is provided in Figure 66; similar sets of plots of thermal performance for the curtain wall assembly having an IGU of higher emissivity (e = 0.84), is given in Figure 67.

The relative thermal performance of the curtain wall assembly in relation to A_R and amongst the different types of IGUs is clearly evident in Figure 66 for the assembly incorporating the low-e IGU; this is much less evident for the assembly with the higher emissivity IGU, as shown in Figure 67. The least performing assembly, irrespective of the emissivity of the glass, was the assembly, having the air filled IGU; the most performing having the Xe filled IGU.

The rate of change, in this instance decreases in R-value, for a corresponding increase in A_R is also provided in the uppermost plot of Figure 66 and Figure 67. The effect is greatest for changes of A_R ranging between 5 and 40%; thereafter, the changes in R-value are less significant for corresponding changes in A_R. The vertical line at A_R = 57% represents the value of A_R of the NFRC compliant curtain wall assembly. It is evident from this information that there is little to be gained in terms of thermal performance for changes in the type of IGU gas for triple-glazed curtain wall assemblies having values of A_R exceeding perhaps 50 %.

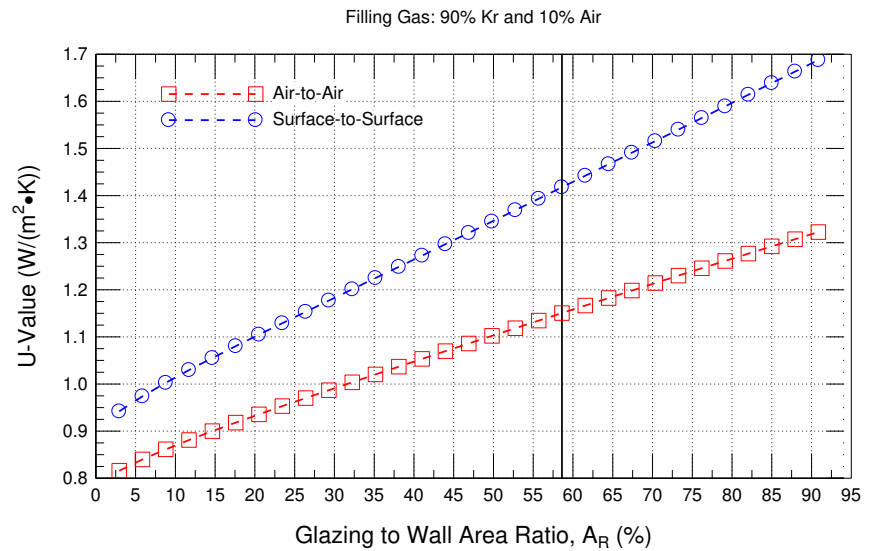
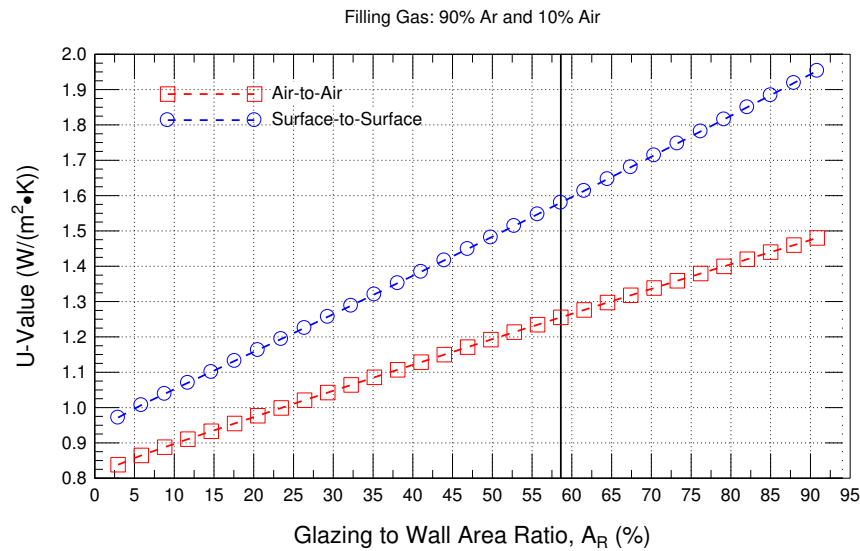
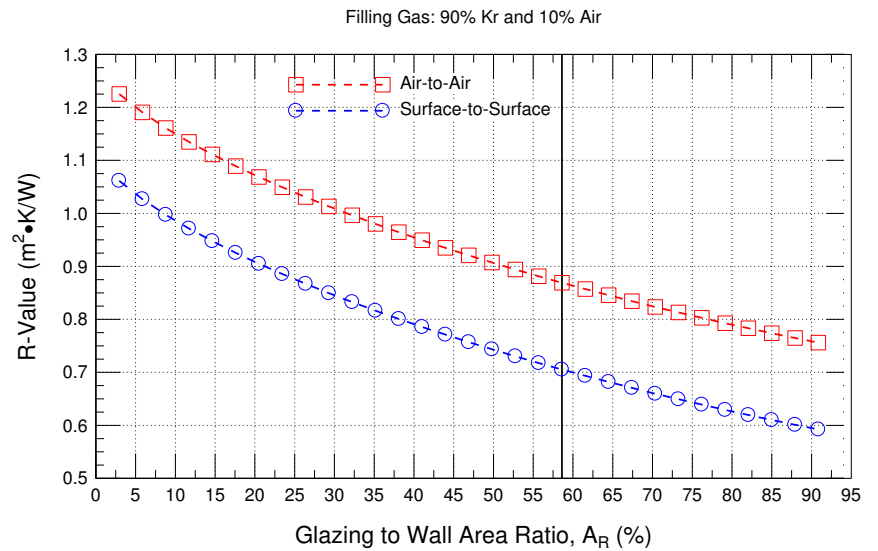
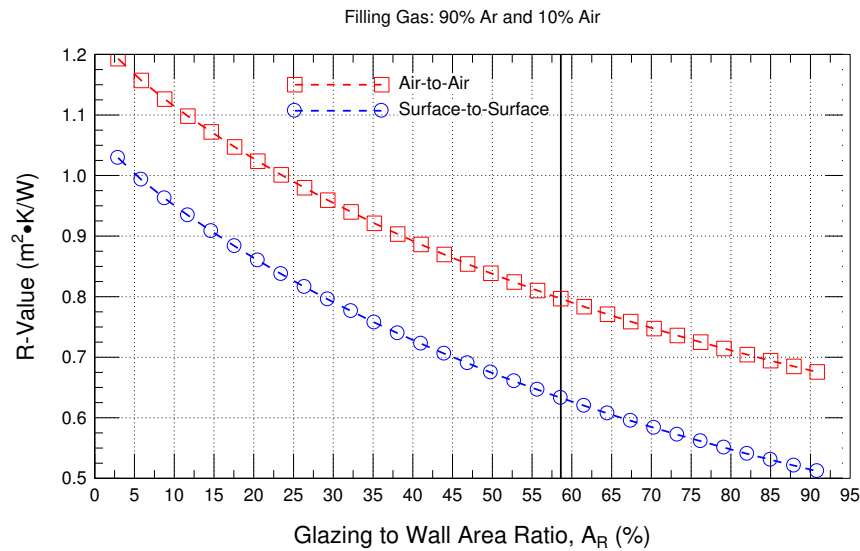


Figure 58 – Predicted (by simulation) (i) R-value and (ii) U-value (air-to-air; surface-to-surface) of triple-glazed low-e ($e = 0.054$) coated thermally broken Curtain Wall in relation to Glazing to Wall Area Ratio for IGU filled with 90 % Ar, 10% Air

Figure 59 – Predicted (by simulation) (i) R-value and (ii) U-value (air-to-air; surface-to-surface) of triple-glazed low-e ($e = 0.054$) coated thermally broken Curtain Wall in relation to Glazing to Wall Area Ratio for IGU filled with 90 % Kr, 10% Air

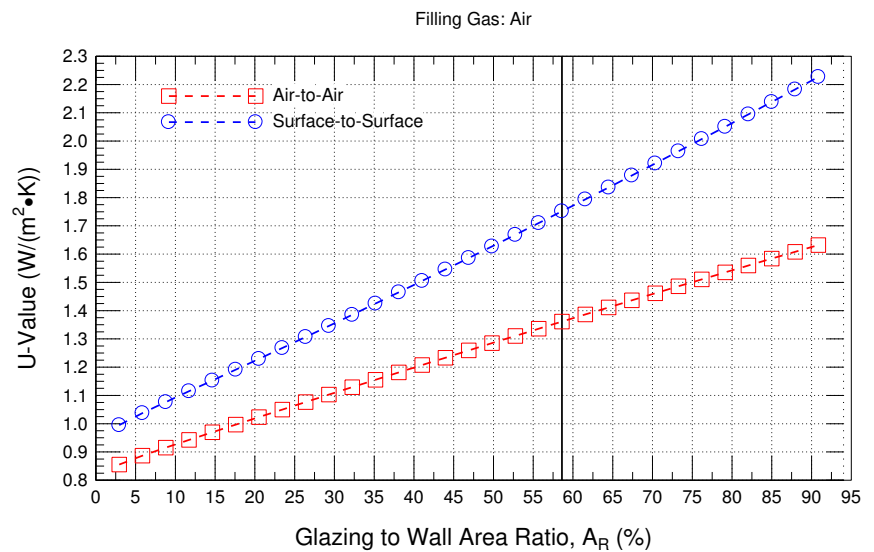
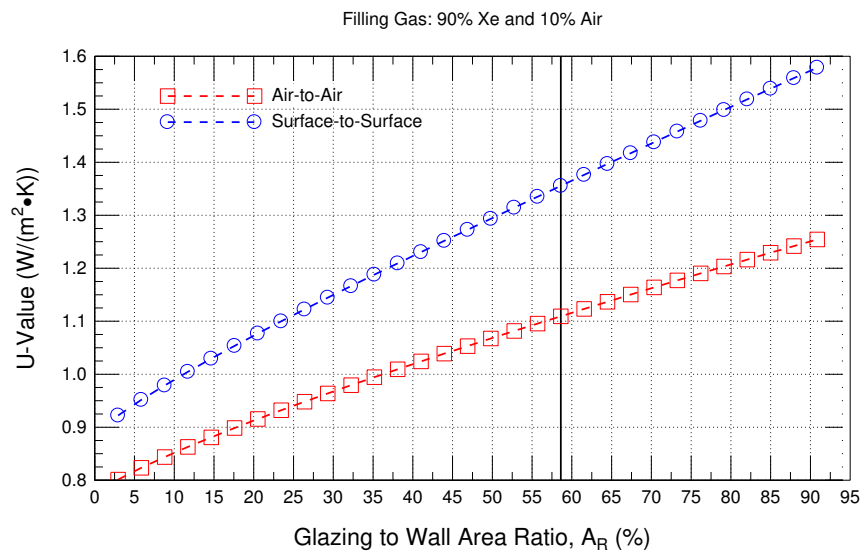
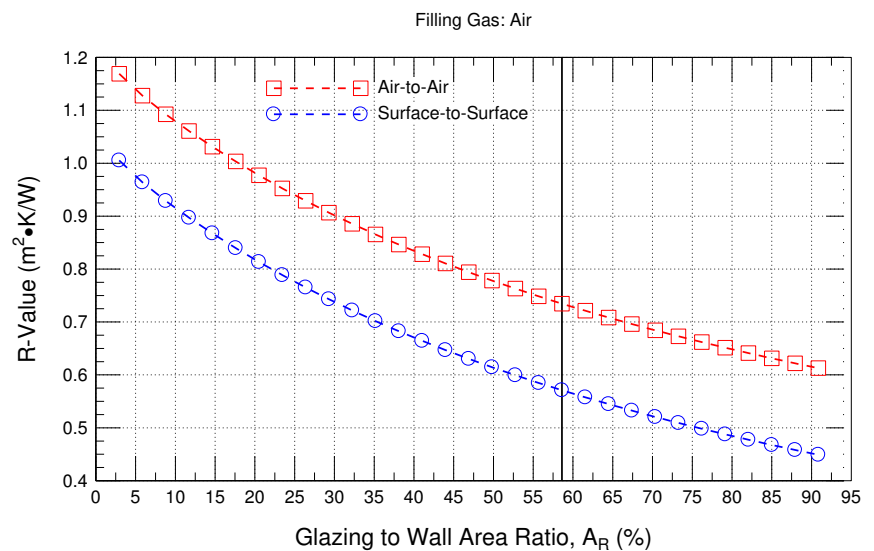
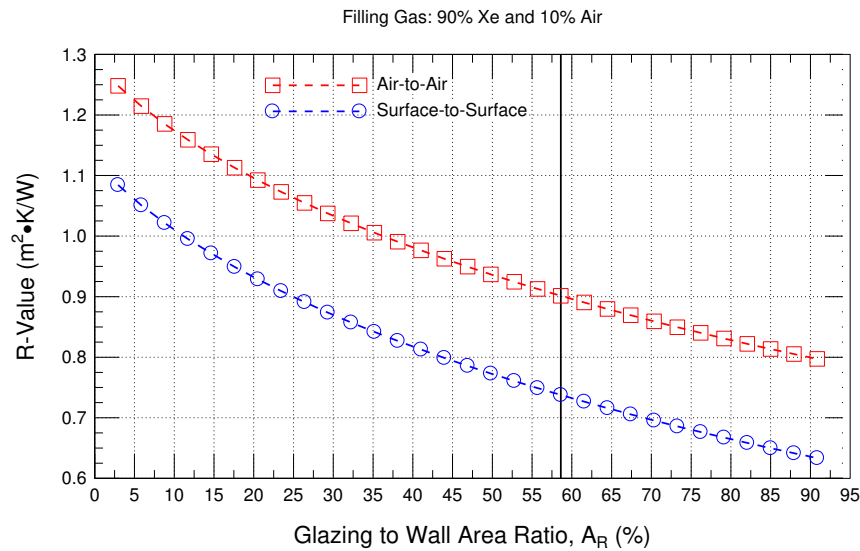


Figure 60 – Predicted (by simulation) (i) R-value and (ii) U-value (air-to-air; surface-to-surface) of triple-glazed low-e ($e = 0.054$) coated thermally broken Curtain Wall in relation to Glazing to Wall Area Ratio for IGU filled with 90 % Xe, 10% Air

Figure 61 – Predicted (by simulation) (i) R-value and (ii) U-value (air-to-air; surface-to-surface) of triple-glazed low-e ($e = 0.054$) coated thermally broken Curtain Wall in relation to Glazing to Wall Area Ratio for IGU filled with 100 % Air

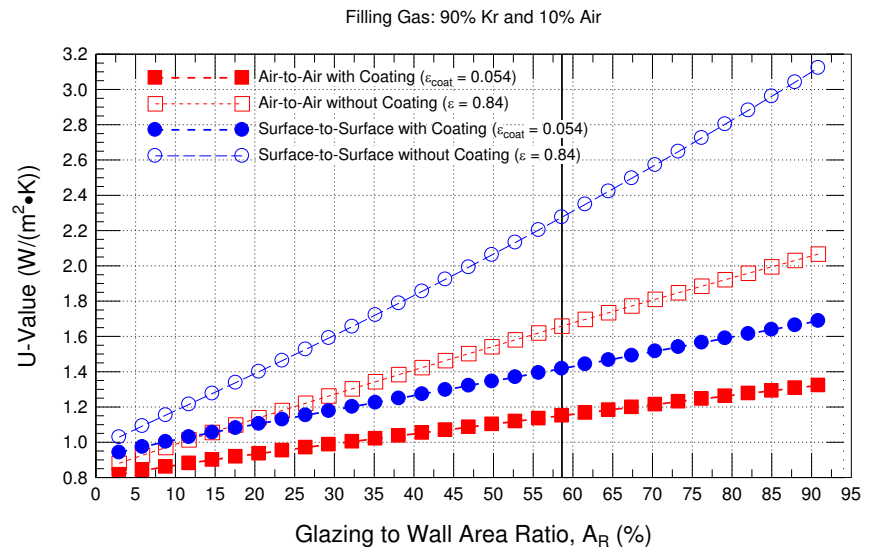
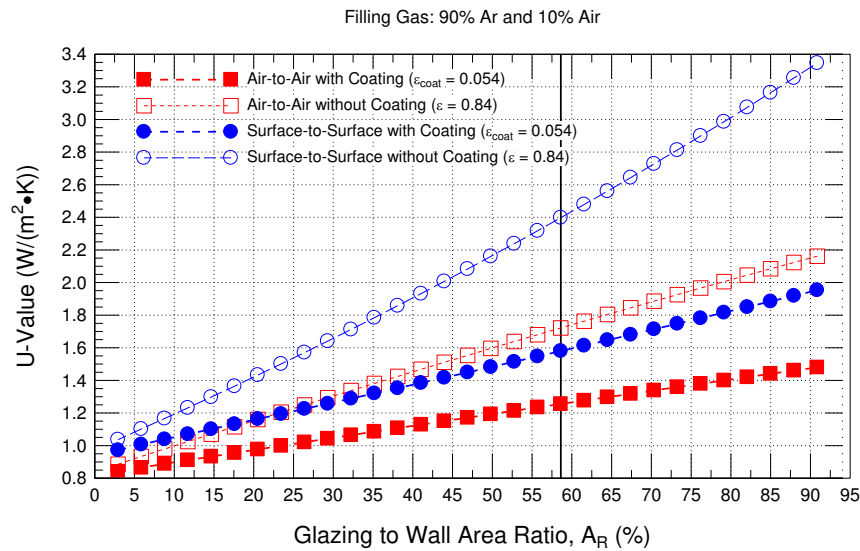
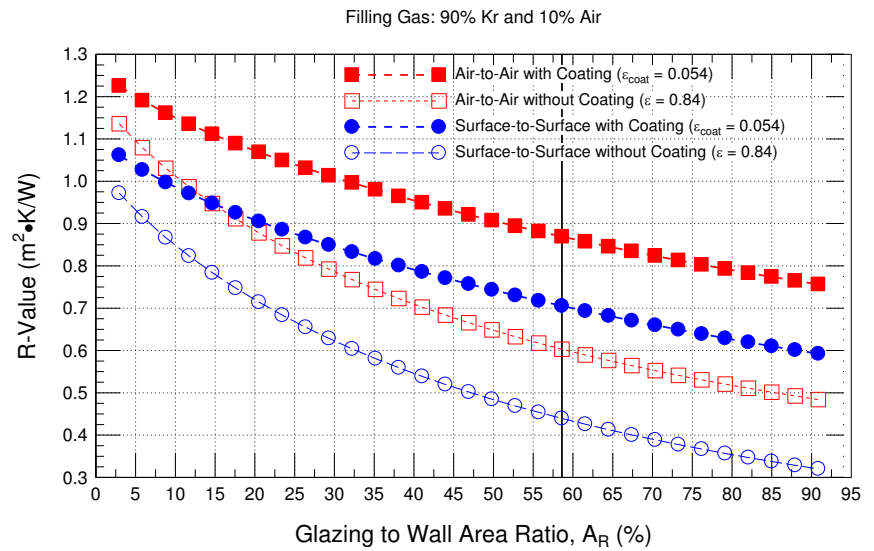
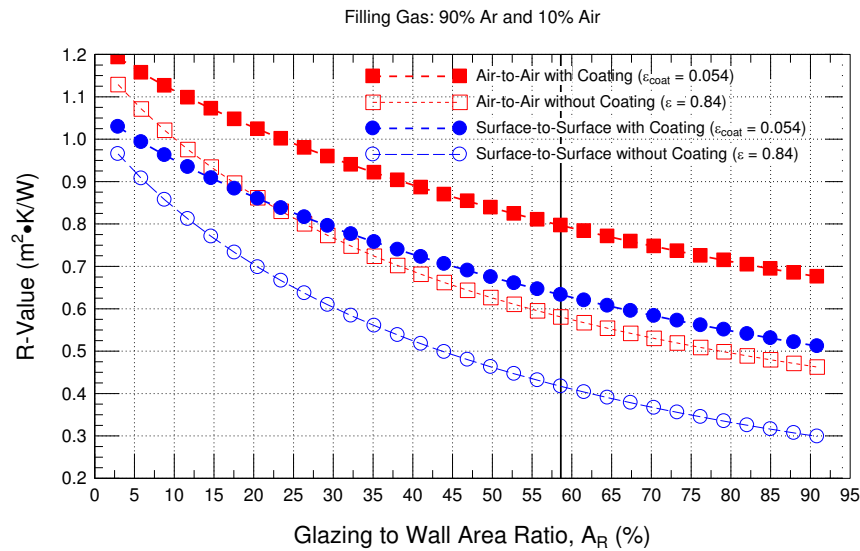


Figure 62 – Predicted (by simulation) (i) R-value and (ii) U-value (air-to-air; surface-to-surface) of triple-glazed low-e ($\epsilon = 0.054$) or no low-e ($\epsilon = 0.84$) coated thermally broken Curtain Wall in relation to Glazing to Wall Area Ratio for IGU filled with 90 % Ar, 10% Air

Figure 63 – Predicted (by simulation) (i) R-value and (ii) U-value (air-to-air; surface-to-surface) of triple-glazed low-e ($\epsilon = 0.054$) or no low-e ($\epsilon = 0.84$) coated thermally broken Curtain Wall in relation to Glazing to Wall Area Ratio for IGU filled with 90 % Kr, 10% Air

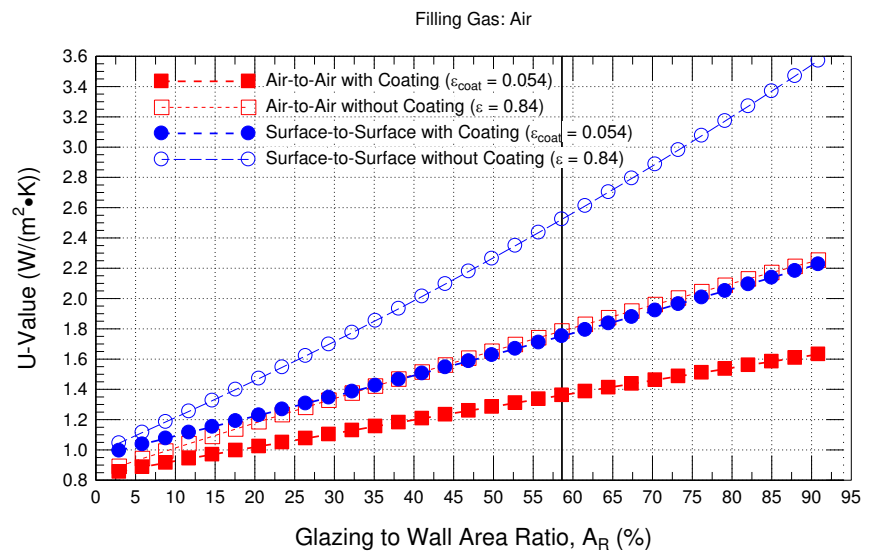
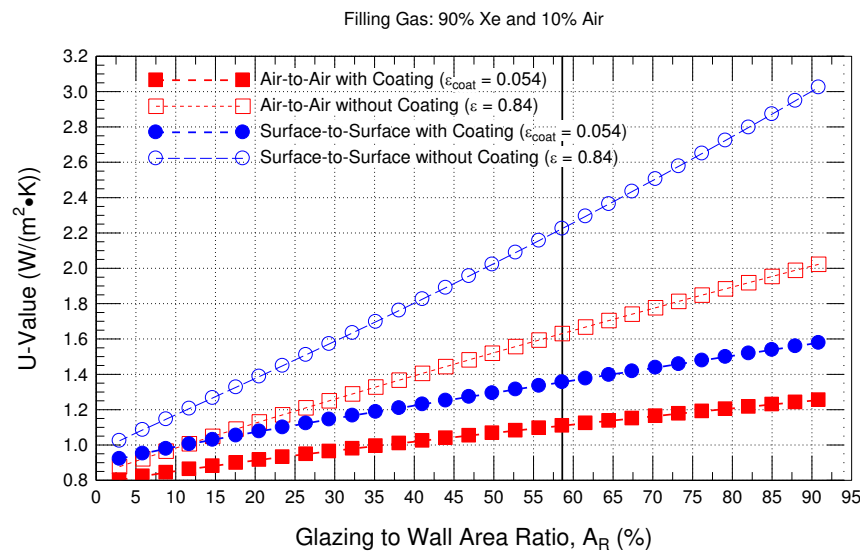
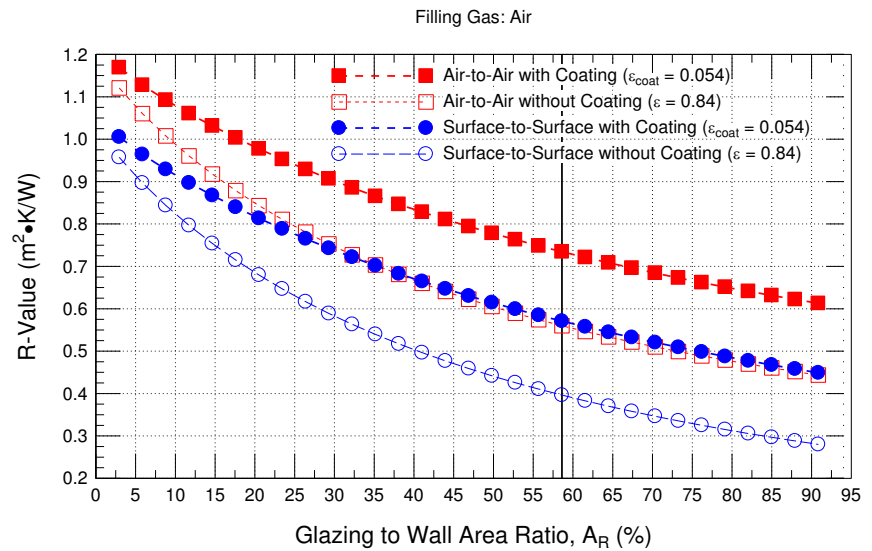
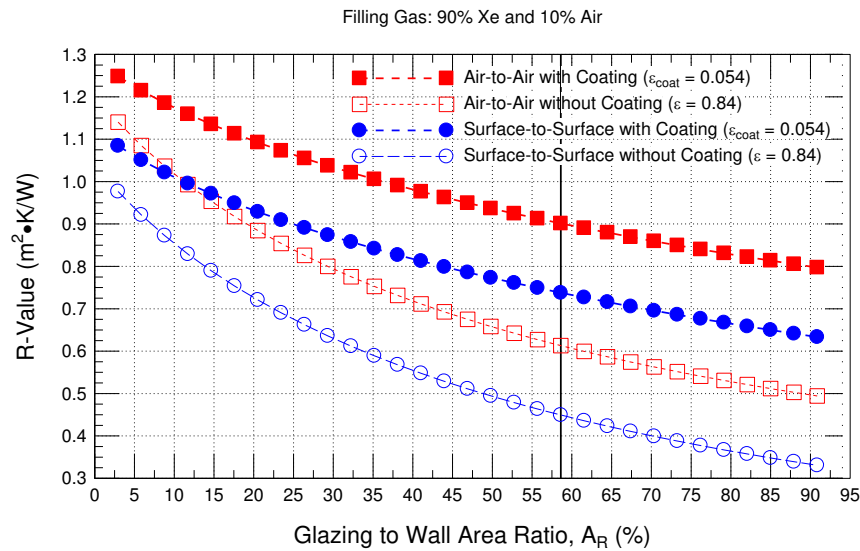


Figure 64 – Predicted (by simulation) (i) R-value and (ii) U-value (air-to-air; surface-to-surface) of triple-glazed low-e ($\epsilon = 0.054$) or no low-e ($\epsilon = 0.84$) coated thermally broken Curtain Wall in relation to Glazing to Wall Area Ratio for IGU filled with 90 % Xe, 10% Air

Figure 65 – Predicted (by simulation) (i) R-value and (ii) U-value (air-to-air; surface-to-surface) of triple-glazed low-e ($\epsilon = 0.054$) or no low-e ($\epsilon = 0.84$) coated thermally broken Curtain Wall in relation to Glazing to Wall Area Ratio for IGU filled with 100 % Air

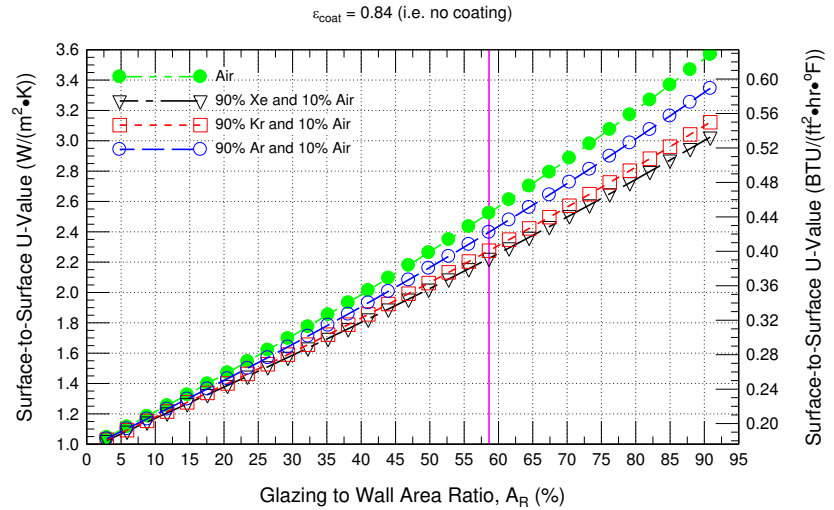
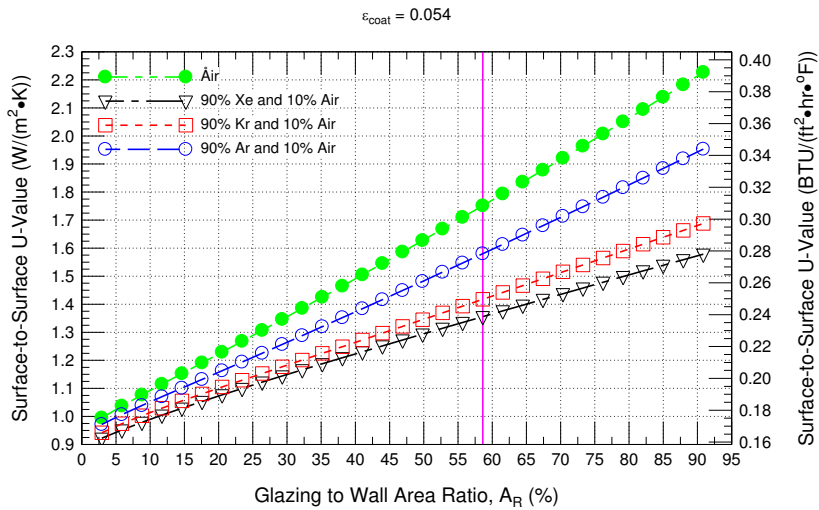
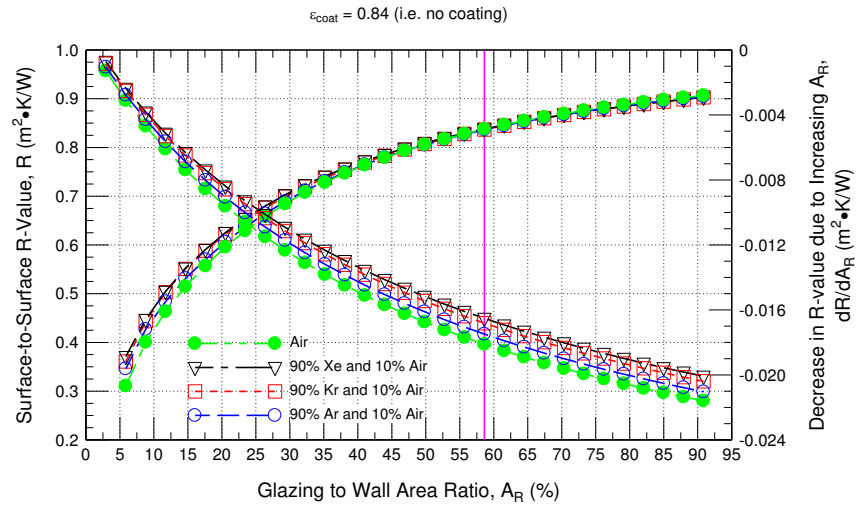
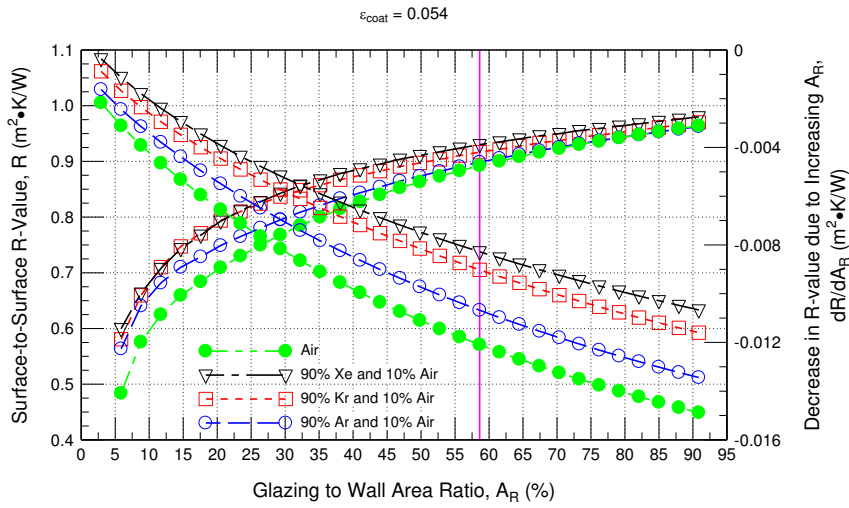


Figure 66 – Predicted (by simulation) (i) R-value and rate of change in R-value in relation to emissivity and; (ii) U-value (surface-to-surface) as a function of Glazing to Wall Area Ratio, for a NFRC-compliant, thermally-broken Curtain Wall, having a triple-glazed, low-e coated ($\epsilon = 0.054$) Air-, Ar-, Xe-, or Kr-filled IGU

Figure 67 – Predicted (by simulation) (i) R-value and rate of change in R-value in relation to emissivity and; (ii) U-value (surface-to-surface) as a function of Glazing to Wall Area Ratio, for a NFRC-compliant, thermally-broken Curtain Wall, having a triple-glazed, Air-, Ar-, Xe-, or Kr-filled IGU (no low-e coating; $\epsilon = 0.84$)

5.2.2.3 — Effect of changes to Coating emissivity

The effect of changes to coating emissivity on the R-values and corresponding U-values of triple-glazed thermally broken NFRC-compliant curtain wall assemblies is elaborated in this section. As well, the influence on the thermal performance of the assembly in relation to the coating emissivity for assemblies incorporating IGUs filled with different gases is also examined.

The results derived from simulation for the air-to-air and surface-to-surface R-value and U-value of a triple-glazed thermally broken curtain wall assembly in relation to the coating emissivity is provided in Figure 68 to Figure 73.

Simulation results for the R-value (uppermost plot) and U-value (lower-most plot) in relation to the coating emissivity (ϵ_{coat}) of surface 2 of the IGU for a triple-glazed curtain wall assembly having an A_R of 0.57, and for which the gas within the IGU was varied, is provided in the initial set of results given in Figure 68 to Figure 71; in the respective 4 figures, starting with Figure 68, the simulation results are given for the IGU incorporating a gas having:

- 90 % Ar and 10 % Air
- 90 % Kr and 10 % Air
- 90 % Xe and 10 % Air
- 100 % Air (Reference value)

From this set of results it is apparent that the R-value (air-to-air, or surface-to-surface) decreases with an corresponding increase in the value of ϵ_{coat} for all of the IGUs simulated, irrespective of the type of gas incorporated in the IGU. The loss in thermal performance with a corresponding increase in value of ϵ_{coat} is completely expected given the increase in transmission of radiation for related increases in emissivity of the glass. The more significant decreases are evidently found for the least performing IGU which is filled with 100% air (Figure 71).

A summary of the effect of changes to coating emissivity on the thermal performance of the triple-glazed curtain wall assembly is given in Figure 72 and Figure 73. In Figure 72, the rate of change in R-value for a NFRC-compliant triple-glazed thermally-broken curtain wall assembly in relation to the emissivity of surface 2 of the IGU is given for IGUs incorporating Air, or combinations of Air and Ar, Xe, or Kr. The vertical line in the plot shows the value of $\epsilon_{\text{coat}} = 0.054$, for which the low- ϵ coating is applied to surface 2. For an IGU having low- ϵ coating, significant changes to thermal performance can arise depending on the type of gas with which the IGU is filled; for $\epsilon_{\text{coat}} = 0.054$ on surface 2 of the IGU, the respective R-values for the curtain wall assembly for which the IGU is filled with air, or mixtures of air and Ar, Kr, or, Xe are: 0.575; 0.625; 0.712; and 0.735 $\text{m}^2\cdot\text{K}/\text{W}$.

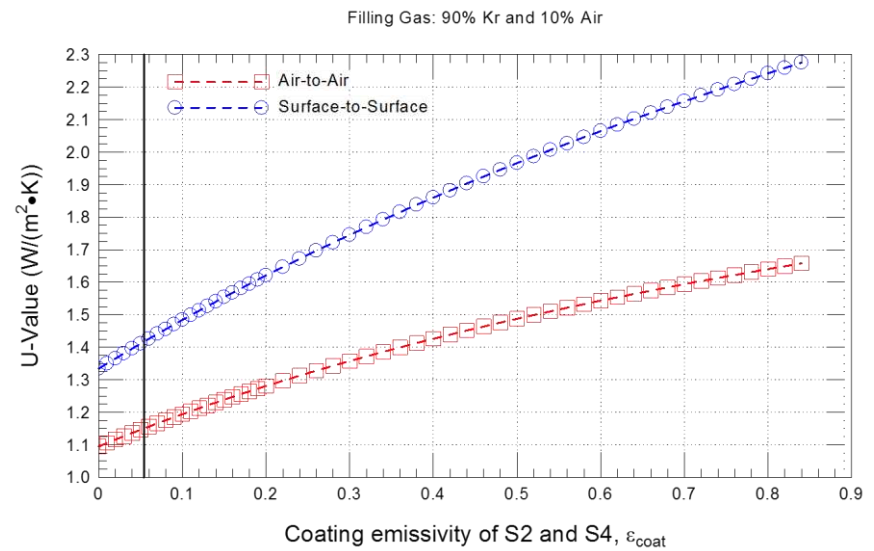
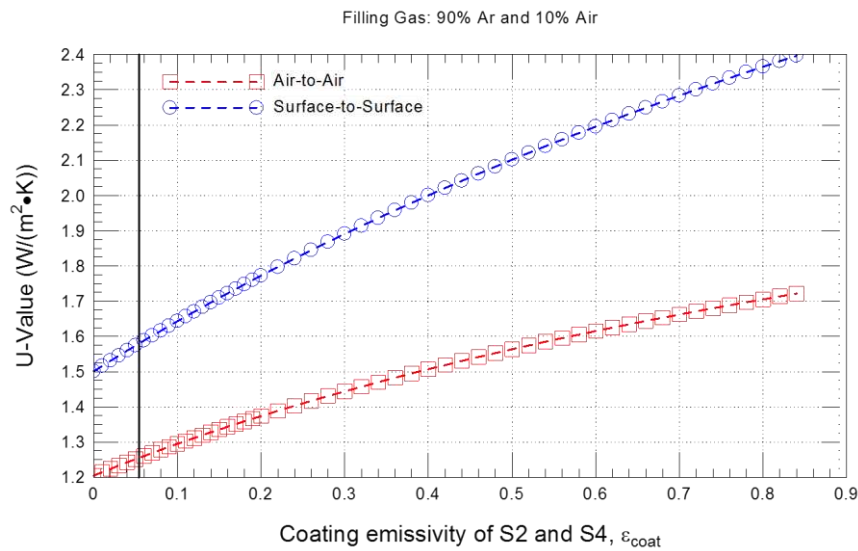
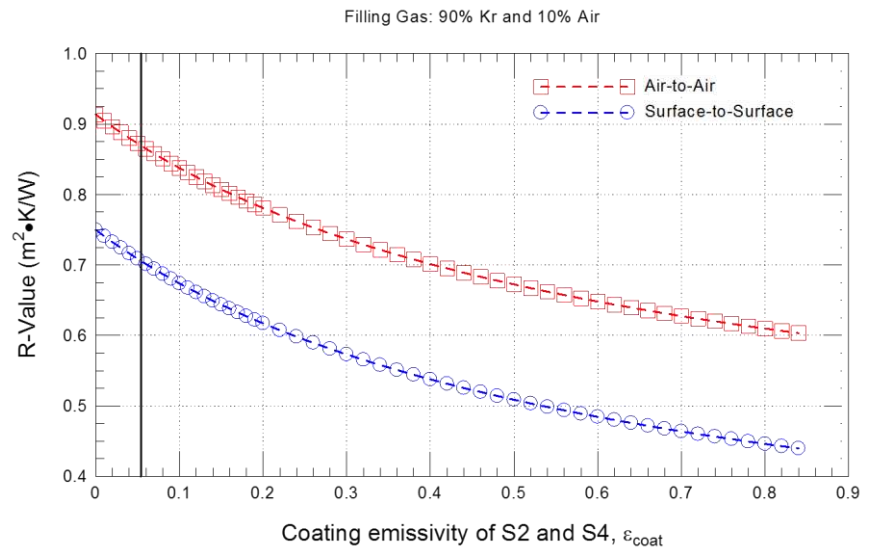
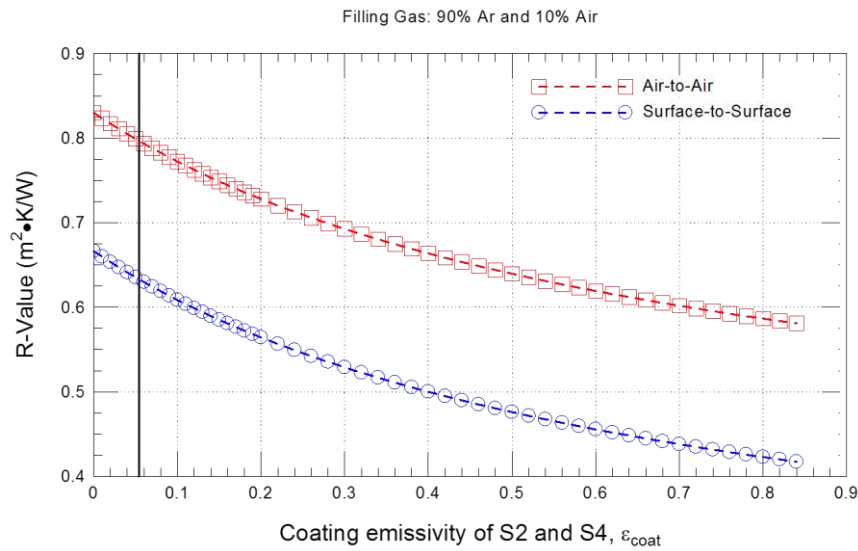


Figure 68 – Predicted (by simulation) R-value (i) ; U-value (ii) (air-to-air; surface-to-surface) of triple-glazed, thermally broken curtain wall as a function of coating emissivity for IGU filled with 90% Ar and 10 % Air

Figure 69 – Predicted (by simulation) R-value (i) ; U-value (ii) (air-to-air; surface-to-surface) of triple -glazed, thermally broken curtain wall as a function of coating emissivity for IGU filled with 90% Kr and 10 % Air

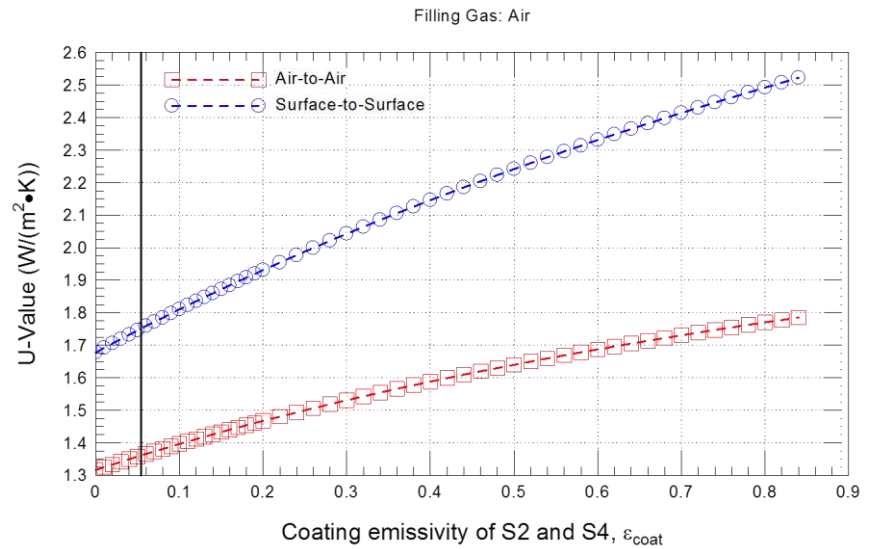
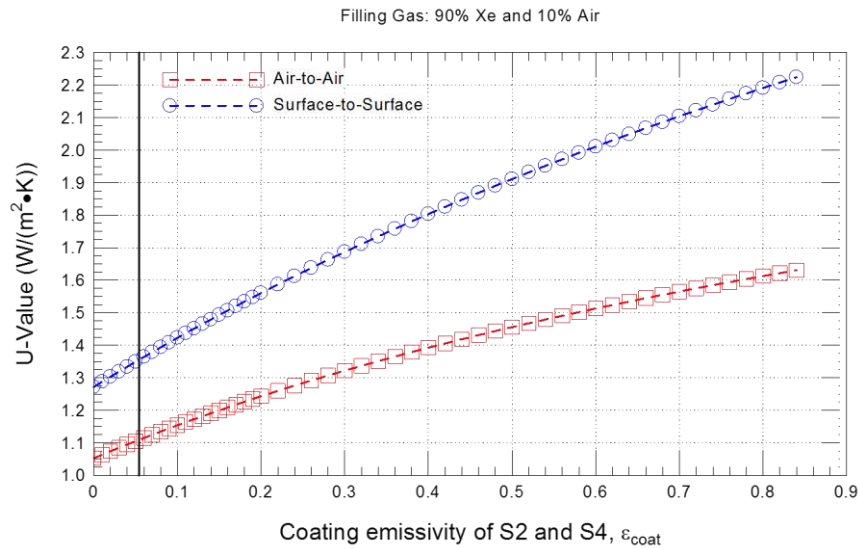
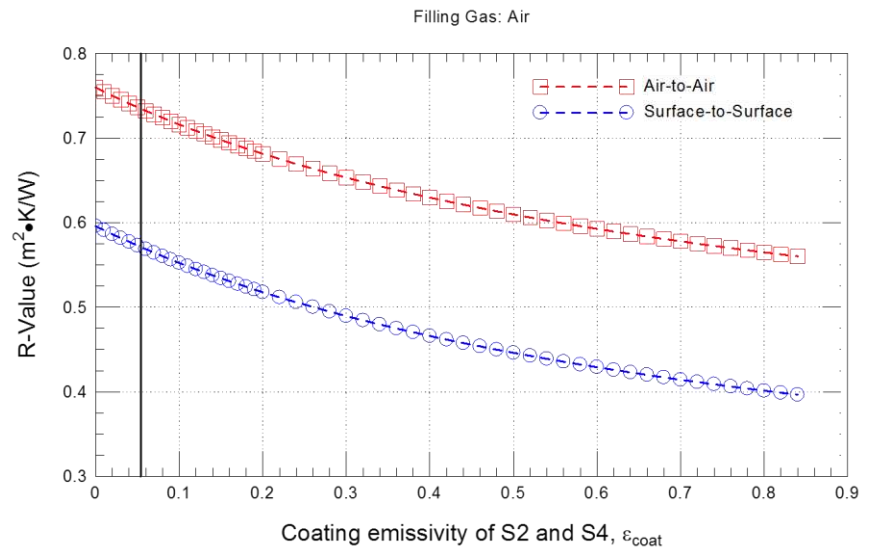
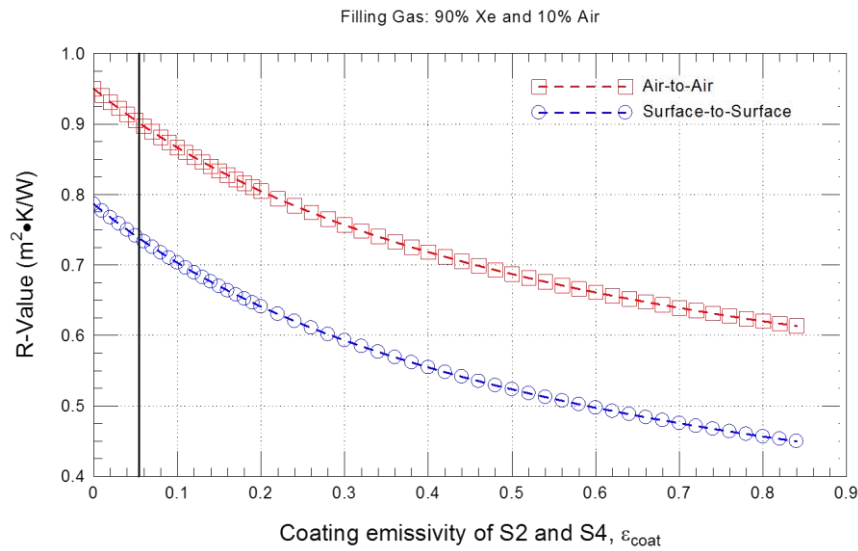


Figure 70 – Predicted (by simulation) R-value (i) ; U-value (ii) (air-to-air; surface-to-surface) of triple-glazed, thermally broken curtain wall as a function of coating emissivity for IGU filled with 90% Xe and 10 % Air

Figure 71 – Predicted (by simulation) R-value (i) ; U-value (ii) (air-to-air; surface-to-surface) of triple -glazed, thermally broken curtain wall as a function of coating emissivity for IGU filled with 100 % Air

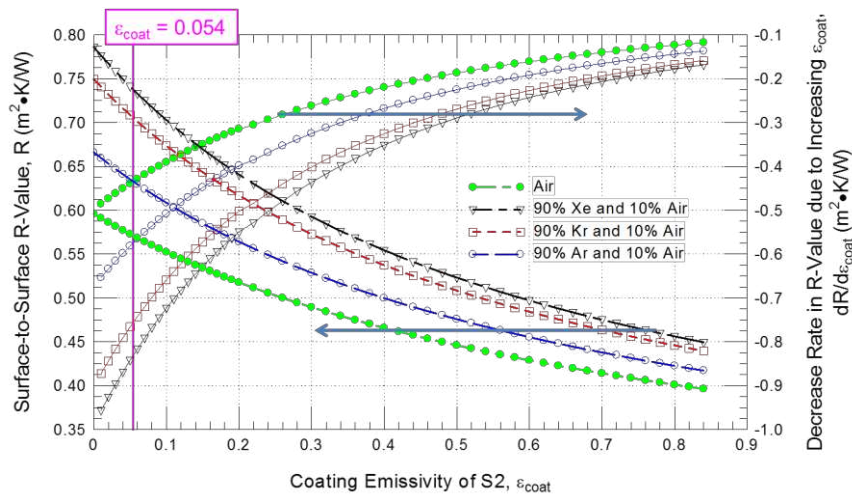


Figure 72 – Predicted (by simulation) (i) R-value (surface-to-surface) as a function of coating emissivity (surface S2) and; (ii) rate of change in R-value in relation to emissivity for a NFRC-compliant, thermally-broken Curtain Wall, with a triple-glazed, Air-, Ar-, Xe-, or Kr-filled IGU

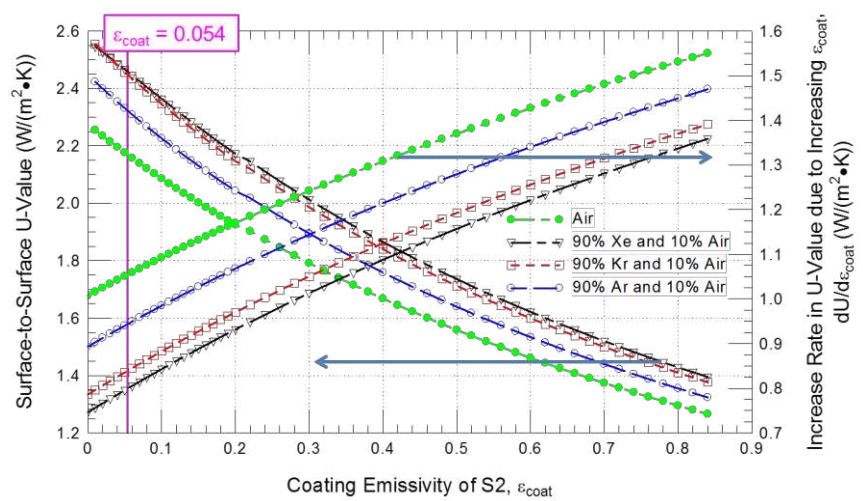


Figure 73 – Predicted (by simulation) (i) U-value (surface-to-surface) as a function of coating emissivity (surface S2) and; (ii) rate of change in U-value in relation to emissivity for a NFRC-compliant, thermally-broken Curtain Wall, with a triple-glazed, Air-, Ar-, Xe-, or Kr-filled IGU

5.2.2.4— *The effect of thermal resistance of the spandrel panel insulation*

The effect of thermal resistance of the spandrel panel insulation on the R-values and corresponding U-values of triple-glazed thermally broken NFRC-compliant curtain wall assemblies is elaborated in this section. As well, the influence on the thermal performance of triple-glazed curtain wall assemblies is also examined in relation to the different gases with which the IGUs are filled and that include Ar, Kr, Xe, and air; this portion also includes assessing the thermal performance of assemblies having IGUs that incorporate, or not, a low-e coating.

The results derived from simulation for the air-to-air and surface-to-surface R-value and U-value of a double-glazed thermally broken curtain wall assembly in relation to the spandrel panel insulation is provided in Figure 74 to Figure 79.

Simulation results for the R-value (uppermost plot) and U-value (lower-most plot) in relation to the spandrel panel thermal resistance ($m^2 \cdot K/W$) for a triple-glazed curtain wall assembly having an A_R of 0.57, and for which the gas within the IGU was varied, is provided in the initial set of results given in Figure 74 to Figure 77; in the respective 4 figures, starting with Figure 74, the simulation results are given for the IGU incorporating a gas having:

- 90 % Ar and 10 % Air
- 90 % Kr and 10 % Air
- 90 % Xe and 10 % Air
- 100 % Air (Reference value)

The vertical line in each of the figures gives the R-value of the spandrel panel insulation for the curtain wall assembly as illustrated in Figure 5 and Figure 11.

From this set of results it is apparent that the R-value (air-to-air, or surface-to-surface) of the curtain wall assembly increases in relation to corresponding increases in thermal resistance of the spandrel panel although such increases are limited to ca. 10% of the initial and lowest R-value for the spandrel panel. The R-value of assemblies having a low- ϵ coated ($\epsilon = 0.054$) IGU are characteristically greater than the assemblies having a non-coated IGU ($\epsilon = 0.84$) although both assemblies have similar trends over the range of increase in thermal resistance of the spandrel panel. The differences in R-value of the curtain wall assembly increase in relation to the type of IGU (i.e. low- ϵ vs. no low- ϵ) and differs depending on the gas which fills the IGU; increases in R-value of the curtain wall assembly were ca. 27%, 38% 49 % and 54%, respectively, for IGUs filled with Air, Ar, Kr, and Xe.

It is to be noted that the values for thermal resistance of the curtain wall, determined for an A_R of ca. 0.57, would not appreciably increase should additional insulation be added to the spandrel panel and thus do not provide a useful avenue for improved overall thermal performance. This is especially evident when reviewing summary results provided in Figure 78 and Figure 79. In Figure 78 is shown the R-value (surface-to-surface) of the same curtain wall assembly having a low-e coated IGU in relation to the thermal resistance of the spandrel panel and for all gases which filled the IGU; whereas Figure 79 provides the same information for an assembly having no low-e coated IGU. In addition, the rate of change in curtain wall R-value to that of the spandrel panel is also provided and for each type of IGU. The trends are now evident, in that only very small changes in assembly R-value can be expected for corresponding changes in spandrel R-value and these are in the order of 1%, or less, for enhancements to the thermal resistance of the spandrel panel beyond the vertical line that delineates the R-value for the spandrel panel of the manufactured product.

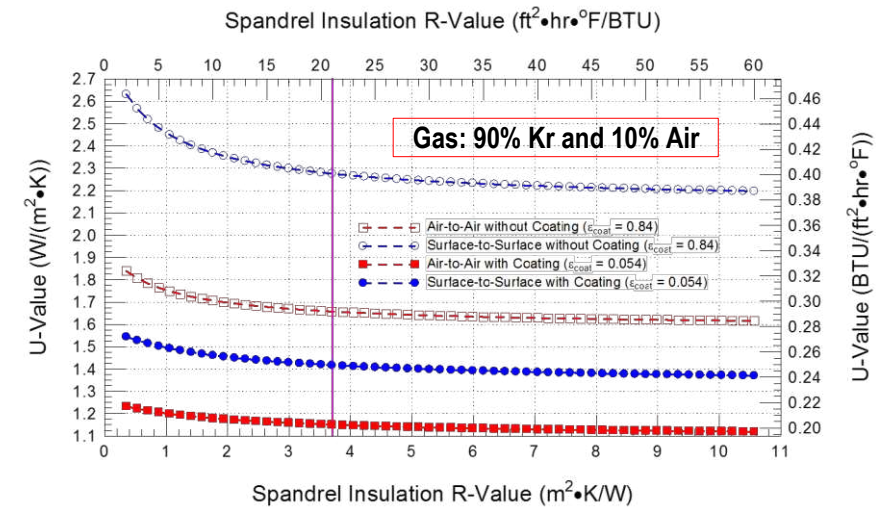
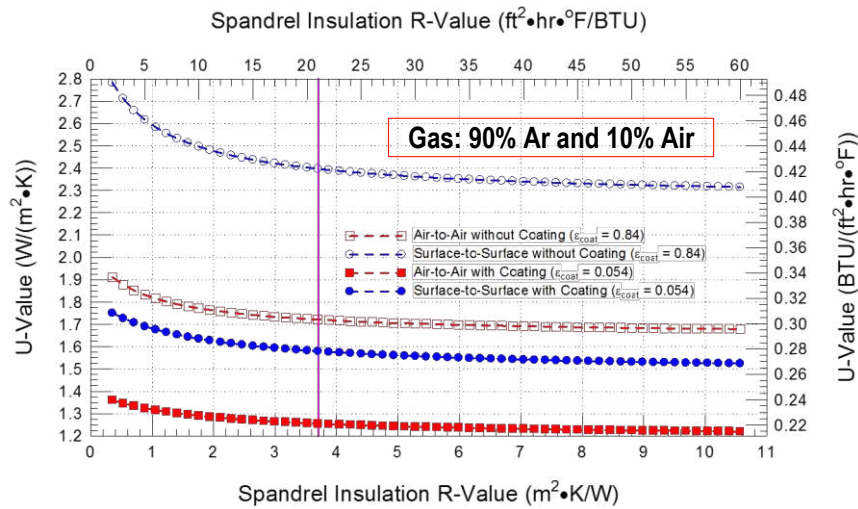
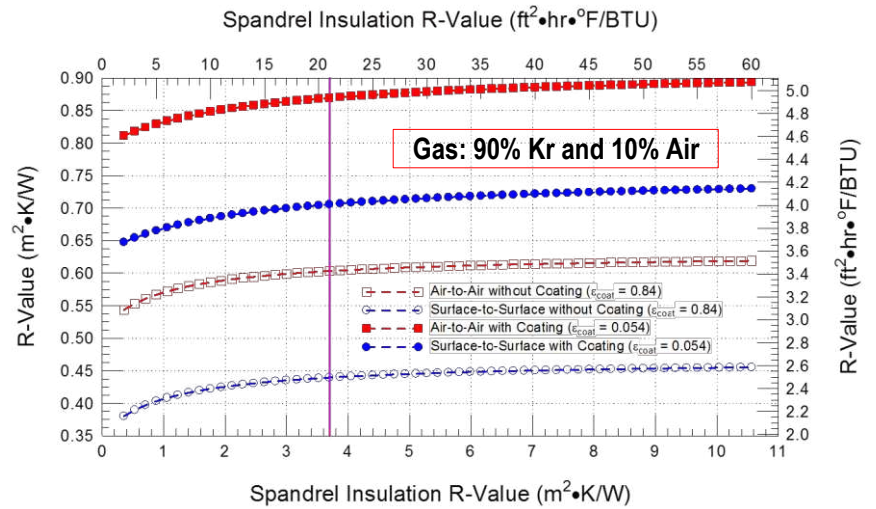
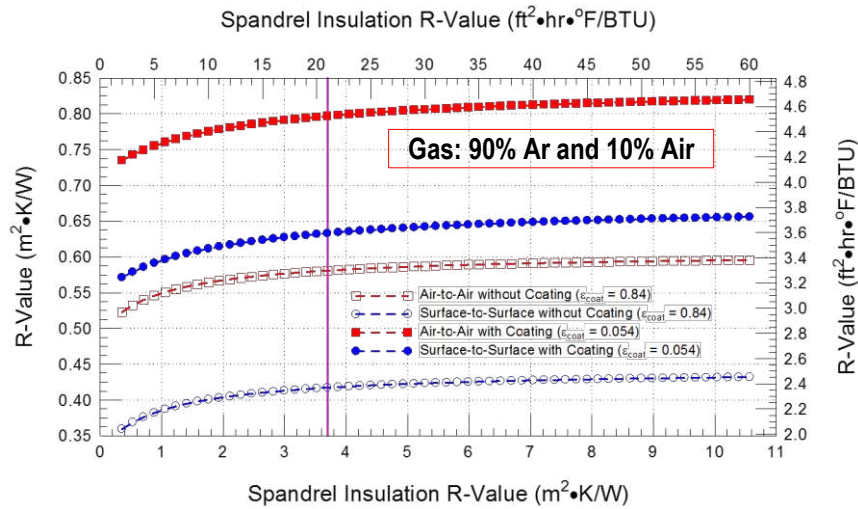


Figure 74 – Predicted (by simulation) (i) R-value and (ii) U-value (air-to-air; surface-to-surface) as a function of Spandrel panel insulation for a NFRC-compliant, thermally-broken triple-glazed Ar-filled IGU curtain wall assembly with and without low-e coating on surface 2

Figure 75 – Predicted (by simulation) (i) R-value and (ii) U-value (air-to-air; surface-to-surface) as a function of Spandrel panel insulation for a NFRC-compliant, thermally-broken triple-glazed Kr-filled IGU curtain wall assembly with and without low-e coating on surface 2

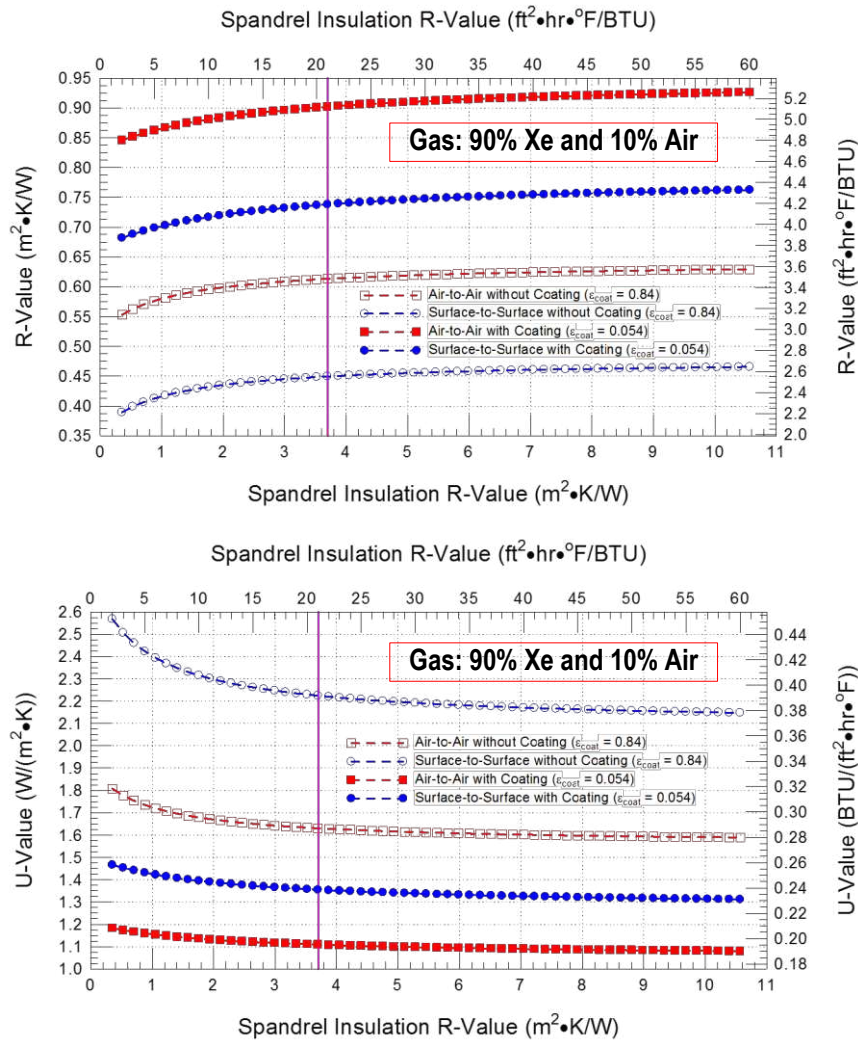


Figure 76 – Predicted (by simulation) (i) R-value and (ii) U-value (air-to-air; surface-to-surface) as a function of Spandrel panel insulation for a NFRC-compliant, thermally-broken triple-glazed Xe-filled IGU curtain wall assembly with and without low-e coating on surface 2

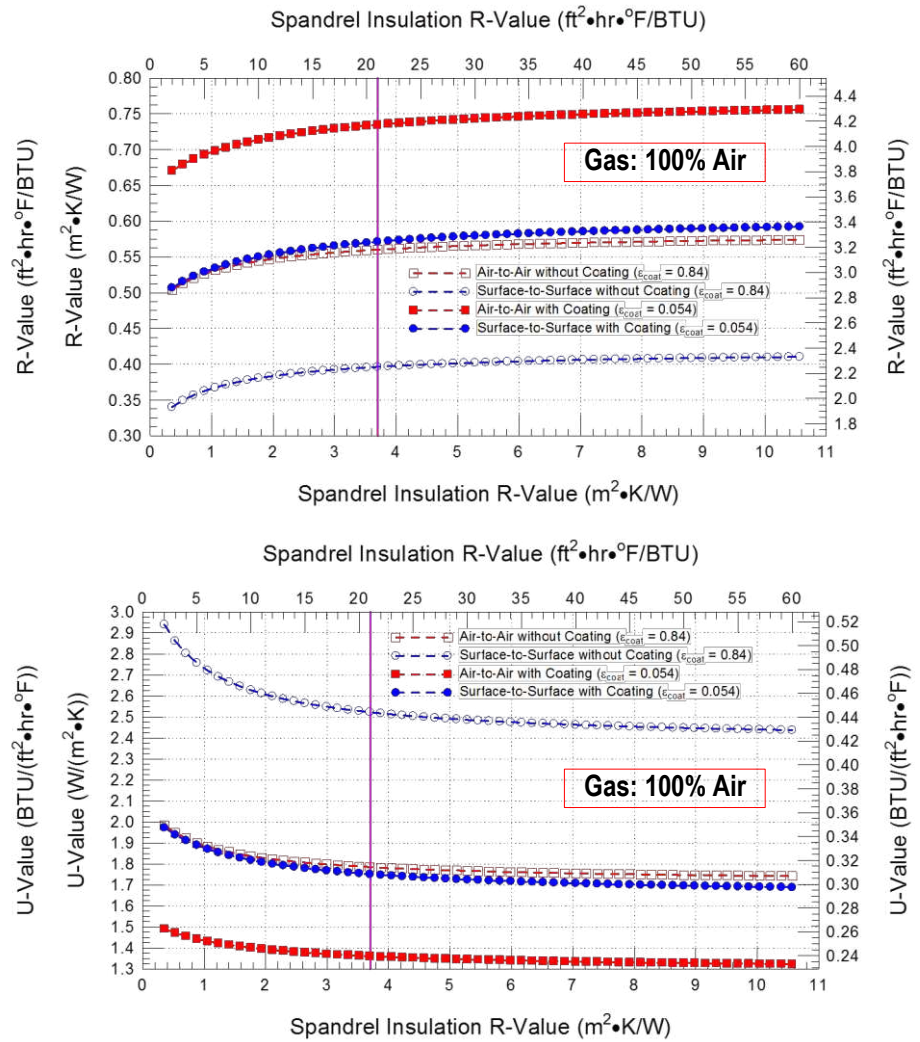


Figure 77 – Predicted (by simulation) (i) R-value and (ii) U-value (air-to-air; surface-to-surface) as a function of Spandrel panel insulation for a NFRC-compliant, thermally-broken triple-glazed Air filled IGU curtain wall assembly with and without low-e coating on surface 2

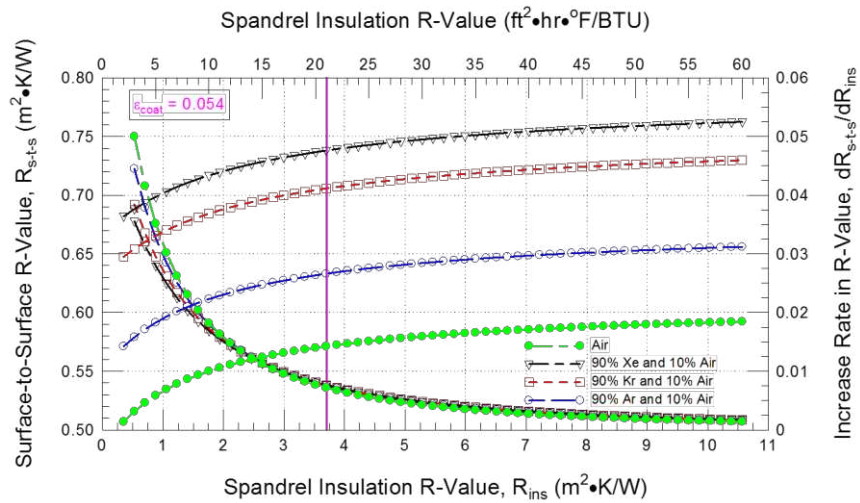


Figure 78 – Predicted (by simulation) (i) R-value and (ii) U-value (air-to-air; surface-to-surface) as a function of Spandrel panel insulation for a NFRC-compliant, thermally-broken triple-glazed curtain wall assembly incorporating an IGU with low- ϵ coating (surface 2) and filled with either Ar, Kr, Xe, or Air

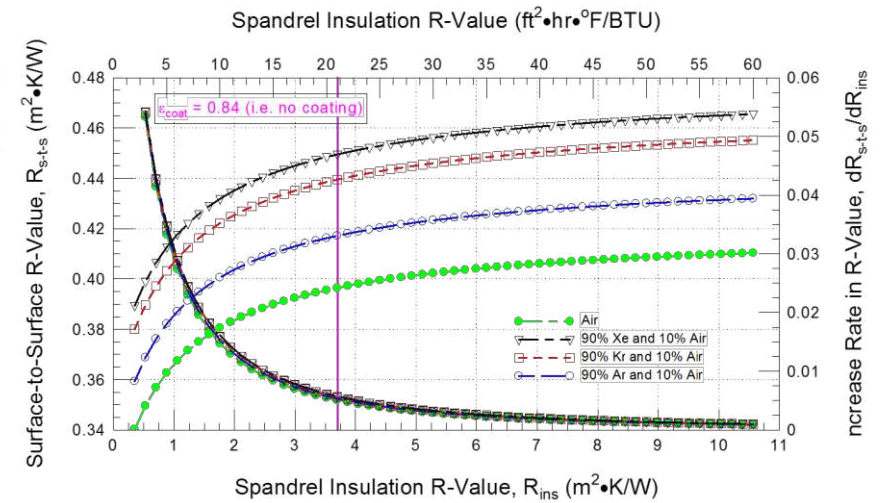


Figure 79 – Predicted (by simulation) (i) R-value and (ii) U-value (air-to-air; surface-to-surface) as a function of Spandrel panel insulation for a NFRC-compliant, thermally-broken triple-glazed curtain wall assembly incorporating an IGU without low- ϵ coating (surface 2) and filled with either Ar, Kr, Xe, or Air

5.2.2.5— *The effect of thermal conductivity of the IGU spacer*

The effect of the IGU spacer thermal properties on the R-values and corresponding U-values of triple-glazed thermally broken NFRC-compliant curtain wall assemblies is elaborated in this section. As well, the influence on the thermal performance of triple-glazed curtain wall assemblies is also examined in relation to the different gases with which the IGUs are filled and that include Ar, Kr, Xe, and air; this section also includes assessing the thermal performance of assemblies having IGUs that incorporate, or not, a low- ϵ coating.

The results derived from simulation for the air-to-air and surface-to-surface R-value and U-value of a triple-glazed thermally broken curtain wall assembly in relation to the thermal conductivity of the IGU spacer is provided in Figure 80 to Figure 85.

Simulation results for the R-value (uppermost plot) and U-value (lower-most plot) in relation to the thermal conductivity of the IGU spacer ($\text{W}/\text{m}\cdot\text{K}$) for a triple-glazed curtain wall assembly having an A_R of 0.57, and for which the gas within the IGU was varied, is provided in the initial set of results given in Figure 80 to Figure 83; in the respective 4 figures, starting with Figure 80, the simulation results are given for the IGU incorporating a gas having:

- 90 % Ar and 10 % Air
- 90 % Kr and 10 % Air
- 90 % Xe and 10 % Air
- 100 % Air (Reference value)

From this set of results it is apparent that the R-value (air-to-air, or surface-to-surface) of the CW assembly decreases in relation to corresponding increases in thermal conductivity of the IGU spacer although such decreases over the range of values for spacer thermal conductivity (i.e. 0-2 $\text{W}/\text{m}\cdot\text{K}$) are limited to ca. 11-15% of the initial and lowest value for thermal conductivity of the IGU spacer. The R-value of assemblies having a low- ϵ coated ($\epsilon = 0.054$) IGU are characteristically greater than the assemblies having a non-coated IGU ($\epsilon = 0.84$) although both assemblies have similar trends over the range in reduction in thermal conductivity of the IGU spacer. The degree of difference in R-value (surface-to-surface) of the CW assembly as relates to whether the IGU is low- ϵ or not low- ϵ , differs depending on the gas which fills the IGU; decreases in the initial R-value (surface-to-surface) of the CW assembly (spacer thermal conductivity: 0.1 $\text{W}/\text{m}\cdot\text{K}$) were ca. 44%, 39%, 44% and 45 %, respectively, for IGUs filled with Air, Ar, Kr, and Xe.

It is to be noted that although the values for thermal resistance of the CW, taken for an A_R of ca. 0.57, do not appreciably decrease over the range of values for the thermal conductivity of the IGU spacer, more performing spacers could provide a useful avenue for improved overall thermal performance. This is especially evident when reviewing summary results provided in Figure 83 and Figure 85. In Figure 85 is shown the R-value (surface-to-surface) of the same CW assembly having a low-e coated IGU in relation to the thermal resistance of the spandrel panel and for all gases which filled the IGU; whereas the same information is provided in Figure 85 for an assembly having non low-e coated IGU. In addition, the rate of change in CW R-value to that of the spacer thermal conductivity is also provided and for each type of IGU. The trends are now evident, in that only very small changes in assembly R-value can be expected for corresponding changes in spacer thermal conductivity beyond 1 $\text{W}/\text{m}\cdot\text{K}$ (ca. < 10% or less); enhancements to the R-value of the CW assembly would require IGU spacer thermal conductivities of < 1 $\text{W}/\text{m}\cdot\text{K}$.

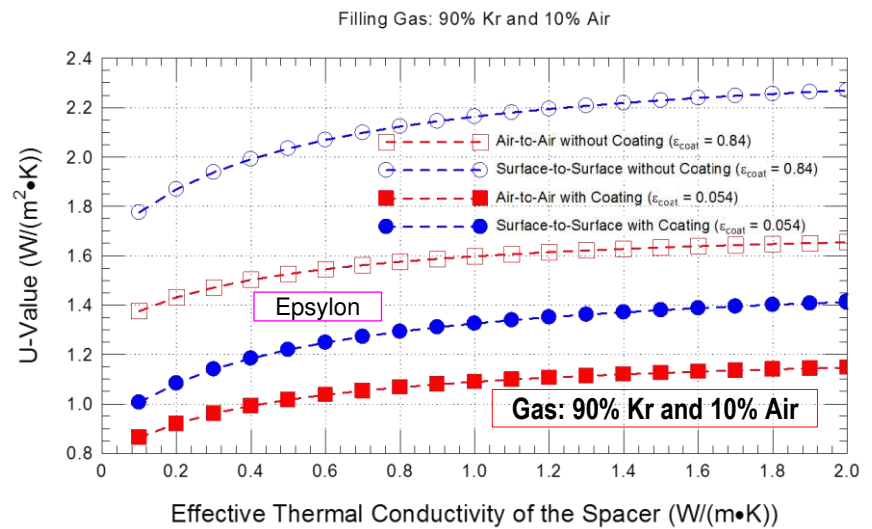
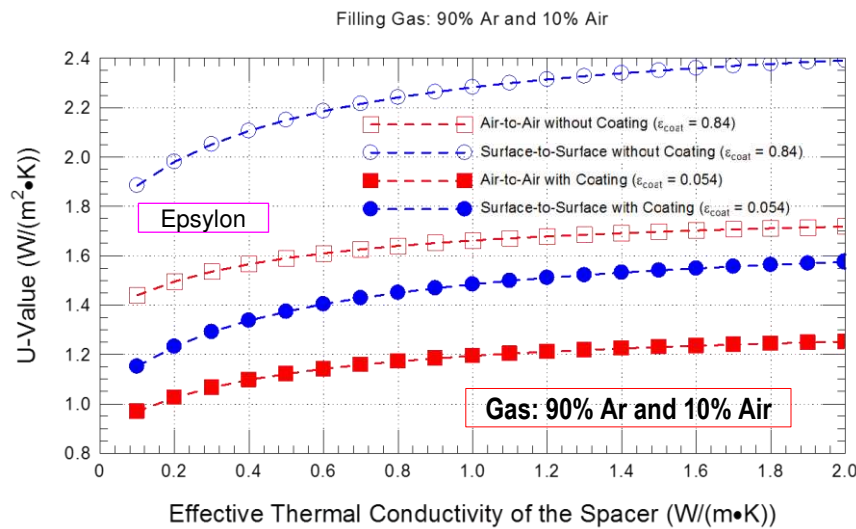
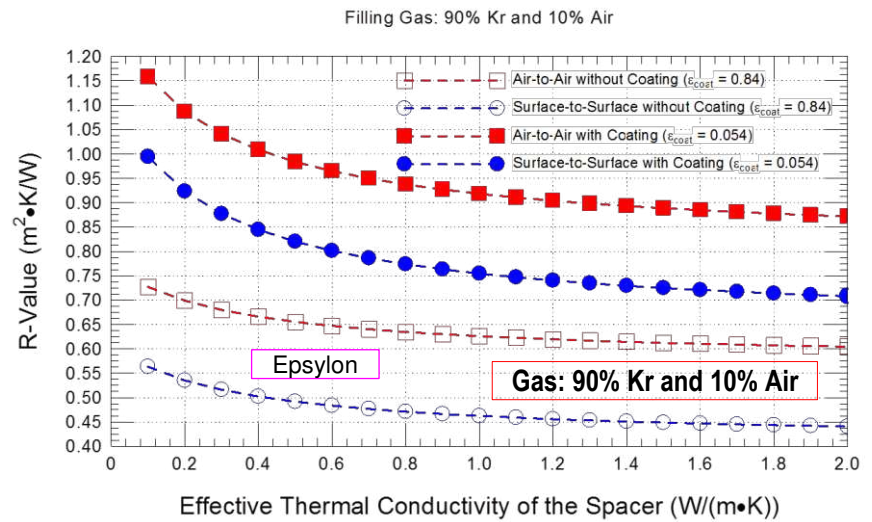
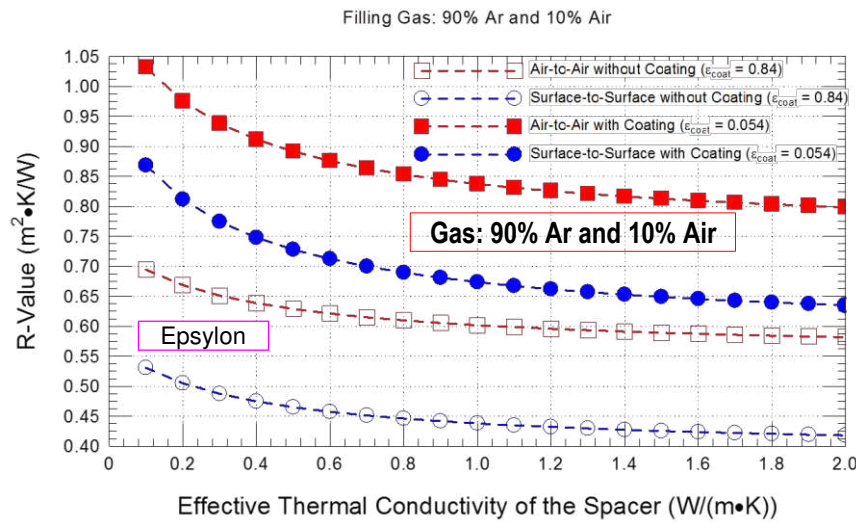


Figure 80 – Predicted (by simulation) (i) R-value and (ii) U-value (air-to-air; surface-to-surface) as a function of thermal conductivity of spacer for a NFRC-compliant, thermally-broken triple-glazed Ar-filled IGU curtain wall assembly with and without low-e coating on surface 2

Figure 81 – Predicted (by simulation) (i) R-value and (ii) U-value (air-to-air; surface-to-surface) as a function of thermal conductivity of spacer for a NFRC-compliant, thermally-broken triple-glazed Kr-filled IGU curtain wall assembly with and without low-e coating on surface 2

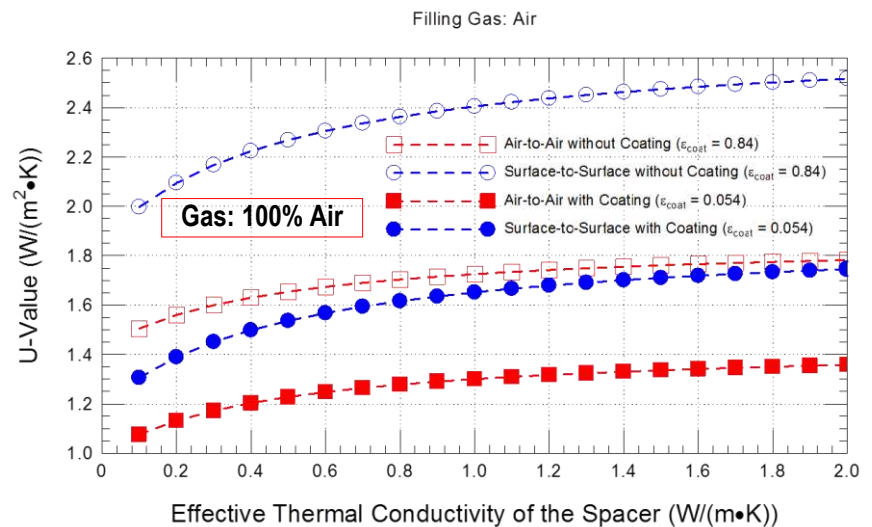
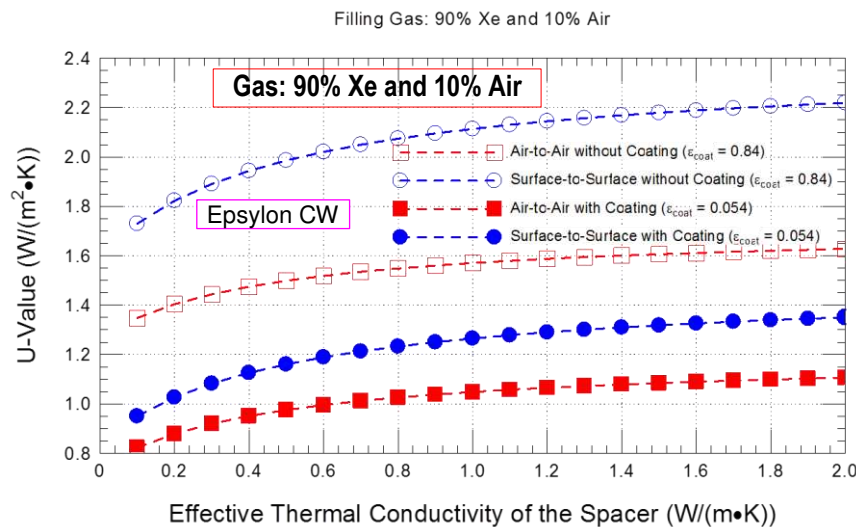
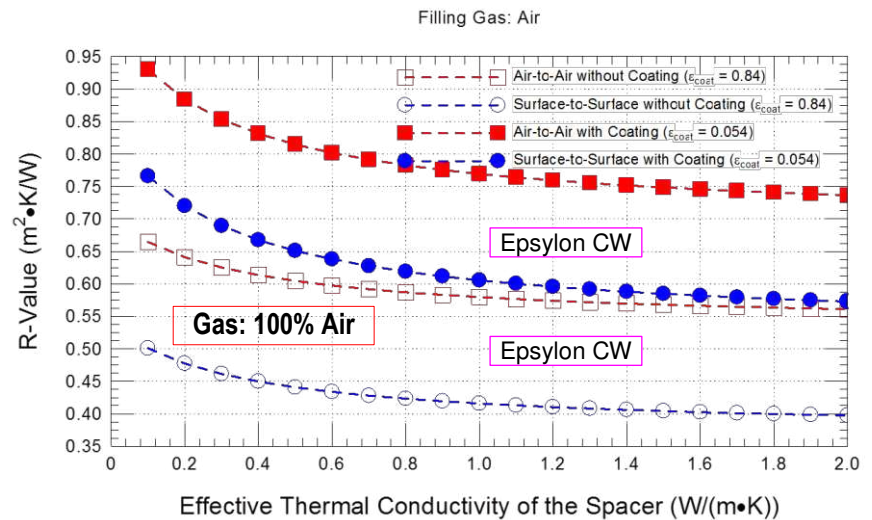
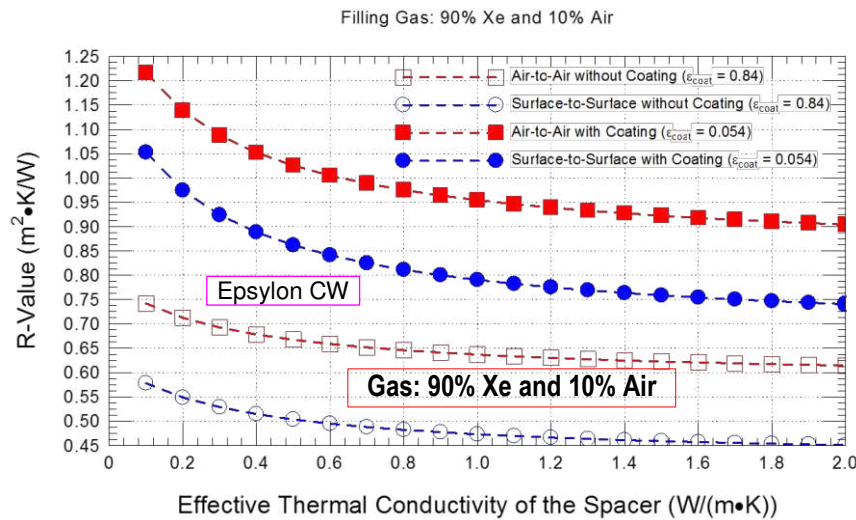


Figure 82 – Predicted (by simulation) (i) R-value and (ii) U-value (air-to-air; surface-to-surface) as a function of thermal conductivity of spacer for a NFRC-compliant, thermally-broken triple-glazed Xe-filled IGU curtain wall assembly with and without low-e coating on surface 2

Figure 83 – Predicted (by simulation) (i) R-value and (ii) U-value (air-to-air; surface-to-surface) as a function of thermal conductivity of spacer for a NFRC-compliant, thermally-broken triple-glazed Air filled IGU curtain wall assembly with and without low-e coating on surface 2

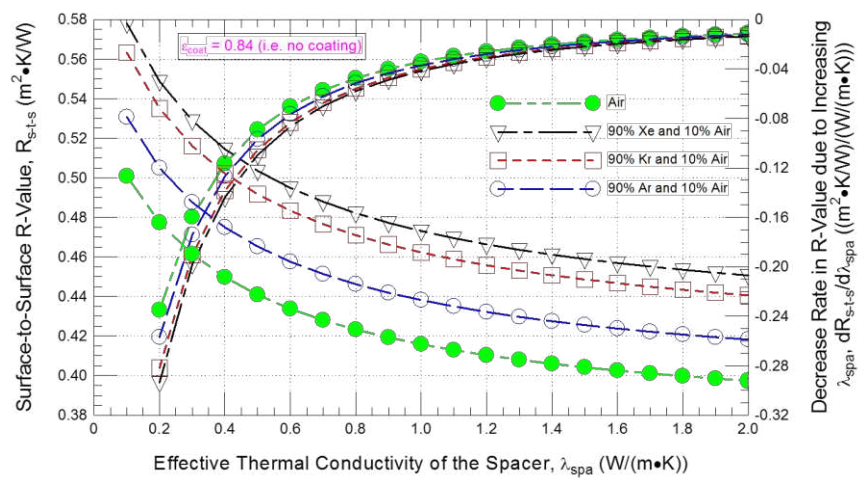
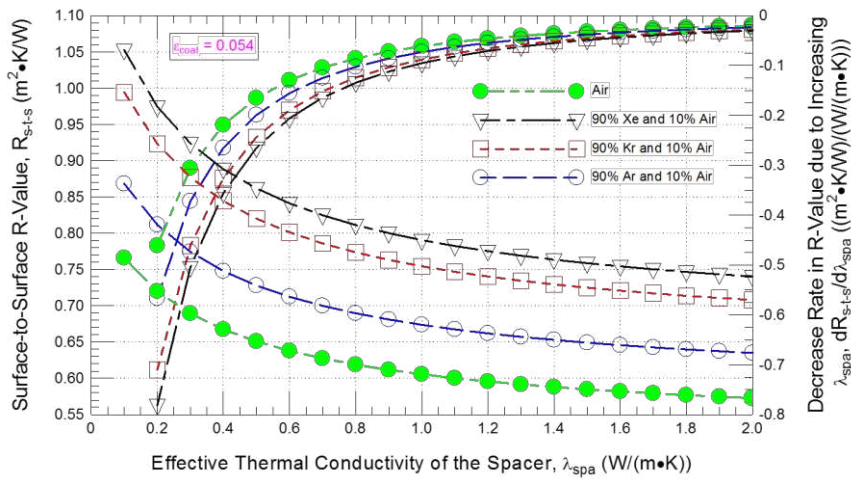


Figure 84 – Predicted (by simulation) R-value (surface-to-surface) as a function of thermal conductivity of Spacer for a NFRC-compliant, thermally-broken triple-glazed curtain wall assembly incorporating an IGU with low- ϵ coating ($\epsilon = 0.054$; surface 2) and filled with either Ar, Kr, Xe, or Air

Figure 85 – Predicted (by simulation) (i) R-value (surface-to-surface) as a function of thermal conductivity of Spacer for a NFRC-compliant, thermally-broken triple-glazed curtain wall assembly incorporating an IGU without low- ϵ coating and filled with either Ar, Kr, Xe, or Air

6. Summary

The results from simulation of double and triple-glazed CW modelling configurations of both manufactured products as well as NFRC compliant CW assemblies using the simulation model hygIRC-C were compared as were results of simulations derived from varying the thermal properties of the CW components.

In respect to results from simulation of manufacturer’s products, results were provided for the risk to condensation of double and triple-glazed CW assemblies. The results showed that both double and triple-glazed CW indeed have components that are potentially vulnerable to the formation of condensation; these are located along the frame at the periphery of the glazing unit.

As regards the NFRC compliant CW assemblies, the results from simulation provided information on the R-value and respective U-values of the assemblies for different gas filling the IGU; a summary of such results are provided in Table 7 for double-glazed and Table 8 for triple-glazed CW assemblies; these results are also summarised in Figure 86.

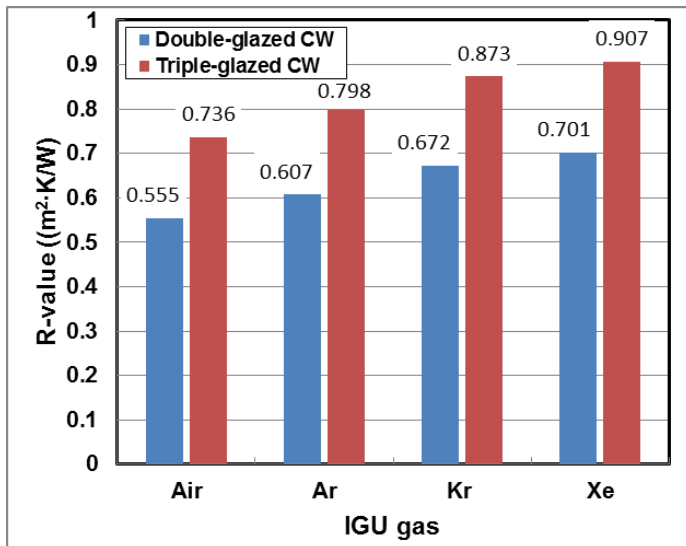


Figure 86 – Summary of Thermal performance of NFRC compliant double- and triple-glazed CW assemblies

As is evident for the information provided in Figure 85, triple-glazed CW assemblies, as expected perform better than the double-glazed assemblies, and the thermal performance is also affected by the type of gas that fills the IGU. Using the R-value of double-glazed Air-filled IGU as reference (i.e. 0.555 m²·K/W), the degree of improvement in R-value is: 9.4%, 21%, 26% respectively, for Ar, Kr, and Xe filled double-glazed IGUs, whereas these values are 8.4%, 18.6%, 23.2% respectively, for Ar, Kr, and Xe filled triple-glazed IGUs, when using the triple-glazed Air-filled IGU as reference (i.e. 0.736 m²·K/W).

Improvements in R-value of the CW assembly for double- to triple-gazed IGUs provide enhancements of 33%, 31.4%, 29.9% and 29.3% when filled respectively, with air, Ar, Kr, and Xe gas.

Improvements in R-value of the CW assembly for double- to triple-gazed IGUs provide

The results from simulation of both the double and triple-glazed NFRC compliant CW assemblies were also provided in terms of:

- (vi.) Risk to the formation of condensation;
- (vii.) Effect of glazing to wall-area ratio;
- (viii.) Effect of changes to coating emissivity;
- (ix.) Effect of thermal resistance of the spandrel panel insulation, and;
- (x.) Effect of IGU spacer thermal conductivity

As regards the results for the Risk to the formation of condensation, the results showed that both double and triple-glazed CW indeed have components that are potentially vulnerable to the formation of condensation as was the case for the manufactured products; locations of vulnerability are along the frame at the periphery of the glazing unit.

Results were then provided in terms of changes to R-value and U-values (both air-to-air and surface to surface) as a function of changes to the specific parameter of interest (i.e. glazing to wall-area ratio, coating emissivity; thermal resistance of the spandrel panel insulation, or IGU spacer thermal conductivity).

At the end of each section of results, summary results were provide together with information on how each of the respective parameters affected changes to the thermal resistance of the CW assembly. Relationships between expected changes in thermal resistance of the CW assembly to corresponding changes in the given simulation parameter permitted gauging the significance of each these effects.

Together this information will provide the basis for developing guidelines to the selection of components of double and triple-gazed metal-glass CW assemblies.

7. References

1. Al-Homoud, M.S., “Performance characteristics and practical applications of common building thermal insulation materials”, *Journal of Building and Environment*, 40: 353–366, 2005.
2. Vrachopoulos, M.G., Koukou, M.K., Stavlas, D. G., Stamatopoulos, V. N., Gonidis, A.F., and Kravvaritis, E.D., “Testing reflective insulation for improvement of buildings energy efficiency”, *Central European Journal of Engineering*, 2(1): 83-90, 2012, [DOI:10.2478/s13531-011-0036-3](https://doi.org/10.2478/s13531-011-0036-3).
3. European Commission, [Green public procurement thermal insulation technical background](#) report. Report for the European Commission – DG Environment by AEA, Harwell, Owner, Editor: European Commission, DG Environment-G2, B-1049, Brussels, 2010.
4. Saber, H.H., Swinton, M.C., Kalinger, P., and Paroli, R.M., “Long-term hygrothermal performance of white and black roofs in North American climates”, *Journal of Building and Environment*, 50: 141-154, 2012, <http://dx.doi.org/10.1016/j.buildenv.2011.10.022>.
5. Saber, H.H., Swinton, M.C., Kalinger, P., and Paroli, R.M., “Hygrothermal simulations of cool reflective and conventional roofs”, *2011 NRC/A International Roofing Symposium, Emerging Technologies and Roof System Performance*, held in Sept. 7-9, 2011, Washington D.C., USA.
6. Glass and Metal Curtain Walls, Best Practice Guide Building Technology, ISBN 0-660-19394-9, Cat. no. NH15-428/2004E, Canada Mortgage and Housing Corporation (CMHC), Canada, 2004.
7. Van Den Bergh S., Hart R., Jelle B.P., and Gustavsen A. “Window spacers and edge seals in insulating glass units: A state-of-the-art review and future perspectives”. *Energy and Buildings* 58: 263-280, 2013.
8. RIMA-I, Reflective Insulation Manufacturers Association International (RIMA-I), *Reflective Insulation, Radiant Barriers and Radiation Control Coatings*. Olathe, KS: RIMA-I, 2002.
9. Yarbrough, D., [Assessment of reflective insulations for residential and commercial applications](#). ORNL/TM-8891, Oak Ridge National Laboratory, Oak Ridge, TN. p. 1-63, 1983.
10. Al-Homoud, M.S., “Performance characteristics and practical applications of common building thermal insulation materials”, *Journal of Building and Environment*, 40: 353–366, 2005.
11. Vrachopoulos, M.G., Koukou, M.K., Stavlas, D. G., Stamatopoulos, V. N., Gonidis, A.F., and Kravvaritis, E.D., “Testing reflective insulation for improvement of buildings energy efficiency”, *Central European Journal of Engineering*, 2(1): 83-90, 2012, [DOI:10.2478/s13531-011-0036-3](https://doi.org/10.2478/s13531-011-0036-3).

Table 7 – Simulation Results of Thermal Performance of NFRC Compliant DOUBLE-Glazed CW Configuration

Double Glazing, Low-e coating of emissivity = 0.054, and XPS Frame Insulation				
Parameter	Gas: Ar	Gas: Kr	Gas: Xe	Gas: Air
	90% Ar	90% Kr	90% Xe	100% Air
Areas				
Projected Area of the Sample (A_p), m^2	7.48	7.48	7.48	7.48
Total Indoor Surface Area (A_i), m^2	9.16	9.16	9.16	9.16
Total Outdoor Surface Area (A_o), m^2	8.08	8.08	8.08	8.08
NFRC Boundary Conditions				
Temperature of warm side air (T_i), °C	21.00	21.00	21.00	21.00
Temperature of cold side air (T_{ii}), °C	-18.00	-18.00	-18.00	-18.00
Interior Test Film (h_i), $W/(m^2 \cdot K)$	7.67	7.67	7.67	7.67
Exterior Test Film (h_{ii}), $W/(m^2 \cdot K)$	30.00	30.00	30.00	30.00
Performance Predications				
Average Area Weighted Room Side Surface Temp. (T_1), °C	13.85	14.57	14.85	13.14
Average Weather Side Area Weighted Surface Temp. (T_2), °C	-15.93	-16.14	-16.22	-15.73
Surface-to-surface Temperature Difference (ΔT), °C	29.78	30.70	31.06	28.87
Net Specimen Heat Loss (Q_s), W	502.26	451.76	432.17	551.66
Derived Performance Parameters				
Conductance of the Sample: $C_s = Q_s/A_p \cdot (T_1 - T_2)$, $W/(m^2 \cdot K)$	2.255	1.967	1.860	2.555
U-value of the sample: $U_s = 1/[(1/C_s) + (1/h_i) + (1/h_{ii})]$, $W/(m^2 \cdot K)$	1.647	1.488	1.426	1.802
Thermal resistance = $1 / C_s$, $(m^2 \cdot K) / W$	0.443	0.508	0.538	0.391
R-value = $1 / U_s$, $(m^2 \cdot K) / W$	0.607	0.672	0.701	0.555
Percentage Increase in Performance due to Using different Filling Gas (%)				
Conductance of the Sample: C_s	13.29	29.88	37.35	N/A
U-value of the sample: U_s	9.37	21.06	26.34	N/A
Thermal resistance = $1 / C_s$	13.29	29.88	37.35	N/A
R-value = $1 / U_s$	9.37	21.06	26.34	N/A

2G, Coating ($e_{coat} = 0.054$), 2 m x 2 m vision and 2 m x 1.2 m spandrel

Table 8 - Simulation Results of Thermal Performance of NFRC Compliant TRIPLE-Glazed CW Configuration

Triple Glazing, Low-e coating of emissivity = 0.054, and XPS Frame Insulation				
Parameter	Gas: Ar	Gas: Kr	Gas: Xe	Gas: Air
	90% Ar	90% Kr	90% Xe	100% Air
Areas				
Projected Area of the Sample (A_p), m ²	7.48	7.48	7.48	7.48
Total Indoor Surface Area (A_i), m ²	9.15	9.15	9.15	9.15
Total Outdoor Surface Area (A_o), m ²	8.00	8.00	8.00	8.00
NFRC Boundary Conditions				
Temperature of warm side air (T_i), °C	21.00	21.00	21.00	21.00
Temperature of cold side air (T_{ii}), °C	-18.00	-18.00	-18.00	-18.00
Interior Test Film (h_i), W/(m ² •K)	7.67	7.67	7.67	7.67
Exterior Test Film (h_{ii}), W/(m ² •K)	30.00	30.00	30.00	30.00
Performance Predications				
Average Area Weighted Room Side Surface Temp. (T_1), °C	15.62	16.09	16.28	15.15
Average Weather Side Area Weighted Surface Temp. (T_2), °C	-16.43	-16.56	-16.62	-16.29
Surface-to-surface Temperature Difference (ΔT), °C	32.04	32.65	32.90	31.43
Net Specimen Heat Loss (Q_s), W	377.63	344.51	331.06	410.75
Derived Performance Parameters				
Conductance of the Sample: $C_s = Q_s/A_p \cdot (T_1 - T_2)$, W/(m ² •K)	1.576	1.411	1.345	1.747
U-value of the sample: $U_s = 1/[(1/C_s) + (1/h_i) + (1/h_{ii})]$, W/(m ² •K)	1.253	1.146	1.103	1.359
Thermal resistance = $1 / C_s$, (m ² •K) / W	0.635	0.709	0.743	0.572
R-value = $1 / U_s$, (m ² •K) / W	0.798	0.873	0.907	0.736
Percentage Increase in Performance due to Using different Filling Gas (%)				
Conductance of the Sample: C_s	10.88	23.86	29.86	N/A
U-value of the sample: U_s	8.46	18.55	23.22	N/A
Thermal resistance = $1 / C_s$	10.88	23.86	29.86	N/A
R-value = $1 / U_s$	8.46	18.55	23.22	N/A

3G, Coating ($e_{coat} = 0.054$), 2m x 2m vision and 2m x 1.2 m spandrel

References, cont'd

12. [European Commission, Green public procurement thermal insulation technical background](#) report. Report for the European Commission – DG Environment by AEA, Harwell, Owner, Editor: European Commission, DG Environment-G2, B-1049, Brussels, 2010.
13. Saber, H.H., Swinton, M.C., Kalinger, P., and Paroli, R.M., “Long-term hygrothermal performance of white and black roofs in North American climates”, *Journal of Building and Environment*, 50: 141-154, 2012, <http://dx.doi.org/10.1016/j.buildenv.2011.10.022>.
14. Saber, H.H., Swinton, M.C., Kalinger, P., and Paroli, R.M., “Hygrothermal simulations of cool reflective and conventional roofs”, *2011 NRCA International Roofing Symposium, Emerging Technologies and Roof System Performance*, held in Sept. 7-9, 2011, Washington D.C., USA.
15. Glass and Metal Curtain Walls, Best Practice Guide Building Technology, ISBN 0-660-19394-9, Cat. no. NH15-428/2004E, Canada Mortgage and Housing Corporation (CMHC), Canada, 2004.
16. Van Den Bergh S., Hart R., Jelle B.P., and Gustavsen A. “Window spacers and edge seals in insulating glass units: A state-of-the-art review and future perspectives”. *Energy and Buildings* 58: 263-280, 2013.
17. RIMA-I, Reflective Insulation Manufacturers Association International (RIMA-I), Reflective Insulation, Radiant Barriers and Radiation Control Coatings. Olathe, KS: RIMA-I, 2002.
18. [Yarbrough, D., Assessment of reflective insulations for residential and commercial applications](#). ORNL/TM-8891, Oak Ridge National Laboratory, Oak Ridge, TN. p. 1-63, 1983.
19. Saber, H.H., and Laouadi, A., “Convective heat transfer in hemispherical cavities with planar inner surfaces (1415-RP)”, *Journal of ASHRAE Transactions*, Volume 117, Part 2, 2011.
20. Saber, H.H., Laouadi, A., Galasiu, A.D., and Arsenaault, C.D., “Convective Heat Transfer Correlations for Low-Profile Spherical Cavities with Planar Bottom Surfaces (1415-RP)”, *HVAC & R Research J.*, 19(1), pp. 10-23, 2013.
21. Laouadi, A., Saber, H.H., Galasiu, A.D., and Arsenaault, C.D., “Tubular Daylighting Devices – Development and Validation of a Thermal Model (1415-RP)”, *HVAC&R Research Journal*, 19(5), pp. 513-535, 2013.
22. [Gross, W.P., and Miller, R.G., “Literature review of measurement and predictions of reflective building insulation system performance”](#), *ASHRAE Transactions*, 95 (2), pp. 651-664, 1989.
23. [Fricker, J.M., and Yarbrough, D.W., “Review of reflective insulation estimation methods](#). Proceedings of Building Simulation”, 12th Conference of International Building Performance Simulation Association, Sydney, 14-16 November 2011, pp. 1989-1996.
24. [Glicksman, L. R., “Two-dimensional heat transfer effects on vacuum and reflective insulations”](#), *Journal of Thermal Insulation*, vol. 14, pp. 281-294, 1991.
25. [Fairey, P., “The measured side-by-side performance of attic radiant barrier systems in hot and humid climates”](#), *19th International Thermal Conductivity Conference*, Cookeville, Tenn., pp. 481–496, 1985.
26. [Han, B.J., Yarbrough, D.W., and Han, S.M., “Thermal resistance of wall cavities containing reflective insulation”](#), *Journal of Solar Energy Engineering*, vol.108, pp. 338-341, 1986.
27. [Desjarlais, A.O., and Tye, R.P., “Research and development data to define the thermal performance of reflective materials used to conserve energy in building applications”](#), ORNL/Sub/88-SA835/1, 1990.
28. [Desjarlais, A.O., and Yarbrough, D.W., “Predictions of the thermal performance of single and multi-air-space reflective insulation materials”](#), *ASTM STP 1116*, R.S. Graves and D.C. Wysocki, Eds., American Society for Testing and Materials, pp. 24-43, 1991.
29. [Medina, M.A., “On the performance of radiant barriers in combination with different attic insulation levels”](#) *Journal of Energy and Buildings*, 33 (1): 31–40, 2000.
30. [Saber, H.H., and Swinton, M.C., “Determining through numerical modeling the effective thermal resistance of a foundation wall system with low emissivity material and furred – airspace”](#), the *2010 International Conference on Building Envelope Systems and Technologies, ICBEST 2010*, Vancouver, British Columbia, Canada, June 27-30, 2010, pp. 247-257.
31. [Craven, C., and Garber-Slaght, R., Product test: reflective insulation in cold climates](#), Technical Report Number TR 2011-01, Cold Climate Housing Research Center (CCHRC), Fairbanks, AK 99708, 2011, www.cchrc.org.

32. Saber, H.H., Maref, W., Swinton, M.C., and St-Onge, C., “Thermal analysis of above-grade wall assembly with low emissivity materials and furred-airspace”, *Journal of Building and Environment*, 46(7): 1403-1414, 2011, [doi:10.1016/j.buildenv.2011.01.009](https://doi.org/10.1016/j.buildenv.2011.01.009).
33. Saber, H.H., Maref, W., and Swinton, M.C., “Numerical investigation of thermal response of basement wall systems with low emissivity material and furred – airspace”, *13th Canadian Conference on Building Science and Technology (13th CCBST) Conference*, held in May 10 – 13, 2011 in Winnipeg, Manitoba, Canada.
34. D’Orazio, M., Di Perna, C., Di Giuseppe, E., and Morodo, M., “Thermal performance of an insulated roof with reflective insulation: Field tests under hot climatic conditions” *Journal of Building Physics*, 36 (3), pp. 229–246, 2012, [doi:10.1177/1744259112448181](https://doi.org/10.1177/1744259112448181).
35. Saber, H.H., and Maref, W., “Effect of furring orientation on thermal response of wall systems with low emissivity material and furred-airspace”, *Building Enclosure Science & Technology (BEST3) Conference*, held in April 2-4, 2012 in Atlanta, Georgia, USA.
36. Saber, H.H., “Investigation of thermal performance of reflective insulations for different applications”, *Journal of Building and Environment*, 55: 32-44, 2012, [doi:10.1016/j.buildenv.2011.12.010](https://doi.org/10.1016/j.buildenv.2011.12.010).
37. Saber, H.H., Maref, W., Sherrer, G., and Swinton, M.C., “Numerical modeling and experimental investigations of thermal performance of reflective insulations”, *Journal of Building Physics*, 36(2): 163-177, 2012, <http://dx.doi.org/10.1177/1744259112444021>.
38. Saber, H.H., Maref, W., and Swinton, M.C., “Thermal response of basement wall systems with low-emissivity material and furred airspace”, *Journal of Building Physics*, 35(4): pp. 353-371, 2012, [DOI: 10.1177/1744259111411652](https://doi.org/10.1177/1744259111411652).
39. Escudero, C., Martin, K., Erkoreka, A., Floresb, I., and Sala, J.M., “Experimental thermal characterization of radiant barriers for building insulation”, *Journal of Energy and Buildings*, vol. 59, pp. 62–72, 2013.
40. Tenpierik, M.J. , and Hasselaar, E., “Reflective multi-foil insulations for buildings: A review”, *Journal of Energy and Buildings*, vol. 56, pp. 233–243, 2013.
41. Saber, H.H., “Thermal performance of wall assemblies with low emissivity”, *Journal of Building Physics*, 36 (3): 308-329, 2013, [DOI: 10.1177/1744259112450419](https://doi.org/10.1177/1744259112450419).
42. Saber, H.H., “Practical correlations for the thermal resistance of vertical enclosed airspaces for building applications”, *Journal of Building and Environment*, vol. 59, pp. 379-396, 2013, <http://dx.doi.org/10.1016/j.buildenv.2012.09.003>.
43. Saber, H.H., “Practical correlation for thermal resistance of horizontal enclosed airspaces with upward heat flow for building applications”, *Journal of Building and Environment*, vol. 61, pp. 169-187, 2013, <http://dx.doi.org/10.1016/j.buildenv.2012.12.016>.
44. Saber, H.H., “Practical correlation for thermal resistance of 45° sloped enclosed airspaces with downward heat flow for building applications”, *Journal of Building and Environment*, vol. 65, pp. 154-169, 2013, <http://dx.doi.org/10.1016/j.buildenv.2013.04.009>.
45. Saber, H.H., “Practical correlation for thermal resistance of horizontal enclosed airspaces with downward heat flow for building applications”, *Journal of Building Physics*, vol. 37 (4), pp. 403-435, 2014, <http://jen.sagepub.com/content/early/2013/08/19/1744259113498473>.
46. Saber, H.H., “Practical correlation for thermal resistance of low-sloped enclosed airspaces with downward heat flow for building applications”, *HVAC&R Research Journal*, 20 (1), pp. 92-112, 2014, <http://dx.doi.org/10.1080/10789669.2013.834779>.
47. ASTM, ASTM C-518: Standard test method for steady-state heat flux measurements and thermal transmission properties by means of the heat flow meter apparatus, Annual Book of Standards, 04.06, 153-164, 2003, American Society for Testing and Materials, Philadelphia, Pa, www.astm.org.
48. Robinson, H.E., Cosgrove, L.A., and Powell, F.J., Thermal resistance of airspaces and fibrous insulations bounded by reflective airspace. Building Material & Structures Report 151, United States National Bureau of Standards, 1956.
49. Robinson, H.E., and Powlitch, F.J., “The thermal insulating value of airspaces”, Housing Research Paper No. 32, National Bureau of Standards Project ME-12, U.S. Government Printing Office, Washington, D.C., 1954.
50. Robinson, H.E., Powlitch, F.J., and Dill, R.S., “The thermal insulation value of airspaces”, Housing Research Paper 32, Housing and Home Finance Agency, 1954.
51. ASTM, ASTM C236-53: Test method for thermal conductance and transmittance of built-up sections by means of a guarded hot box, American Society for Testing and Materials, 1953.

52. IEA Annex XII, International Energy Agency, Energy Conservation in Buildings and Community Systems Programme, Annex XII, Windows and Fenestration, Step 2, Thermal and Solar Properties of Windows, Expert Guide, December, 1987.
53. ASHRAE, 2009 *ASHRAE Handbook – Fundamentals*, Chapter 26: Heat, air, and moisture control in building assemblies – material properties., SI Edition. Atlanta, GA: American Society of Heating, Refrigeration and Air-Conditioning Engineers, Inc., 2009.
54. ASTM, ASTM C-1363: Standard test method for the thermal performance of building assemblies by means of a hot box apparatus, 2006 Annual Book of ASTM Standards 04.06:717–59, www.astm.org.
55. Saber, H.H., Maref, W., Elmahdy, A.H., Swinton, M.C., and Glazer, R., “3D thermal model for predicting the thermal resistances of spray polyurethane foam wall assemblies”, *Building XI Conference*, December 5-9, 2010, Clearwater Beach, Florida, USA.
56. Saber, H.H., Maref, W., Lacasse, M.A., Swinton, M.C., Kumaran, M.K., “Benchmarking of hygrothermal model against measurements of drying of full-scale wall assemblies”, *2010 International Conference on Building Envelope Systems and Technologies, ICBEST 2010*, Vancouver, British Columbia, Canada, June 27-30, 2010, pp. 369-377.
57. Saber, H.H., Maref, W., Elmahdy, A.H., Swinton, M.C., and Glazer, R., 3D heat and air transport model for predicting the thermal resistances of insulated wall assemblies. *International Journal of Building Performance Simulation*, 5(2): 75–91, 2012, <http://dx.doi.org/10.1080/19401493.2010.532568>.
58. Air-Ins Inc., Performance evaluation of Enermax product tested for CCMC evaluation purposes as per CCMC technical guide master format 07 21 31.04, Confidential Test Report Prepared for Products of Canada Corp., AS-00202-C, August 17th, 2009.
59. Elmahdy, A.H., Maref, W., Swinton, M.C., Saber, H.H., and Glazer, R., “Development of energy ratings for insulated wall assemblies”, *2009 Building Envelope Symposium*, held in San Diego, CA, October, 26, 2009, pp. 21-30.
60. Saber, H.H., Maref, W., and Abdulghani, K., Determining through numerical modeling the effective thermal resistance of a foundation wall system with a low emissivity material bonded to thermal insulation and furred-air-space assembly – Phase II, report number B-1265.3 (A1-000440), Client Report. NRC - Construction, pp. 1-71, November, 2012.
61. Saber, H.H., Maref, W., and Abdulghani, K., Determining through numerical modeling the effective thermal resistance of a foundation wall system with a low emissivity material bonded to thermal insulation and furred-air-space assembly – Phase I, report number B-1265.2 (A1-000440), Client Report. NRC - Construction, pp. 1-111, September, 2012.
62. Saber, H.H., and Maref, W., Determining through numerical modeling the effective thermal resistance of a foundation wall system with a low emissivity material bonded to thermal insulation and furred-air-space assembly: Model benchmarking and sensitivity analyses, Client Report. NRC Institute for Research in Construction, pp. 1-7, October 2011 (B-1265.1).
63. Saber, H.H., Maref, W., Armstrong, M.M., Swinton, M.C., Rousseau, M.Z., and Ganapathy, G., "Benchmarking 3D Thermal Model against Field Measurement on the Thermal Response of an Insulating Concrete Form (ICF) Wall in Cold Climate", Eleventh International Conference on Thermal Performance of the Exterior Envelopes of Whole Buildings XI (Clearwater, FL, USA, December 4-9, 2010).
64. Saber, H.H., Maref, W., Gnanamurugan, G., and Nicholls, M., “Energy Retrofit Using VIPs: - an Alternative Solution for Enhancing the Thermal Performance of Wood-Frame Walls”, *Journal of Building Physics*, vol. 39(1), pp. 35-68, 2015.
65. Saber, H.H., Maref, W., Gnanamurugan, G. and Nicholls, M., “Model Benchmarking for Field Energy Retrofit towards Highly Insulated Residential Wood-Frame Construction Using VIPs” 11th International Vacuum Insulation Symposium (IVIS2013), September 19-20, 2013, Empa, Switzerland.
66. Mukhopadhyaya, P., and Van Reenen, D., Heat Flow Characterization of Three GDDC (Geometrically Defined Drainage Cavity) Specimens, Client Report: A1-003165.1, National Research Council of Canada, Construction Portfolio, Ottawa, Canada, July 2013.
67. ASTM C 177-04, Standard Test Method for Steady-State Heat Flux Measurements and Thermal Transmission Properties by Means of the Guarded-Hot-Plate Apparatus, Section 4, vol. 04.06, Thermal Insulation, 2012 Book of ASTM Standards.

APPENDIX 1

Table A9 – Material Properties

Material NO.	English	Material name	Thermal conductivity (W/m.K)
1	Mullion	Anodized Aluminum	237
2	Rigid Insulation block	XPS or EPS	XPS: 0.029 / EPS: 0.037
3	Dry gasket	Silicone (confirmed)	0.35
4	Dry gasket	Silicone	0.35
5	Cap	Clear anodized aluminum?	237
6	Pressure plate	Aluminum	237
7	Mullion	Anodized Aluminum	237
8	Mullion	Anodized Aluminum	237
9	Back pan Insulation	Roxul (Curtain Rock)	0.0343
10	Back pan	Steel	50
11	Dry gasket	Silicone	0.35
12		Aluminum	237
13	Dry gasket	Silicone	0.35
14	Dry gasket	Anodized Aluminum	237
15	Mullion	Anodized Aluminum	237
16	Mullion	Anodized Aluminum	237
17	Dry gasket	Silicone	0.35
18	Mullion	Anodized Aluminum	237
19	Fill gas	Argon (90% Ar and 10% Air)	f(T)
20	Silicon sealant	Silicon	0.35
21	Thermal brick	Polyamide (confirmed)	0.3
22	Metallic spacer	Stainless steel (product data)	15
23	Desiccant bead	Silica gel loose fill?	0.03
24	IG secondary seal	Silicon (confirmed)	0.35
25	Setting Block	Silicon (confirmed)	0.35
26	Desiccant Container		15
27	Glass		1

APPENDIX 2

RESULTS OF SIMULATION OF DOUBLE-GLAZED CURTAIN WALL MANUFACTURED PRODUCTS

- 2-Glz (Epsilon) – TO Benchmark report
 - 2-Glz – durability – Ar/Air depletion ($e_{\text{coat}} = 0.054$)
 - 2-Glz – coating emissivity ($e_{\text{coat}} = 0$ to 0.84)

A2.1 Predicted to total heat loss through curtain wall panel derived from simulation

The predicted total heat loss through the curtain wall panel derived from simulation and in relation to the fraction (by volume) of air present in the low-e (0.054) IGUs is given in Figure A91. The predicted overall heat loss when the Argon gas fraction in the IGUs diminishes from 1 to 0 is 11%. The red marker in Figure A91 shows the value obtained in the test if it is assumed that the IGUs are 90% filled with Argon gas. Similar estimates as those for thermal resistance could be made for heat loss as a function of time using the information provided in Figure A91 and assuming a 1% loss in Argon concentration per year.

A2.2 Predicted R-value in relation to emissivity of glazing as derived from simulation

The predicted R-value (surface-to-surface) of a curtain wall panel, derived from simulation, and in relation to the glazing emissivity on surface 2 of the IGUs is given Figure A92. The prediction is based on having 90% Argon gas filled IGUs in the curtain wall panel. The emissivity may increase over time from the degradation of the IGU. As the IGU deteriorates, over time the Argon gas concentration diminishes as air and moisture replace the inert gas. Any moisture present in the air may at times condense on the glass surfaces thereby increasing the emissivity of the coated surface. The net effect on the R-value can be estimated from the information provided in Figure A92.

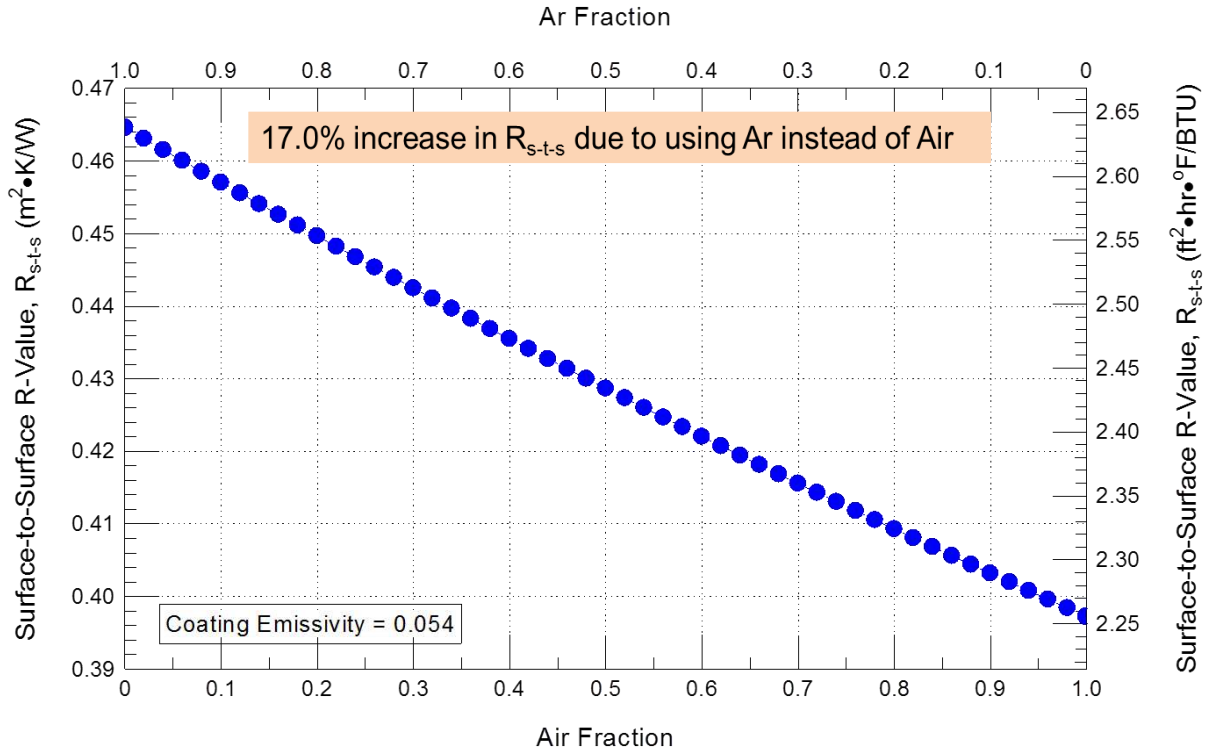


Figure A87 – Predicted (by simulation) R-value (surface-to-surface) of double-glazed thermally broken curtain wall panel in relation to fraction (by volume) of air present in the low-e (0.054) IGUs

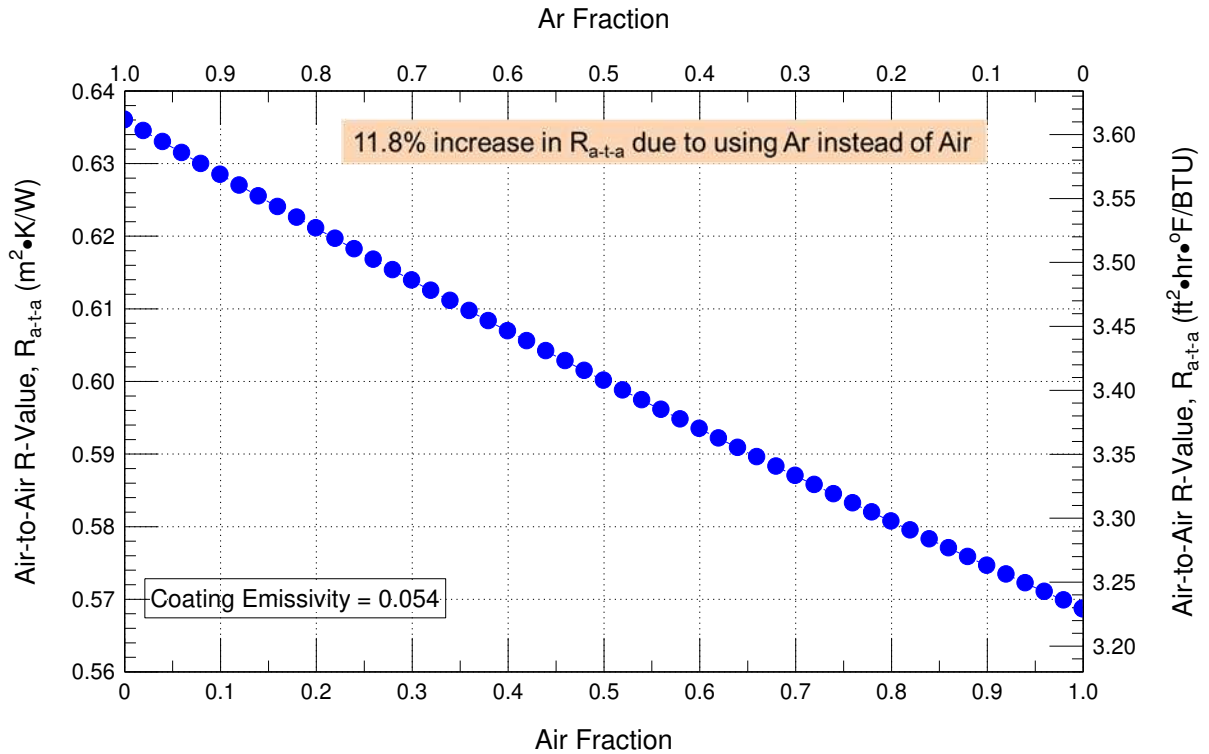


Figure A88 – Predicted (by simulation) R-value (air-to-air) of double-glazed thermally broken curtain wall panel in relation to fraction (by volume) of air present in the low-e (0.054) IGUs

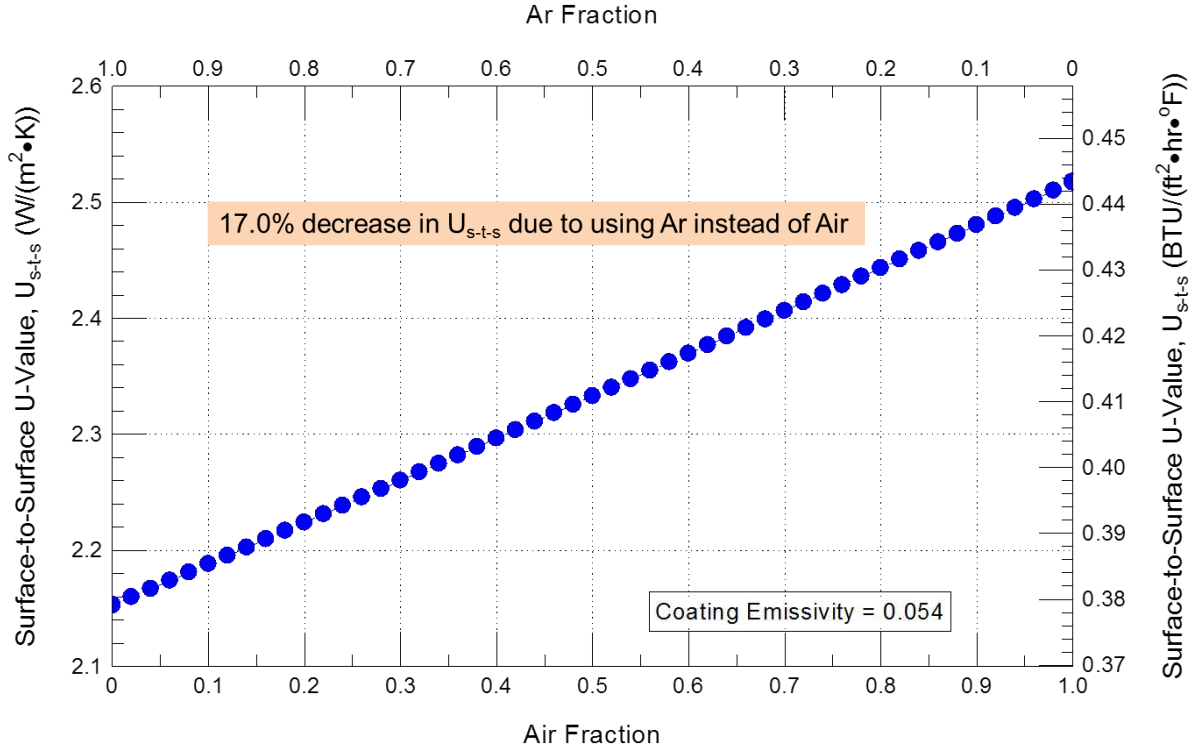


Figure A89 - Predicated (by simulation) U-value (surface -to-surface) of double-glazed thermally broken curtain wall panel in relation to fraction (by volume) of air present in the low-e (0.054) IGUs

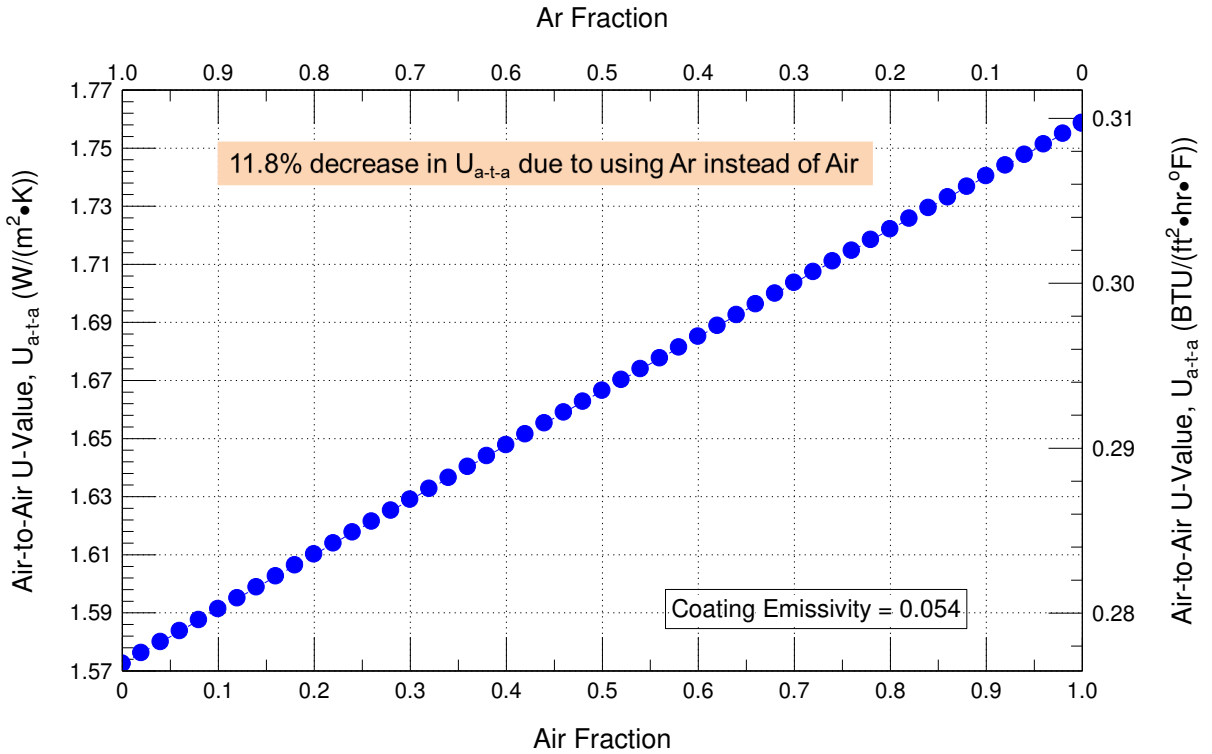


Figure A90 – Predicated (by simulation) U-value (air-to-air) of double-glazed thermally broken curtain wall panel in relation to fraction (by volume) of air present in the low-e (0.054) IGUs

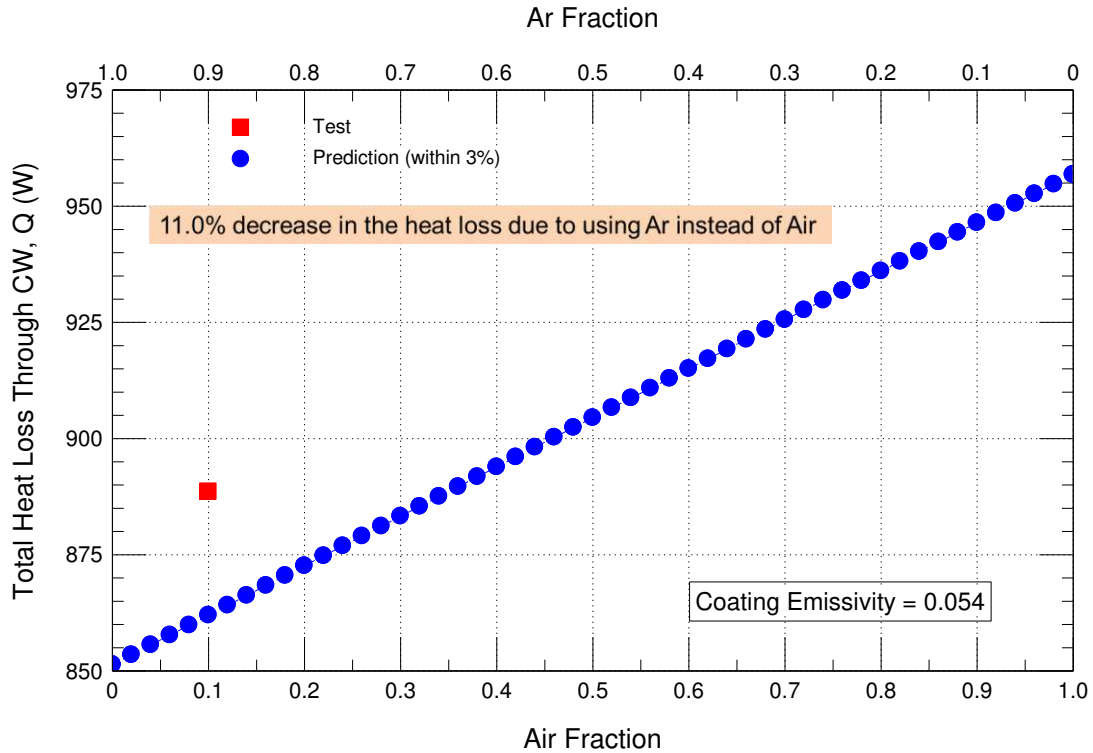


Figure A91 - Predicated (by simulation) total heat loss through double-glazed thermally broken curtain wall panel in relation to fraction (by volume) of air present in the low-e (0.054) IGUs; red marker shows test value

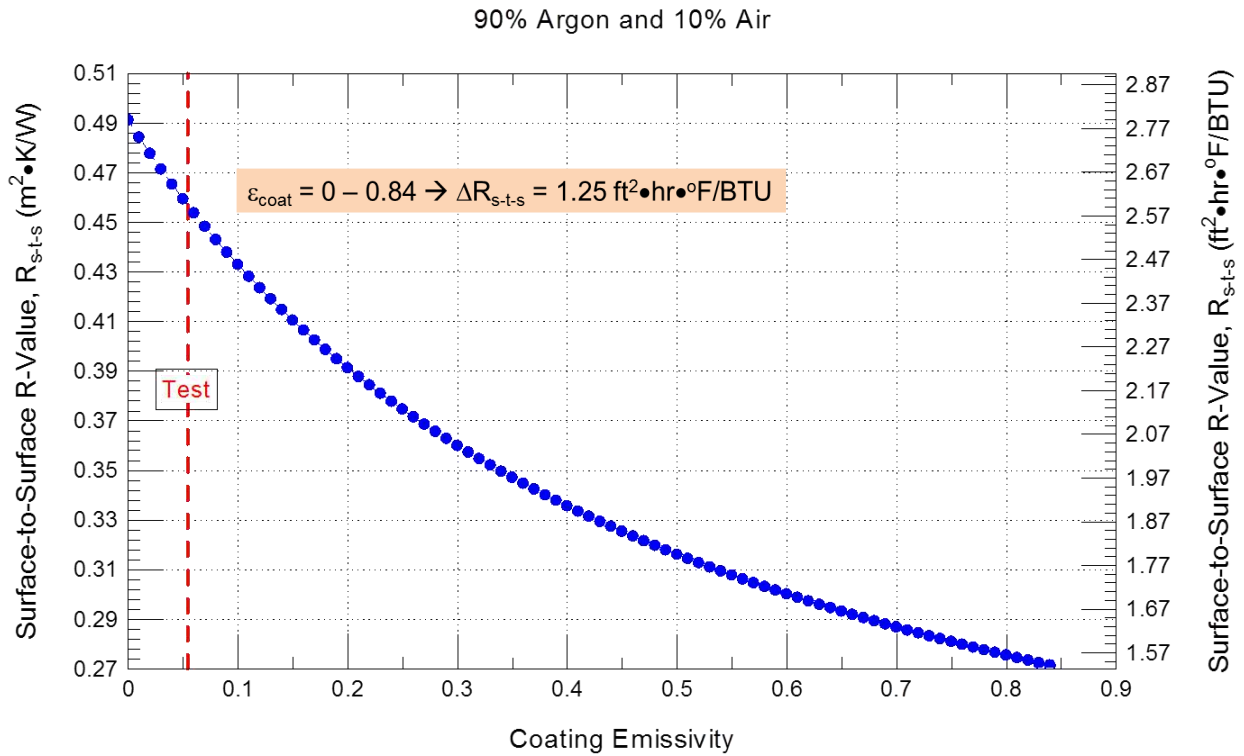


Figure A92 - Predicted (by simulation) R-value (surface-to-surface) of double-glazed thermally broken curtain wall panel in relation to glazing emissivity on surface 2 of IGUs; 90% Ar filled IGU

90% Argon and 10% Air

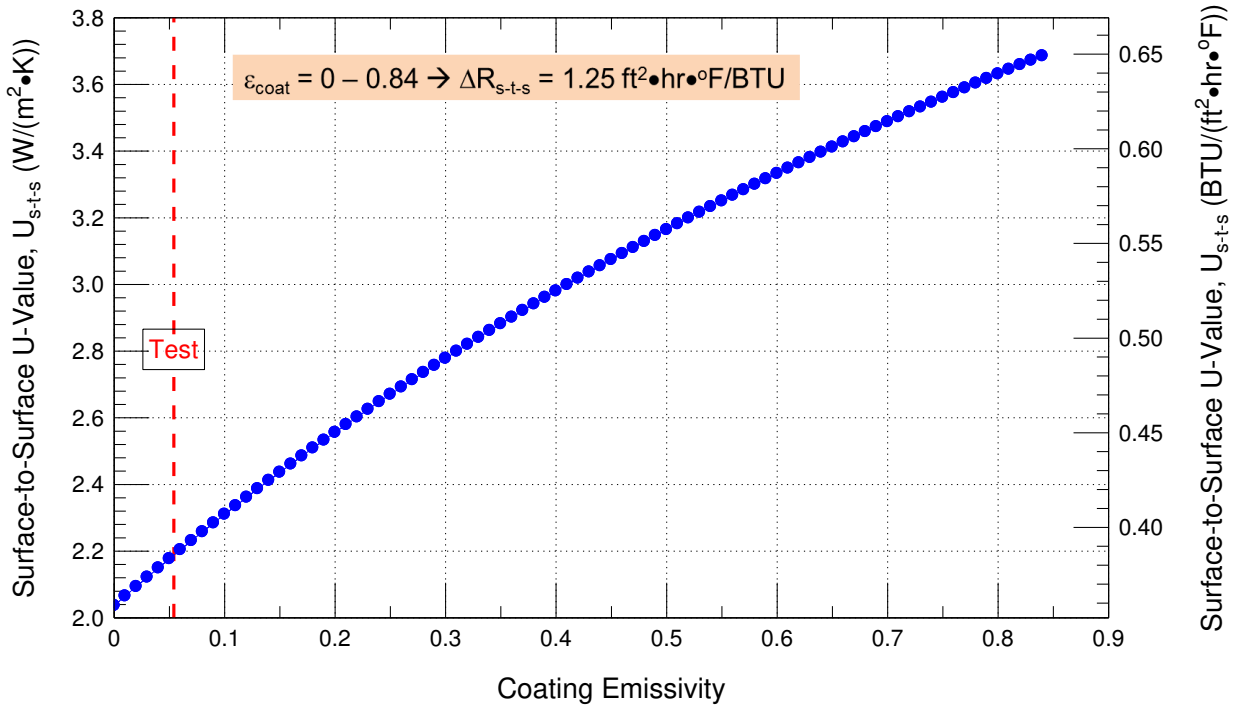


Figure A93 - Predicted (by simulation) U-value (surface-to-surface) of double-glazed thermally broken curtain wall panel in relation to glazing emissivity on surface 2 of IGUs; 90% Ar filled IGU

90% Argon and 10% Air

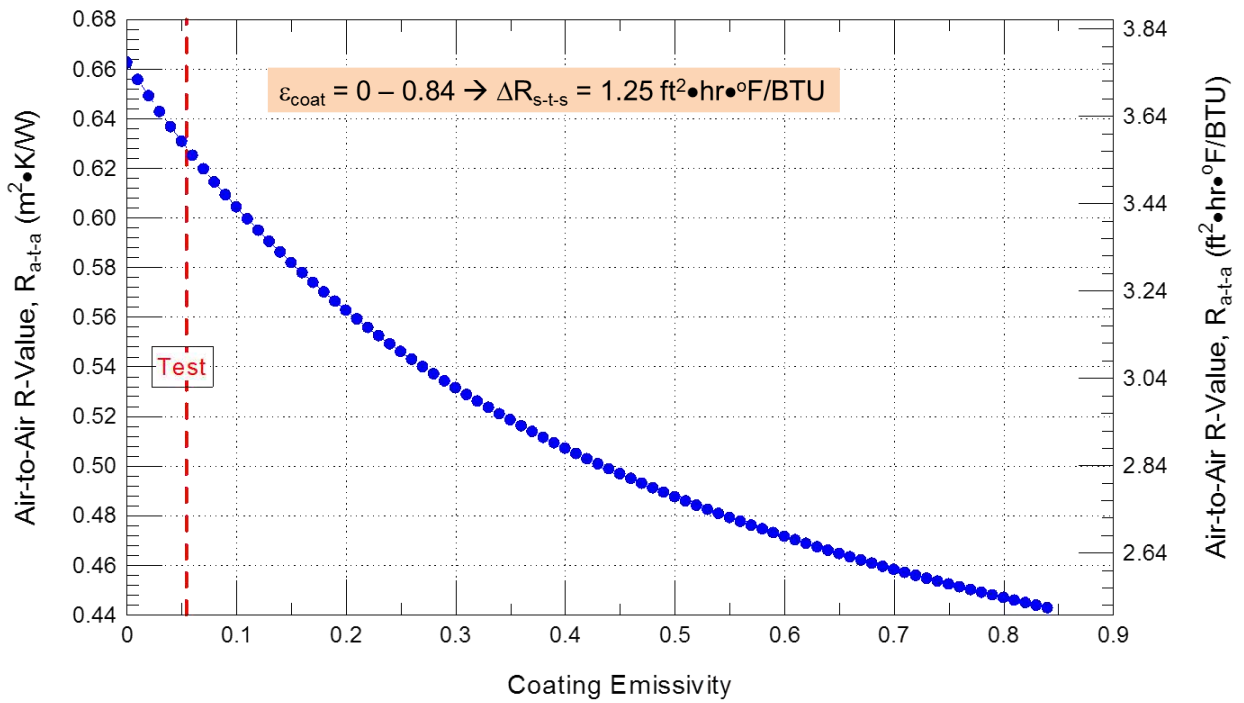


Figure A94 - Predicted (by simulation) R-value (air-to-air) of double-glazed thermally broken curtain wall panel in relation to glazing emissivity on surface 2 of IGUs; 90% Ar filled IGU

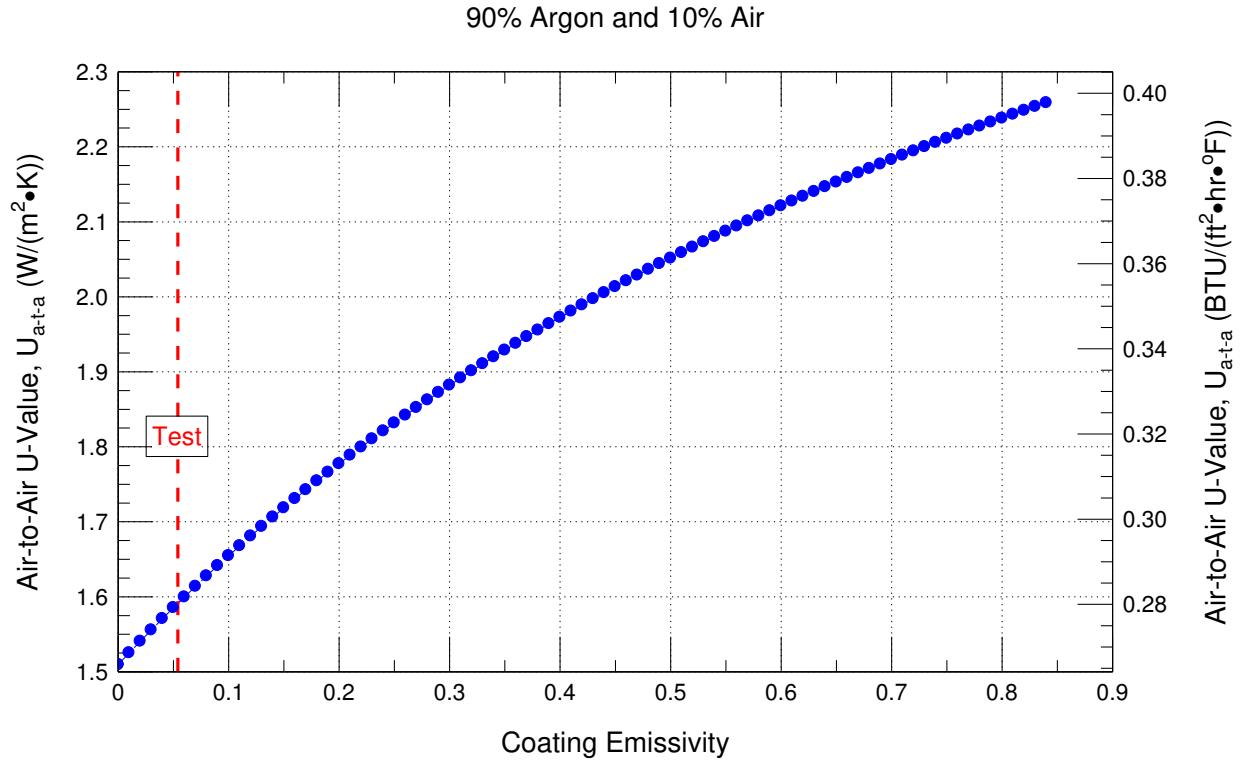


Figure A95 - Predicted (by simulation) U-value (air-to-air) of double-glazed thermally broken curtain wall panel in relation to glazing emissivity on surface 2 of IGUs; 90% Ar filled IGU

APPENDIX 3

RESULTS OF SIMULATION OF TRIPLE-GLAZED CURTAIN WALL MANUFACTURERS PRODUCT

Effect of Glazing to Wall Area Ratio / Case-I: 90% Ar and 10% Air, Low-e Coating ($\epsilon_{coat} = 0.054$)

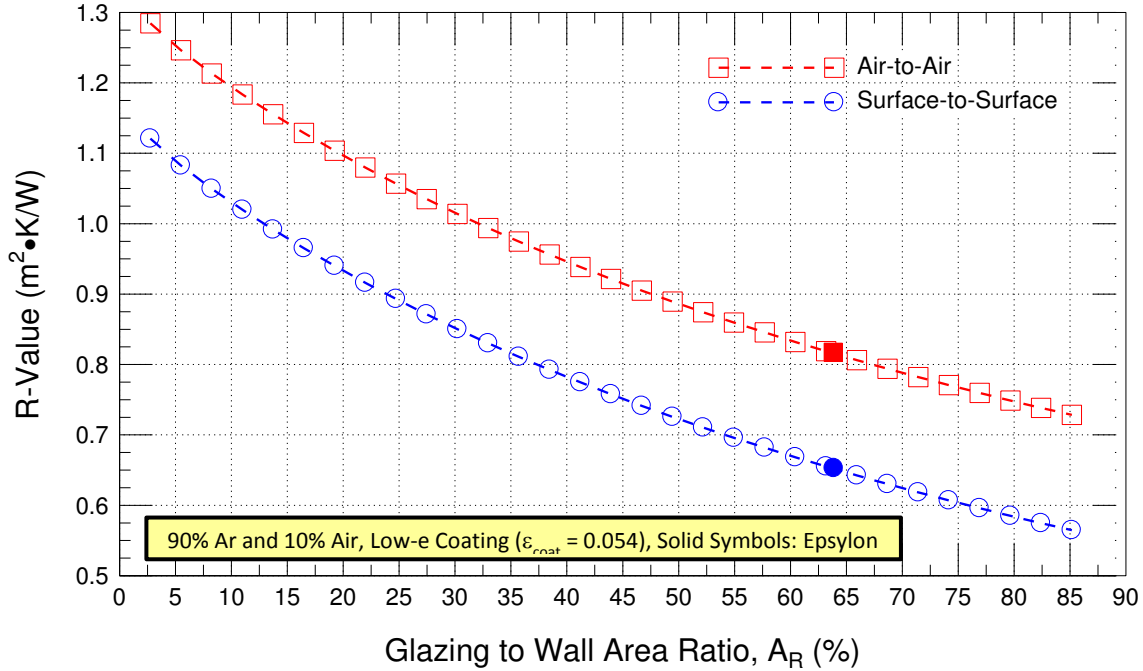


Figure A96 - Predicted (by simulation) R-value (air-to-air; surface-to-surface) of triple-glazed low-e coated ($\epsilon = 0.054$) thermally broken curtain wall panel in relation to glazing to Wall Area Ratio; 90% Ar filled IGU

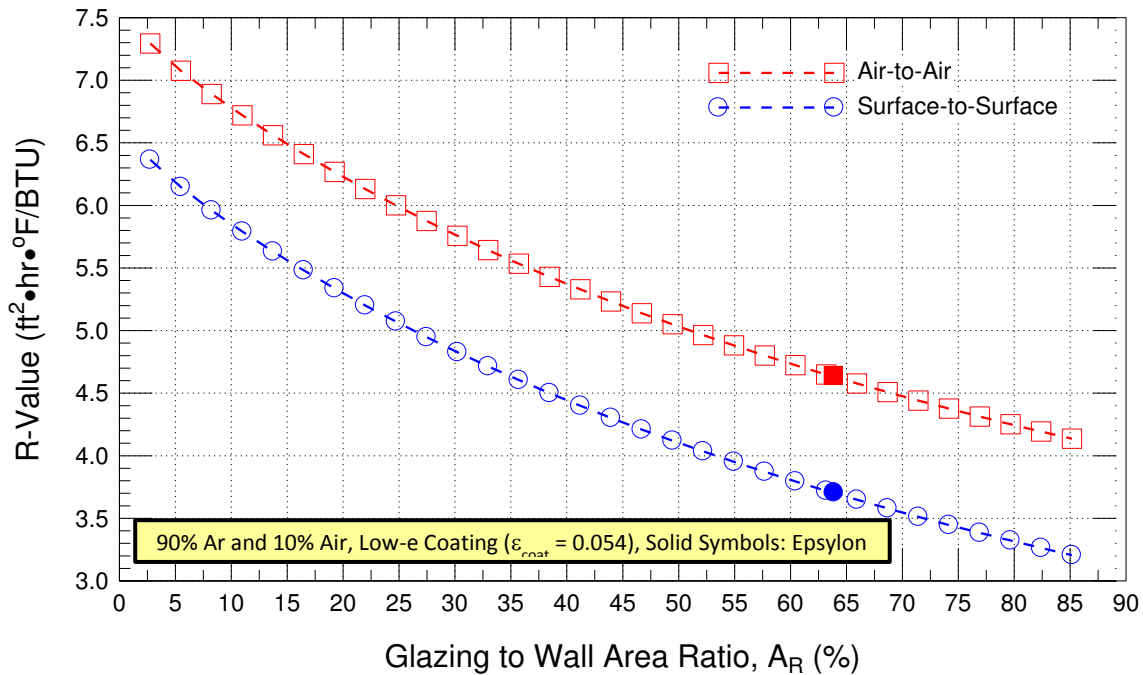


Figure A97 - Predicted (by simulation) R-value (air-to-air; surface-to-surface) of triple-glazed low-e coated ($\epsilon = 0.054$) thermally broken curtain wall panel in relation to glazing to Wall Area Ratio; 90% Ar filled IGU

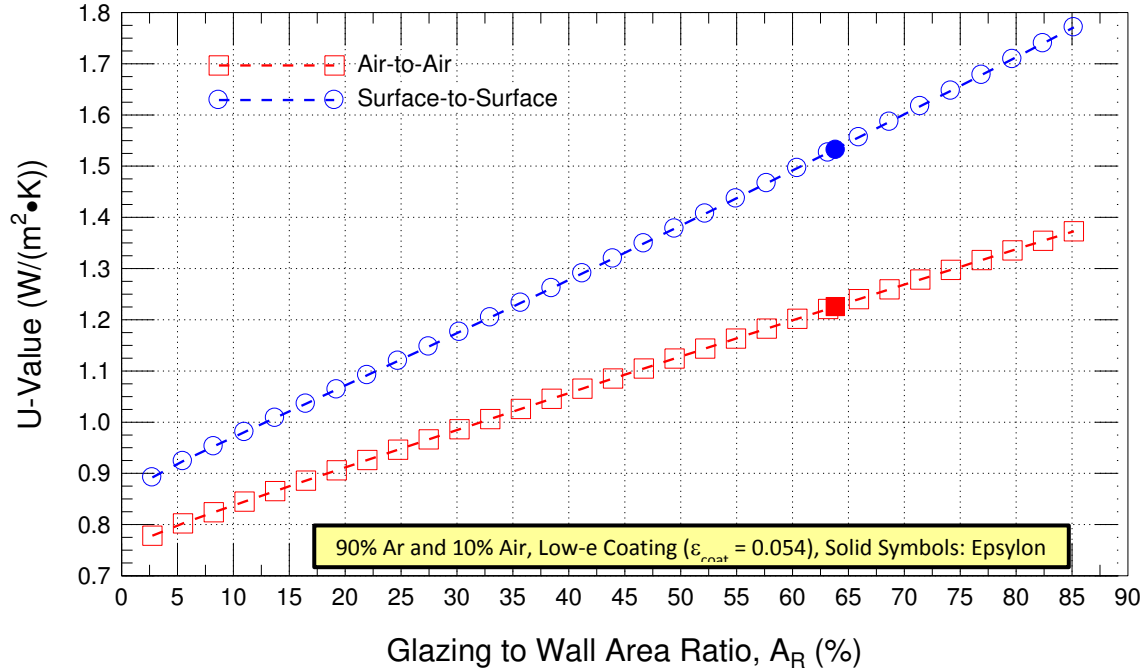


Figure 98 - Predicted (by simulation) U-value (air-to-air; surface-to-surface) of triple-glazed low-e coated ($e = 0.054$) thermally broken curtain wall panel in relation to glazing to Wall Area Ratio; 90% Ar filled IGU

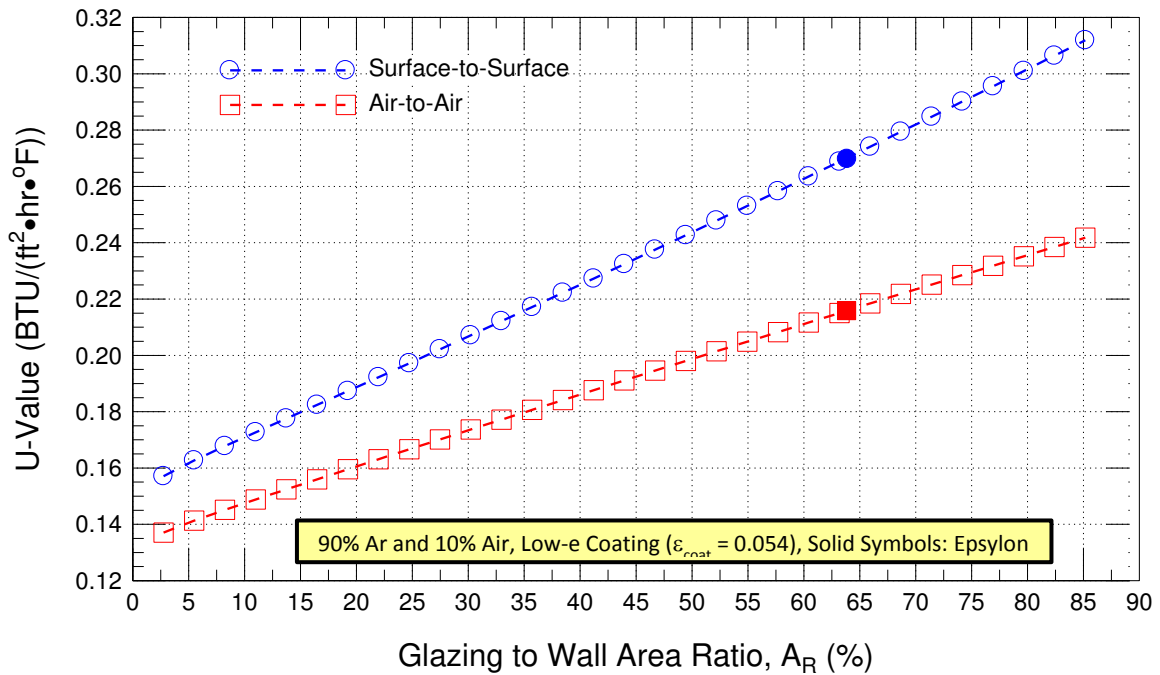


Figure 99 - Predicted (by simulation) U-value (air-to-air; surface-to-surface) of triple-glazed low-e coated ($e = 0.054$) thermally broken curtain wall panel in relation to glazing to Wall Area Ratio; 90% Ar filled IGU

Effect of Glazing to Wall Area Ratio / **Case-II: 90% Kr and 10% Air, Low-e Coating ($\epsilon_{coat} = 0.054$)**

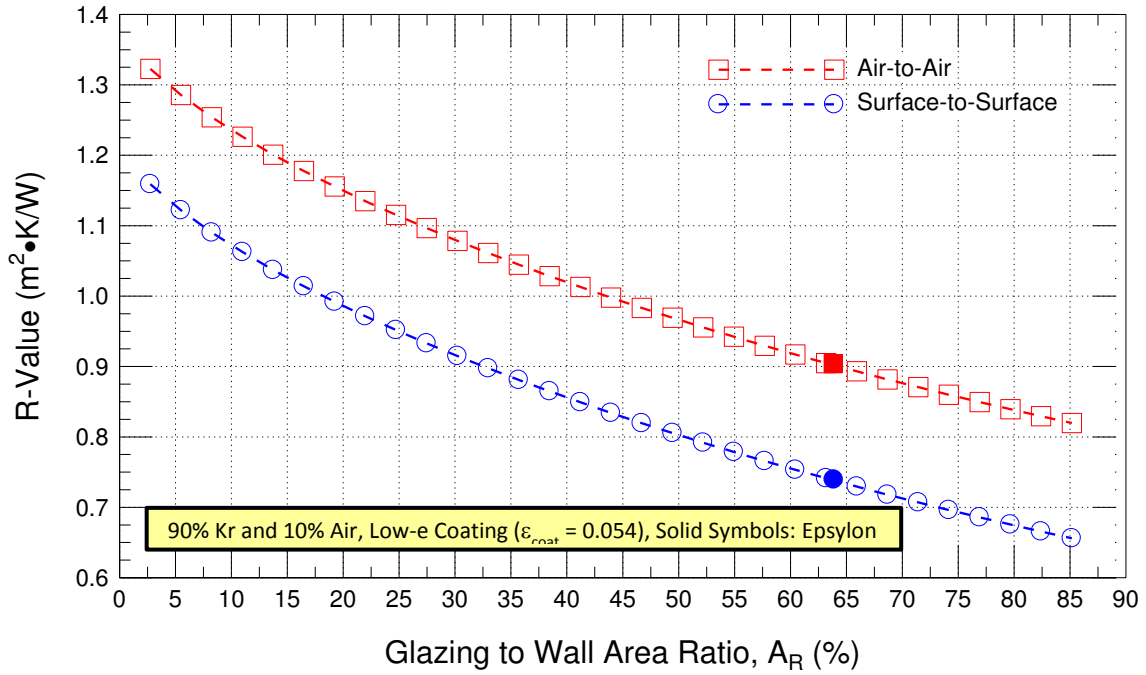


Figure A100 – Predicted (by simulation) R-value (air-to-air; surface-to-surface) of triple-glazed low-e coated ($\epsilon = 0.054$) thermally broken curtain wall panel in relation to glazing to Wall Area Ratio; 90% Kr filled IGU

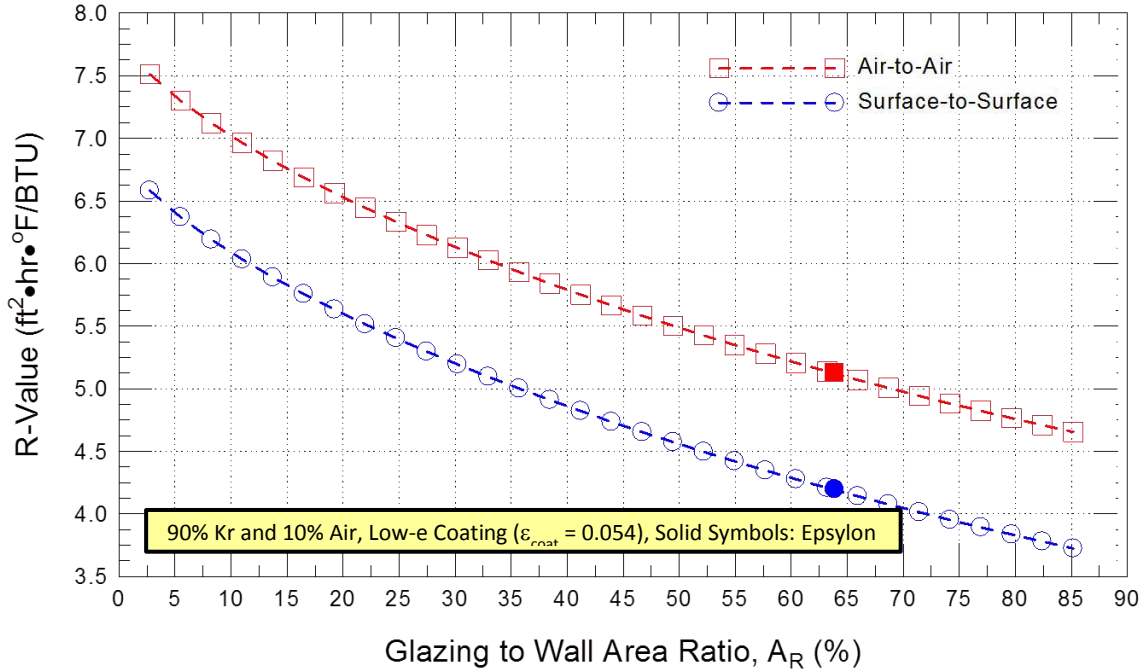


Figure A101 - Predicted (by simulation) R-value (air-to-air; surface-to-surface) of triple-glazed low-e coated ($\epsilon = 0.054$) thermally broken curtain wall panel in relation to glazing to Wall Area Ratio; 90% Kr filled IGU

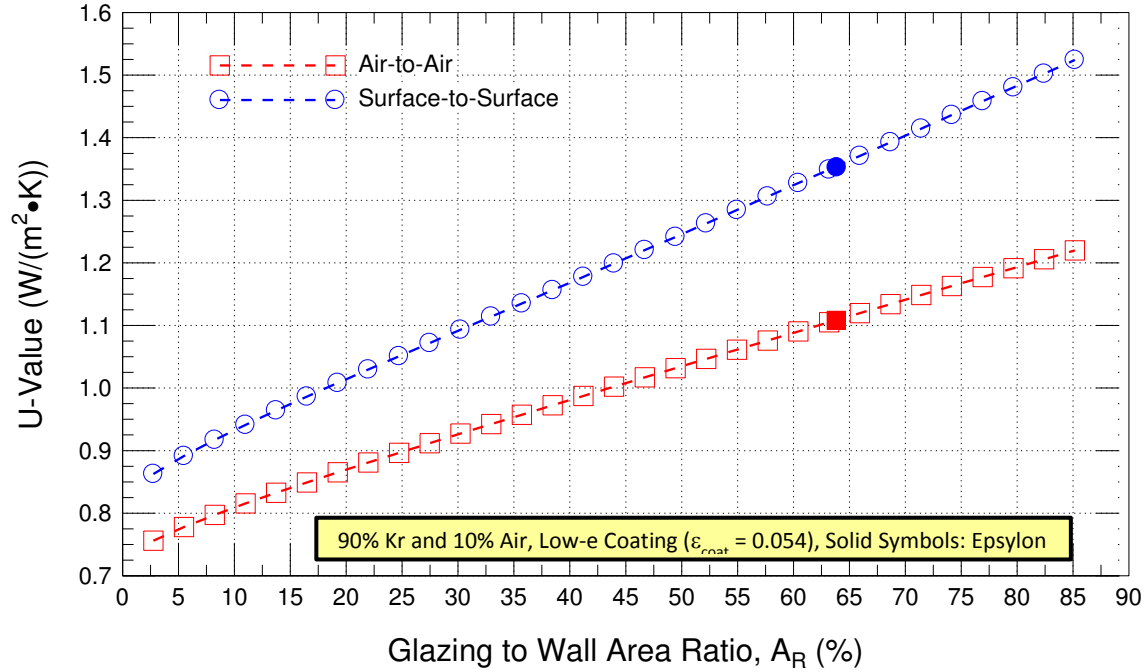


Figure A102 - Predicted (by simulation) U-value (air-to-air; surface-to-surface) of triple-glazed low-e coated ($e = 0.054$) thermally broken curtain wall panel in relation to glazing to Wall Area Ratio; 90% Kr filled IGU

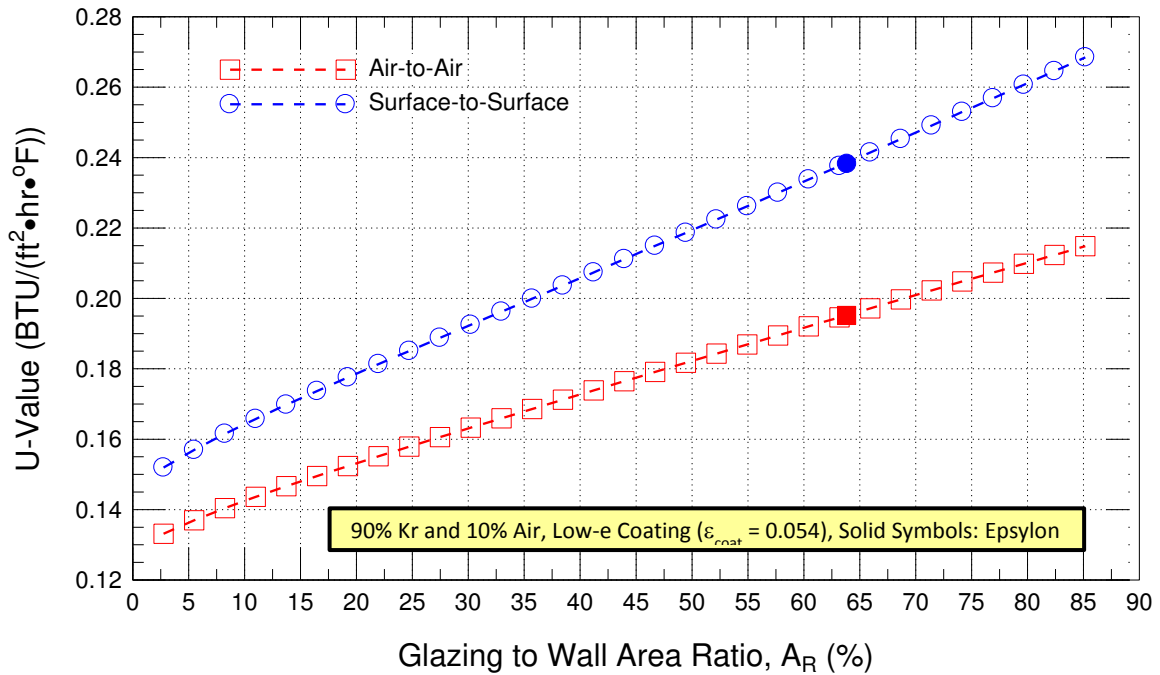


Figure A103 - Predicted (by simulation) U-value (air-to-air; surface-to-surface) of triple-glazed low-e coated ($e = 0.054$) thermally broken curtain wall panel in relation to glazing to Wall Area Ratio; 90% Kr filled IGU

Effect of Glazing to Wall Area Ratio / Case-III: 90% Xe and 10% Air, Low-e Coating (ecoat = 0.054)

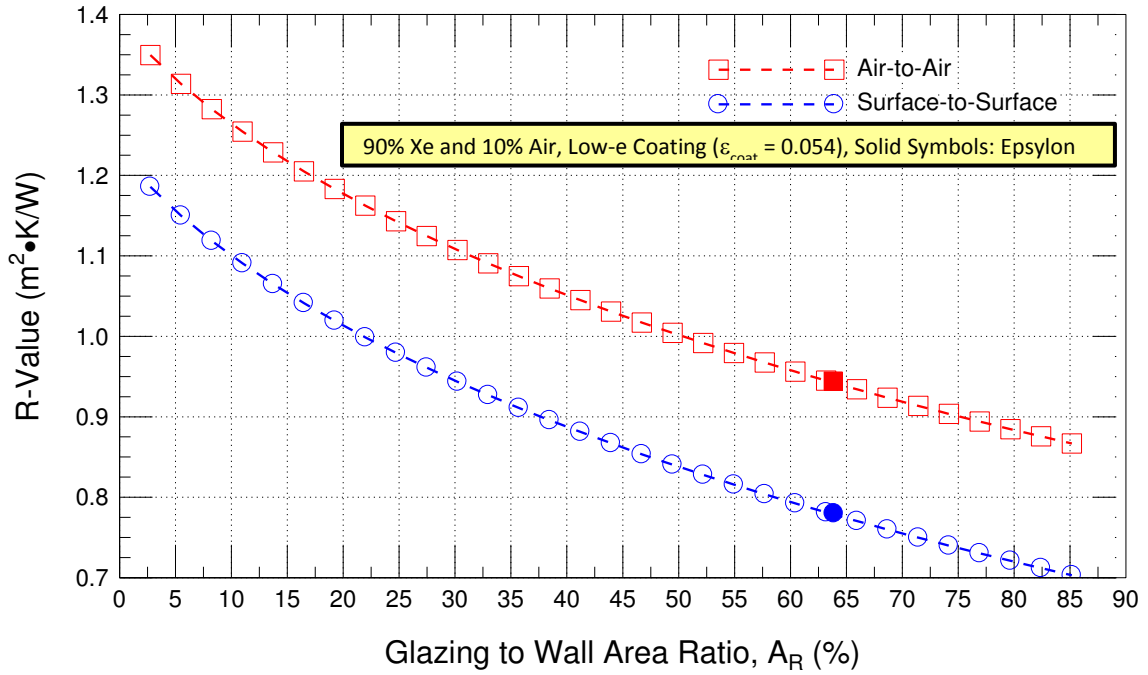


Figure A104 - Predicted (by simulation) R-value (air-to-air; surface-to-surface) of triple-glazed low-e coated ($e = 0.054$) thermally broken curtain wall panel in relation to glazing to Wall Area Ratio; 90% Xe filled IGU

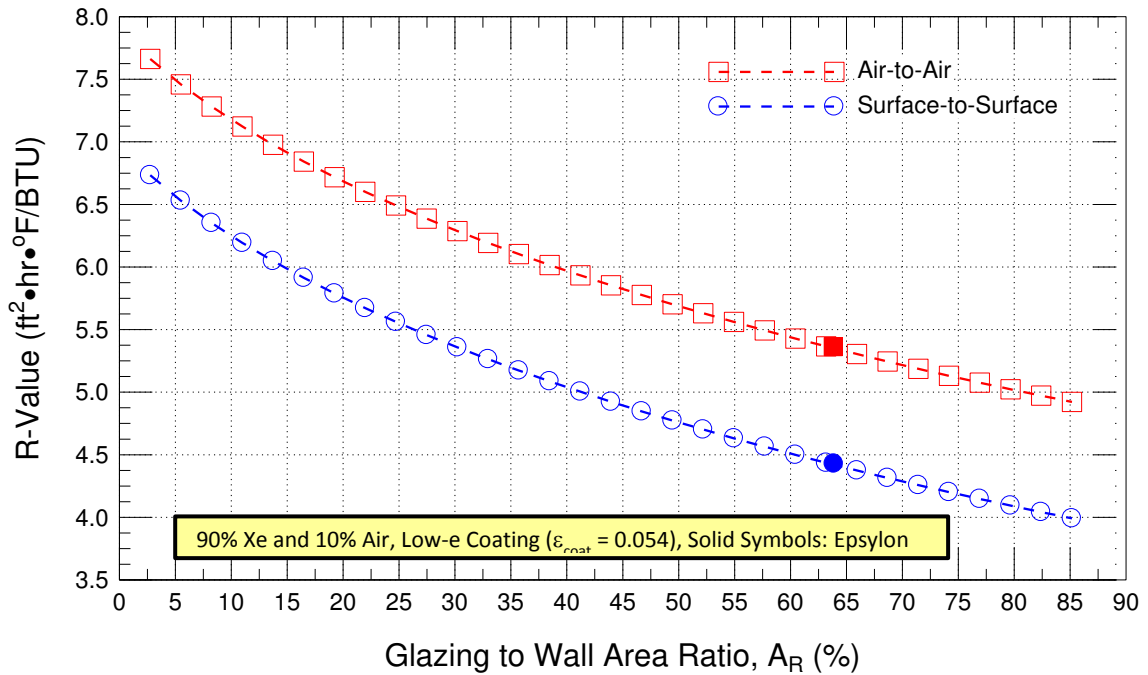


Figure A105 - Predicted (by simulation) R-value (air-to-air; surface-to-surface) of triple-glazed low-e coated ($e = 0.054$) thermally broken curtain wall panel in relation to glazing to Wall Area Ratio; 90% Xe filled IGU

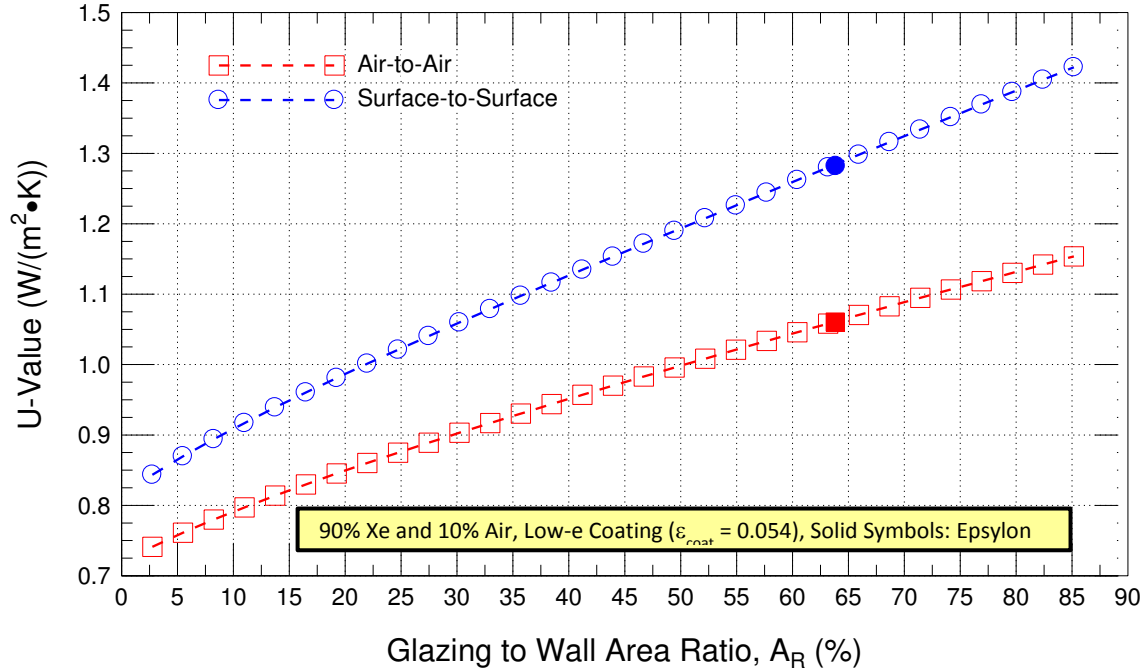


Figure A106 - Predicted (by simulation) U-value (air-to-air; surface-to-surface) of triple-glazed low-e coated ($\epsilon = 0.054$) thermally broken curtain wall panel in relation to glazing to Wall Area Ratio; 90% Xe filled IGU

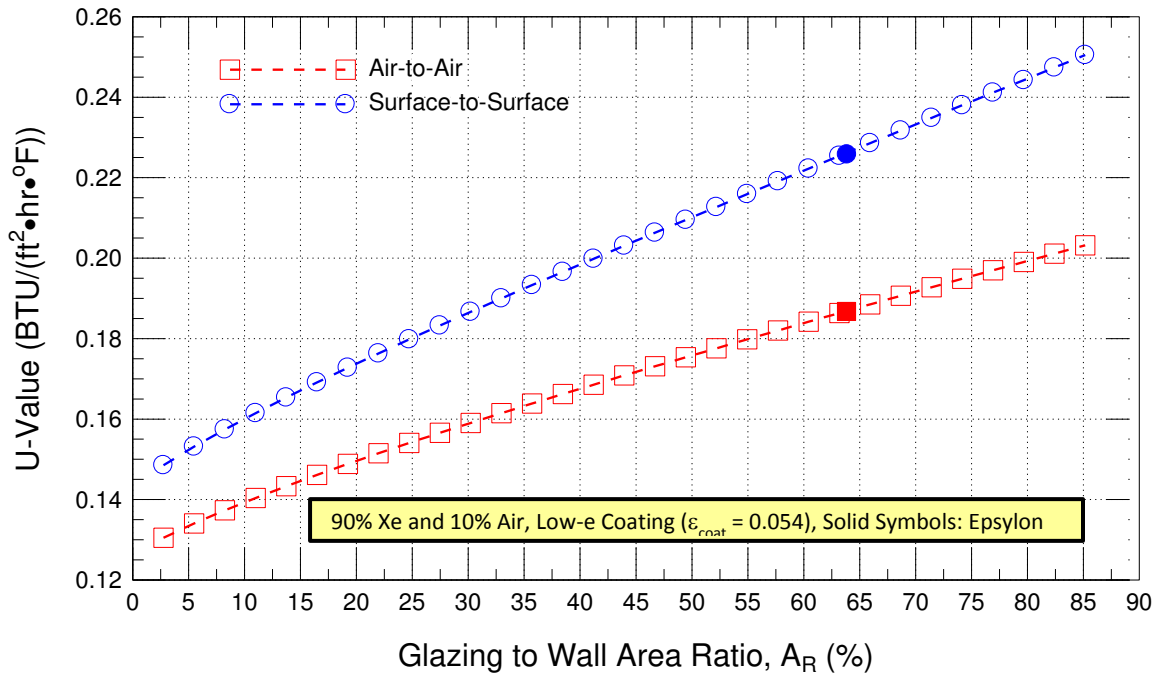


Figure 107 - Predicted (by simulation) U-value (air-to-air; surface-to-surface) of triple-glazed low-e coated ($\epsilon = 0.054$) thermally broken curtain wall panel in relation to glazing to Wall Area Ratio; 90% Xe filled IGU

Effect of Glazing to Wall Area Ratio / Air, Low-e Coating ($\epsilon_{coat} = 0.054$)

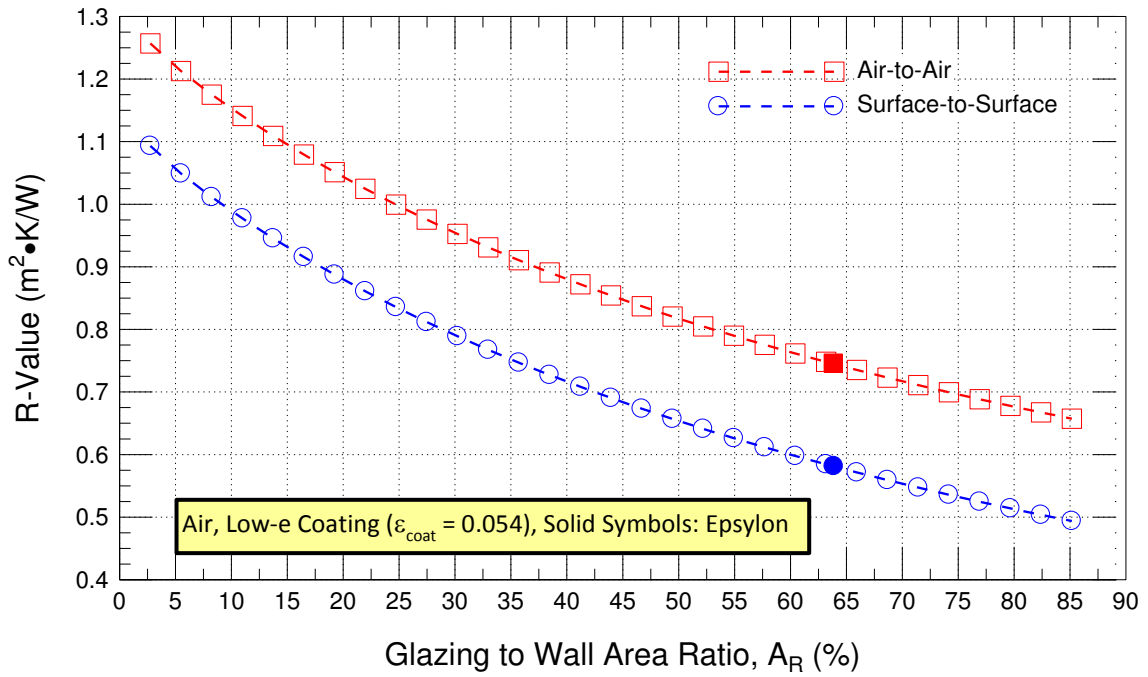


Figure A108 - Predicted (by simulation) R-value (air-to-air; surface-to-surface) of triple-glazed low-e coated ($e = 0.054$) thermally broken curtain wall panel in relation to glazing to Wall Area Ratio; Air filled IGU

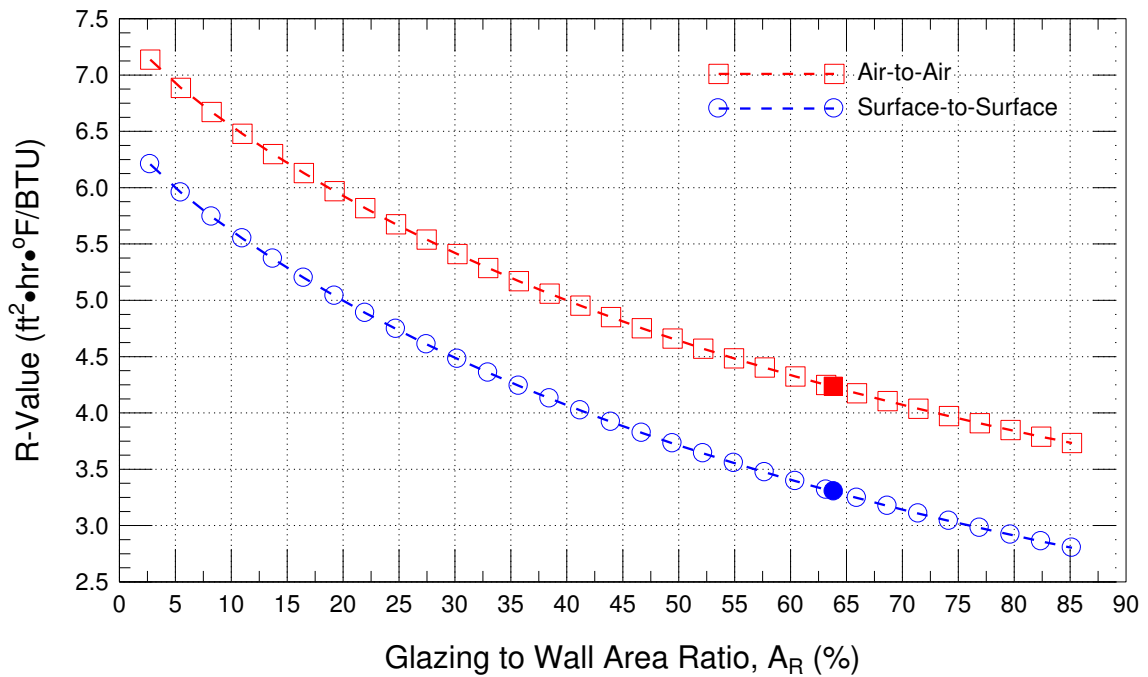


Figure A109 - Predicted (by simulation) R-value (air-to-air; surface-to-surface) of triple-glazed low-e coated ($e = 0.054$) thermally broken curtain wall panel in relation to glazing to Wall Area Ratio; Air filled IGU

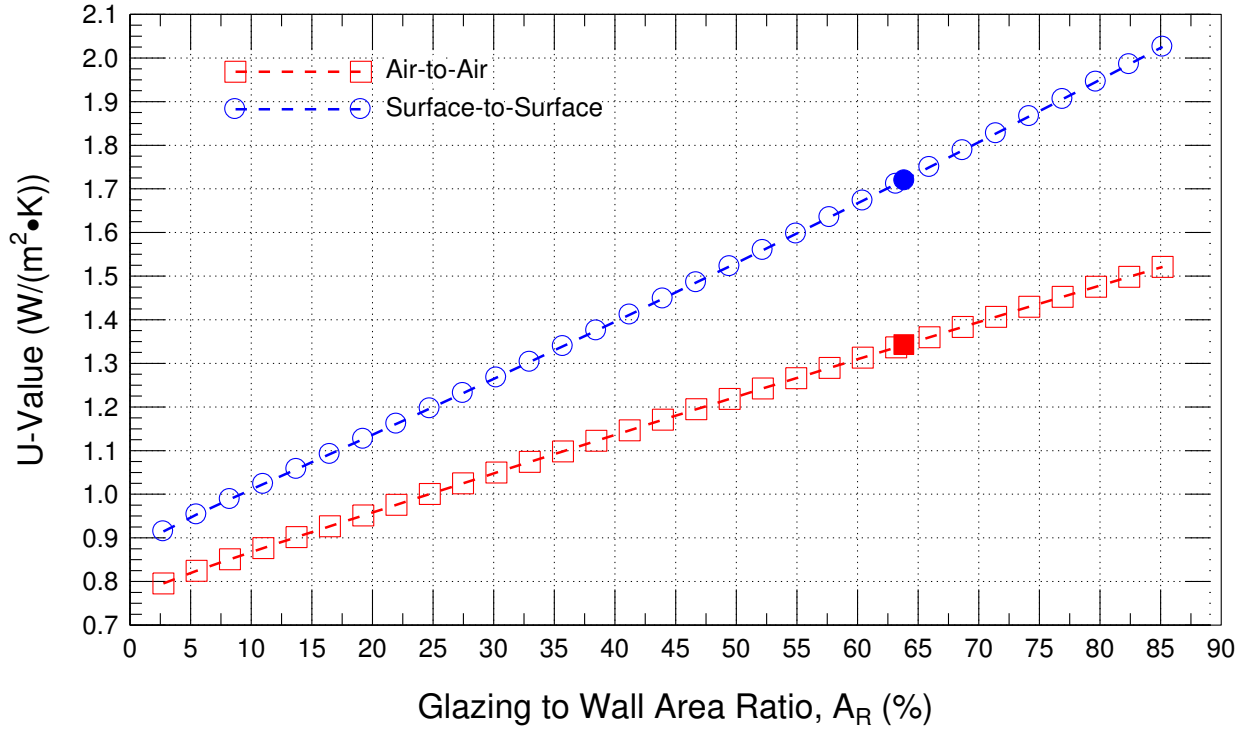


Figure A110 - Predicted (by simulation) U-value (air-to-air; surface-to-surface) of triple-glazed low-e coated ($e = 0.054$) thermally broken curtain wall panel in relation to glazing to Wall Area Ratio; Air filled IGU

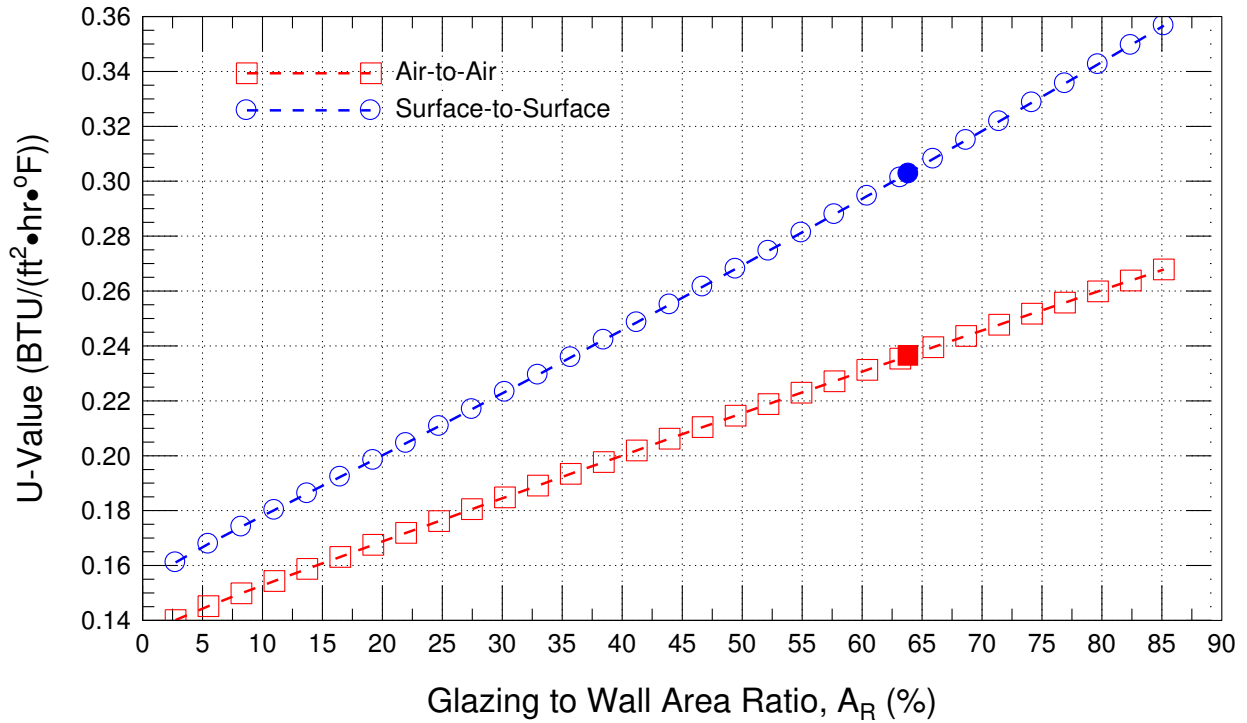


Figure A111 - Predicted (by simulation) U-value (air-to-air; surface-to-surface) of triple-glazed low-e coated ($e = 0.054$) thermally broken curtain wall panel in relation to glazing to Wall Area Ratio; Air filled IGU

Effect of Glazing to Wall Area Ratio/Case-IV: Air filled IGU;
 Low-e Coating vs. no Coating ($\epsilon_{\text{coat}}=0.054 / \epsilon=0.84$)

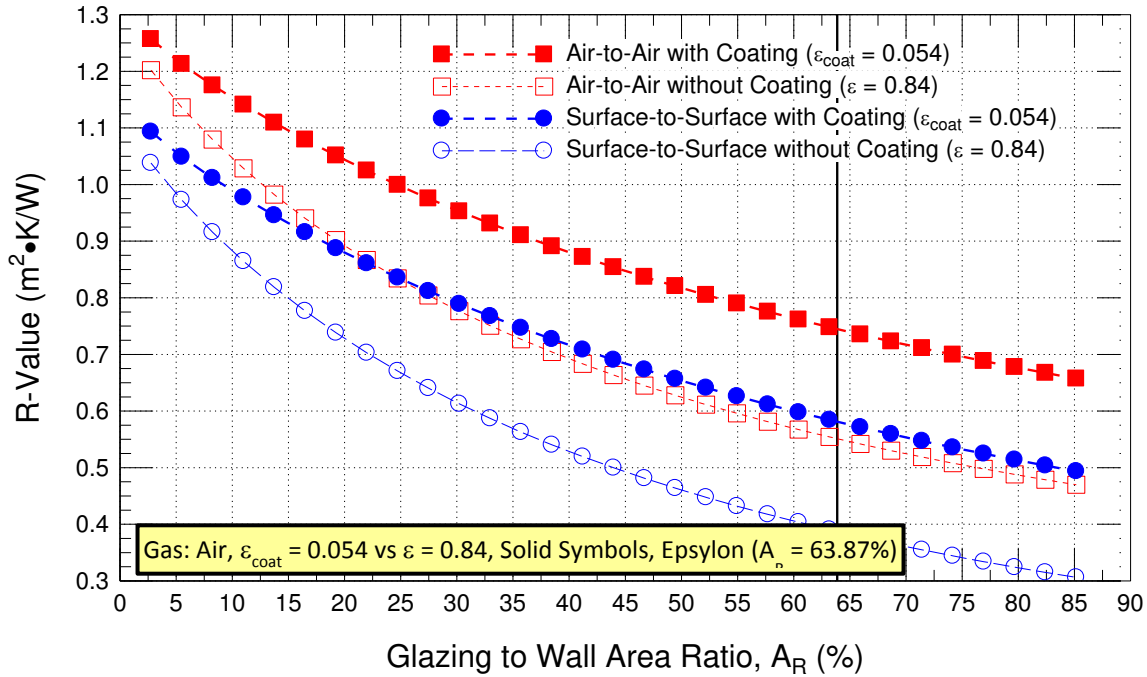


Figure A112 – Predicted (by simulation) R-value (air-to-air; surface-to-surface) of triple-glazed low-e coated ($\epsilon = 0.054$) or not coated ($\epsilon = 0.84$) thermally broken curtain wall in relation to glazing to Wall Area Ratio; Air filled IGU

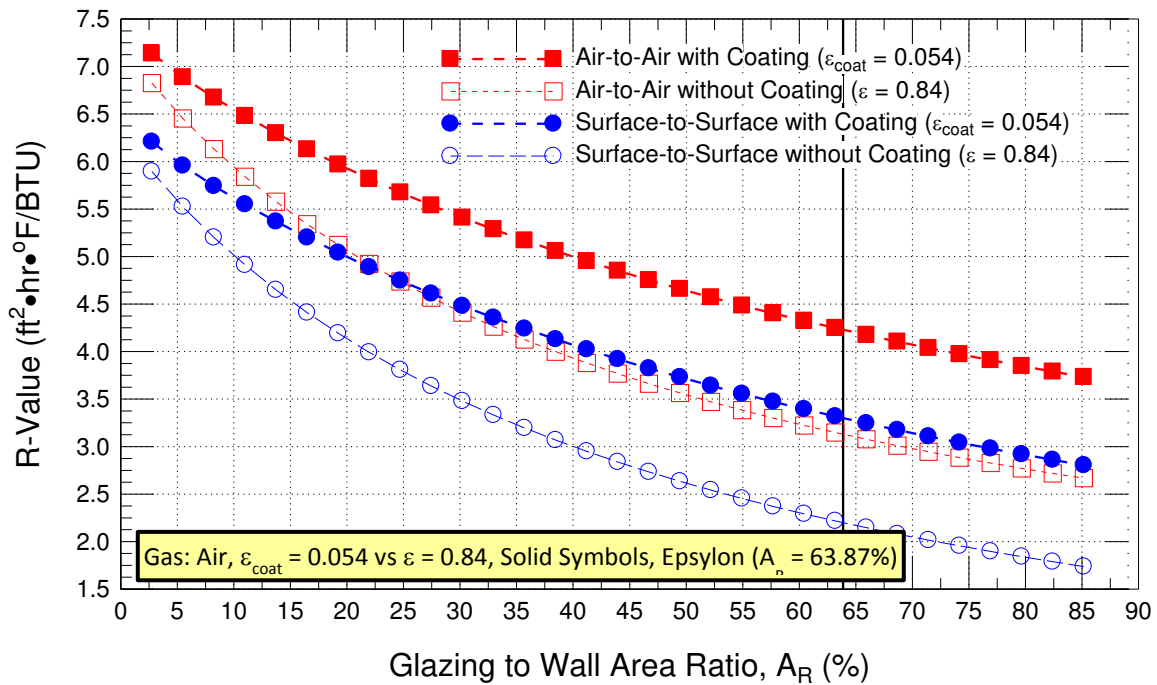


Figure A113 - Predicted (by simulation) R-value (air-to-air; surface-to-surface) of triple-glazed low-e coated ($\epsilon = 0.054$) or not coated ($\epsilon = 0.84$) thermally broken curtain wall in relation to glazing to Wall Area Ratio; Air filled IGU

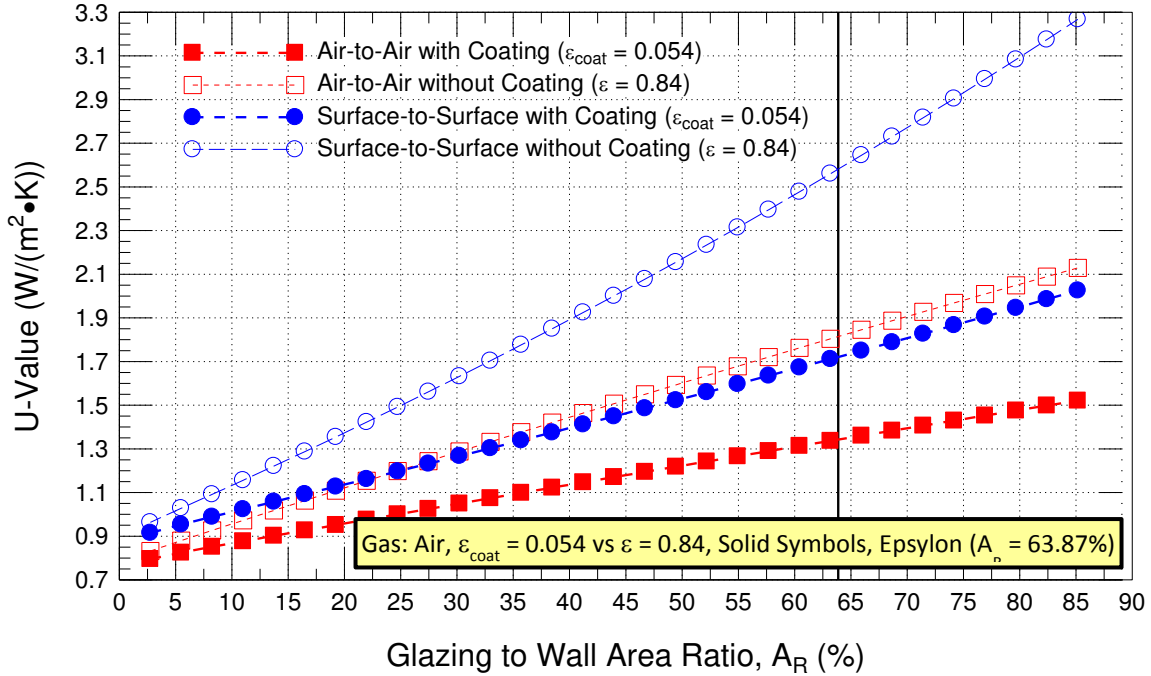


Figure A114 – Predicted (by simulation) U-value (air-to-air; surface-to-surface) of triple-glazed low-e coated ($\epsilon = 0.054$) or not coated ($\epsilon = 0.84$) thermally broken curtain wall in relation to glazing to Wall Area Ratio; Air filled IGU

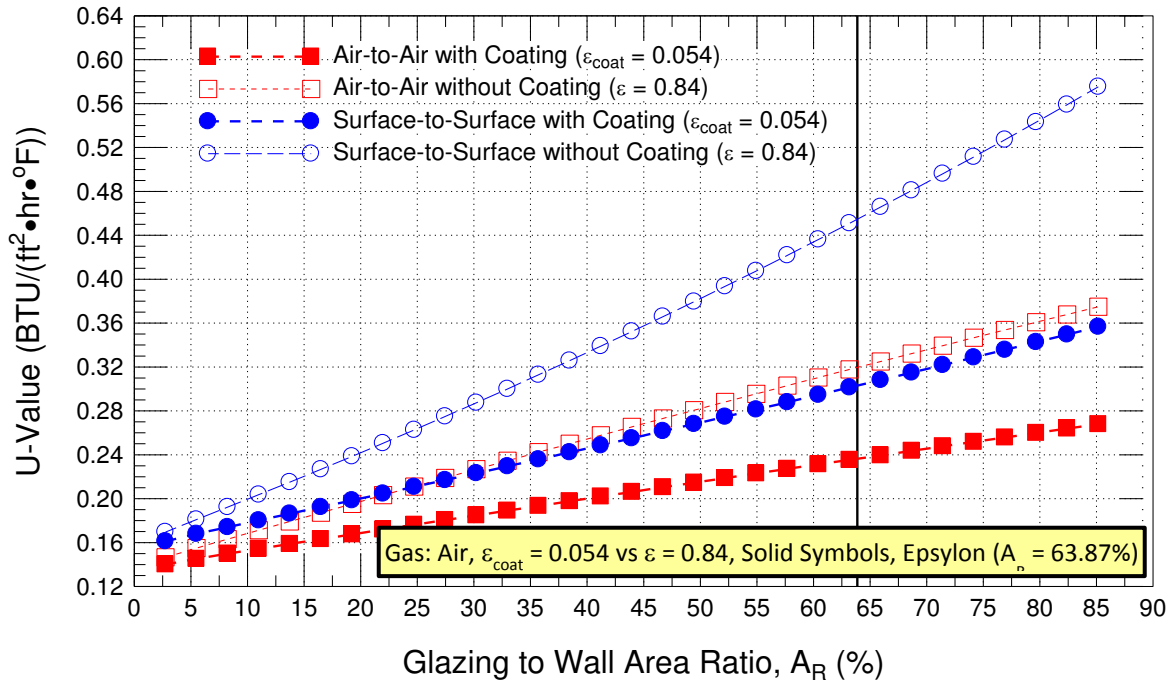


Figure A115 - Predicted (by simulation) U-value (air-to-air; surface-to-surface) of triple-glazed low-e coated ($\epsilon = 0.054$) or not coated ($\epsilon = 0.84$) thermally broken curtain wall in relation to glazing to Wall Area Ratio; Air filled IGU

**Effect of Glazing to Wall Area Ratio/Case-IV: 90 % Ar, 10 % Air-filled IGU;
Low-e Coating vs. no Coating ($\epsilon_{coat}=0.054$ / $\epsilon=0.84$)**

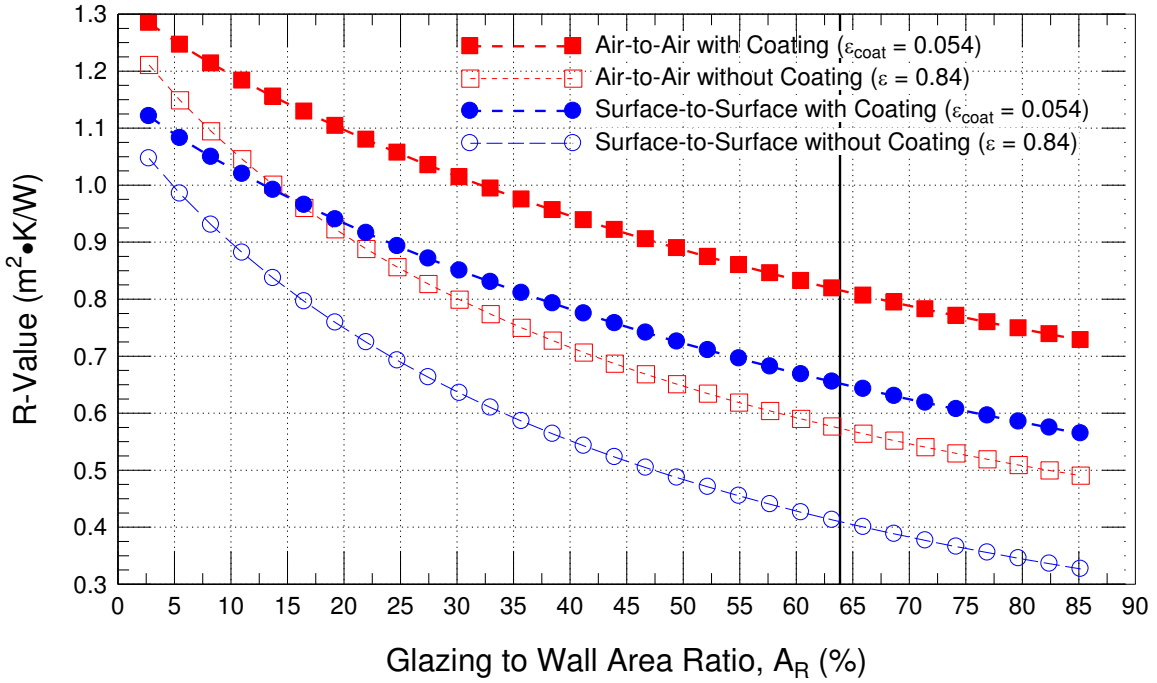


Figure A116 - Predicted (by simulation) R-value (air-to-air; surface-to-surface) of triple-glazed low-e coated ($\epsilon = 0.054$) or not coated ($\epsilon = 0.84$) thermally broken curtain wall in relation to glazing to Wall Area Ratio; 90 % Ar, 10 % Air-filled IGU

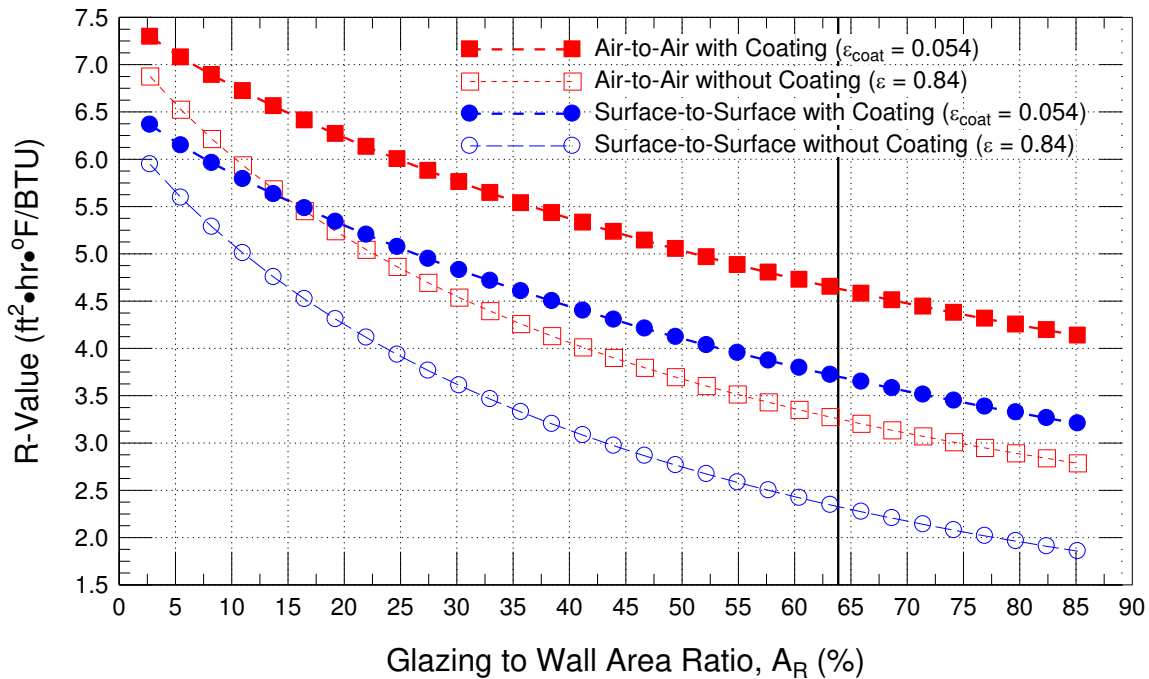


Figure A117 - Predicted (by simulation) R-value (air-to-air; surface-to-surface) of triple-glazed low-e coated ($\epsilon = 0.054$) or not coated ($\epsilon = 0.84$) thermally broken curtain wall in relation to glazing to Wall Area Ratio; 90 % Ar, 10% Air-filled IGU

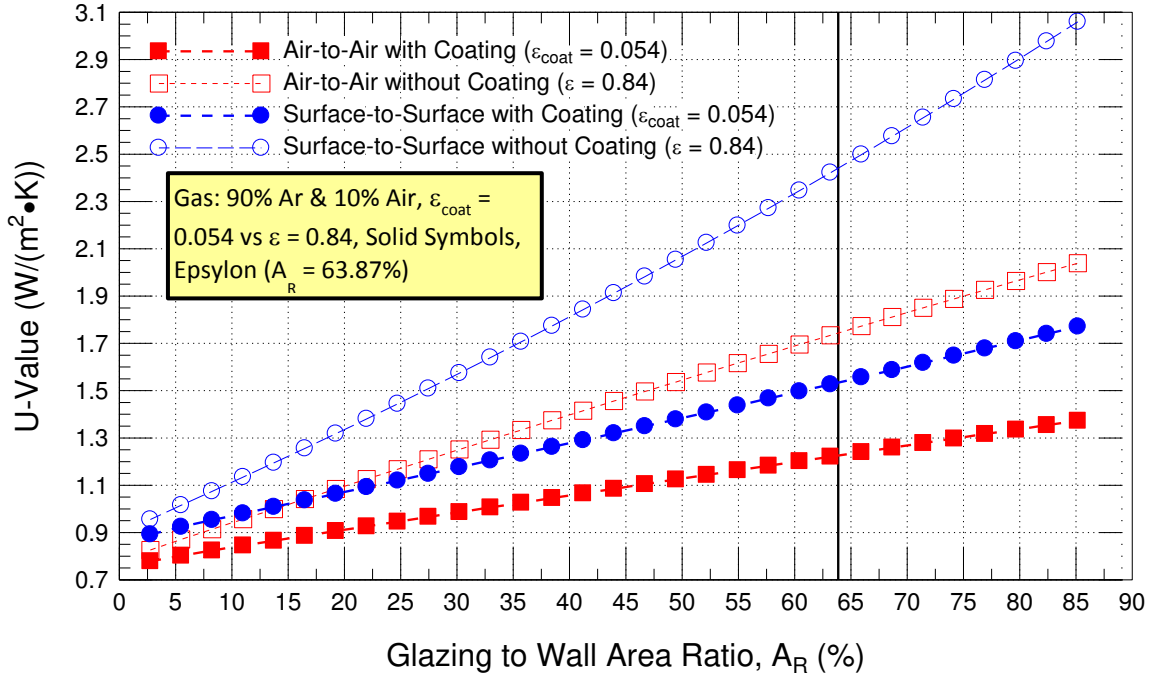


Figure A118 - Predicted (by simulation) U-value (air-to-air; surface-to-surface) of triple-glazed low-e coated (e = 0.054) or not coated (e = 0.84) thermally broken curtain wall in relation to glazing to Wall Area Ratio; 90 % Ar, 10 % Air-filled IGU

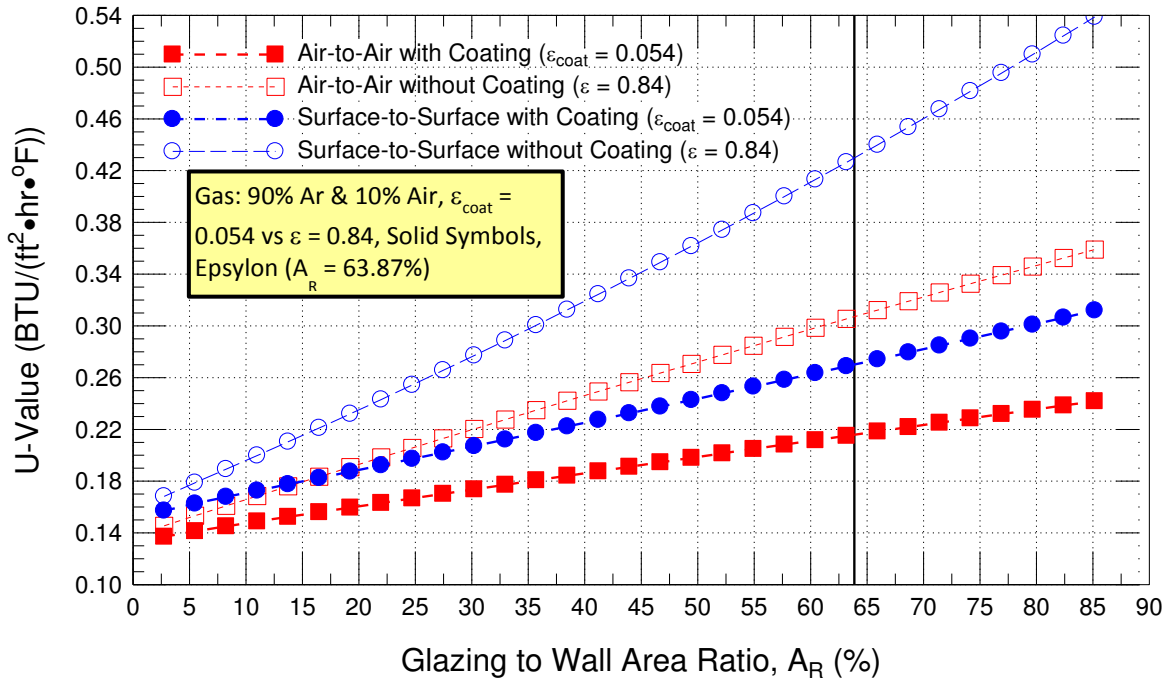


Figure A119 - Predicted (by simulation) U-value (air-to-air; surface-to-surface) of triple-glazed low-e coated (e = 0.054) or not coated (e = 0.84) thermally broken curtain wall in relation to glazing to Wall Area Ratio; 90 % Ar, 10 % Air-filled IGU

**Effect of Glazing to Wall Area Ratio/Case-IV: 90 % Kr, 10 % Air-filled IGU;
Low-e Coating vs. no Coating ($\epsilon_{\text{coat}}=0.054 / \epsilon=0.84$)**

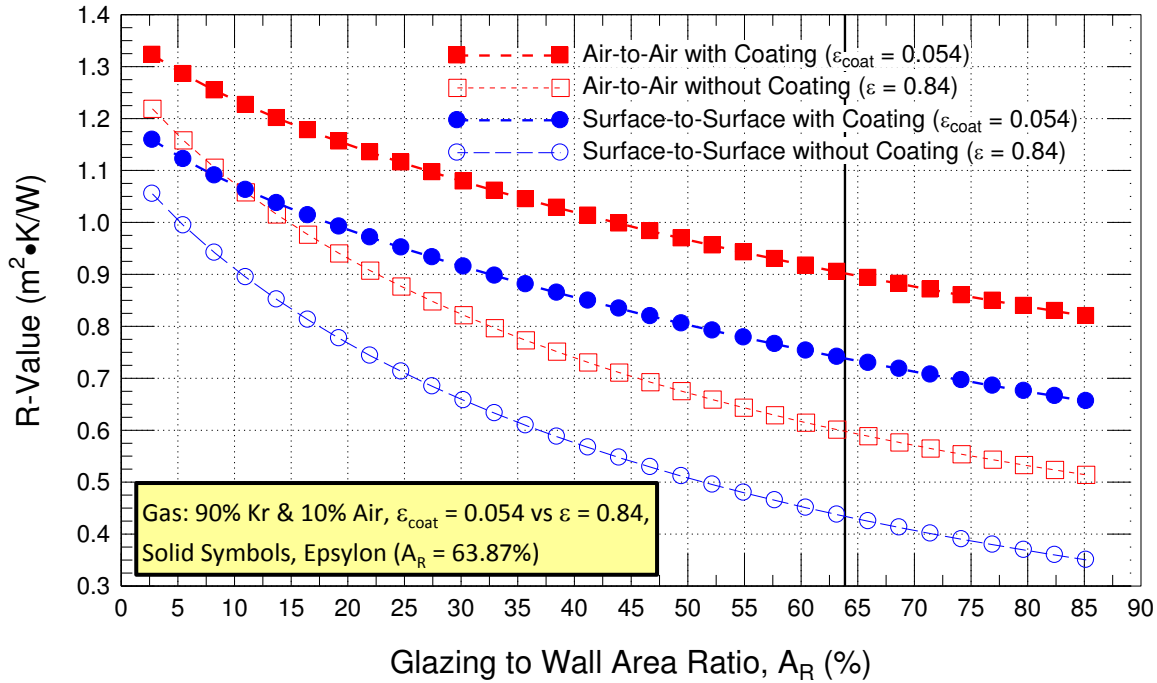


Figure A120 - Predicted (by simulation) R-value (air-to-air; surface-to-surface) of triple-glazed low-e coated ($\epsilon = 0.054$) or not coated ($\epsilon = 0.84$) thermally broken curtain wall in relation to glazing to Wall Area Ratio; 90 % Kr, 10 % Air-filled IGU

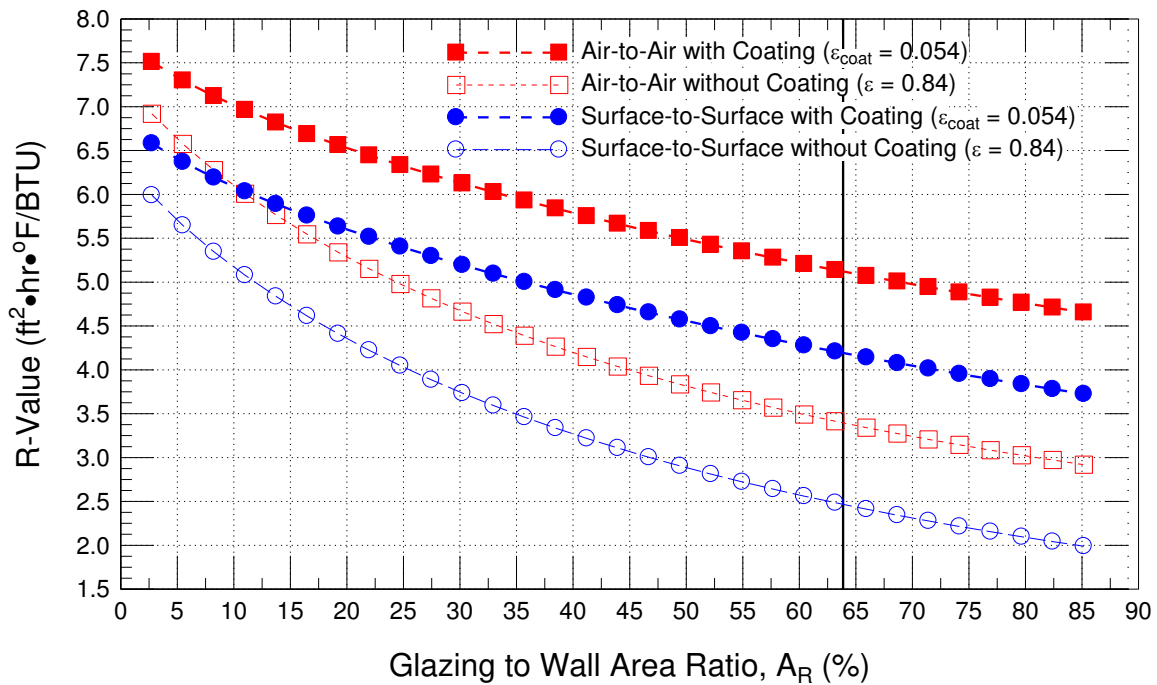


Figure A121 - Predicted (by simulation) R-value (air-to-air; surface-to-surface) of triple-glazed low-e coated ($\epsilon = 0.054$) or not coated ($\epsilon = 0.84$) thermally broken curtain wall in relation to glazing to Wall Area Ratio; 90 % Kr, 10 % Air-filled IGU

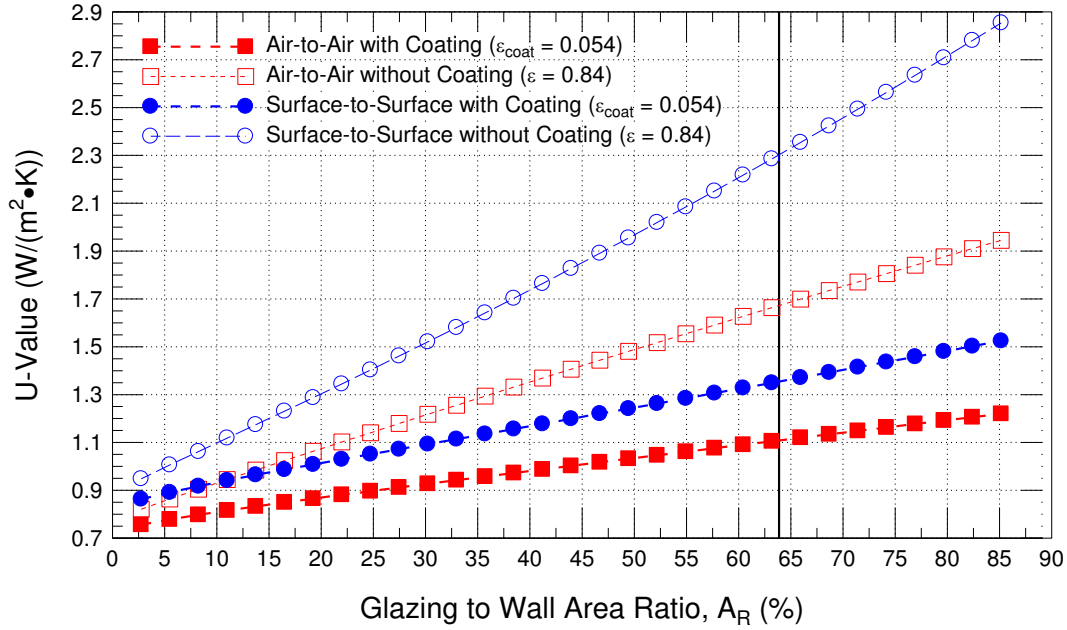


Figure A122 – Predicted (by simulation) U-value (air-to-air; surface-to-surface) of triple-glazed low-e coated ($\epsilon = 0.054$) or not coated ($\epsilon = 0.84$) thermally broken curtain wall in relation to glazing to Wall Area Ratio; 90 % Kr, 10 % Air-filled IGU

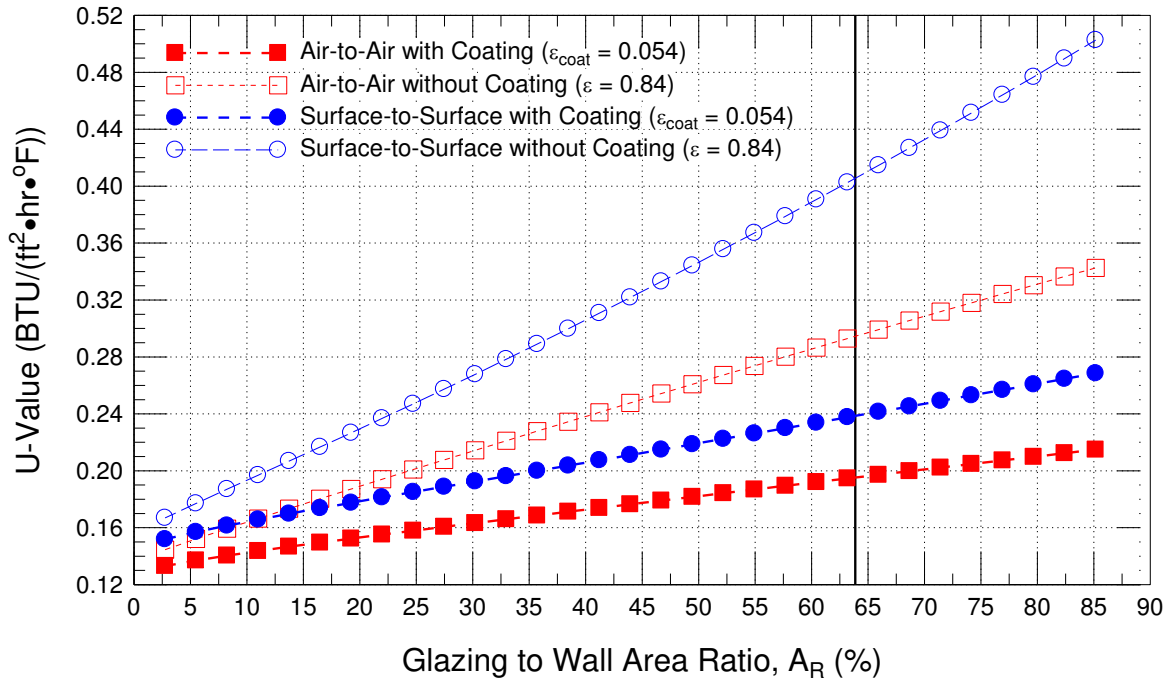


Figure A123 - Predicted (by simulation) U-value (air-to-air; surface-to-surface) of triple-glazed low-e coated ($\epsilon = 0.054$) or not coated ($\epsilon = 0.84$) thermally broken curtain wall in relation to glazing to Wall Area Ratio; 90 % Kr, 10 % Air-filled IGU

Effect of Glazing to Wall Area Ratio/Case-IV: 90 % Xe, 10 % Air-filled IGU;
 Low-e Coating vs. no Coating ($\epsilon_{coat}=0.054 / \epsilon=0.84$)

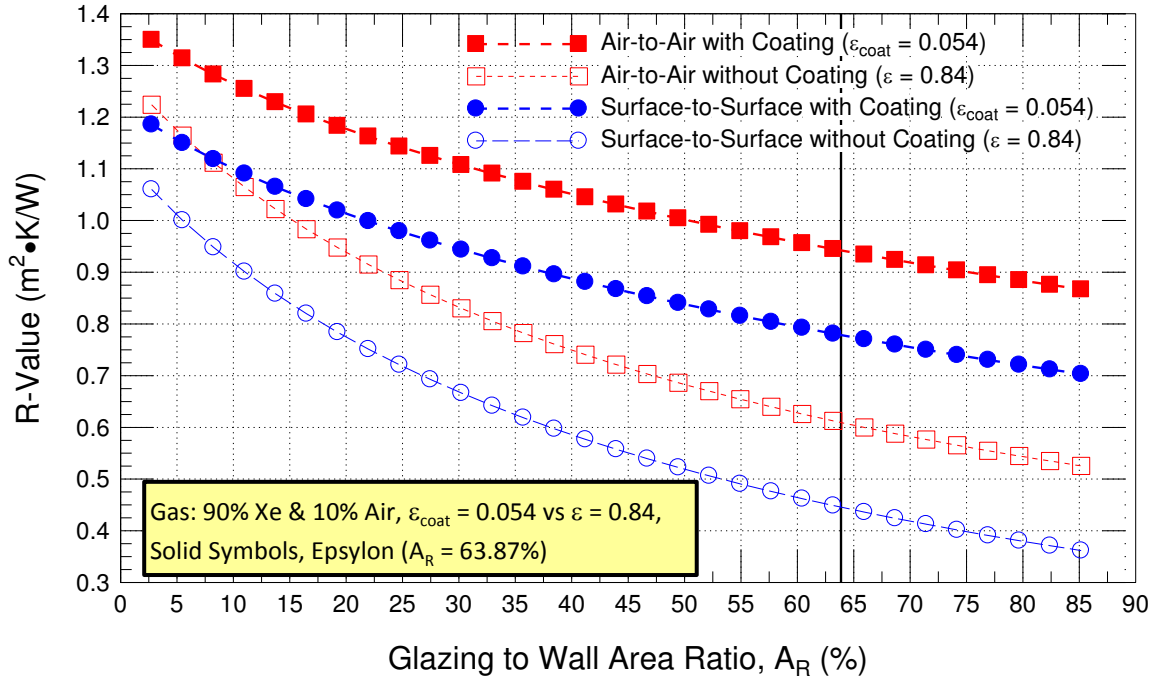


Figure A124 - Predicted (by simulation) R-value (air-to-air; surface-to-surface) of triple-glazed low-e coated ($\epsilon = 0.054$) or not coated ($\epsilon = 0.84$) thermally broken curtain wall in relation to glazing to Wall Area Ratio; 90 % Xe, 10 % Air-filled IGU

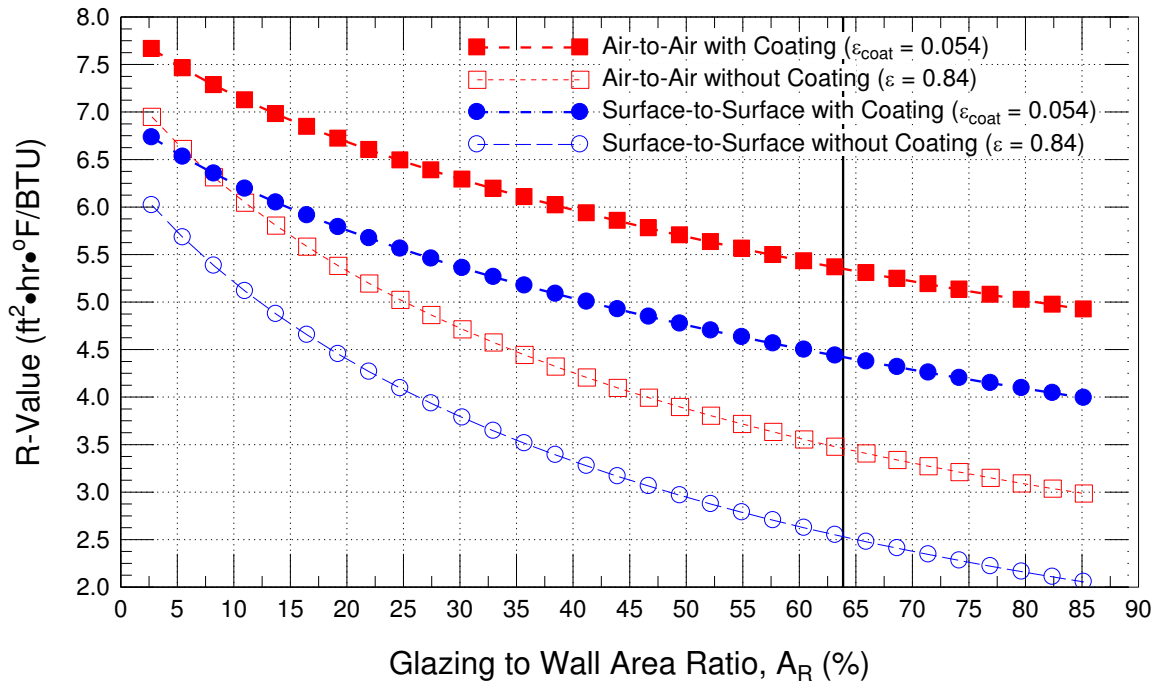


Figure A125 - Predicted (by simulation) R-value (air-to-air; surface-to-surface) of triple-glazed low-e coated ($\epsilon = 0.054$) or not coated ($\epsilon = 0.84$) thermally broken curtain wall in relation to glazing to Wall Area Ratio; 90 % Xe, 10 % Air-filled IGU

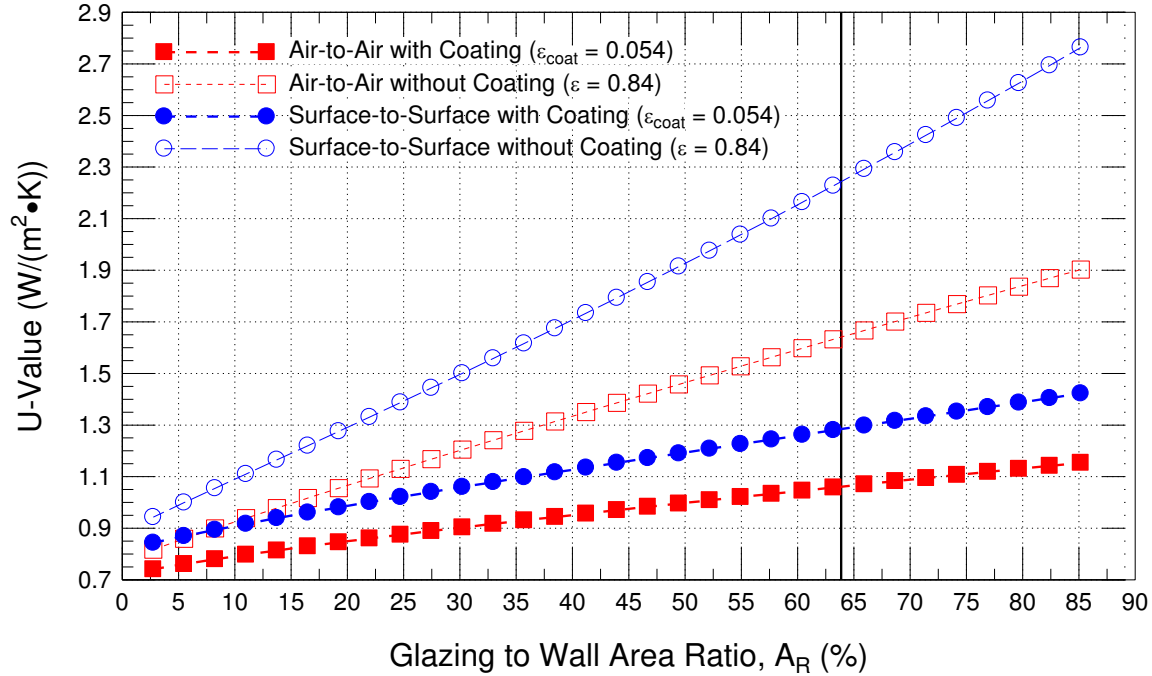


Figure A126 - Predicted (by simulation) U-value (air-to-air; surface-to-surface) of triple-glazed low-e coated ($\epsilon = 0.054$) or not coated ($\epsilon = 0.84$) thermally broken curtain wall in relation to glazing to Wall Area Ratio; 90 % Xe, 10 % Air-filled IGU

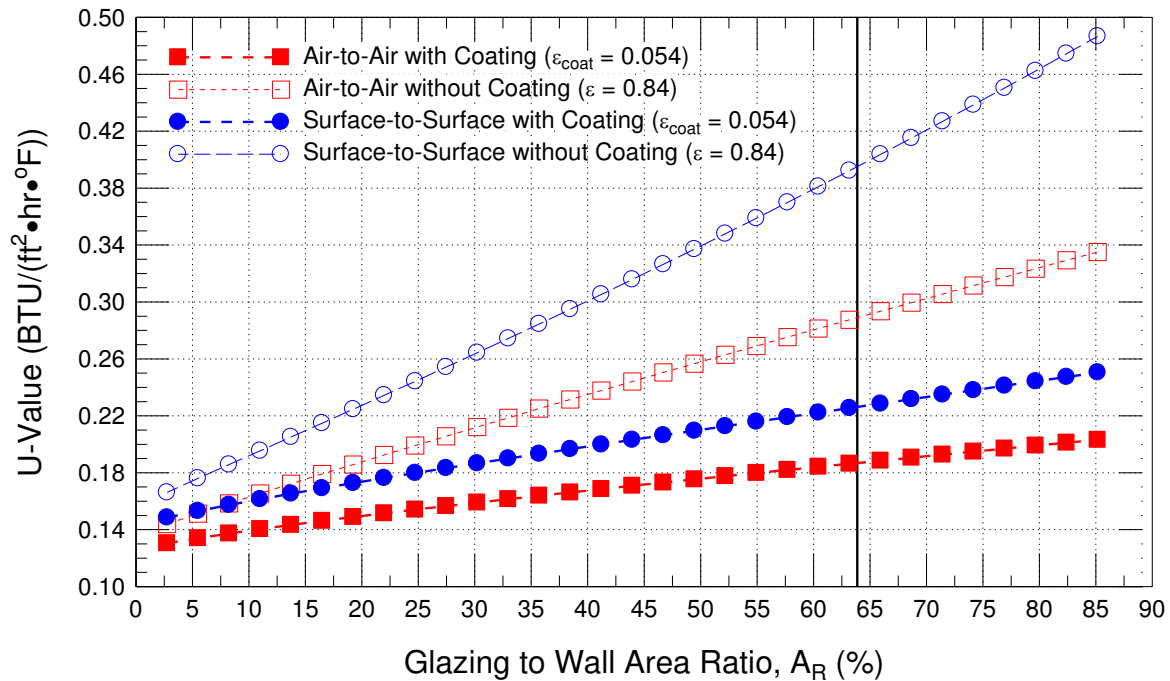


Figure A127 - Predicted (by simulation) U-value (air-to-air; surface-to-surface) of triple-glazed low-e coated ($\epsilon = 0.054$) or not coated ($\epsilon = 0.84$) thermally broken curtain wall in relation to glazing to Wall Area Ratio; 90 % Xe, 10 % Air-filled IGU

Effect of Coating ($\epsilon_{\text{coat}} = 0 - 0.84$), 90 % Ar, 10 % Air-filled IGU; Solid Symbols: Epsilon CW having triple-glazed vision and spandrel panel

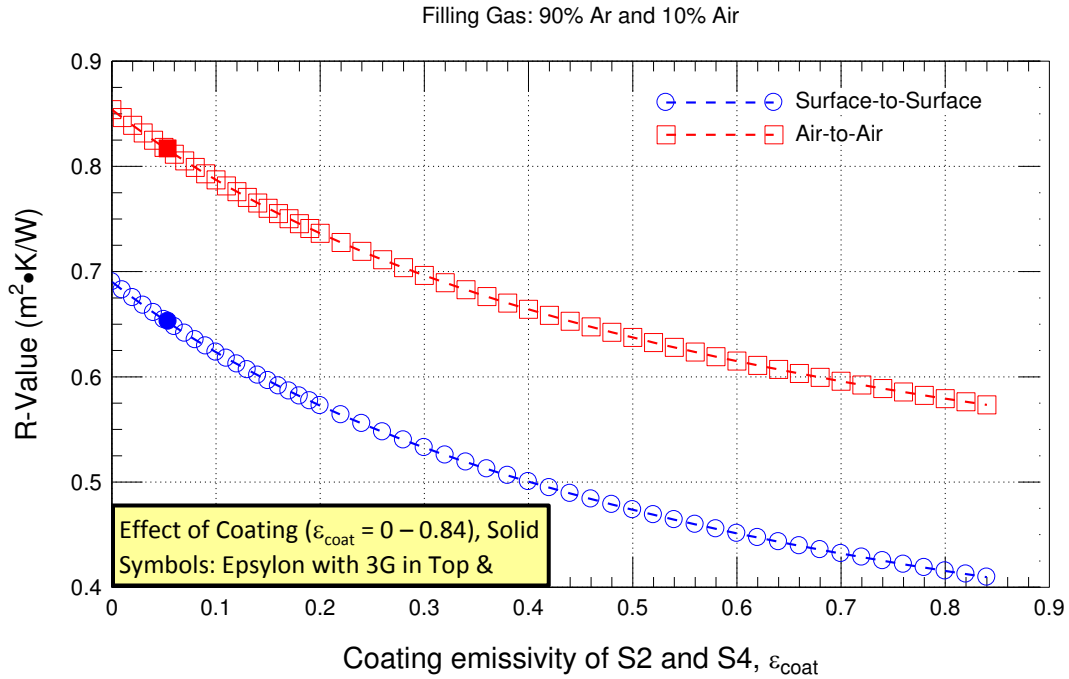


Figure A128 - Predicted (by simulation) R-value (air-to-air; surface-to-surface) of triple-glazed vision & spandrel panel low-e coated ($e = 0.054$; surfaces S2 and S4) thermally broken curtain wall in relation to coating emissivity; 90 % Ar, 10 % Air-filled IGU

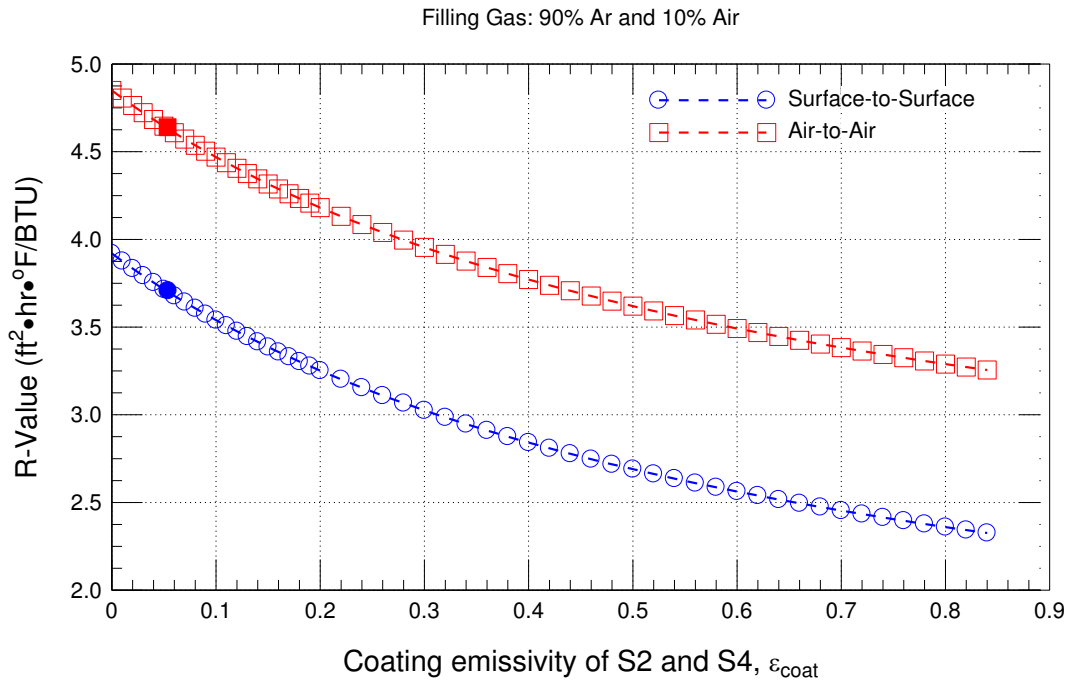


Figure 129 - Predicted (by simulation) R-value (air-to-air; surface-to-surface) of triple-glazed vision & spandrel panel low-e coated ($e = 0.054$; surfaces S2 and S4) thermally broken curtain wall in relation to coating emissivity; 90 % Ar, 10 % Air-filled IGU

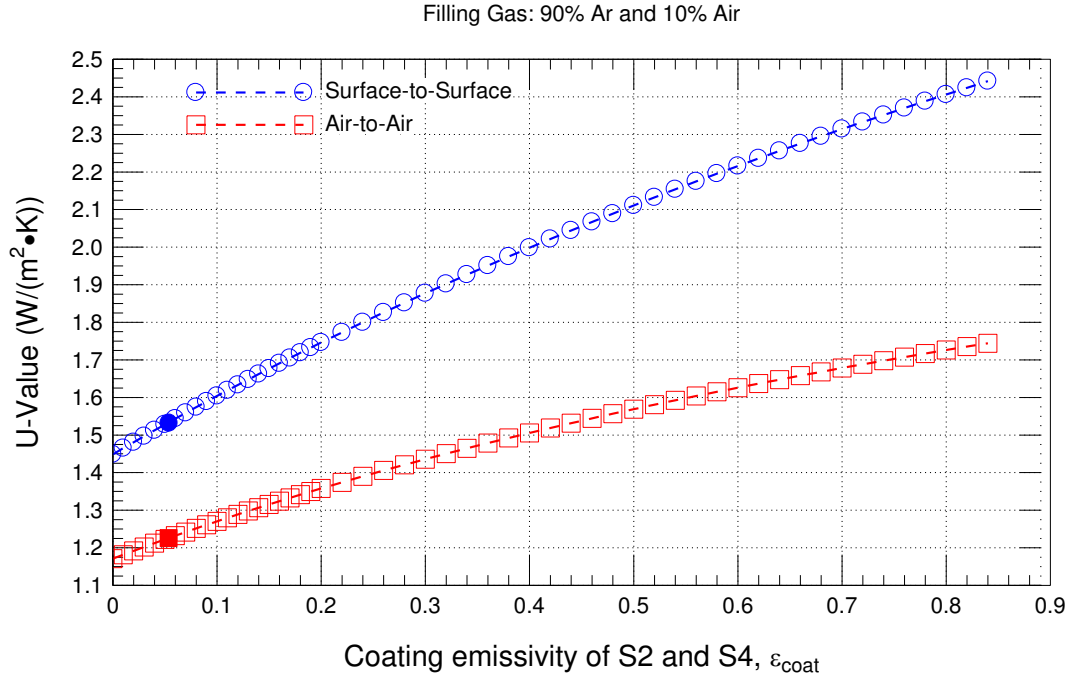


Figure A130 - Predicted (by simulation) U-value (air-to-air; surface-to-surface) of triple-glazed vision & spandrel panel low-e coated ($e = 0.054$; surfaces S2 and S4) thermally broken curtain wall in relation to coating emissivity; 90 % Ar, 10 % Air-filled IGU

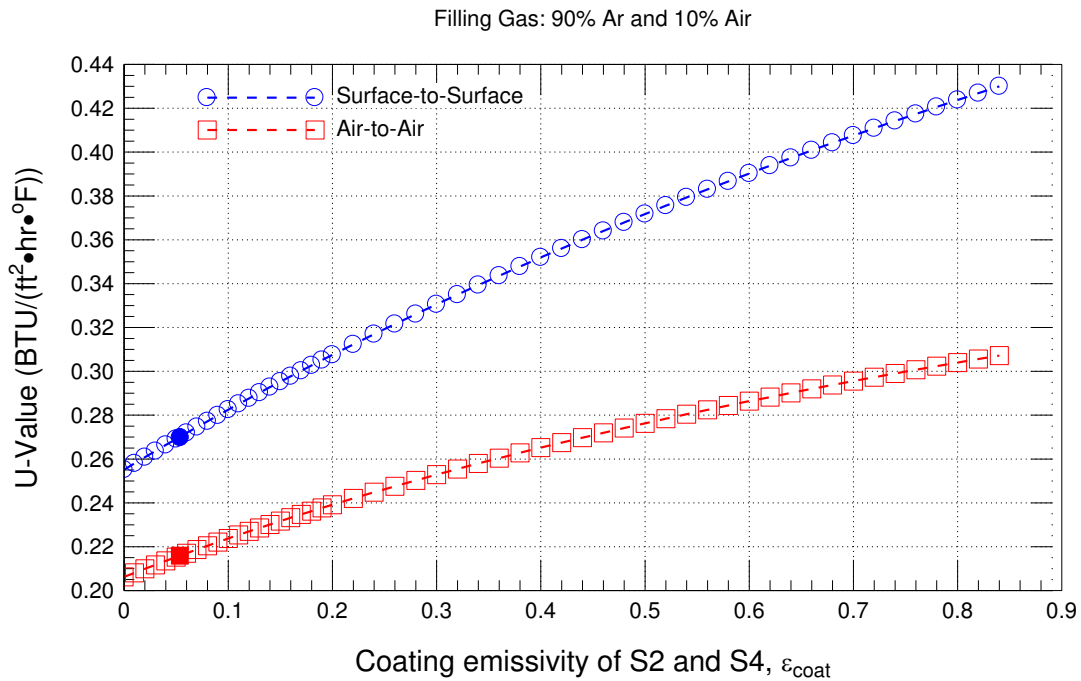


Figure 131 - Predicted (by simulation) U-value (air-to-air; surface-to-surface) of triple-glazed vision & spandrel panel low-e coated ($e = 0.054$; surfaces S2 and S4) thermally broken curtain wall in relation to coating emissivity; 90 % Ar, 10 % Air-filled IGU

Effect of Coating ($\epsilon_{\text{coat}} = 0 - 0.84$), 90 % Kr, 10 % Air-filled IGU; Solid Symbols: Epsilon CW having triple-glazed vision and spandrel panel

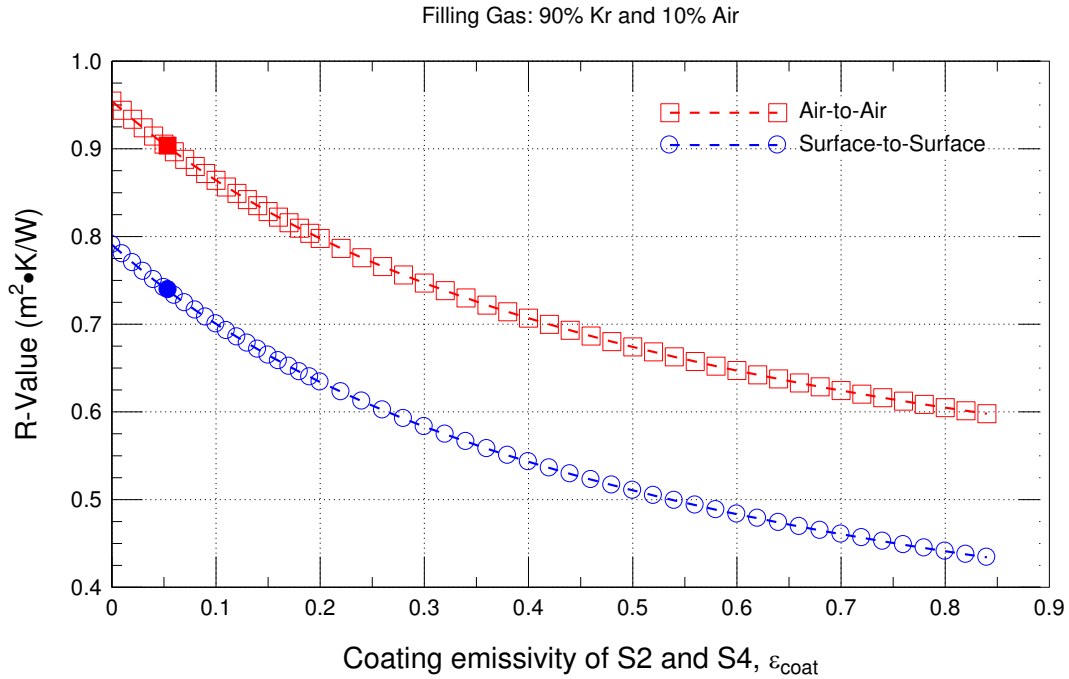


Figure A132 - Predicted (by simulation) R-value (air-to-air; surface-to-surface) of triple-glazed vision & spandrel panel low-e coated ($e = 0.054$; surfaces S2 and S4) thermally broken curtain wall in relation to coating emissivity; 90 % Kr, 10 % Air-filled IGU

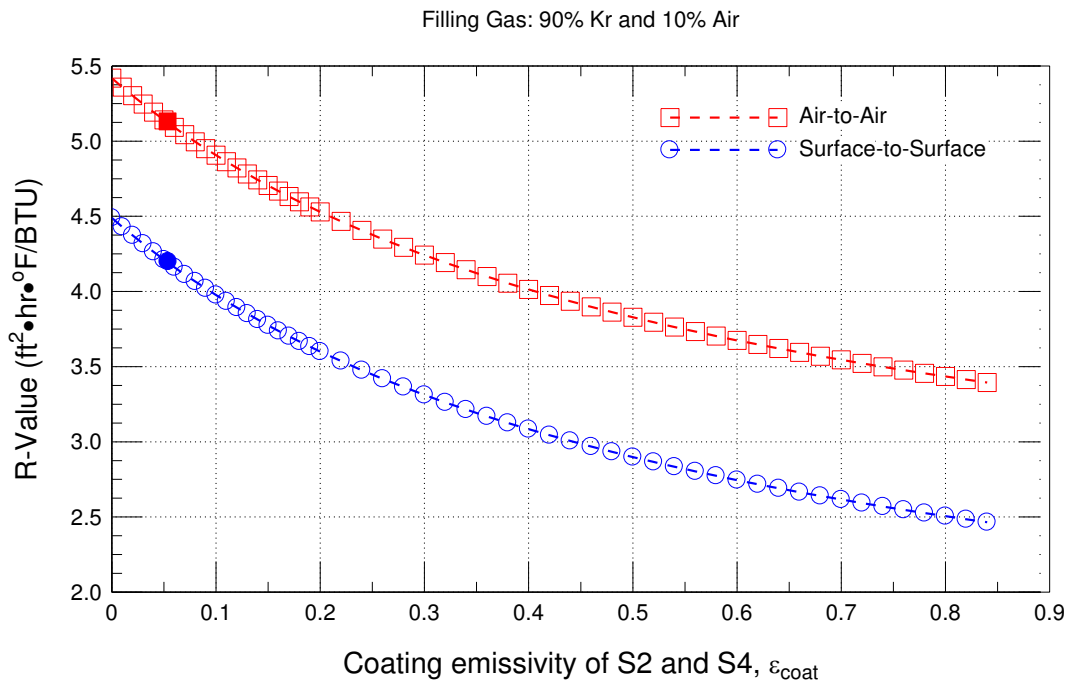


Figure A133 - Predicted (by simulation) R-value (air-to-air; surface-to-surface) of triple-glazed vision & spandrel panel low-e coated ($e = 0.054$; surfaces S2 and S4) thermally broken curtain wall in relation to coating emissivity; 90 % Kr, 10 % Air-filled IGU

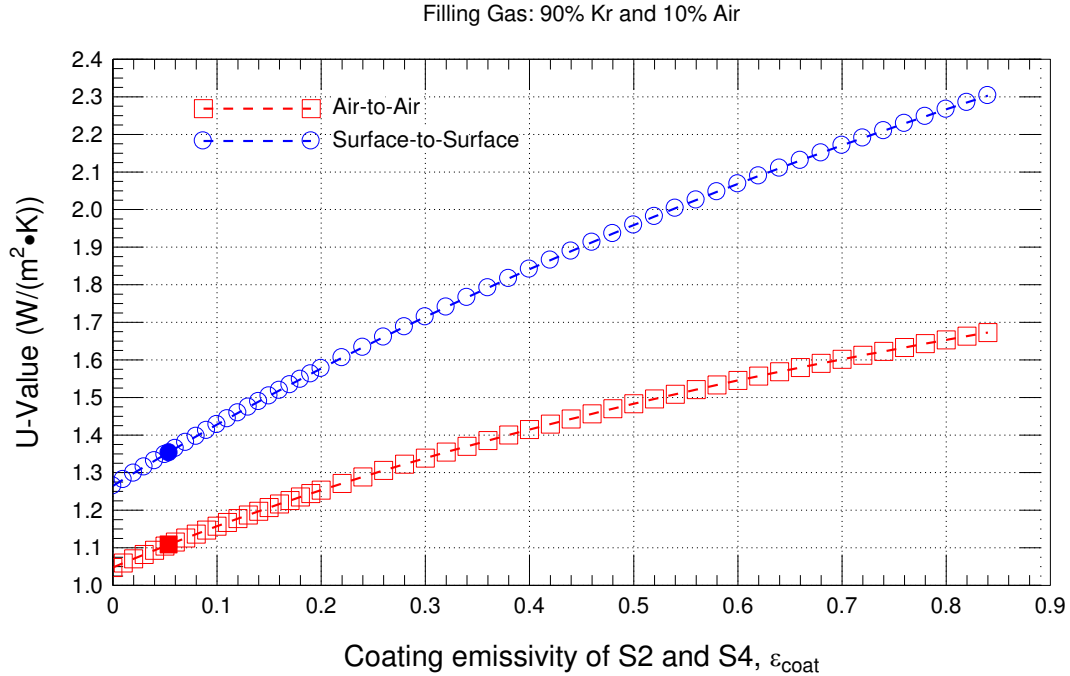


Figure A134 – Predicted (by simulation) U-value (air-to-air; surface-to-surface) of triple-glazed vision & spandrel panel low-e coated ($e = 0.054$; surfaces S2 and S4) thermally broken curtain wall in relation to coating emissivity; 90 % Kr, 10 % Air-filled IGU

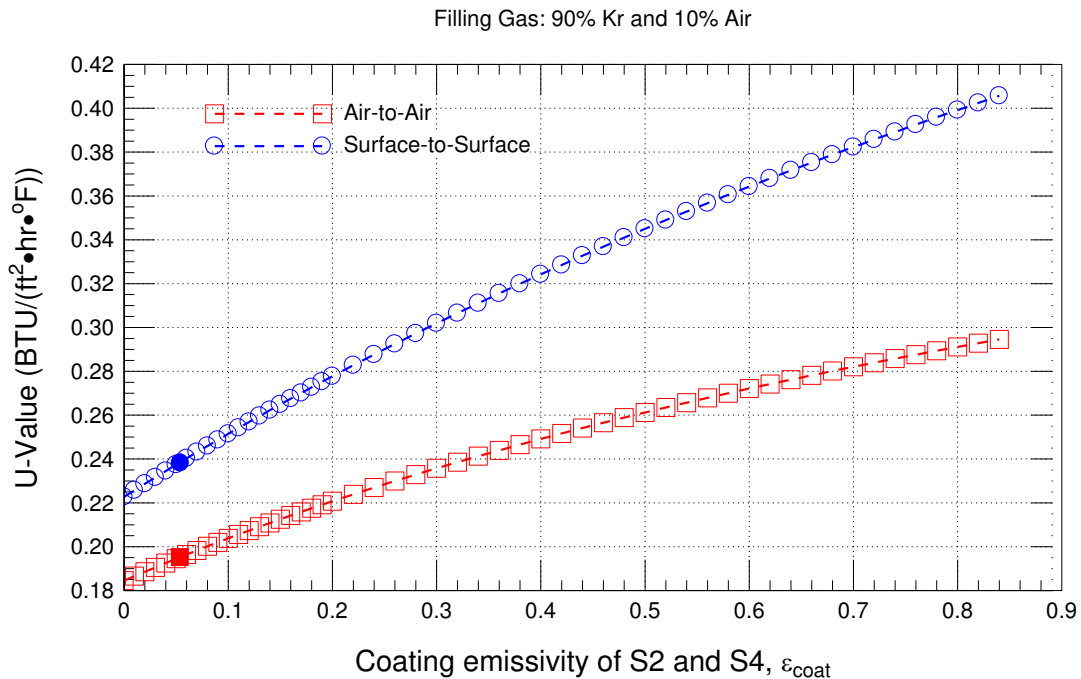


Figure A135 - Predicted (by simulation) U-value (air-to-air; surface-to-surface) of triple-glazed vision & spandrel panel low-e coated ($e = 0.054$; surfaces S2 and S4) thermally broken curtain wall in relation to coating emissivity; 90 % Kr, 10 % Air-filled IGU

Effect of Coating ($\epsilon_{\text{coat}} = 0 - 0.84$), 90 % Xe, 10 % Air-filled IGU;
 Solid Symbols: Epsilon CW having triple-glazed vision and spandrel panel

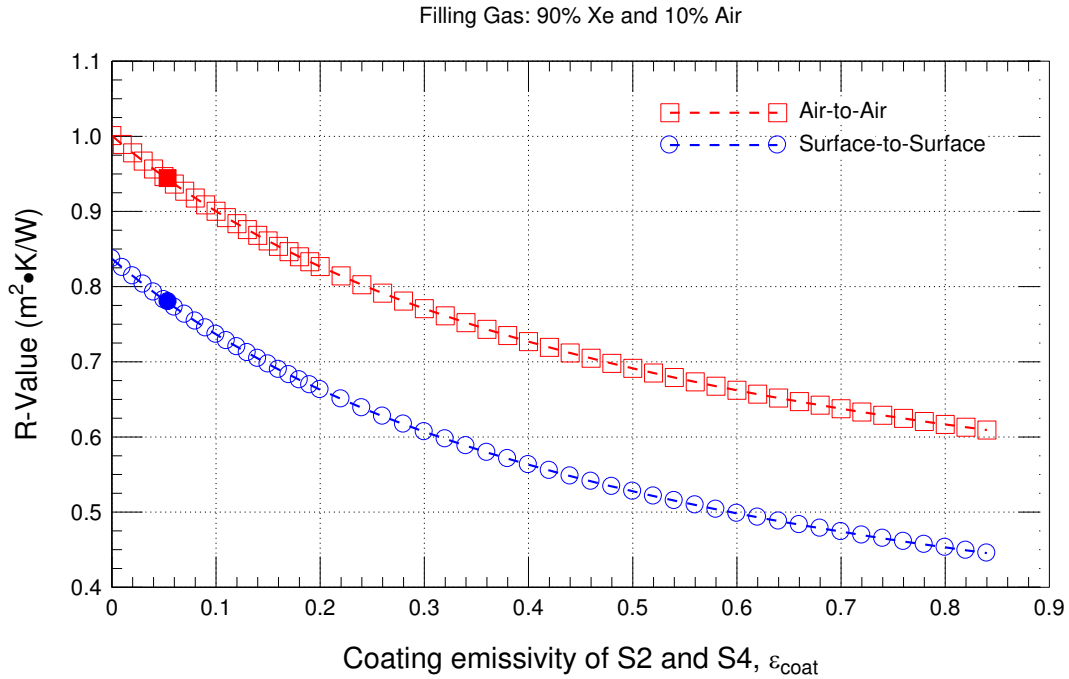


Figure A136 - Predicted (by simulation) R-value (air-to-air; surface-to-surface) of triple-glazed vision & spandrel panel low-e coated ($e = 0.054$; surfaces S2 and S4) thermally broken curtain wall in relation to coating emissivity; 90 % Xe, 10 % Air-filled IGU

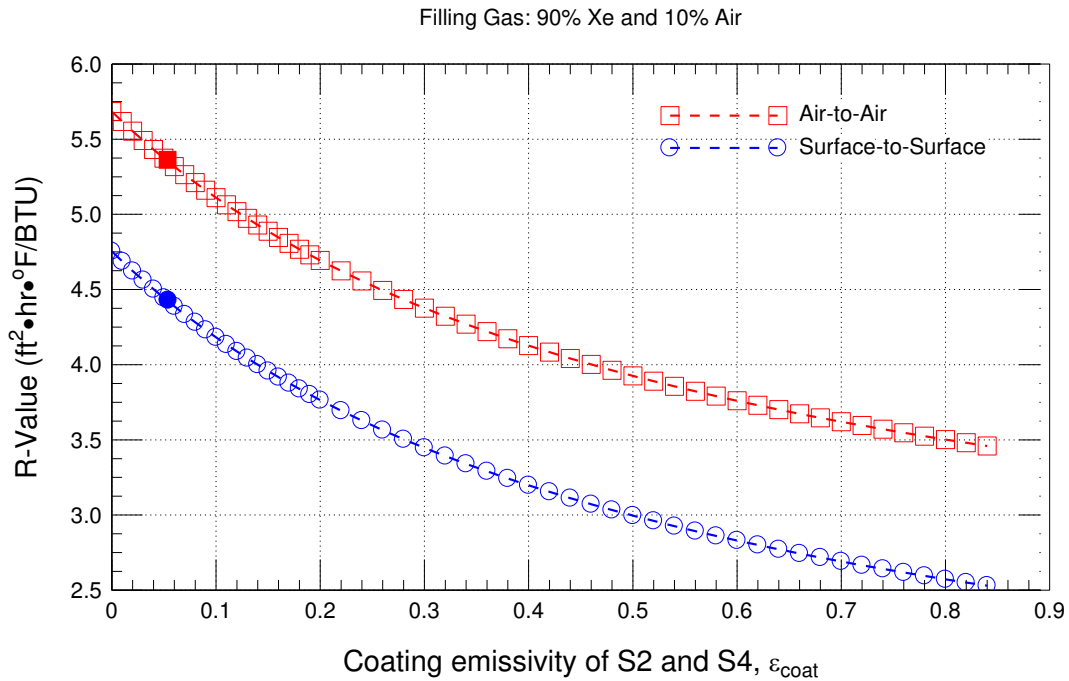


Figure A137 - Predicted (by simulation) R-value (air-to-air; surface-to-surface) of triple-glazed vision & spandrel panel low-e coated ($e = 0.054$; surfaces S2 and S4) thermally broken curtain wall in relation to coating emissivity; 90 % Xe, 10 % Air-filled IGU

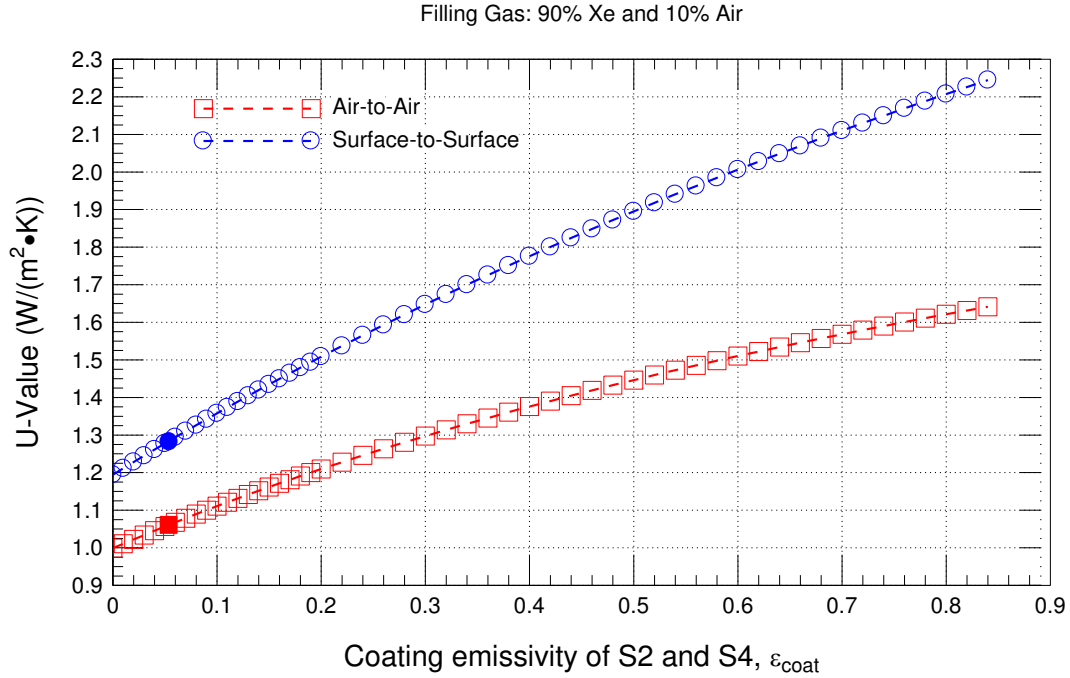


Figure A138 - Predicted (by simulation) U-value (air-to-air; surface-to-surface) of triple-glazed vision & spandrel panel low-e coated ($e = 0.054$; surfaces S2 and S4) thermally broken curtain wall in relation to coating emissivity; 90 % Xe, 10 % Air-filled IGU

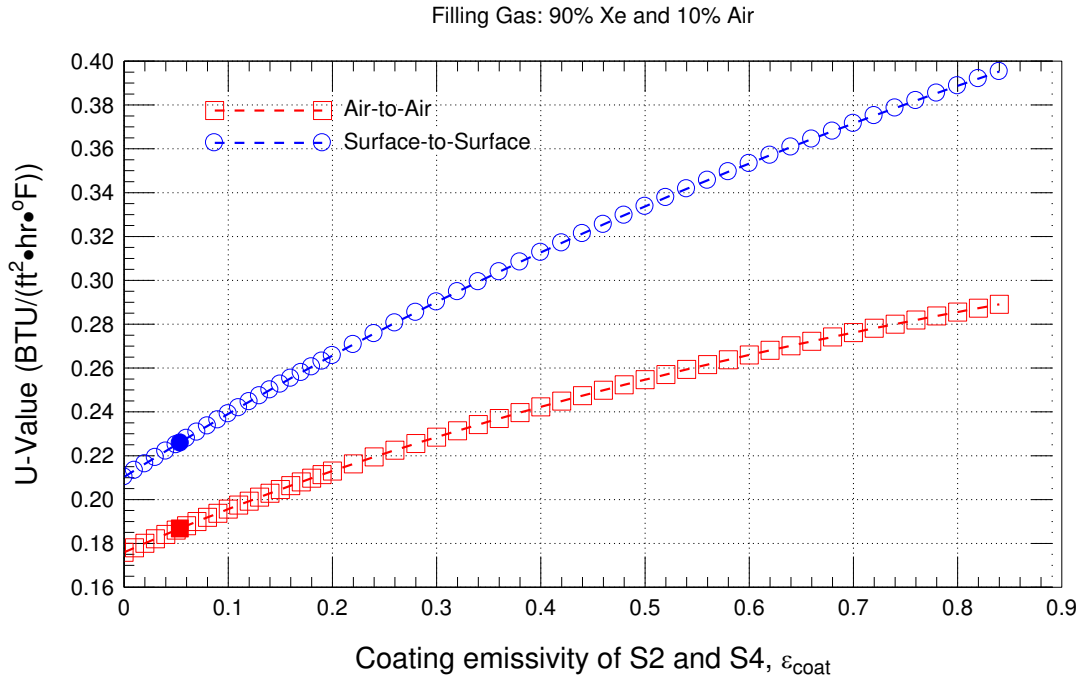


Figure A139 - Predicted (by simulation) U-value (air-to-air; surface-to-surface) of triple-glazed vision & spandrel panel low-e coated ($e = 0.054$; surfaces S2 and S4) thermally broken curtain wall in relation to coating emissivity; 90 % Xe, 10 % Air-filled IGU

Effect of Coating ($\epsilon_{\text{coat}} = 0 - 0.84$), Air-filled IGU;
Solid Symbols: Epsilon CW having triple-glazed vision and spandrel panel

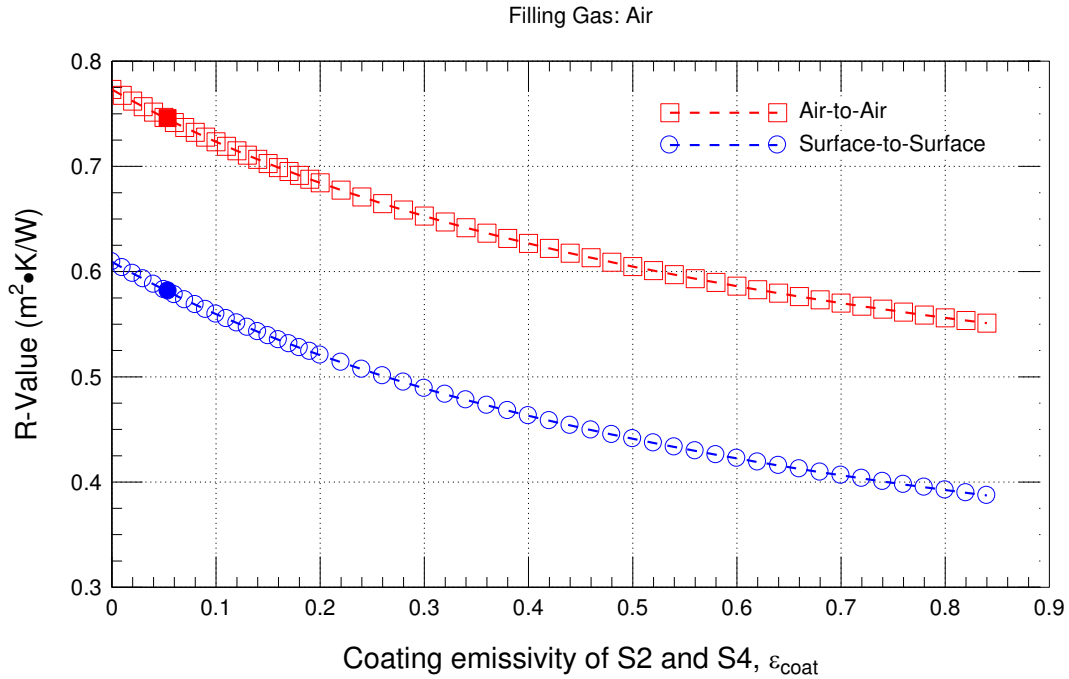


Figure A140 - Predicted (by simulation) R-value (air-to-air; surface-to-surface) of triple-glazed vision & spandrel panel low-e coated ($e = 0.054$; surfaces S2 and S4) thermally broken curtain wall in relation to coating emissivity; Air-filled IGU

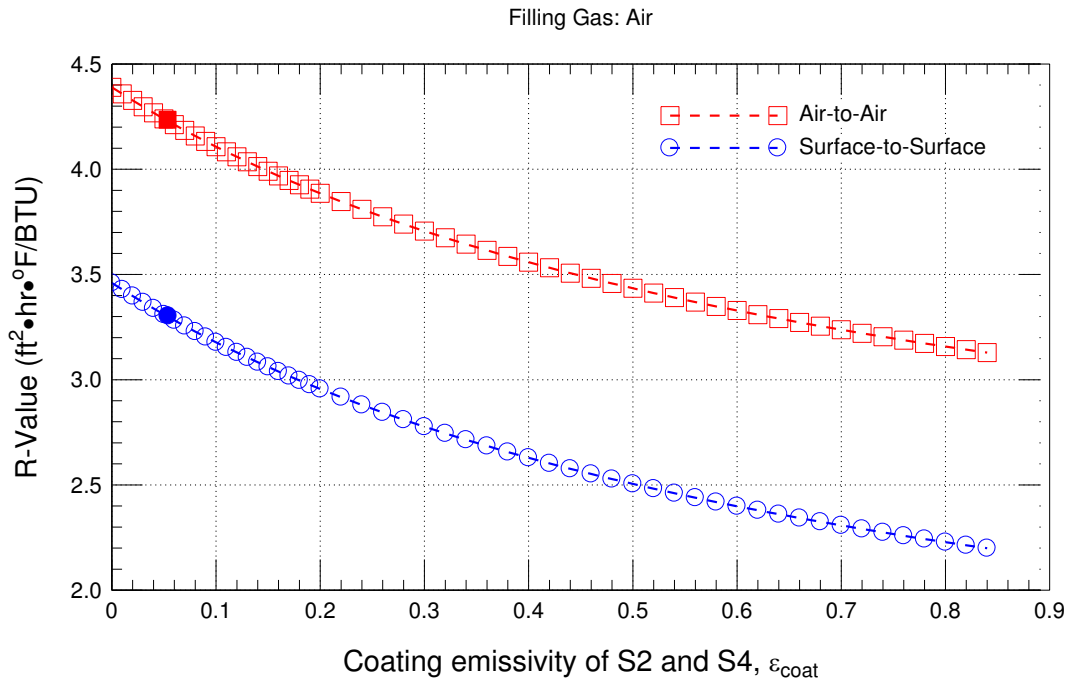


Figure A141 - Predicted (by simulation) R-value (air-to-air; surface-to-surface) of triple-glazed vision & spandrel panel low-e coated ($e = 0.054$; surfaces S2 and S4) thermally broken curtain wall in relation to coating emissivity; Air-filled IGU

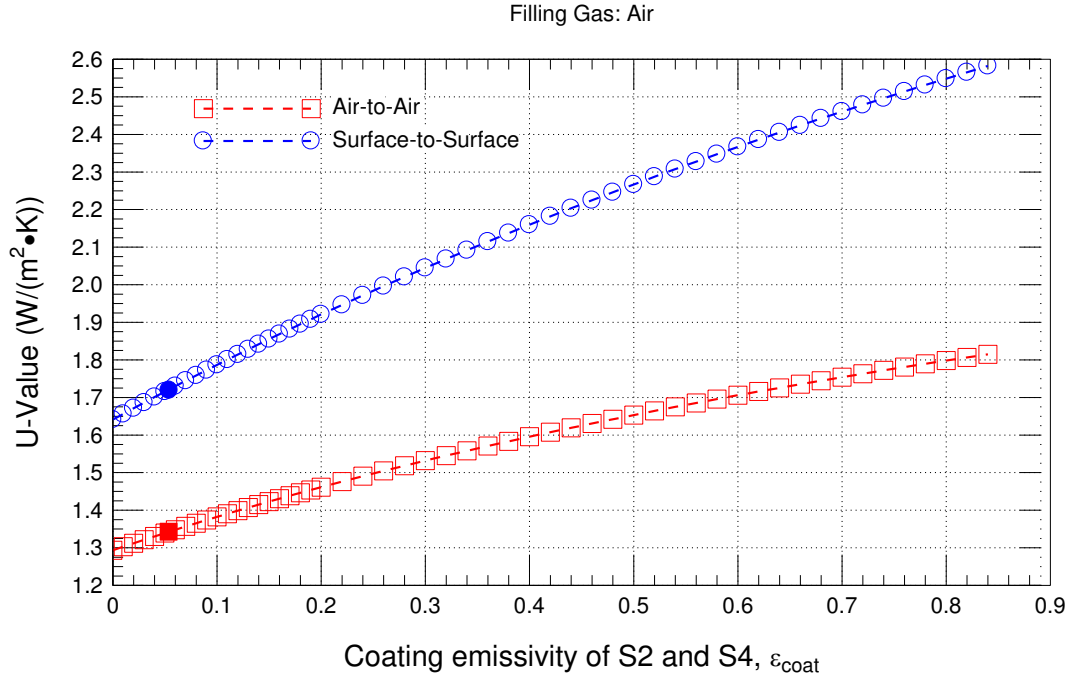


Figure A142 - Predicted (by simulation) U-value (air-to-air; surface-to-surface) of triple-glazed vision & spandrel panel low-e coated ($e = 0.054$; surfaces S2 and S4) thermally broken curtain wall in relation to coating emissivity; Air-filled IGU

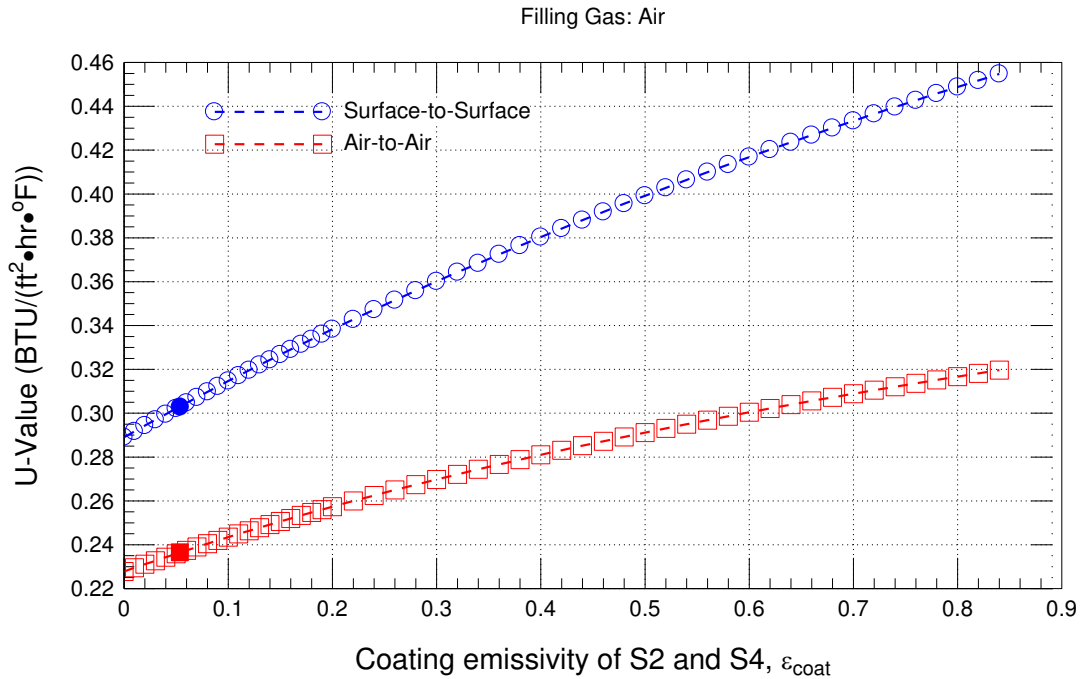


Figure A143 - Predicted (by simulation) U-value (air-to-air; surface-to-surface) of triple-glazed vision & spandrel panel low-e coated ($e = 0.054$; surfaces S2 and S4) thermally broken curtain wall in relation to coating emissivity; Air-filled IGU

Table A10 – Test Results & Calculated U-value for curtain wall assembly for Ar (90%) filled IGU; model dimensions (M) used as basis for calculations

90% Ar and 10% Air, Frame Insulations: XPS				
Parameter	Test (T)	Model (M)	Difference M - T	Deviation (%)
Areas				
Projected Area of the Sample (A_p), m ²	13.38	13.31	-0.07	-0.52%
Total Indoor Surface Area (A_i), m ²	15.81	16.21	0.40	2.56%
Total Outdoor Surface Area (A_o), m ²	14.09	14.30	0.21	1.52%
Test and Boundary Conditions				
Temperature of warm side air (T_i), °C	21.09	21.09	N/A	N/A
Temperature of cold side air (T_o), °C	-17.99	-17.99	N/A	N/A
Interior Test Film (h_i), W/(m ² ·K)	8.37	8.37	N/A	N/A
Exterior Test Film (h_o), W/(m ² ·K)	19.25	19.25	N/A	N/A
Measurements and Predictions				
Average Area Weighted Room Side Surface Temp. (T_1), °C	13.16	14.74	1.58	11.98%
Average Weather Side Area Weighted Surface Temp. (T_2), °C	-14.54	-14.86	-0.32	2.20%
Surface-to-surface Temperature Difference (DT), °C	27.70	29.60	1.90	6.85%
Net Specimen Heat Loss (Q_s), W	888.56	861.99	-26.57	-2.99%
Derived Performance Parameters				
Conductance of the Sample: $C_s = Q_s/A_p \cdot (T_1 - T_2)$, W/(m ² ·K)	2.40	2.19	-0.21	-8.73%
U-value of the sample: $U_s = 1/[(1/C_s) + (1/h_i) + (1/h_o)]$, W/(m ² ·K)	1.70	1.59	-0.11	-6.35%
Thermal resistance = $1/C_s$, (m ² ·K) / W	0.42	0.46	0.04	9.57%
R-value = $1/U_s$, (m ² ·K) / W	0.59	0.63	0.04	6.78%
90% Ar and 10% Air, Frame Insulations: EPS				
Measurements and Predictions				
Average Area Weighted Room Side Surface Temp. (T_1), °C	13.16	14.73	1.57	11.91%
Average Weather Side Area Weighted Surface Temp. (T_2), °C	-14.54	-14.85	-0.31	2.16%
Surface-to-surface Temperature Difference (DT), °C	27.70	29.58	1.88	6.79%
Net Specimen Heat Loss (Q_s), W	888.56	863.35	-25.21	-2.84%
Derived Performance Parameters				
Conductance of the Sample: $C_s = Q_s/A_p \cdot (T_1 - T_2)$, W/(m ² ·K)	2.40	2.19	-0.20	-8.54%
U-value of the sample: $U_s = 1/[(1/C_s) + (1/h_i) + (1/h_o)]$, W/(m ² ·K)	1.70	1.59	-0.11	-6.21%
Thermal resistance = $1/C_s$, (m ² ·K) / W	0.42	0.46	0.04	9.34%
R-value = $1/U_s$, (m ² ·K) / W	0.59	0.63	0.04	6.62%

Table A11 – Test Results & Calculated U-value for curtain wall assembly with overfilling of Argon in IGU; model dimensions (M) used as basis for calculations

100% Ar and 0% Air, Frame Insulations: XPS				
Parameter	Test (T)	Model (M)	Difference M - T	Deviation (%)
Areas				
Projected Area of the Sample (A_p), m^2	13.38	13.31	-0.07	-0.52%
Total Indoor Surface Area (A_i), m^2	15.81	16.21	0.40	2.56%
Total Outdoor Surface Area (A_o), m^2	14.09	14.30	0.21	1.52%
Test and Boundary Conditions				
Temperature of warm side air (T_i), °C	21.09	21.09	N/A	N/A
Temperature of cold side air (T_o), °C	-17.99	-17.99	N/A	N/A
Interior Test Film (h_i), $W/(m^2 \cdot K)$	8.37	8.37	N/A	N/A
Exterior Test Film (h_o), $W/(m^2 \cdot K)$	19.25	19.25	N/A	N/A
Measurements and Predictions				
Average Area Weighted Room Side Surface Temp. (T_1), °C	13.16	14.82	1.66	12.58%
Average Weather Side Area Weighted Surface Temp. (T_2), °C	-14.54	-14.90	-0.36	2.46%
Surface-to-surface Temperature Difference (DT), °C	27.70	29.71	2.01	7.27%
Net Specimen Heat Loss (Q_s), W	888.56	851.34	-37.22	-4.19%
Derived Performance Parameters				
Conductance of the Sample: $C_s = Q_s/A_p \cdot (T_1 - T_2)$, $W/(m^2 \cdot K)$	2.40	2.15	-0.24	-10.22%
U-value of the sample: $U_s = 1/[(1/C_s) + (1/h_i) + (1/h_o)]$, $W/(m^2 \cdot K)$	1.70	1.57	-0.13	-7.46%
Thermal resistance = $1 / C_s$, $(m^2 \cdot K) / W$	0.42	0.46	0.05	11.38%
R-value = $1 / U_s$, $(m^2 \cdot K) / W$	0.59	0.64	0.05	8.06%
100% Ar and 0% Air, Frame Insulations: EPS				
Measurements and Predictions				
Average Area Weighted Room Side Surface Temp. (T_1), °C	13.16	14.81	1.65	12.50%
Average Weather Side Area Weighted Surface Temp. (T_2), °C	-14.54	-14.89	-0.35	2.43%
Surface-to-surface Temperature Difference (DT), °C	27.70	29.70	2.00	7.22%
Net Specimen Heat Loss (Q_s), W	888.56	852.70	-35.86	-4.04%
Derived Performance Parameters				
Conductance of the Sample: $C_s = Q_s/A_p \cdot (T_1 - T_2)$, $W/(m^2 \cdot K)$	2.40	2.16	-0.24	-10.03%
U-value of the sample: $U_s = 1/[(1/C_s) + (1/h_i) + (1/h_o)]$, $W/(m^2 \cdot K)$	1.70	1.57	-0.12	-7.32%
Thermal resistance = $1 / C_s$, $(m^2 \cdot K) / W$	0.42	0.46	0.05	11.15%
R-value = $1 / U_s$, $(m^2 \cdot K) / W$	0.59	0.64	0.05	7.90%

Table A12 – Test Results and Calculated U-value for Curtain Wall Assembly Specimen size of 12 ft. x 12 ft., as reported in test for Ar (90%) filled IGU

90% Ar and 10% Air, Frame Insulations: XPS				
Parameter	Test (T)	Model (M)	Difference M - T	Deviation (%)
Areas				
Projected Area of the Sample (A_p), m^2	13.38	13.38	0.00	-0.01%
Total Indoor Surface Area (A_i), m^2	16.29	16.29	0.49	3.08%
Total Outdoor Surface Area (A_o), m^2	14.38	14.38	0.28	2.02%
Test and Boundary Conditions				
Temperature of warm side air (T_i), °C	21.09	21.09	N/A	N/A
Temperature of cold side air (T_o), °C	-17.99	-17.99	N/A	N/A
Interior Test Film (h_i), $W/(m^2 \cdot K)$	8.37	8.37	N/A	N/A
Exterior Test Film (h_o), $W/(m^2 \cdot K)$	19.25	19.25	N/A	N/A
Measurements and Predictions				
Average Area Weighted Room Side Surface Temp. (T_1), °C	13.16	14.73	1.57	11.97%
Average Weather Side Area Weighted Surface Temp. (T_2), °C	-14.54	-14.86	-0.32	2.19%
Surface-to-surface Temperature Difference (DT), °C	27.70	29.59	1.89	6.83%
Net Specimen Heat Loss (Q_s), W	888.56	866.69	-21.87	-2.46%
Derived Performance Parameters				
Conductance of the Sample: $C_s = Q_s/A_p \cdot (T_1 - T_2)$, $W/(m^2 \cdot K)$	2.40	2.19	-0.21	-8.69%
U-value of the sample: $U_s = 1/[(1/C_s) + (1/h_i) + (1/h_o)]$, $W/(m^2 \cdot K)$	1.70	1.59	-0.11	-6.32%
Thermal resistance = $1 / C_s$, $(m^2 \cdot K) / W$	0.42	0.46	0.04	9.51%
R-value = $1 / U_s$, $(m^2 \cdot K) / W$	0.59	0.63	0.04	6.74%
90% Ar and 10% Air, Frame Insulations: EPS				
Measurements and Predictions				
Average Area Weighted Room Side Surface Temp. (T_1), °C	13.16	14.72	1.56	11.89%
Average Weather Side Area Weighted Surface Temp. (T_2), °C	-14.54	-14.85	-0.31	2.15%
Surface-to-surface Temperature Difference (DT), °C	27.70	29.58	1.88	6.78%
Net Specimen Heat Loss (Q_s), W	888.56	868.05	-20.51	-2.31%
Derived Performance Parameters				
Conductance of the Sample: $C_s = Q_s/A_p \cdot (T_1 - T_2)$, $W/(m^2 \cdot K)$	2.40	2.19	-0.20	-8.50%
U-value of the sample: $U_s = 1/[(1/C_s) + (1/h_i) + (1/h_o)]$, $W/(m^2 \cdot K)$	1.70	1.59	-0.10	-6.17%
Thermal resistance = $1 / C_s$, $(m^2 \cdot K) / W$	0.42	0.46	0.04	9.29%
R-value = $1 / U_s$, $(m^2 \cdot K) / W$	0.59	0.63	0.04	6.58%

Table A13 –Test Results and Calculated U-value for Curtain Wall Assembly of 12 ft. x 12 ft. Specimen size, as reported in test with overfilling of Argon in IGU

100% Ar and 0% Air, Frame Insulations: XPS				
Parameter	Test (T)	Model (M)	Difference M - T	Deviation (%)
Areas				
Projected Area of the Sample (A_p), m^2	13.38	13.38	0.00	-0.01%
Total Indoor Surface Area (A_i), m^2	16.29	16.29	0.49	3.08%
Total Outdoor Surface Area (A_o), m^2	14.38	14.38	0.28	2.02%
Test and Boundary Conditions				
Temperature of warm side air (T_i), °C	21.09	21.09	N/A	N/A
Temperature of cold side air (T_o), °C	-17.99	-17.99	N/A	N/A
Interior Test Film (h_i), $W/(m^2 \cdot K)$	8.37	8.37	N/A	N/A
Exterior Test Film (h_o), $W/(m^2 \cdot K)$	19.25	19.25	N/A	N/A
Measurements and Predictions				
Average Area Weighted Room Side Surface Temp. (T_1), °C	13.16	14.81	1.65	12.56%
Average Weather Side Area Weighted Surface Temp. (T_2), °C	-14.54	-14.90	-0.36	2.45%
Surface-to-surface Temperature Difference (DT), °C	27.70	29.71	2.01	7.26%
Net Specimen Heat Loss (Q_s), W	888.56	855.96	-32.60	-3.67%
Derived Performance Parameters				
Conductance of the Sample: $C_s = Q_s/A_p \cdot (T_1 - T_2)$, $W/(m^2 \cdot K)$	2.40	2.15	-0.24	-10.17%
U-value of the sample: $U_s = 1/[(1/C_s) + (1/h_i) + (1/h_o)]$, $W/(m^2 \cdot K)$	1.70	1.57	-0.13	-7.43%
Thermal resistance = $1 / C_s$, $(m^2 \cdot K) / W$	0.42	0.46	0.05	11.33%
R-value = $1 / U_s$, $(m^2 \cdot K) / W$	0.59	0.64	0.05	8.03%
100% Ar and 0% Air, Frame Insulations: EPS				
Measurements and Predictions				
Average Area Weighted Room Side Surface Temp. (T_1), °C	13.16	14.80	1.64	12.49%
Average Weather Side Area Weighted Surface Temp. (T_2), °C	-14.54	-14.89	-0.35	2.42%
Surface-to-surface Temperature Difference (DT), °C	27.70	29.70	2.00	7.20%
Net Specimen Heat Loss (Q_s), W	888.56	857.32	-31.24	-3.52%
Derived Performance Parameters				
Conductance of the Sample: $C_s = Q_s/A_p \cdot (T_1 - T_2)$, $W/(m^2 \cdot K)$	2.40	2.16	-0.24	-9.99%
U-value of the sample: $U_s = 1/[(1/C_s) + (1/h_i) + (1/h_o)]$, $W/(m^2 \cdot K)$	1.70	1.58	-0.12	-7.29%
Thermal resistance = $1 / C_s$, $(m^2 \cdot K) / W$	0.42	0.46	0.05	11.09%
R-value = $1 / U_s$, $(m^2 \cdot K) / W$	0.59	0.63	0.05	7.86%

Triple Glazing, Low-e coating of emissivity = 0.054, and XPS Frame Insulation							
Parameter	Gas: Ar		Gas: Kr		Gas: Xe		Gas: Air
	90% Ar	100% Ar	90% Kr	100% Kr	90% Xe	100% Xe	100% Air
Areas							
Projected Area of the Sample (A_p), m^2	13.32	13.32	13.32	13.32	13.32	13.32	13.32
Total Indoor Surface Area (A_i), m^2	16.20	16.20	16.20	16.20	16.20	16.20	16.20
Total Outdoor Surface Area (A_o), m^2	14.17	14.17	14.17	14.17	14.17	14.17	14.17
NFRC Boundary Conditions							
Temperature of warm side air (T_i), °C	21.00	21.00	21.00	21.00	21.00	21.00	21.00
Temperature of cold side air (T_{ii}), °C	-18.00	-18.00	-18.00	-18.00	-18.00	-18.00	-18.00
Interior Test Film (h_i), $W/(m^2 \cdot K)$	7.67	7.67	7.67	7.67	7.67	7.67	7.67
Exterior Test Film (h_{ii}), $W/(m^2 \cdot K)$	30.00	30.00	30.00	30.00	30.00	30.00	30.00
Performance Predictions							
Average Area Weighted Room Side Surface Temp. (T_1), °C	15.72	15.77	16.24	16.33	16.45	16.54	15.20
Average Weather Side Area Weighted Surface Temp. (T_2), °C	-16.46	-16.47	-16.61	-16.63	-16.67	-16.70	-16.30
Surface-to-surface Temperature Difference (ΔT), °C	32.18	32.25	32.85	32.96	33.12	33.24	31.50
Net Specimen Heat Loss (Q_s), W	656.20	649.25	591.54	580.45	565.36	554.00	721.09
Derived Performance Parameters							
Conductance of the Sample: $C_s = Q_s/A_p \cdot (T_1 - T_2)$, $W/(m^2 \cdot K)$	1.532	1.512	1.352	1.323	1.282	1.252	1.719
U-value of the sample: $U_s = 1/[(1/C_s) + (1/h_i) + (1/h_{ii})]$, $W/(m^2 \cdot K)$	1.225	1.212	1.107	1.087	1.060	1.039	1.342
Thermal resistance = $1/C_s$, $(m^2 \cdot K) / W$	0.653	0.661	0.739	0.756	0.780	0.799	0.582
R-value = $1/U_s$, $(m^2 \cdot K) / W$	0.817	0.825	0.903	0.920	0.944	0.963	0.745
Percentage Increase in Performance due to Using different Filling Gas (%)							
Conductance of the Sample: C_s	12.24	13.70	27.11	30.00	34.10	37.34	N/A
U-value of the sample: U_s	9.55	10.69	21.16	23.41	26.61	29.14	N/A
Thermal resistance = $1/C_s$	12.24	13.70	27.11	30.00	34.10	37.34	N/A
R-value = $1/U_s$	9.55	10.69	21.16	23.41	26.61	29.14	N/A

Triple Glazing, Low-e coating of emissivity = 0.054, and EPS Frame Insulation							
Parameter	Gas: Ar		Gas: Kr		Gas: Xe		Gas: Air
	90% Ar	100% Ar	90% Kr	100% Kr	90% Xe	100% Xe	100% Air
Areas							
Projected Area of the Sample (A_p), m^2	13.32	13.32	13.32	13.32	13.32	13.32	13.32
Total Indoor Surface Area (A_i), m^2	16.20	16.20	16.20	16.20	16.20	16.20	16.20
Total Outdoor Surface Area (A_o), m^2	14.17	14.17	14.17	14.17	14.17	14.17	14.17
NFRC Boundary Conditions							
Temperature of warm side air (T_i), °C	21.00	21.00	21.00	21.00	21.00	21.00	21.00
Temperature of cold side air (T_{ii}), °C	-18.00	-18.00	-18.00	-18.00	-18.00	-18.00	-18.00
Interior Test Film (h_i), $W/(m^2 \cdot K)$	7.67	7.67	7.67	7.67	7.67	7.67	7.67
Exterior Test Film (h_{ii}), $W/(m^2 \cdot K)$	30.00	30.00	30.00	30.00	30.00	30.00	30.00
Performance Predications							
Average Area Weighted Room Side Surface Temp. (T_1), °C	15.71	15.77	16.23	16.32	16.44	16.53	15.19
Average Weather Side Area Weighted Surface Temp. (T_2), °C	-16.45	-16.47	-16.61	-16.63	-16.67	-16.69	-16.30
Surface-to-surface Temperature Difference (ΔT), °C	32.16	32.24	32.84	32.95	33.11	33.23	31.49
Net Specimen Heat Loss (Q_s), W	657.39	650.44	592.73	581.64	566.55	555.18	722.28
Derived Performance Parameters							
Conductance of the Sample: $C_s = Q_s/A_p \cdot (T_1 - T_2)$, $W/(m^2 \cdot K)$	1.535	1.515	1.356	1.326	1.285	1.255	1.723
U-value of the sample: $U_s = 1/[(1/C_s) + (1/h_i) + (1/h_{ii})]$, $W/(m^2 \cdot K)$	1.227	1.214	1.109	1.089	1.062	1.041	1.344
Thermal resistance = $1/C_s$, $(m^2 \cdot K) / W$	0.651	0.660	0.738	0.754	0.778	0.797	0.580
R-value = $1/U_s$, $(m^2 \cdot K) / W$	0.815	0.824	0.901	0.918	0.942	0.961	0.744
Percentage Increase in Performance due to Using different Filling Gas (%)							
Conductance of the Sample: C_s	12.23	13.68	27.07	29.95	34.05	37.28	N/A
U-value of the sample: U_s	9.54	10.67	21.12	23.36	26.56	29.08	N/A
Thermal resistance = $1/C_s$	12.23	13.68	27.07	29.95	34.05	37.28	N/A
R-value = $1/U_s$	9.54	10.67	21.12	23.36	26.56	29.08	N/A

Appendix 4 Effect of Inclination Angle and Direction of Heat Flow

The sloped reflective insulation products and IGUs are being used in many building applications such as sloped roof and skylight systems. In these particular applications, it might be difficult to adapt one of the available test methods such as the ASTM C-518 [47] and ASTM C-1363 [54] in order to measure the R-value of sloped specimens. For instance, the ASTM C-518 test method could be used in the case of specimen with horizontal and vertical orientations only [47]. After gaining confidence in the present model, as described in this report, in predicting the R-value of specimen with horizontal orientation (e.g., see [37]) and specimen with vertical orientation (e.g., see [32]), it was then used to quantify the contribution of enclosed spaces bounded by surfaces having different values of emissivity to the R-value of specimen with different orientations.

In a recent study by Saber [36], a parametric study was conducted to investigate the effect of inclination angle (θ) and direction of heat flow on the effective R-value of EPS sample stack shown in Figure 144. For the case of IGUs, however, the EPS layers in the sample stack can be replaced by glass plates. Note that the rate of heat transfer by both convection and radiation in the air cavity depends on its size and the temperature difference across the sample stack (ΔT). As such, the effective R-value depends on both ΔT and the size of the air cavity. The results presented in this section are obtained for *only* one ΔT of 22.4°C ($T_c = 12.7^\circ\text{C}$, and $T_h = 35.1^\circ\text{C}$) and one size of the air cavity as shown in Figure 144.

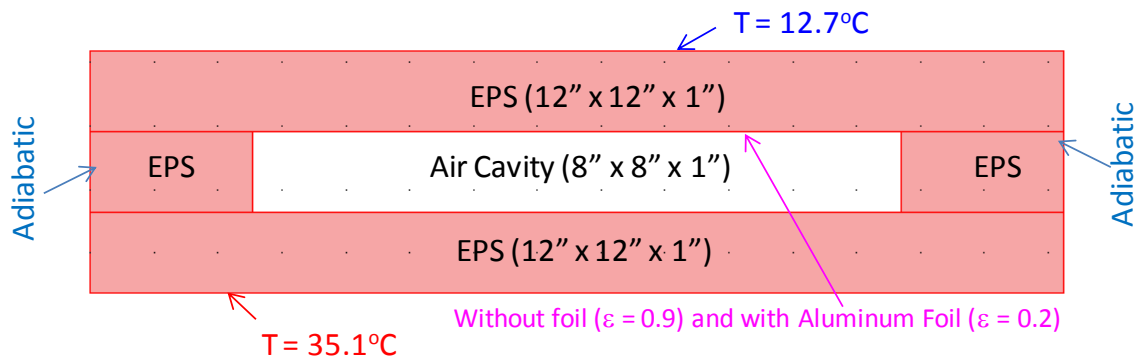


Figure 144. Sample stacks tested at NRC [37]

In the case of foil emissivity of 0.05, Figure 145 and Figure 146 show the vertical velocity (v) and horizontal velocity (u) contours and the airflow field in the cavity for different inclination angles (θ) when the sample stack was heated from the top and the bottom. As shown in these figures, in the case of sample stack heated from the top with $\theta = 30^\circ$ and vertical sample stack heated from the left ($\theta = 90^\circ$), a mono-cellular with one vortex cell airflow (i.e. convection loop) is developed in the air cavity due to bouncy effect. In the case of sample stack heated from the bottom with $\theta = 30^\circ$, a multi-cellular airflow is developed in the cavity with three vortex cells. For horizontal sample stack ($\theta = 0^\circ$) heated from the bottom and top, multi-cellular airflow is developed in the cavity with six and two vortex cells, respectively.

Figure 145 and Figure 146 show that the value of the air velocity in the cavity is greatly affected by both the inclination angle (θ) and direction of heat flow through the sample stack. For horizontal sample stack ($\theta = 0^\circ$), the air velocity in the case of downward heat flow (sample heated from the top, $v_{\uparrow}(\max) = 0.6$ mm/s,

$u \rightarrow (\max) = 3.2$ mm/s) is much smaller than that in the case of upward heat flow (sample heated from the bottom, $v \uparrow (\max) = 18.7$ mm/s, $u \rightarrow (\max) = 22.1$ mm/s). This is due to a downward heat flow encourages a relatively stable stratification of air due to differences in buoyancy compared to the case with upward heat flow. As such, a sample stack with downward heat flow results in a greater R-value (12.19 ft²hr°F/BTU) than that with upward heat flow (10.82 ft²hr°F/BTU) (see Figure 147a). By subtracting the R-value of both the top and bottom EPS layers (8.33 ft²hr°F/BTU) from the total R-value of the sample stack, the middle layer (i.e. the spacer in the case of IGUs) with the air cavity contributed to the R-value by 3.86 ft²hr°F/BTU and 2.49 ft²hr°F/BTU in the cases of horizontal sample stack heated from the top and bottom, respectively (Figure 147b). Similarly, for $\theta = 30^\circ$, the air velocity in the cavity of sample stack heated from the top ($v \uparrow (\max) = 10.6$ mm/s, $u \rightarrow (\max) = 18.5$ mm/s) is also smaller than that heated from the bottom ($v \uparrow (\max) = 14.1$ mm/s, $u \rightarrow (\max) = 23.3$ mm/s). Consequently, the contribution of middle layer with air cavity to the R-value for the former (3.26 ft²hr°F/BTU) is greater than that for the latter (2.65 ft²hr°F/BTU) (Figure 147b). For vertical sample stack ($\theta = 90^\circ$) heated from the left or right, the contribution of the middle layer with air cavity to the R-value is 2.63 ft²hr°F/BTU.

Using a heavier gas than air to fill the cavity of the sample stack such as Argon (Ar), Krypton (Kr), or Xenon (Xe), listed in Coatings for *glass lites* — Reflective and low-emissivity (low-e) coatings made of thin pure metal or metal oxide layers can also be applied for solar (ultraviolet and infrared radiation) control, as either hard (e.g., cobalt, iron, chrome, tin) or soft coatings (e.g., silver, copper, chrome, titanium, stainless steel) products. Soft coatings are vulnerable to scratching and corrosion and are sealed within the space in the IGU (surface S2 or S4, see Figure 2). Reflective coatings act like a mirror reflecting the heat back to the exterior, whereas low- ϵ , would result in an increase the overall thermal resistance as shown in Figure 149 through Figure 153. This is due to in the following:

1. Obtaining lower gas velocity on the cavity than that provided in Figure 145 and Figure 146 for air resulting in reducing the heat transfer by convection inside the cavity; and
2. Reducing the heat transfer by conduction through the cavity due to lower thermal conducting of these gases compared to air (Coatings for *glass lites* — Reflective and low-emissivity (low-e) coatings made of thin pure metal or metal oxide layers can also be applied for solar (ultraviolet and infrared radiation) control, as either hard (e.g., cobalt, iron, chrome, tin) or soft coatings (e.g., silver, copper, chrome, titanium, stainless steel) products. Soft coatings are vulnerable to scratching and corrosion and are sealed within the space in the IGU (surface S2 or S4, see Figure 2). Reflective coatings act like a mirror reflecting the heat back to the exterior, whereas low- ϵ).

Figure 148a and Figure 148b show the effect of the foil emissivity on the effective R-value and the contribution of the middle layer with air cavity to the R-value, respectively, for sample stack with different inclination angles and different directions of heat flow. As shown in these figures, for all values of foil emissivity, the horizontal sample stack heated from the top (downward heat flow) resulted in the highest R-values while the horizontal sample stack heated from the bottom (upward heat flow) resulted in the lowest R-values. These two cases, respectively, represent the application of using reflective insulations and IGUs in flat roof in the summer season and winter season.

As provided in references [35-38], the emissivity of surfaces of foil or low-e coating materials can increase due to oxidation, accumulation of dust and/or vapor condensation on these surfaces. For IGU applications in

curtain walls, to avoid dust accumulation and vapor condensation on these surfaces, primary and secondary sealants and desiccant are currently being used in the IGUs (see

). Increasing the emissivity from 0.05 to 0.9 resulted in a decrease in the R-value by 20.7% and 8.2% for horizontal sample stack heated from the top and bottom, respectively (Figure 148a). Note that the emissivity of 0.9 represents the case of no foil or low-e coating installed on the system. Moreover, as the emissivity increases from 0.05 to 0.9, the contribution of the air cavity to the R-value decreases by 118% (from 3.86 ft²hr°F/BTU to 1.77 ft²hr°F/BTU) and 49% (from 2.49 ft²hr°F/BTU to 1.67 ft²hr°F/BTU) for horizontal sample stack heated from the top and bottom, respectively (Figure 148b).

In the case of sample stack with inclination angle of 30° (e.g., application of reflective insulations in sloped roofs and flat skylight systems), increasing the emissivity from 0.05 to 0.9 resulted in a decrease in the R-value by 15.0% and 9.5% for sample stack heated from the top (summer season) and bottom (winter season), respectively (Figure 148a). Also, Figure 148b shows that as the emissivity increases from 0.05 to 0.9, the contribution of the air cavity to the R-value decreases by 86% (from 3.26 ft²hr°F/BTU to 1.75 ft²hr°F/BTU) and 56% (from 2.65 ft²hr°F/BTU to 1.70 ft²hr°F/BTU) for sample stack heated from the top and bottom, respectively. Furthermore, in the case of vertical sample stack (e.g., application of reflective insulations in wall systems, windows and curtain walls), increasing the emissivity from 0.05 to 0.9 resulted in a decrease in the R-value by 11.0% (Figure 148a). In this case the contribution of the air cavity to the R-value decreases by 68% (from 2.81 ft²hr°F/BTU to 1.67 ft²hr°F/BTU).

In the case of no foil or low-e coating materials installed in sample stack, or the case of the bounded surfaces of the space are fully covered by dust and/or vapor condensation (i.e. $\epsilon = 0.9$), both inclination angle and direction of heat flow through the specimen have insignificant effect on the effective R-value (i.e. resultant lines tend to converge as ϵ tends to 0.9, see Figure 148a). In this case, the maximum change in the contribution of the middle layer and the air cavity to the R-value is only 6% (from 1.77 ft²hr°F/BTU to 1.67 ft²hr°F/BTU, Figure 148b). Therefore, for accurate energy calculations for roofs, walls and fenestration systems with reflective insulations or low-e coating materials, subjected to different climate conditions, it is important to conduct hygrothermal simulations instead of thermal simulations in order to investigate whether or not vapor condensation occurs on the surfaces bounded the space.

The effect of the type of filling gas and foil/coating emissivity on the effective resistance of sample stack (see Figure 144) are shown in Figure 149 for the case of vertical sample stack, Figure 150 for the case of horizontal sample stack heated from bottom, Figure 151 for the case sample stack heated from top, Figure 152 for the case of sloped sample stack of $\theta = 30^\circ$ heated from bottom, and Figure 153 for the case of sloped sample stack of $\theta = 30^\circ$ heated from top. As shown in these figures, the sample stack with Xe has the highest R-value while that with air has the lowest R-value. Also, these figures show that the effect of the type of gas has a significant effect on the R-value when the foil/coating emissivity is approximately lower than 0.5. However, when the foil/coating emissivity is approximately greater than 0.5, the type of gas has insignificant effect on the R-value. As such, in case of not using foil/coating with low emissivity, it is not recommended using heavy gases (e.g. Ar, Kr or Xe) in the IGUs of fenestration systems.

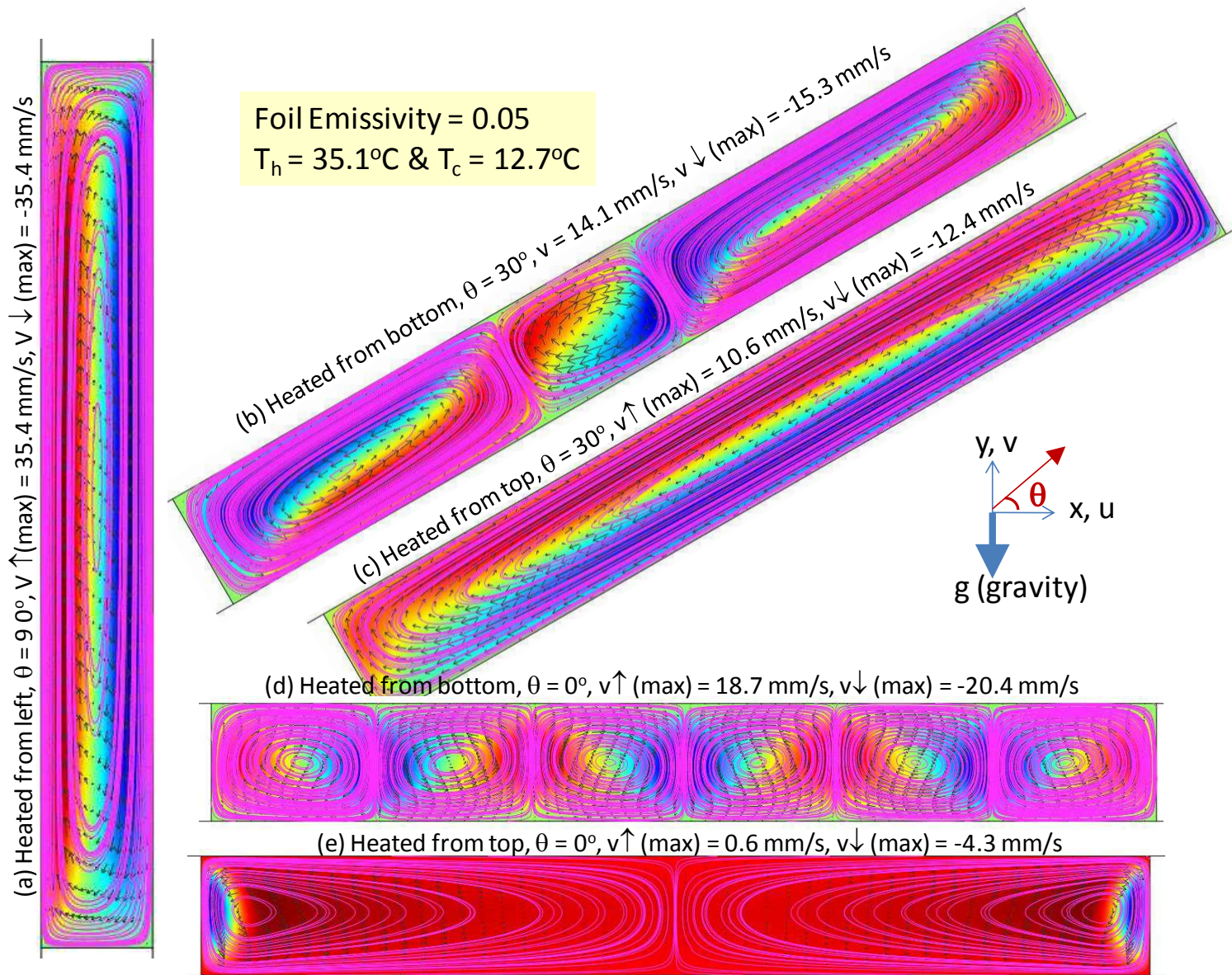


Figure 145. Vertical velocity contours and flow field in the air cavity of sample stacks with different inclinations

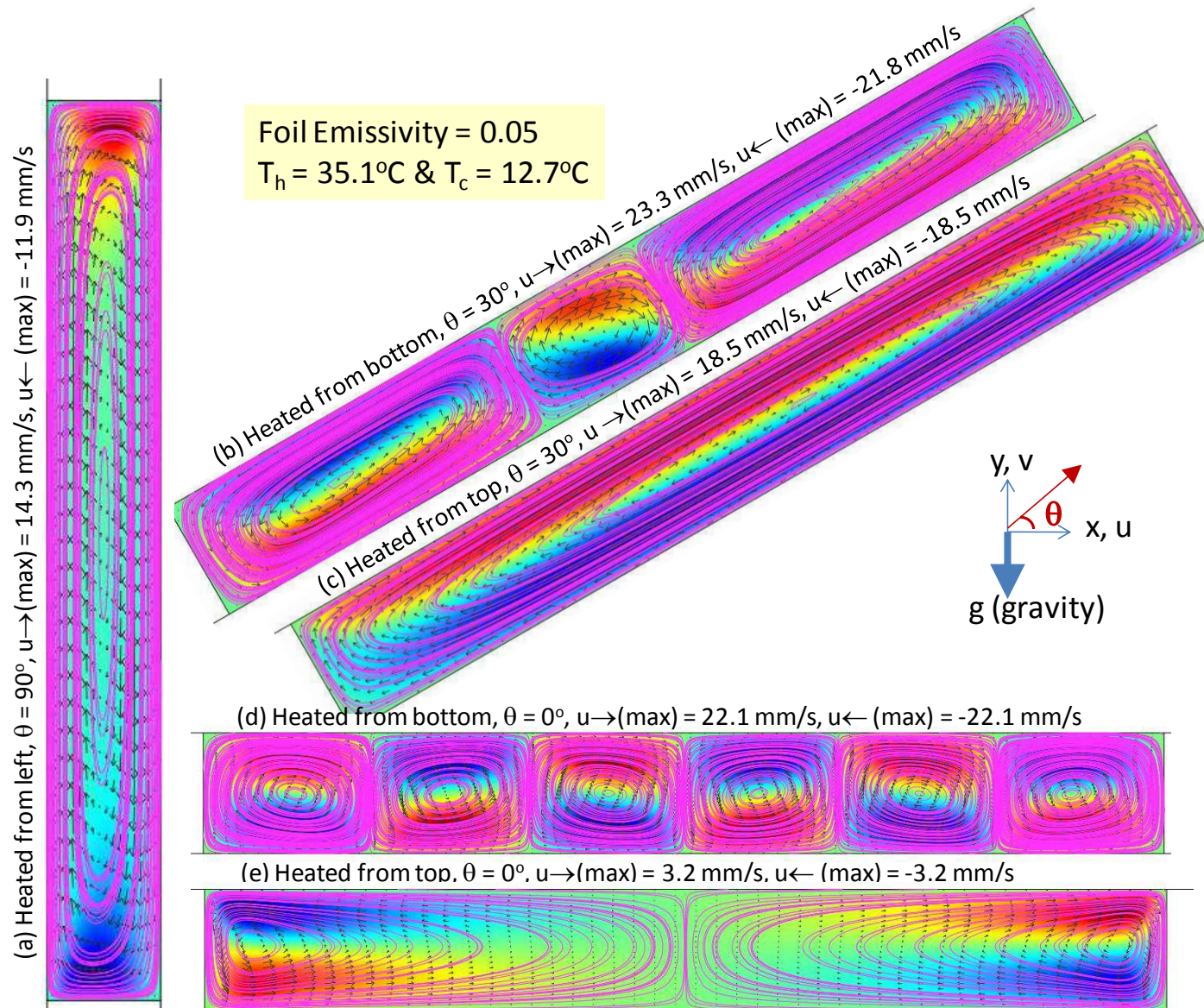


Figure 146. Horizontal velocity contours and flow field in the air cavity of sample stacks with different inclinations

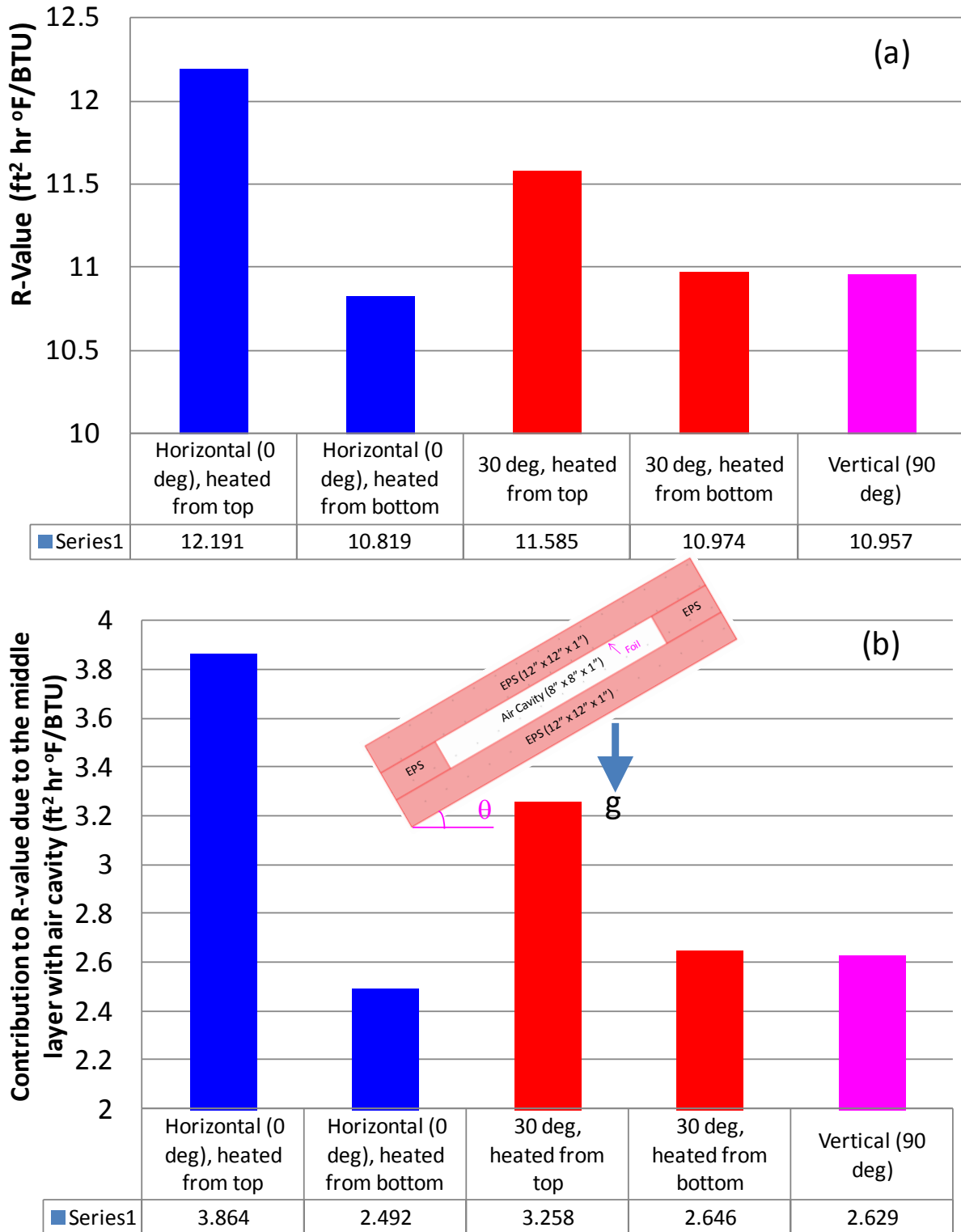


Figure 147. Effect of inclination angle of sample stack and direction of heat flow on the effective R-value in the case of foil emissivity of 0.05

Cavity filled with air

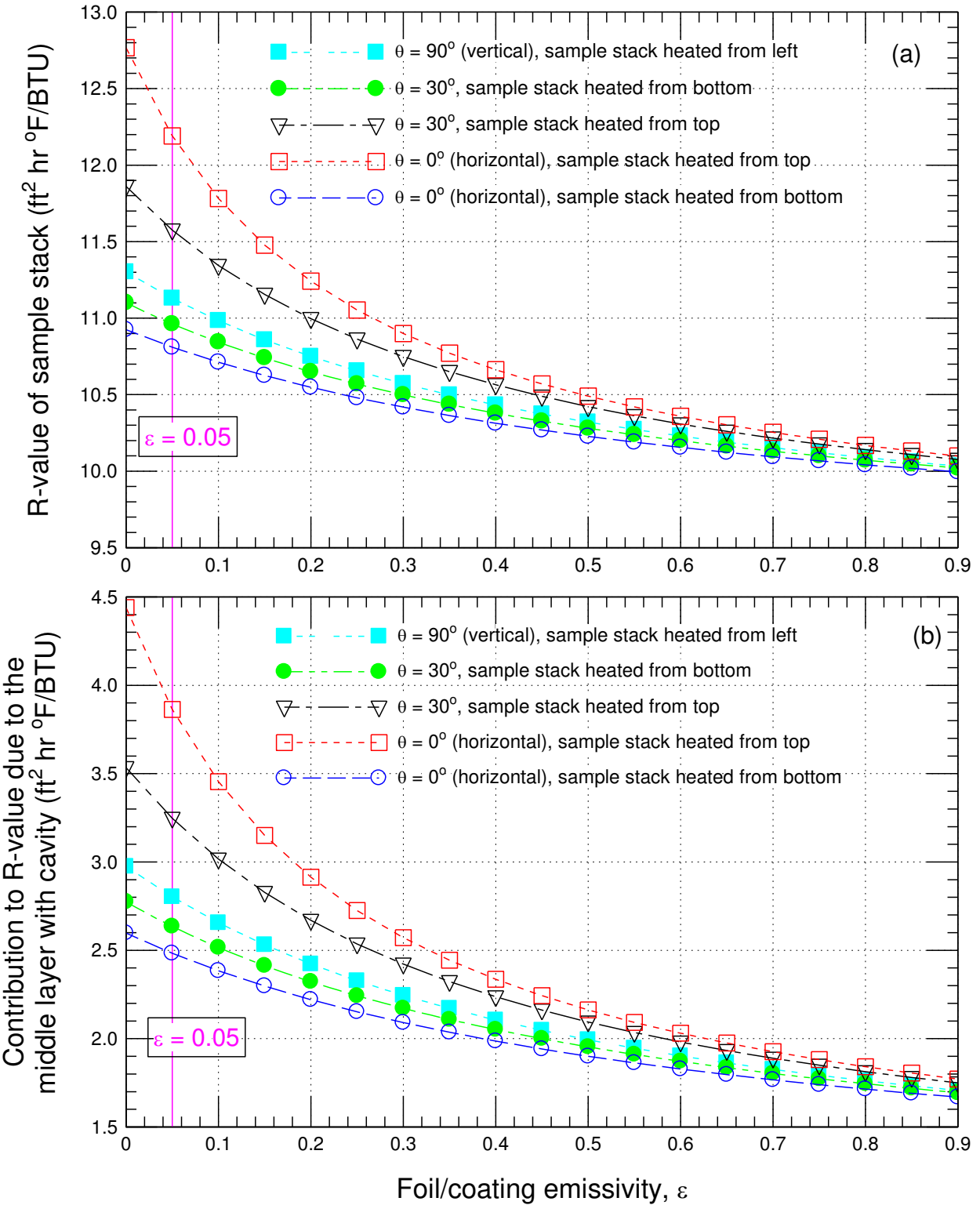


Figure 148. Effect of inclination angle of sample stack shown in Figure 144, foil/coating emissivity and direction of heat flow on the effective R-value

$\theta = 90^\circ$ (vertical), sample stack heated from left

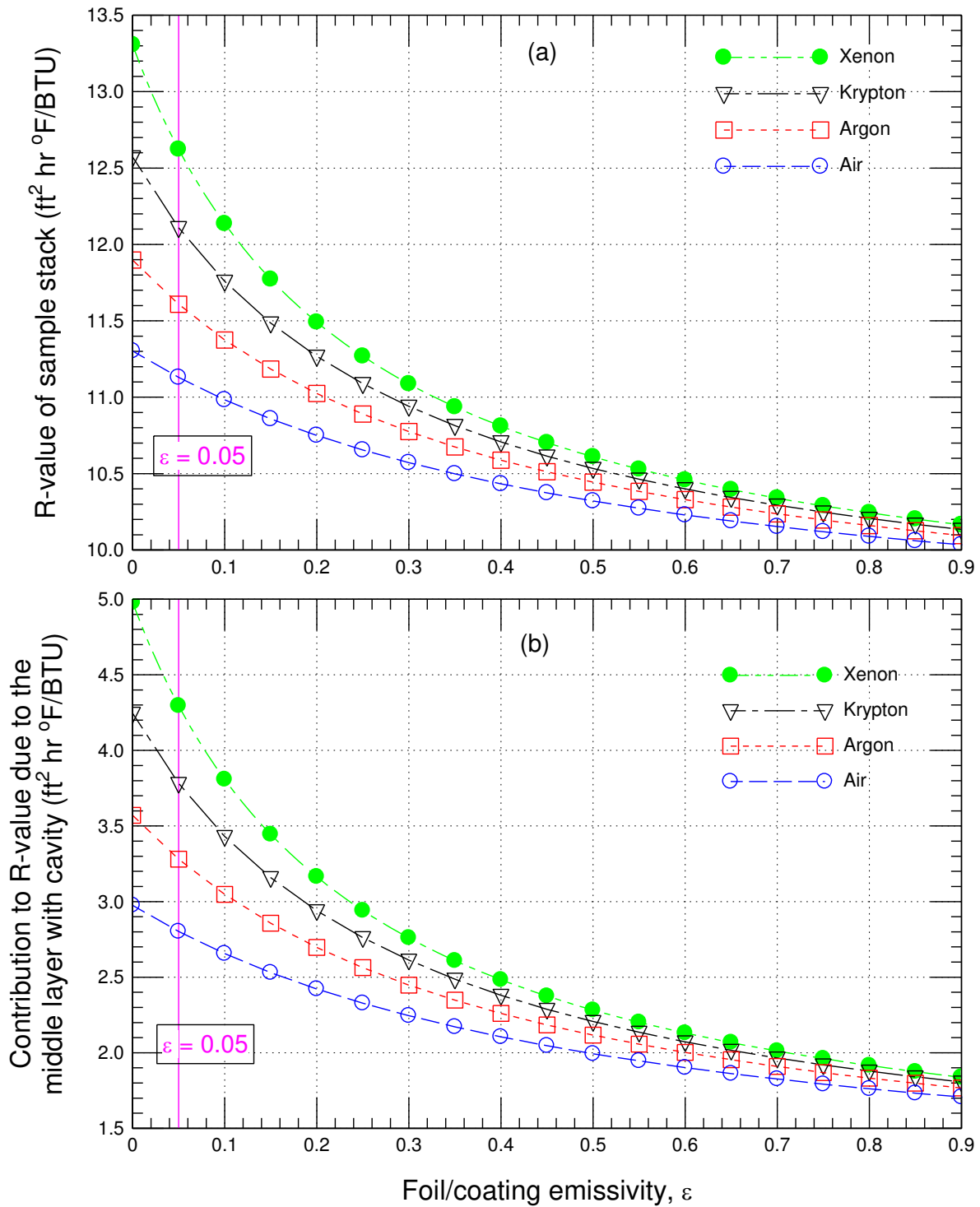


Figure 149. Effect filling gas in sample stack shown in Figure 144 and foil/coating emissivity on the effective R-value for the case of $\theta = 90^\circ$ (vertical)

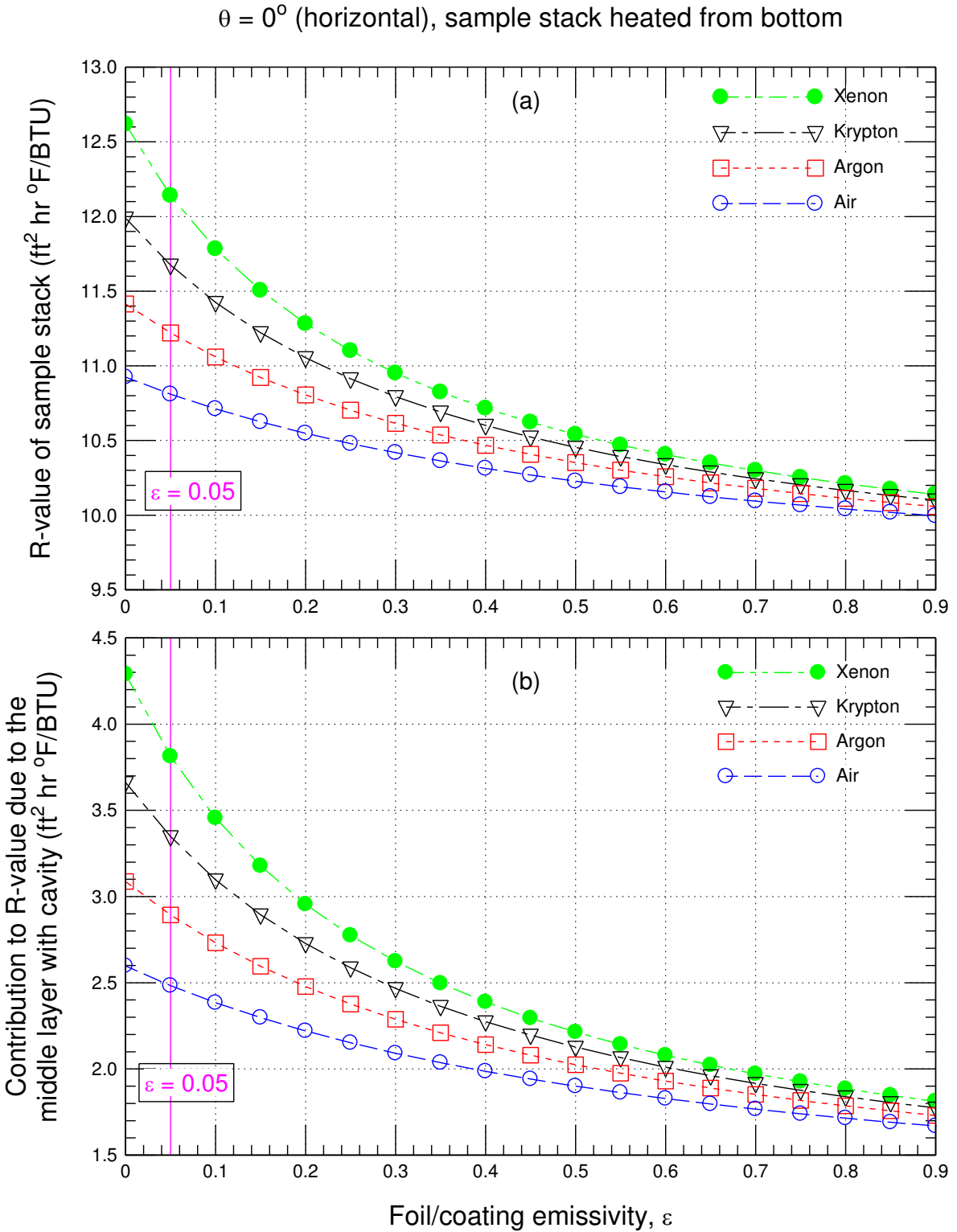


Figure 150. Effect filling gas in sample stack heated from bottom and shown in Figure 144 and foil/coating emissivity on the effective R-value for the case of $\theta = 0^\circ$ (horizontal)

$\theta = 0^\circ$ (horizontal), sample stack heated from top

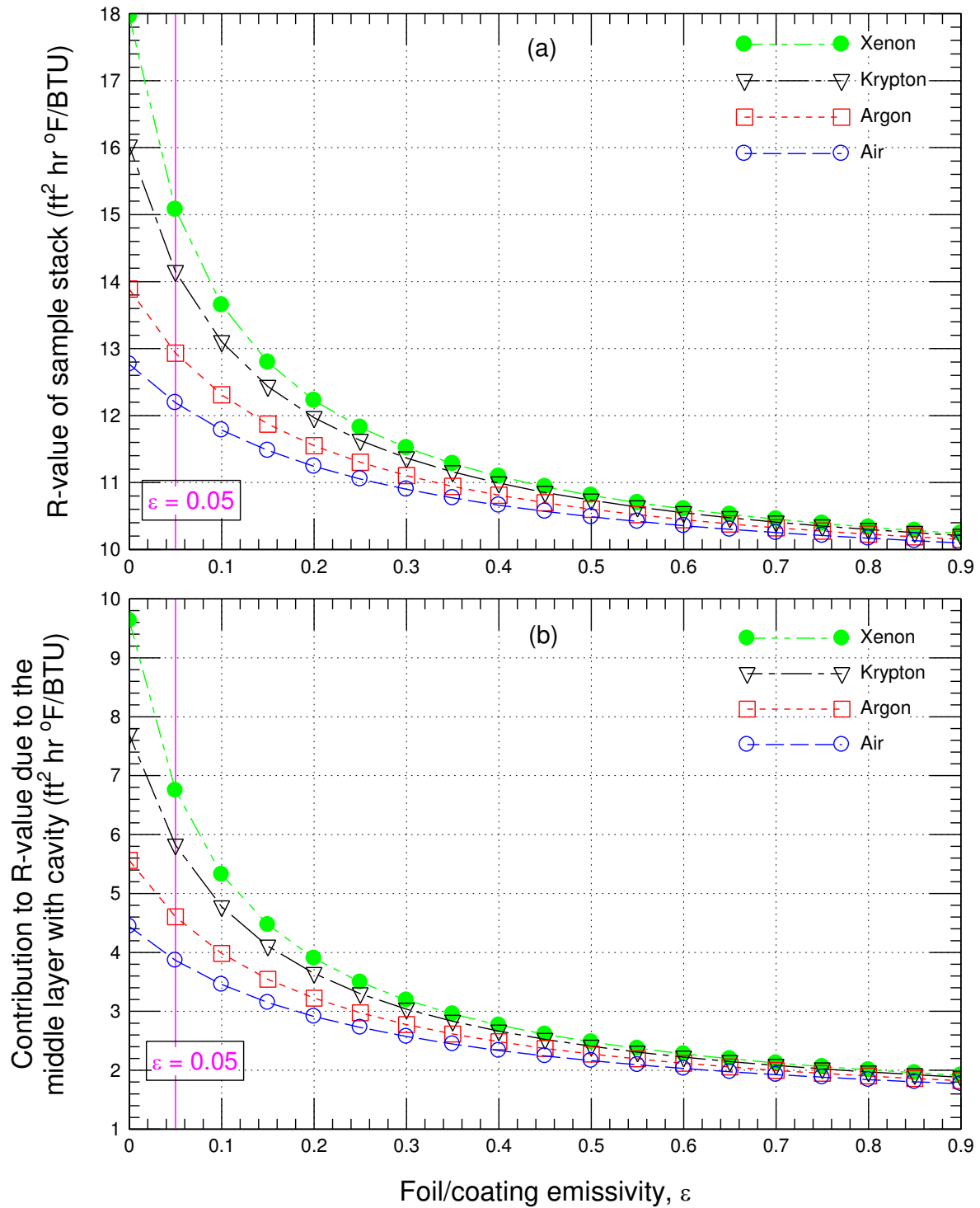


Figure 151. Effect filling gas in sample stack heated from top and shown in Figure 144 and foil/coating emissivity on the effective R-value for the case of $\theta = 0^\circ$ (horizontal)

$\theta = 30^\circ$, sample stack heated from bottom

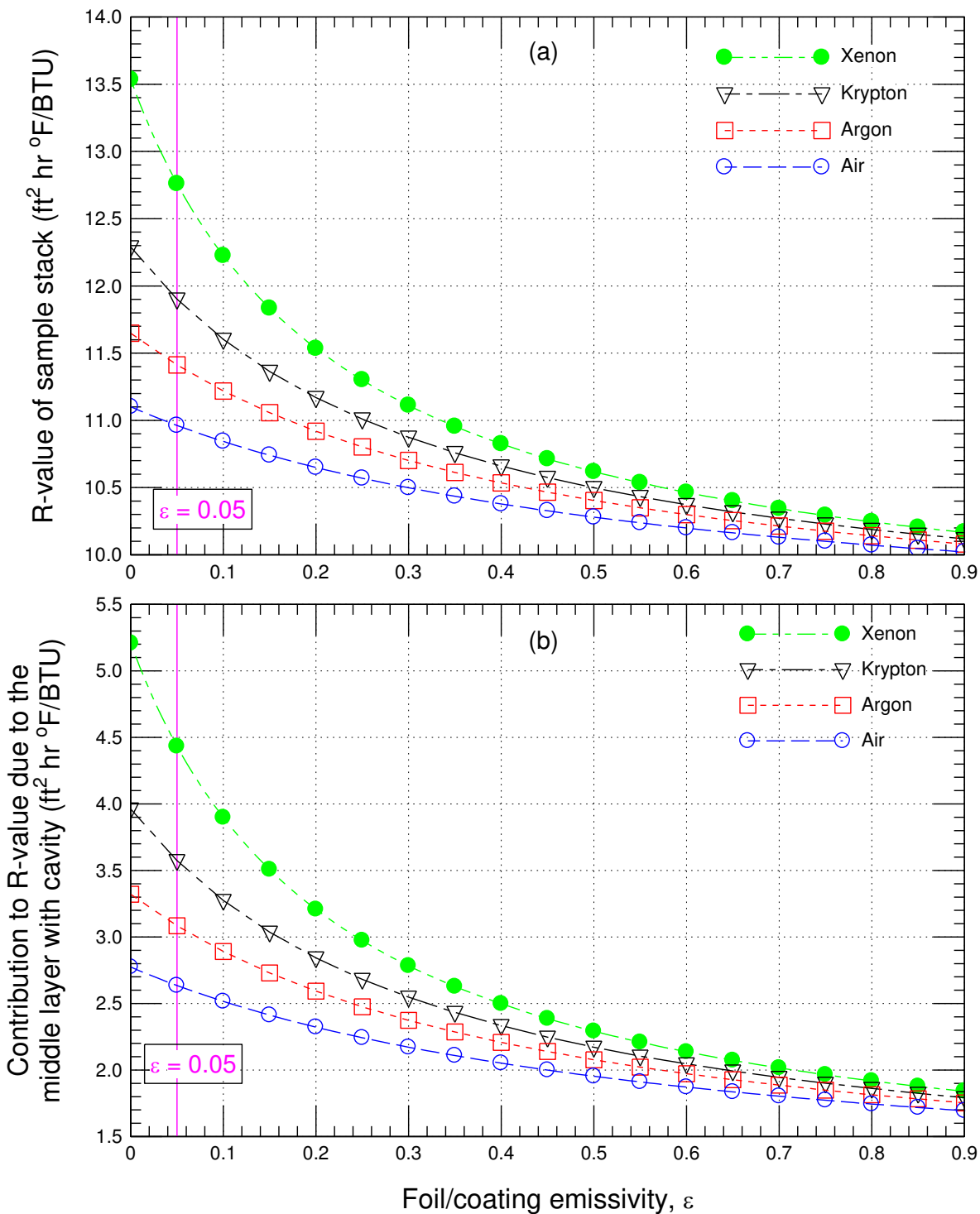


Figure 152. Effect filling gas in sample stack heated from bottom and shown in Figure 144 and foil/coating emissivity on the effective R-value for the case of $\theta = 30^\circ$ (sloped)

$\theta = 30^\circ$, sample stack heated from top

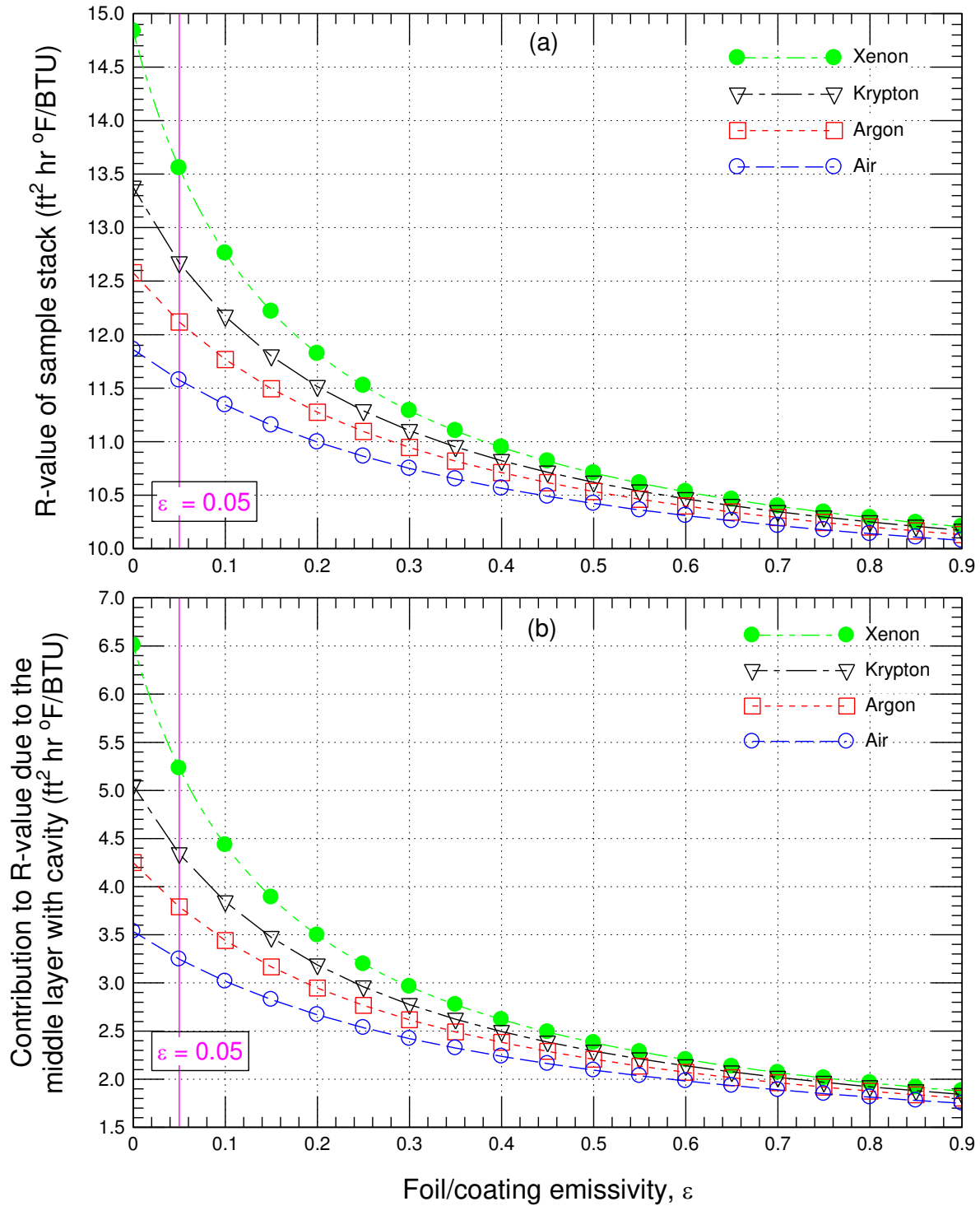


Figure 153. Effect filling gas in sample stack heated from top and shown in Figure 144 and foil/coating emissivity on the effective R-value for the case of $\theta = 30^\circ$ (sloped)

Appendix 5 - Summary of Previous Model Benchmarking

The numerical model, hygIRC-C, was used to investigate the thermal performance of curtain wall systems. The model solves simultaneously the 2D and 3D moisture transport equation, energy equation, surface-to-surface radiation equation (e.g., surface-to-surface radiation in enclosed airspace such as shown in **Error! eference source not found.**) and air transport equation in the various material layers. The air transport equation is the Navier-Stokes equation for the airspace (e.g., air cavity), and Darcy equation (Darcy Number, $DN < 10^{-6}$) and Brinkman equation ($DN > 10^{-6}$) for the porous material layers (see [13-14, 32-33, 37-38, 55-57] for more details).

The numerical model had been previously benchmarked in a number of building applications. For the applications that are similar to this study, the numerical model was benchmarked against the thermal performance data for a full-scale wall assembly with and without reflective insulation products. In a previous project called “Wall Energy Rating (WER)”, the three-dimensional version of this model was used to conduct numerical simulations for different full-scale 2 x 6 wall assemblies incorporating, or not, penetrations representative of a window installation, such that the effective thermal resistance (R-value) of the assemblies could be predicted, taking into consideration air leakage across the assembly. The stud-cavity of these walls incorporated open cell polyurethane foam, closed cell spray polyurethane foam or glass fibre insulation. The predicted R-values for these walls were in good agreement (within $\pm 5\%$ which is the same as the uncertainty of test data, see [55, 57, 59]) with the measured R-values that were obtained from testing in the NRC’s Guarded Hot Box (GHB) according to the ASTM C-1363 standard test method [54].

For test samples featuring reflective insulation products, the data obtained using a GHB in accordance with ASTM C-1363 test method [54] and ASTM C-518 standard test method [47] were compared with the model predictions. Results showed that the R-value predicted by the model for above-grade wall assembly with low emissivity materials and furred-airspace was in good agreement with the measured R-value (within 1.2%) [32, 58]. Furthermore, the numerical model was benchmarked against a number of tests that were conducted at the Cold Climate Housing Research Center (CCHRC) [31] and the National Research Council of Canada (NRC) [36-37]. These tests were conducted using heat flow meters in accordance with the ASTM C-518 test method [47] to examine the thermal performance of different types of reflective insulation assemblies. The results showed that the heat fluxes predicted by the model were in good agreements with the measured heat fluxes (within $\pm 1.0\%$). The accurate calculations of the airflow and temperature distributions within the test specimens resulted in that the predictions of the present model for the R-values were in good agreements with the measured R-values. Furthermore, the model was used to determine the reductions in the R-values of the specimens as a result of increasing the foil emissivity due to water vapour condensation and/or dust accumulation on the surface of the foil. Thereafter, the model was used to investigate the contribution of reflective insulations to the R-value for specimens having three inclination angles ($\theta = 0^\circ$, 45° and 90°), different directions of heat flow through the specimens, and a wide range of foil emissivity [36].

In previous studies, the model was used to determine the R-values of vertical enclosed airspaces ($\theta = 90^\circ$) [42], horizontal enclosed airspaces ($\theta = 0^\circ$) with upward heat flow [43] and downward heat flow [45], and high-sloped enclosed airspaces ($\theta = 45^\circ$) with downward heat flow [44]. In those studies, the predicted R-values were compared with the ASHRAE R-values [53] for enclosed airspaces of different thicknesses and different operating conditions. Also, the model was used to determine the R-values of low-sloped enclosed airspaces ($\theta = 30^\circ$) and subjected to downward heat flow conditions [46]. As indicated earlier, in these same

studies, the dependence of the R-value on a wide range of the airspace aspect ratio (i.e. ratio of the length or height of the airspace to its thickness) of the enclosed airspace was also investigated. Additionally, practical correlations were developed for determining the R-values of enclosed airspaces of different thicknesses, and for a wide range of values for various parameters, namely, aspect ratio, temperature differential, average temperature, and emissivity of the different surfaces of the airspaces [42-46]. These correlations are ready to be implemented in energy simulations models such as Energy Plus, ESP-r and DOE.

For the cases of open and closed airspaces in wall systems, the model was used to determine the effective thermal resistance of a number of foundation wall systems with a low emissivity material bonded to thermal insulation and furred-airspace assembly, and subjected to different climatic conditions of Canada (Toronto, Quebec, Sept-Îles, Ottawa, and Victoria) [60-62]. In that study, for the case of open airspace, the effect of infiltration and exfiltration on the effective R-value was accounted for [60].

Also, the present model was benchmarked and thereafter used to assess the effect of thermal mass on the thermal performance of Insulated Concrete Form (ICF) wall systems when placed in NRC-Construction's Field Exposure of Walls Facility (FEWF) and subjected to yearly periods of local Canadian climate [63]. Results showed that the predictions of the present model for the temperature and heat flux distributions within the ICF wall systems were in good agreements with the test data. Recently, the present model was benchmarked against field data obtained in the NRC's FEWF of highly insulated residential wood-frame construction in which Vacuum Insulation Panels (VIPs) were used as the primary insulation components; the results from this work showed that the model predictions were in good agreement with the test data [64, 65].

More recently, the hygIRC-C model was benchmarked against test results of a number of samples of Exterior Insulation and Finishing Systems (EIFS) [66]. The test results were obtained using the NRC's Guarded-Hot-Plate (GHP) apparatus in accordance of the ASTM C-177 standard test method [67]. The accurate calculations of the airflow and temperature distribution within the test specimens had resulted that the model predictions for the R-values of different samples were in good agreements with the test results (within $\pm 5\%$). Thereafter, the present model was used to investigate the effect of air leakage due to infiltration and exfiltration on the effective R-values of different EIFS assemblies, subjected to different climatic conditions. The results of this study will be published at a later date. A full description of the present model and more details about model benchmarking are available in previous publications [13-14, 30, 32, 33, 35, 37-38, 54-56, 59]. Having previously benchmarked the present model to several tests undertaken in controlled laboratory conditions as described previously, it is important to benchmark the model against the test results of curtain wall before using it to assess the thermal performance of curtain wall systems as described in this report.